

**Silica Cell Wall Morphogenesis and
Cytoskeletal Dynamics of the Centric
Diatom *Odontella sinensis***

Volume 1

Yin Zhang

Institute of Cellular & Molecular Botany (IZMB)
Mathematisch-Naturwissenschaftliche Fakultät
Rheinische Friedrich-Wilhelms-Universität Bonn

A Dissertation presented for the degree of
Doctor of Natural Sciences
in the subject of Plant Sciences

Bonn, 2018

Angefertigt mit Genehmigung der Mathematisch-Naturwissenschaftlichen Fakultät der Rheinischen Friedrich-Wilhelms-Universität Bonn.

Erstgutachter: Prof. Dr. Diedrik Menzel

Zweitgutachter: PD Dr. František Baluška

Tag der Promotion: 21.12.2018

Erscheinungsjahr: 2019

Declaration

I declare that this thesis is my own work in design and execution; and all material that I have used or quoted have been indicated and acknowledged by means of complete references.

Bonn, September 2018

Yin Zhang



Preface

This thesis is dedicated to

ROBERT LAUTERBORN

WHO DESCRIBED DELICATE INTRACELLULAR STRUCTURES IN THE DIATOMS FOR THE FIRST TIME AND STUDIED THEIR DYNAMICS ALREADY IN THE YEAR 1896,

And to

JEREMY PICKETT-HEAPS

WHO REVEALED THEIR CYTOSKELETAL NATURE IN MODERN TIMES.

About the Dissertation

Recent perception of the diatom cytoskeleton is still lacking recognition of how the cytoskeleton dynamically changes its architecture and composition to perform growth and morphogenesis of the silica wall during the cell cycle. This thesis, consisting of three parts, is making a contribution to understanding this problem. The general background of the centric diatom species *Odontella sinensis* is introduced in Part I of this thesis. In Part II, data of *O. sinensis* are presented and discussed in three chapters: The fine structure of the silica cell wall observed by electron microscopy illustrates the frustule characteristics in Chapter 1. In Chapter 2 the sequences of morphogenetic events, which shape the frustule, and the characteristics of the cytoskeleton are imaged throughout the cell cycle by means of silica probe staining and immunocytochemistry, respectively. This leads to a model of how cells accomplish the task of frustule shaping while passing from one generation to the next. Chapter 3 describes what happens in the frustule morphogenesis, when microtubules or microfilaments are interfered with by drugs (additional but yet preliminary results of myosin inhibitions and that of other drug treatments are shown in the Appendix, only included in the accompanying CD). In comparison to the observed cytoskeletal interactions gathered from control cells in Chapter 2, abnormal features of inhibited cells are revealed and the role of the cytoskeleton in frustule morphogenesis is discussed and compared to features of the cytoskeleton dynamics in animals and plants. A short excursion into some other diatom species is added in Part III, the General Discussion, to illustrate the diversity but also common features of the cytoskeleton in centric diatoms. This is backed up by some preliminary observations made on the centric diatoms, which however have remained incomplete (see the Appendix on CD).

- ❖ Please note: Because of the large size, the thesis is printed as two volumes. The flow-text with some illustrations is compiled in Volume 1, all corresponding image plates of the results sections are presented together with the legends in Volume 2. The digital version of the two-volume thesis together with the appendix is provided in the accompanying CD.

Acknowledgement

This thesis has taken a long time to mature. During the study through the past 6 years, I have received a lot of help, guidance and care from my supervisor, colleagues and student friends. I was also fortunate to be helped and encouraged by loved friends and family.

In the following, I would like to especially thank those, who have directly been concerned with my research project:

The support from the CSC scholarship sponsor is gratefully acknowledged. Prof. Caixia Zheng, Prof. Fenglan Li, Prof. Rongfu Gao, Prof. Xinli Xia and Prof. Wei Gao are thanked for recommending me and for opening the chance to me to pursue my Master degree and my PhD work in Germany.

Prof. Dr. Diedrik Menzel, my supervisor, has offered me careful guidance even beyond his retirement. My gratitude to him is beyond expression. This thesis would not have been possible without his help in each stage of the work. Ursula Mettbach has been very important to me as senior technician in the Menzel lab. She has helped me a lot as experienced bench worker, reliable guide and trusted friend through the past 6 years. Dr. Chao Yue, my husband, who is an ecologist from the LSCE-Institute Pierre Simon Laplace in Paris, has given me unconditional support and encouragement, which kept me going in tough times, and I also thank him for his help with proofreading.

I thank Hans-Jürgen Ensikat from the NEES Institute, who patiently and skillfully helped in all aspects of scanning electron microscopy. The use of the SEM facility of the NEES Institute was made possible by the courtesy of Prof. Dr. Maximilian Weigend. PD. Dr. Boris Voigt was of great help, in guiding me through the intricacies of confocal microscopy. Paul Blasczyck, the head of the Mechatronics Lab & Workshop at the IZMB and his team have offered me valuable help in improving experimental tools, especially I would like to mention Marc Schulz, who was my guardian of the computer-based work, which was of great importance. I also thank Prof. Dr. Walter Witke, from the Institute of Genetics for letting me test their new actin antibody.

I am also grateful to Dr. M. A. Tiffany (San Diego State University), who shared her newest paper with me even before its publication.

Dr. David G. Mann (Royal Botanic Garden, Edinburgh), who shared the conference publication of the late Dr. A.M.M Schmid with me and Prof. Dr. Dusan Losic (Adelaide University, Australia), who shared his recent publication with me.

Lastly, I would like to thank Prof. Frantisek Baluska for co-supervising my work and the people of the Menzel lab for helping me through this great experience.

Volume 1

Contents

Part I. General Introduction	9
1 Diatoms	10
1.1 Frustule Structure and Its Ornamented Pattern	11
1.2 Silica Cell Wall Formation and the Potential Involvement of Cytoskeleton	13
1.2.1 Uptake and Transportation of Silicic Acid	14
1.2.2 Assembly of a Two-dimensional Pattern in the Silica Layer	14
1.2.3 Assembly of a Three-dimensional Silica Framework	15
2 Species Selection for this Study	16
3 Odontella sinensis	16
4 My Previous Work on Odontella sinensis	19
5 References	22
Part II. Frustule Morphogenesis	29
Chapter 1 Fine Structure of the Odontella Frustule	30
Abstract	30
1 Introduction	31
2 Materials and Methods	33
2.1 Culturing	33
2.2 Fixation	34
2.3 Preparations for Scanning Electron Microscopy (SEM)	35
2.3.1 Cell Treatments	35
2.3.1.1 Post-fixation Treatment — SDS Extraction	35
2.3.1.2 Pre-fixation Treatment — Enzyme Digestion	36

2.3.1.3 Post-fixation Treatment — Acid Wash	36
2.3.2 Drying Methods	37
2.3.3 Sputter Coating & SEM Observation	38
2.4 Preparations for Transmission Electron Microscopy (TEM)	38
2.4.1 Imaging of Ultra-thin Sections	38
2.4.2 Shadow Imaging of Acid Cleaned Frustules	39
2.4.3 TEM Observation	39
2.5 Terminology	40
2.6 Acknowledgement	40
3 Results	40
3.1 Observations by SEM and TEM-Shadow Imaging	40
3.1.1 General Morphology of the Frustule	41
3.1.1.1 Frustule Compositions	41
3.1.1.2 Young SDV beneath the Epitheca	41
3.1.1.3 Porous Surface	44
3.1.2 Structures of the Girdle Band	44
3.1.2.1 Expansion Gap	44
3.1.2.2 Edge Morphology of the Girdle Band	45
3.1.2.3 Orientation of the Girdle Band	46
3.1.2.4 Organic Layer	46
3.1.3 Structures of the Valve	47
3.1.4 Development Stages of the Frustule	49
3.1.5 Substructures of the Cell Wall	50
3.2 TEM	52
3.2.1 Structures of the Mature Frustule	52
3.2.2 Young Cell Wall and Membrane Morphogenesis	53
3.2.3 Fibrous Balls and Fibrous Layer	54
3.2.4 Summary of the Cell Wall Growing Process	56
4 Discussion	57
4.1 Different Treatment Effects on Diatom Structures when Preparing Samples	57
4.1.1 Rationale for the Choice of Various Pretreatment Regimes	58
4.1.2 Unique Effects of Various Pretreatments	59
4.1.2.1 Appearance of Enzyme-digested Samples Before Fixation	59
4.1.2.2 The Appearance of Cells after the Post-fixation Treatments	59
4.2 Overall Architecture of the Frustule	61
4.2.1 The Head Plate and the Annuli	61
4.2.2 Interlocking Structures of the Girdle Bands	62
4.2.3 Connecting Lace	63
4.2.4 Immature SDV Locating beneath eGB2	64
4.3 Internal Construction of the Frustule Cell Wall	65

4.3.1 Cell Wall Construction Revealed by Cracked Open Samples	66
4.3.2 Cell Wall Construction Revealed by Shadow Imaging	67
4.3.3 Frustule Structure and Morphogenesis Interpreted from Ultrathin Sections	68
4.3.3.1 Structure of a Cell Wall Pattern Unit — the Areola Chamber	68
4.3.3.2 Organic Layer	69
4.3.3.3 The Morphogenesis of the Silicella Lumen	70
5 References	73
Chapter 2 Frustule Morphogenesis, Cell Cycle Activities and Cytoskeleton Dynamic	79
Abstract	79
1 Introduction	79
1.1 The Composition of the Diatom Cytoskeleton	79
1.2 Current Background on the General Architecture and Function of the Diatom Cytoskeleton	80
1.3 Observing Frustule Structures and Cytoskeleton of <i>O. sinensis</i> by Fluorescence Microscopy	83
1.3.1 Silica Probes	84
1.3.2 Double Immunolabeling in Lysosensor Stained Cells of <i>O. sinensis</i>	85
1.3.3 Chitin Probes	86
2. Materials and Methods	88
2.1 Culturing	88
2.2 Fluorescent Staining on SDV	88
2.2.1 Single Silica Probe Staining in Live Cell	88
2.2.2 Consecutive Staining by Two Different Probes in Live Cell	88
2.2.3 WGA Staining in Fixed Cell	89
2.3 Double-Aldehyde Fixation	89
2.4 Cytoskeleton Immunolabeling	89
2.4.1 Single Indirect Immunolabeling (Method 1)	89
2.4.2 Double Indirect Immunolabeling: a Mixture of 1st Antibodies plus a Mixture of 2nd Antibodies (Method 2)	92
2.4.3 Double Indirect Immunolabeling: A Mixture of 1st Antibodies Followed by the Separate Label of Each 2nd Antibodies (Method 3)	93
2.5 Confocal Microscopy	94
2.5.1 Preparing Mounted Samples	94
2.5.2 Imaging	94
3. Results	96
3.1 Interphase: Morphogenesis of SDV and Cytoskeleton	96
3.1.1 The SDV Develops under the Cover of the Last Epithelial Girdle Band	96

3.1.2 Chitin Plays a Role in Sealing between Silica Frustule Components	98
3.1.3 Distribution of Microtubules and Microfilaments at Interphase	99
3.1.4 The Spatial Relationship of the SDV with the Cytoskeleton	100
3.2 From Late Interphase to Anaphase: Development of the Spindle and the Occurrence of the Cytokinetic Actin Ring	100
3.3 From Telophase to Cytokinesis: Formation of the Horn Bundles, Reappearance of the MC and Constriction of the Cytokinetic Actin Ring	102
3.4 Post-cytokinetic Phase (Early Interphase): Valve Morphogenesis involving the Valvar SDV and the Cytoskeleton	103
4. Discussion	104
4.1 Interphase	105
4.1.1 GB-SDV Development and the Mode of Frustule Elongation	105
4.1.2 Configuration of the Interphase Cytoskeleton	109
4.1.2.1 The Interphase Microfilament System	109
4.1.2.2 The Actin Ring	110
4.1.2.3 The Microtubule Cytoskeleton	111
4.1.2.4 The Spatial Relationship among Cytoskeleton, Nucleus and the SDV	113
4.1.3 Involvement of Chitin in Controlling Axial Cell Expansion	117
4.2 Mitosis	120
4.2.1 Transformation of Mitotic Structures: MC, PC and Spindle	120
4.2.2 Origin of the MT-Horn Bundles at Late Mitosis	121
4.2.3 The Development of the Cytokinetic Ring	122
4.2.3.1 Proof of Actin in the Cytokinetic Ring	122
4.2.3.2 The Timing of Setting up the Cytokinetic Ring	122
4.2.3.3 The Initiation of the Assembly of the Cytokinetic Actin Ring	123
4.2.3.3.1 The Role of the GB-Actin Ring	123
4.2.3.3.2 The Role of the PC Precursor	125
4.3 Localization of Horn Bundles during Cytokinesis	127
4.4 Post-cytokinetic Valve Morphogenesis	128
4.4.1 Silicification of the LPs	128
4.4.2 Formation of the Head Plate	129
4.4.3 Bending of the Microtubule Horn Bundles	132
4.5 Developmental Road Map	133
5 References	137
Chapter 3 Cytoskeletal Dynamics in Consecutive Stages of Frustule Morphogenesis Challenged by Inhibitors	146
1 Introduction	146
1.1 The Inhibition of the Microtubule System	146

1.2 The Inhibition of Actin Cytoskeleton	147
2 Materials and Methods	148
2.1 Oryzalin	148
2.1.1 Short-term Incubations	148
2.1.2 Long-term Incubations	149
2.2 Taxol	149
2.3 Jasplakinolide	150
2.4 Phalloidin	150
3 Results	151
3.1 Oryzalin	151
3.1.1 Setting the Incubation Parameters by Tests of Short-term Treatment	151
3.1.1.1 Effects of Short-term Treatment on Post-cytokinetic Cells	152
3.1.1.2 Recovery following Short-term Treatment on Post-cytokinetic Cells	153
3.1.1.3 Staining under Control and Short-term Inhibition on a Same Cell at Mid-interphase	154
3.1.2 Cells after Long-term Inhibition	156
3.1.2.1 Cells at Post-cytokinetic Stage — Cell Division without Preceding Mitosis	157
3.1.2.2 Cells at Late-interphase — before Transition to Mitosis	158
3.1.2.3 Cells at Cytokinetic Stage — Morphology of Cytokinetic Actin Ring	159
3.1.2.4 Repetitive Constricting Pulses during Cytokinesis	160
3.1.2.5 Formation of Lateral Frustule Components	161
3.1.2.5.1 Formation of the Lateral Valve Complex: Inhibition Starting from Interphase	161
3.1.2.5.2 Formation of Lateral Girdle Band: Inhibition Starting from Interphase	162
3.1.2.5.3 Partially Connected Valves: Inhibition at Mid-cytokinesis	164
3.1.3 Inhibitory Phenotypes of Long-term Inhibition with Oryzalin	164
3.2 Taxol	171
3.2.1 Inhibition at Interphase	171
3.2.2 Inhibition at Preprophase and Prophase	172
3.2.3 Inhibition at Telophase	173
3.2.4 Inhibition in the Course of Cytokinesis	173
3.2.5 Inhibition at Post-cytokinetic Phase	174
3.3 Jasplakinolide	176
3.3.1 Inhibition at Interphase of the Mother Generation	176
3.3.2 Inhibition until the Daughter Generation without Cell Division	177
3.3.2.1 Silica Development of the Daughter Generation with Preceding Nuclear Division	177
3.3.2.2 Silica Development of the Daughter Generation without Preceding Nuclear Division	180
3.3.3 Inhibition until the Daughter Generation with Cell Division	181

3.3.4 Inhibitory Phenotypes of Long-term Inhibition with JAS	182
3.4 Phalloidin	188
3.4.1 Inhibition at the Post-cytokinetic (Valve-formation) Stage	188
3.4.2 Inhibition from Mid-Interphase to Prophase	190
3.4.3 Inhibition on Prospective Cytokinesis	192
4. Discussion	194
4.1 Oryzalin	194
4.1.1 General Effects of Oryzalin	194
4.1.1.1 Dynamic of the Microtubule System under Inhibition	194
4.1.1.2 Are Microtubules Required for the Silicic Acid Supply?	197
4.1.1.3 Sometimes Silica Deposition is Inhibited	198
4.1.1.4 Lateral Valves are Absent if the 2-hour Pre-Inhibition has been Applied	198
4.1.2 The Potential Role of MTs in the SDV Shaping and Functioning	199
4.1.2.1 Role in Girdle Band Morphogenesis	199
4.1.2.2 Role of Microtubules in Valve Morphogenesis	201
4.1.2.2.1 Aberrant Morphology of Separated Valves	202
4.1.2.2.2 Lateral-Valve Formation Induced by Oryzalin	204
4.1.3 Pulsing Cytokinesis	206
4.1.3.1 Repetitive Pulses of Cytokinesis	206
4.1.3.2 Role of the PC Precursor in the Location of the Cytokinetic Actin Ring	208
4.2 Taxol	209
4.2.1 Potential Side Effects of Taxol Treatment	209
4.2.1.1 Phosphorylation Status on Serine/Threonine and Tyrosine Residues of Regulatory Proteins	209
4.2.1.2 The Side Effects of Taxol on Ca-homeostasis	210
4.2.2 Interphase: Disturbance of the Pace of Silicification and Axial Expansion	211
4.2.3 From Mitosis to Post-cytokinesis: Over-stabilization of the Central Spindle and Over-extension of the Microtubule Horn Bundle	212
4.3 Jasplakinolide	214
4.3.1 General Effect of JAS	214
4.3.2 The Potential Role of F-actin in the SDV Stabilization, Shaping and Initiation	216
4.3.3 Nuclear Status in JAS Treated Cells	220
4.3.4 Lateral-Valve Formation Induced by JAS	221
4.3.5 One Missing Inhibitory Phenotype	222
4.4 Phalloidin	223
4.4.1 General Effects of Phalloidin	223
4.4.2 Post-cytokinetic Stage: The Role of F-Actin in Valve Morphogenesis	224
4.4.2.1 Disturbance of Valve Morphogenesis Stages Starting from Head Plate Formation	224
4.4.2.2 Disturbance of Morphogenesis before Head Plate Formation	227

4.4.3 From Mid-Interphase to Prophase: Configuration of the Cytoskeleton after Valve Morphogenesis	228
4.4.3.1 Case 1: Disturbance on Actin Ring Anchorage	229
4.4.3.2 Case 2: Loss of Capacity to Counteract Turgor Pressure and to Exocytose Frustule Parts	230
4.4.3.3 Case 3: Enhancement of Radial Symmetry in the Cytoskeleton	231
4.4.4 Cytokinesis: The Failure of Prospective Constriction	233
5 References	234
Part III. General Discussion	241
1 Fidelity of Structural Preservation and Immunolabeling	242
2 The Evolutionary Trends in Silica Pattern Formation	243
2.1 Silica Pattern of the Frustule	243
2.2 The Rise of Areola in Diatom Cell Wall	246
3 Involvement of the Cytoskeleton in Valve Morphogenesis	247
3.1 The Geometry Pattern of the Valve Head Plate	247
3.2 Possible Origin of the hb-MTOCs	249
3.3 Placement of Initial SDVs	251
3.3.1 A Comparison among Bipolar, Monopolar and Radial Centrics	251
3.3.2 Comparison of Valve Initiation between Pennates and Bipolar Centrics	255
3.4 Cytoskeletal Interactions during Stages of Valve Morphogenesis	257
3.4.1 Functions of the Microtubules	257
3.4.2 Functions of the Actin System	258
3.4.2.1 Head Plate Morphogenesis with a Deconstructed Cytokinetic Actin Ring	258
3.4.2.2 Valve Morphogenesis in Cells with an Over-stabilized Actin System	259
3.4.2.3 SDV Expansion and the Cytoskeletal Composition of the Valve Actin Ring	260
3.4.2.4 Role of the Distal Actin Patch in the Formation of the Ocellar Plate	261
3.4.2.5 The Credibility of the PM-MFN-SDV Model	263
4 Dynamics of the Cytoskeleton during Girdle Band Formation and Axial Expansion	265
4.1 Tensional Force Centers on the Nucleus not on the MC	265
4.2 The Girdle Band Actin Ring	266
4.2.1 The Role of Chimeric Chitin Synthases in Anchoring the Actin Ring	267
4.2.2 Secretion of Chitin Fibres when the Axial Expansion is Inhibited	269
5 The Diversity of Circumferential Actin Rings	269
5.1 For Adhesion	269
5.2 For Constriction	270
5.3 Two Different Types of Actin Rings Sitting Side by Side	271

6 The Cytokinetic Actin Ring of Odontella	272
6.1 Does the PC Precursor/ PCs of the Diatom Spindle Controls the Cleavage Plane Determination?	272
6.2 How Common is the Pulsed Contraction?	273
7 References	275
Summary	280

Part I. General Introduction

1 Diatoms

Diatoms are unicellular organisms commonly grouped within the algae. Many taxa of the diatoms live as phytoplankton suspended in marine or fresh waters. They are major primary producers in the food chain, contributing around 20% of the global photosynthetic carbohydrates (Nelson et al., 1995). Taxonomically, diatoms belong to the pigmented heterokonts (Medlin et al., 1997b). They are speculated to have arisen through endosymbiosis of a unicellular red alga with a colorless, predatory heterokont (Lee, 2008).

The microfossil record of diatoms dates from the early Jurassic period (190 Ma) (Sims et al., 2006), when the atmospheric CO₂ level (1200–1500 ppmv) (Royer, 2006) was 3 times more than that of present day (~400 ppmv) (US Department of Commerce, NOAA, Earth System Research Laboratory, 2005); but according to molecular clock calculations based on small subunit ribosomal RNA (ssu rRNA) sequences and from frustule morphology analysis, the earliest existence of diatoms is speculated to have occurred in the Permian-Triassic period (238–266 Ma) (Kooistra and Medlin, 1996; Medlin et al., 1997a). Thus, considering their photosynthetic capability, diatoms may have had a substantial contribution to the Earth's climate change over the past geological ages.

The rank of diatoms in taxonomic classifications is controversial. They may be ranked as class (*Bacillariophyceae*) or as division (*Bacillariophyta*) (Medlin and Kaczmarska, 2004; Pickett-Heaps et al., 1990; Round et al., 1990). Regardless the rank, there are two major orders: the centric diatoms (*Centrales*) and the pennate diatoms (*Pennales*). The centrics could be further divided into radial centrics and polar centrics according to the symmetry status of the valve. As for the pennates, they are further classified by the possession or absence of a raphe (raphids or araphids), which is a slit-shaped opening in the valves. Generally, centrics as well as araphid pennates lack the ability of locomotion, while raphid pennates are able to glide by secreting mucilage strands through the raphe (Edgar and Pickett-Heaps, 1983). According to phylogenetic analysis (Medlin and Kaczmarska, 2004), the branch of radial centrics (*Coscinodiscophyceae*) arose first, followed by the branch of bi/multi polar centrics and the branch of other centrics (*Mediophyceae*), and then the araphids (*Bacillariophyceae*) and raphids (*Bacillariophyceae*) emerged.

1.1 Frustule Structure and Its Ornamented Pattern

In nature, several groups of organisms such as algae (e.g., *Chrysophyceae*, diatoms), land plants (e.g., cereals, rice, grasses), protozoans (e.g., radiolaria), and some lower aquatic animals (e.g., sponges), have developed some kind of external or internal silica skeletons (1981). In the diatoms, the silica skeleton is an external cell wall termed frustule, which provides a rigid, transparent casing, protecting the cell from environmental stress and from attack by predators. In contrast to softer, more flexible types of cell walls, which are commonly found in phototrophic protists and algae, this type of rigid wall limits cell motility and shape changes, restricting its capability to chase the sunlight. As a result, various mechanisms relieving this disadvantage have developed: some types of diatoms rely on turbulent water currents to suspend in the surface water (Gross and Zeuthen, 1948); some adjust their lipid storage (Armbrust et al., 2004; Dunstan et al., 1993) or secrete chitin fibers to control their buoyancy (Round et al., 1990); some sink down to the ground in shallow waters (Staats et al., 2000), where most of these diatoms locomote towards the sun-lit zones. Most diatoms grow their frustule by absorbing silicic acid from surrounding aquatic environment, with some specific taxa as the exception. For example, the araphid pennate *Phaeodactylum tricornutum* is able to form a silica frustule but can also survive without it — by forming a soft, organic cell wall in the absence of silicon (Lewin et al., 1958).

A frustule consists of two similar halves — the epitheca and the hypotheca. The hypotheca is always a little smaller than the epitheca, so that it fits in by a smaller circumference within the epitheca like the two halves of a petri-dish. This fitting feature between the two thecae and the rigidness of the silica frustule of diatoms imply inevitable changes in cell size during vegetative cell division (Macdonald, 1869; Pfitzer, 1869; Round et al., 1990): In the process of vegetative cell division, a pair of daughter protoplasts are formed in the mother frustule by cytokinesis following mitosis. Both daughter protoplasts inherit a theca (either the epi- or the hypotheca) from its mother frustule. Subsequently they complement this inherited theca by generating a new corresponding theca: the daughter protoplast situated within the epithecal half of the mother cell produces a new hypotheca, and the original epi-hypo polar direction is thus maintained; in contrast, the other daughter cell inherits the hypotheca from the mother cell, which becomes the epitheca in the new cell, in this case a smaller new hypotheca is generated and the polar direction is reversed. As a result, after generations, there is a gradual decrease in cell size in the branch of cells who inherited the hypotheca from the mother.

In general, diminished cell size ultimately triggers sexual reproduction: when a cell reaches a minimal size threshold or alternatively meets some specific environmental conditions (e.g., illumination, temperature, nutrition stress, salinity, bacteria) (Chepurnov et al., 2004; Edlund and Stoermer, 1997; Halse and Syvertsen, 1996; Round et al., 1990), formation of gametes will be triggered. The zygote of diatom is termed “auxospore” when its surface is covered by silica scales. The auxospore expands its volume up to a genetically determined maximum size of its species (Chepurnov et al., 2004). Then it gives rise to an initial cell, which is the first asexual generation followed by many vegetative divisions until eventually the minimal size threshold is reached triggering the next round of sexual reproduction. The first pair of siliceous valves are built by the initial cells, which sometimes show the same morphology as the valves of normal vegetative cells (Drebes, 1974). But more often, the siliceous valves of the initial cell have a different shape, and in that case, the species-specific morphology is re-established gradually with the formation of the new hypovalves through two consecutive vegetative divisions (Ross et al., 1979; Schmid, 1987; Zhang, 2012).

The fascinating ornamentations of the diatom frustule have triggered researchers' interest in the mechanisms of cell wall morphogenesis from nano- to micrometer scale (Gordon et al., 2009a; Sumper and Brunner, 2006). This made the emphasis of the frustule research shift from the traditional morphology characterization towards mechanisms of biomineralization. With the advent of electron microscopy, the construction of the silica cell walls was studied in many diatom species (Borowitzka and Volcani, 1978; Boyle et al., 1984; Chiappino and Volcani, 1977; Edgar and Pickett-Heaps, 1984; Gordon and Drum, 1994; Schmid, 1979, 1994; Schmid and Volcani, 1983; Tiffany, 2002, 2005, 2008, 2015), as well as the formation of the labiate processes (Li and Volcani, 1985a, 1985b) i.e., a special spine- or knob-like extension of the frustule. Schmid, Pickett-Heaps and their colleagues raised the expectation that frustule formation is related with cytoskeletal activities (van de Meene and Pickett-Heaps, 2002; Pickett-Heaps and Kowalski, 1981; Schmid, 1980; Van de Meene and Pickett-Heaps, 2004). More recently, Hildebrand and Tesson speculated on the involvement of motor proteins in valve morphogenesis (Davis and Hildebrand, 2010; Tesson and Hildebrand, 2010a, 2010b). Further discussion of this topic is offered in Chapter 3. As another aspect regarding the mechanism of silica deposition, researchers illustrated that organic templates are involved in biosilica formation (Kröger and Poulsen, 2008; Sumper et al., 2004) (see Section 1.2.2).

The potential elucidation of diatom morphogenesis mechanisms may open new avenues for its practical application, besides the traditional usages already well known to the society. In

traditional industrial manufacture, diatomaceous earth excavated from sediment strata is used for construction works, or as blackboard chalk or filling material in explosives (Dynamite). Thanks to the porous nature of the silica wall and other material properties, diatom frustule has become a natural role model in bionic engineering for developing ultra-lightweight structures with high mechanical resistance (Garcia and Buehler, 2010; Hamm et al., 2003). Also, the new branch of nanomechanical engineering might profit from imitating the design of interlocking spine-like frustule structures in some diatoms (Gebeshuber and Crawford, 2006). Further, based on the porous nature of silica walls, development of microcapsules (Gordon et al., 2009b; Vasani et al., 2015), or nanoporous filters has been envisioned as means to exclude viruses or other deleterious chemicals from solvent mixtures (Losic et al., 2006a). Last but not the least, the porous biosilica of diatoms can be considered as a photonic crystal, which moderates the wavelength of refractive light (Fuhrmann et al., 2004) or concentrates the transmitted light into a spot (De Stefano et al., 2007, 2009), or traps light which could enhance the optical absorption ability of thin-film solar cells (Chen et al., 2015), or may be used as diffraction grating to split light into color beams radiating in different directions (Kieu et al., 2014). Other applications include using fine structures of diatom frustules as templates for MEMS (micro electro mechanical systems) or exploiting silica templates coated with minerals for microfluidic systems (Bao et al., 2007; Cai et al., 2005; Drum and Gordon, 2003; Losic et al., 2006b; Zyga, 2007) or as bio/chemical-sensors (De Stefano et al., 2009; Losic et al., 2009; Yang et al., 2011). The converted biosilica could even be used in accumulating quantum dots for the color illumination in electronic screens technology (Sumper and Brunner, 2006).

1.2 Silica Cell Wall Formation and the Potential Involvement of Cytoskeleton

Organisms that use silica for the formation of intra- or extracellular skeletons must be capable of biosilicification, i.e., the condensation of silicic acid from the dissolved aqueous state into the solid state. In this process, individual silicic acid molecules are mixed with organic materials and are compacted as colloidal nanoparticles (Currie and Perry, 2007; Kröger and Poulsen, 2008; Mann and Perry, 1986), constructing the silica from nano- to micrometer scale. It differs from the process of crystallization, where monomeric molecules/atoms are strictly arranged in a unique order to generate crystals from the nano- to millimeter scale.

1.2.1 Uptake and Transportation of Silicic Acid

The global marine average concentration of orthosilicic acid (Si(OH)_4) is 70 μM (Hildebrand, 2006). In diatoms, orthosilicic acids are taken up by transmembrane proteins — silicon transporters (SITs) (Hildebrand, 2006; Hildebrand et al., 1997, 1998; Thamatrakoln et al., 2006) and then transported into the silica deposition vesicle (SDV), within which the silicon concentration is much higher than that in the environment (e.g., 20–100mM in *T. pseudonana*) (Sumper and Brunner, 2008). So far, the intracellular transportation of silicic acid is supposed to be achieved by transmembrane transport via intracellularly localized silicon transport proteins and ionophore-mediated transport proteins, and long distance transport via silicon transport vesicles (STV), which will eventually fuse with the SDV (Hildebrand, 2006). In Chapter 1, a kind of small cytoplasmic vesicles is presented in a TEM sample of *O. sinensis* for the first time, which are supposed to be the potential candidates for STVs.

1.2.2 Assembly of a Two-dimensional Pattern in the Silica Layer

In the field of chemical engineering, amorphous silica nanoparticles can be compacted in laboratory procedures under the condition of neutral pH and moderate temperature (60 °C), into a lamella called “mesoporous silica” with arrays of hexagonally arranged pores with diameters at the nanometer scale (Berggren et al., 2005; Kim et al., 2000a, 2000b, 2001; Nandiyanto et al., 2009; Perry, 2003).

In diatoms, pore patterns are created within the growing frustule, where the pores are much bigger, reaching to the micrometer scale, e.g., the areolae of *Coscinodiscus sp.* have a diameter of 1.7–2.3 μm (Jantschke et al., 2014). This difference may be caused by different types of proteins (e.g., silaffins, cingulins) and long-chain polyamines (LCPA). These are components said to be involved in the so-called self-assembly process of silica deposition from small deposits to big sheets inside the SDV whereby these organic compounds serve as kind of a matrix or template (Kröger and Poulsen, 2008; Sumper et al., 2004). But some other complicated ornaments (e.g., the shape of a silica sheet) requires a higher level of regulation. So far, by intriguing observations which have been made in several species of centric diatoms, microfilaments assembling into a ring (termed "actin ring") are found to accompany the periphery of the valve SDV (van de Meene and Pickett-Heaps, 2002; Schmid, 1980; Tesson and

Hildebrand, 2010a, 2010b; Van de Meene and Pickett-Heaps, 2004), which may function in the outwards extension and morphogenesis of the SDV across the plasma membrane (Pickett-Heaps et al., 1979, 1990; Tesson and Hildebrand, 2010a). Microfilaments assembling in radial arrays are reported to be responsible for the formation of ribs in the valve (Tesson and Hildebrand, 2010a, 2010b), or they assembling into actin networks may probably stabilize and shape the SDV (Tesson and Hildebrand, 2010b). Microtubules arranging in radial arrays have been also observed in a few species, most spectacular in the large cells of *Coscinodiscus*, showing microtubules running from the nucleus in a radial fashion to the margin of the valve (Tesson and Hildebrand, 2010a). Microtubules have been assumed to aid the expansion of the valve SDV via motor molecules (Davis and Hildebrand, 2010), involve in silicon-transportation (Schmid, 1980, 2003) or stabilize the SDV (Pickett-Heaps et al., 1990; Schmid, 2003). However, the role of either cytoskeletal element in the SDV formation has not been clarified yet. Further study of this topic is provided in Chapter 3.

1.2.3 Assembly of a Three-dimensional Silica Framework

Fine structure work using TEM of ultrathin sections has revealed that the frustule is not just a single layer of silica, but a three-dimensional framework, often composed of a multitude of small, regularly spaced chambers, termed areolae. As is summarized in the form of beautiful drawings by A.-M. Schmid for the frustules of *Thalassiosira eccentrica* (Schmid and Schulz, 1979), and *Coscinodiscus wailesii* (Schmid, 1994; Schmid and Volcani, 1983), position and size of the chambers may be determined by “spacer vesicles”, around which the expanding SDV folds. In *Odontella*, such vesicles have not been described so far, and there remains the question, whether other mechanisms are involved to shape the areola lumen. In almost all diatoms, the upper wall of the chambers facing the outside and the inner wall facing the protoplast are perforated with various types of pores in a species-specific manner. In addition, the outer wall may carry all sorts of knobs, spines and ridges, generating species-specific ornaments, which are inherited from mother to daughter throughout countless generations in a given evolutionary branch of diatoms (e.g., frustule patterns shown in Chapter 1).

2 Species Selection for this Study

The size of *O. sinensis* is conveniently bigger among the centric diatoms allowing single cell manipulation as well as batch culture manipulation. On the other hand, its size is not too big to mount cells between coverslip and glass slide, so that microscopic observation can be performed without causing major pressure damage to the cells. The frustule structure of *O. sinensis* (Fig.1) is relatively simple; this allows its detailed structure being clearly observed with 40x or 60x objective lenses as routinely used in fluorescence or confocal microscopes. Their compressed, oblong cell shape causes *Odontella* cells to always present the girdle side to the observer under the microscope. This allows the observation of many cell activities throughout the cell cycle such as mitosis, cytokinesis and the growth process of the silica theca along the length axis of the cell.

While in this thesis the emphasis only lies on *Odontella sinensis*. The availability of another member in the same order – *O. regia*, and two bipolar centrics without ocelli – *Ditylum sp.* and *Lithodesmium sp.*, as well as one bipolar centric without either labiate processes or ocelli – *Mediopyxis sp.*, has made it possible to compare *O. sinensis* with some of its phylogenetically related relatives (Ashworth, 2013; Theriot, 2010). And two members of the radial centrics such as *Coscinodiscus sp.* and *Actinocyclus sp.* have also been used as side investigations, which allows observer to see the spatial distribution of their cytoskeleton in valve view. Though the comparison with these diatoms will not be discussed in this thesis, the data of these diatoms would still be presented in the supplement.

3 *Odontella sinensis*

The size range of *Odontella sinensis* was firstly reported, based on samples collected from british coastal waters (Hendey, 1964). The distance along the apical axis of the valve between the two opposite ocelli ranges from 120–260 μm (see Fig. 2 for the planes of the axes). The transapical axis, running perpendicular to the apical axis (Fig. 2), is around 60–80 μm , and cell length along the peralvar axis is around 300 μm (Hendey, 1964). The cells collected from the Helgoland Sea were all similar in size but the variation in length was larger, between 90 and 440 μm (Hoppenrath et al., 2009). Cells of this bipolar centric diatom were often linked together in

chains, which may reduce cell dispersal as an adaptation against predation and as a means to increase the success rate of sexual reproduction.

Odontella sinensis was previously recorded as *Biddulphia chinensis* collected from Hong Kong Harbour in 1866 (Greville, 1866), then reported to be found in the North Sea waters around Helgoland in 1903. It has since been considered a common member in the North Sea phytoplankton (Gómez and Souissi, 2010; Ostenfeld, 1908). This species has been speculated to originate from the Red Sea, the Indian Ocean or the Atlantic coast of North America then spread through navigating ships to far destinations (Gómez and Souissi, 2010; Ostenfeld, 1908).

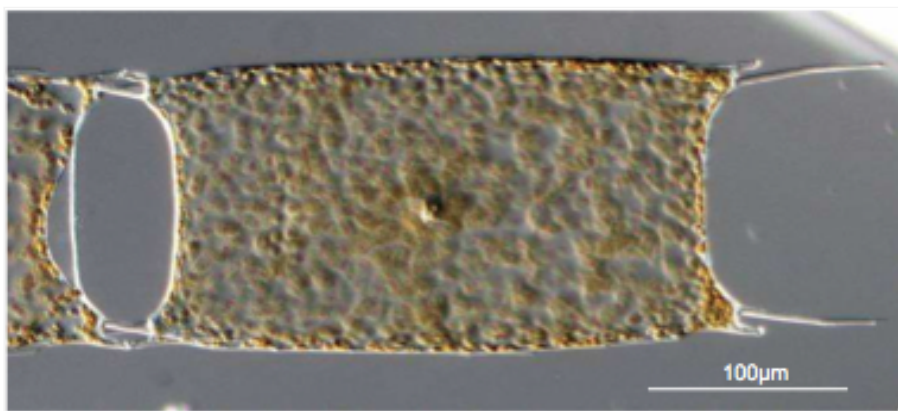


Fig. 1 The overall habitus of *O. sinensis* in a phytoplankton sample collected from the sea around Helgoland, Germany. All other images shown in this thesis are from cell cultures derived from this collection. See Fig. 2 for details of frustule construction.

Taxonomically, *Odontella sinensis* has been renamed several times due to different assessments of its cytomorphological features. The most recent evaluation placed it and its two closest relatives *O. regia* and *O. mobiliensis* into a newly erected genus, *Trieres*, whereas other members were maintained in the genus *Odontella* (Table 1) (Guiry, 2002; Lavigne et al., 2015). The genera *Odontella* and *Trieres* belong to the family *Triceratiaceae* (Guiry, 2011) (with two symmetrically placed ocellate elevations along the apical axis of the valve); the genus *Biddulphia* is maintained in the family *Biddulphiaceae* (with pseudo-ocellate elevations) (Lavigne et al., 2015; Round et al., 1990). The recent transfer of *O. sinensis* to the newly erected clade *Trieres* is based on both cytomorphological and molecular analysis (Ashworth et al., 2013). Here in this thesis the popular name, *Odontella sinensis*, is used in consistency with previous studies.

Table 1. Taxonomy of *Odontella sinensis*

Genus	sp.	Taxonomic Editor	Re-editor	Year	Synonyms
<i>Biddulphia</i>	<i>chinensis / sinensis</i>	Greville	–	1866	Basionym
<i>Odontella</i>	<i>chinensis / sinensis</i>	(Greville)	Grunow	1884	Homotypic synonym of <i>Trieres</i>
<i>Trieres</i>	<i>chinensis / sinensis</i>	(Greville)	M.P.Ashworth & E.C.Theriot	2013	Homotypic synonym of <i>Odontella</i>

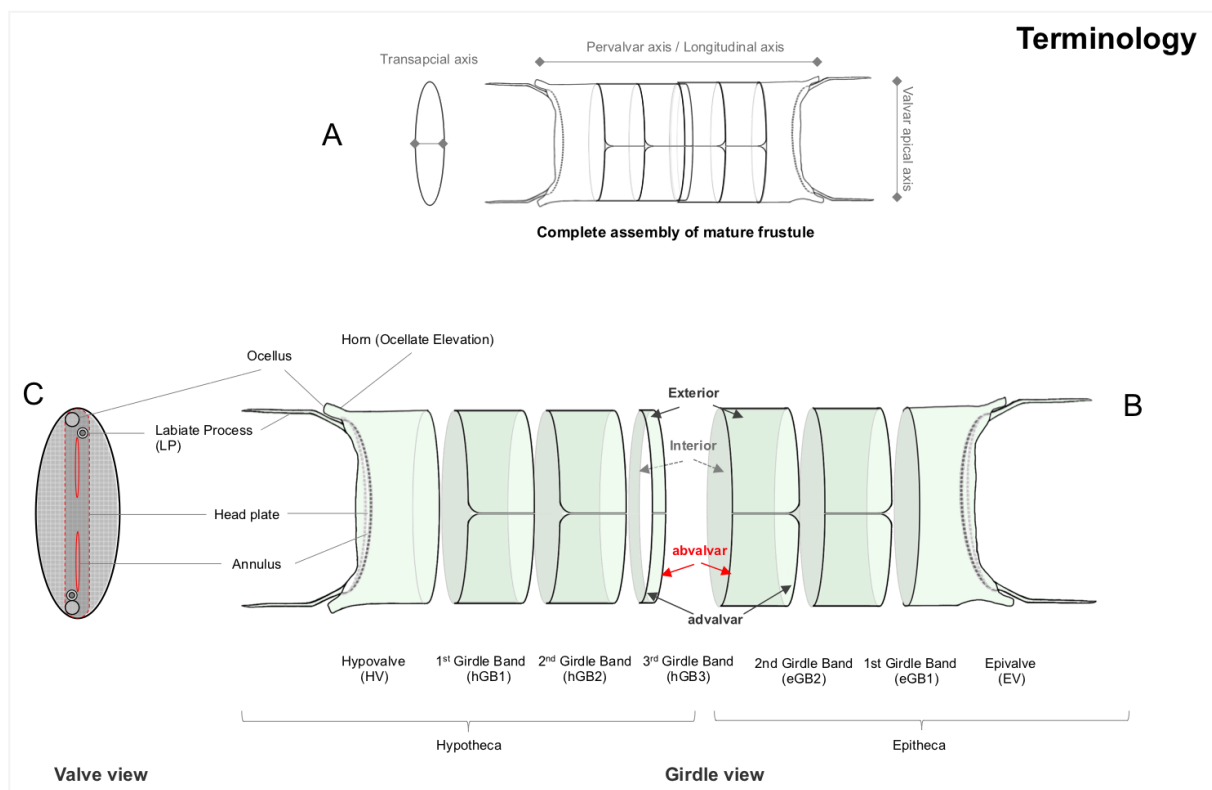


Fig. 2 A simplified drawing of frustule assembly in *Odontella sinensis* in girdle view. (A) Complete assembly of the mature frustule at the end of interphase. Major axes are indicated. (B) The frustule is presented in a way that its components are segregated, with the descriptive terms noted under each component. Throughout the thesis, images of *Odontella* from microscope observations will present the cells in the same orientation as in this figure, i.e., hypotheca to the left, epitheca to the right. Ocellus is the front plate of the horn, with fine pores in it. Notably, the last narrow girdle band, hGB3, connecting hypotheca with epitheca may not be present in all cells. (C) Front view of the valve. The outermost ellipse

indicates the outline of the whole valve; the inner long, narrow ellipse represents the head plate (encircled by the red stipple line; comprising two compressed annuli that are indicated by red line) between the two horns (circles) and the positions of the LPs (double line circles). Note the centrosymmetry of LPs.

The *Odontella sinensis* frustule consists of two major parts (Fig. 2) – the epitheca (right half in the figure) and the hypotheca (left half), each of which consists of one valve plus two or three girdle bands. The third girdle band is usually very narrow. At each end of the head plate, there is a narrow, stretched region along the apical axis termed “annulus” (Fig. 2 lower left image). The cell has two of these annuli separated from each other in the middle of the head plate (see Chapter 1 for further details). The outermost structures on the valvar apical axis are the horns (also referred to as “ocellate elevations” in other studies) each with a specially sculptured front plate, the ocellus. Slightly inside from the horns along the valve apical axis is a pair of long, drawn-out labiate processes.

Despite the fact that *Odontella sinensis* is known for quite a long time, frustule morphogenesis research on this species is limited. Pickett-Heaps and colleagues investigated some aspects of *Odontella* division and fine structures (Pickett-Heaps et al., 1990). They also presumed mucilage secretion through the hollow labiate processes, which they say would indirectly cause the subtle trembling of the cell when observed by optical microscopy (Pickett-Heaps et al., 1986). A similar mechanism was also implied to explain the same behavior of the centric species *Actinocyclus sp.* (Medlin et al., 1986). Moreover, Li and Volcani studied the labiate process formation in *O. sinensis* and *O. aurita*, but also in *Stephanopyxis turris* and *Ditylum brightwellii*. They discovered that in all these centrics, a special structure was associated with the silica lemma on the inner side of the SDV, which they termed the labiate process forming apparatus (LPA), suggesting that this structure has a role in LP-formation (Li and Volcani, 1985a). Further details will be discussed in Chapter 1.

4 My Previous Work on *Odontella sinensis*

The work presented here is based on my observations described in a preceding study (Zhang, 2012), which has shown that:

(1) The normal cell cycle of *O. sinensis* takes 48–60 hours under laboratory culture conditions.

(2) New frustule components could be well visualized by the lysosensor dye (PDMPO), which can bind to the silica material in acidic SDV (Parambath et al., 2016).

(3) Expansion in longitudinal axis is not a continuous growth process but it occurs as an interval event between each silicification. **(This assumption is later modified with additional data in this thesis.)**

(4) The nucleus is always placed at the location, where silica is depositing, i.e., underneath a developing valve or girdle band. As to the girdle bands, each of them always originates from a narrow, circular band, and then grows to the mature, wide size.

(5) The fabrication time of a girdle band varies from 2 to 4 hours under continuous illumination (Fig. 3).

(6) It is postulated that the two hypothecal girdle bands are extruded to the protoplast surface sequentially (i.e., one-by-one) from the mature SDV positioned underneath the cover of the first epithecal girdle band (eGB1), which is then followed by axial cell expansion, so eventually this new hypothecal silica structure will be deployed to the abvalvar side of the epitheca. This assumption is based on time-lapse observations of cell growth showing two phases of axial expansion **(In the current thesis additional data will be presented leading to a modification of this interpretation, see Chapter 2).**

In order to familiarize the reader with the time scale of the developmental processes occurring through the vegetative cell cycle and successive steps of frustule morphogenesis, the graphical sketches of Fig. 3 show a summary of my previous interpretation (Zhang, 2012).

(7) Most importantly, the spatial correlation of the actin cytoskeleton with frustule morphogenesis has been demonstrated by immunolabeling actin in PDMPO stained cells. Normally, a ring of actin filaments is always detected at the abvalvar edge of the girdle bands, where silica is added. Once an actin inhibitor (Latrunculin B or Jasplakinolide) is applied, the silica deposition shows prominent patterning defects.

(8) The motile behavior of the nucleus was also affected by Jasplakinolide. In a normal cell, the nucleus moves with each insertion of an hGB during axial expansion. But when a cell encounters Jasplakinolide, its nucleus moves erratically throughout the cell. Interestingly, similar erratic movement also occurred in young auxospores, but the nucleus moves regularly in between two ends of the cell even though the cell has not yet developed two intrinsic polarity. This suggests that the proper anchoring of the nucleus to the site of the forming girdle band is depending on a clearly defined polar axis, and this axis may probably be defined by actin.

(9) Lysosensor staining and SEM examination revealed a narrow gap across the width of the girdle band, which is interpreted as an expansion joint allowing the girdle band to accommodate to the wider diameter after it has become deployed on the protoplast surface. This expansion joint is then further explored by SEM in chapter 1 of this PhD thesis.

(10) Preliminary evidences suggest that chitin or a related β -1,4-linked polysaccharide, visualized by calcofluor-white-staining, is used as filling material in the circumferential edges among adjacent frustule components. The rest of the frustule is more dimly stained.

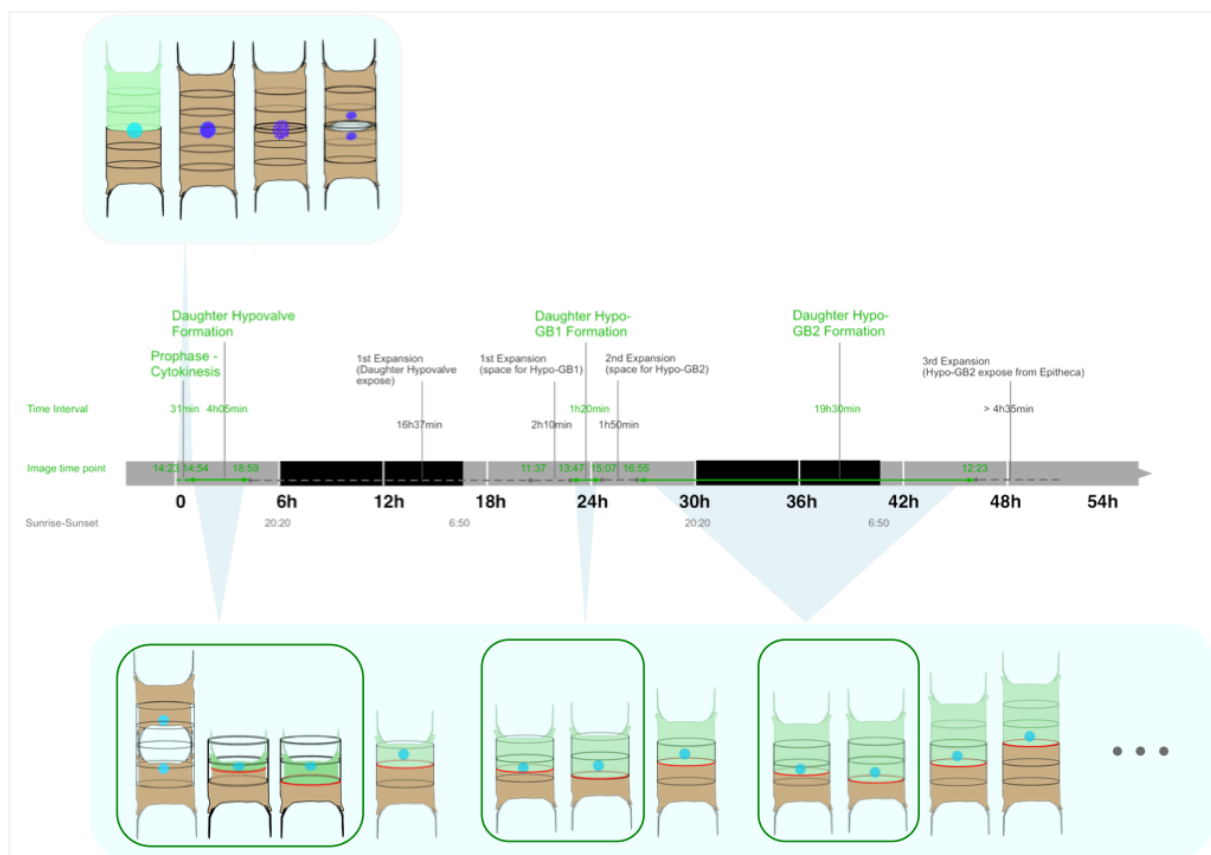


Fig. 3 Summary scheme of the vegetative developmental cycle of *O. sinensis*. Duration of silica fabrication and the cell elongation are illustrated along the time scale bar according to a live observation recorded by the time-lapse movie (Zhang, 2012). Actin ring is shown in red; nucleus is shown in blue, and nuclei of mitotic stages are shown in darker blue. Mother frustule is transparent, exposing the protoplast in khaki-grey. Green theca represents hypotheca. Solid green frames indicate the silicification states, when new frustule components form in an SDV.

5 References

- Armbrust, E.V., Berges, J.A., Bowler, C., Green, B.R., Martinez, D., Putnam, N.H., Zhou, S., Allen, A.E., Apt, K.E., Bechner, M., et al. (2004). The genome of the diatom *Thalassiosira pseudonana*: ecology, evolution, and metabolism. *Science* *306*, 79–86.
- Ashworth, M.P. (2013). Rock snot in the age of transcriptomes: using a phylogenetic framework to identify genes involved in diatom extracellular polymeric substance-secretion pathways. Doctoral dissertation.
- Ashworth, M.P., Teofil, N., and Theriot, E.C. (2013). Revisiting Ross and Sims (1971): toward a molecular phylogeny of the Biddulphiaceae and Eupodiscaceae (Bacillariophyceae). *J. Phycol.* *49*, 1207–1222.
- Bao, Z., Weatherspoon, M.R., Shian, S., Cai, Y., Graham, P.D., Allan, S.M., Ahmad, G., Dickerson, M.B., Church, B.C., Kang, Z., et al. (2007). Chemical reduction of three-dimensional silica micro-assemblies into microporous silicon replicas. *Nature* *446*, 172–175.
- Berggren, A., Palmqvist, A.E.C., and Krister, H. (2005). Surfactant-templated mesostructured materials from inorganic silica. *Soft Matter* *1*, 219.
- Borowitzka, M.A., and Volcani, B.E. (1978). THE POLYMORPHIC DIATOM PHAEODACTYLUM TRICORNUTUM: ULTRASTRUCTURE OF ITS MORPHOTYPES^{1,2}. *J. Phycol.* *14*, 10–21.
- Boyle, J.A., Pickett-Heaps, J.D., and Czarnecki, D.B. (1984). VALVE MORPHOGENESIS IN THE PENNATE DIATOM ACHNANTHES COARCTATA. *J. Phycol.* *20*, 563–573.
- Cai, Y., Ye, C., Allan, S.M., Sandhage, K.H., and Zalar, F.M. (2005). Three-Dimensional Magnesia-Based Nanocrystal Assemblies Via Low-Temperature Magnesiothermic Reaction of Diatom Microshells. *J. Am. Ceram. Soc.* *88*, 2005–2010.
- Chen, X., Wang, C., Baker, E., and Sun, C. (2015). Numerical and experimental investigation of light trapping effect of nanostructured diatom frustules. *Sci. Rep.* *5*, 11977.
- Chepurnov, V.A., Mann, D.G., Sabbe, K., and Vyverman, W. (2004). Experimental studies on sexual reproduction in diatoms. *Int. Rev. Cytol.* *237*, 91–154.
- Chiappino, M.L., and Volcani, B.E. (1977). Studies on the biochemistry and fine structure of silicia shell formation in diatoms VII. Sequential cell wall development in the pennate *Navicula pelliculosa*. *Protoplasma* *93*, 205–221.
- Currie, H.A., and Perry, C.C. (2007). Silica in plants: biological, biochemical and chemical studies. *Ann. Bot.* *100*, 1383–1389.
- Davis, A.K., and Hildebrand, M. (2010). Molecular Processes of Biosilicification in Diatoms. In *From Nature to Application*, pp. 255–294.
- De Stefano, L., Rea, I., Rendina, I., De Stefano, M., and Moretti, L. (2007). Lensless light focusing with the centric marine diatom *Coscinodiscus walesii*. *Opt. Express* *15*, 18082–18088.

- De Stefano, L., Maddalena, P., Moretti, L., Rea, I., Rendina, I., De Tommasi, E., Mocella, V., and De Stefano, M. (2009). Nano-biosilica from marine diatoms: A brand new material for photonic applications. *Superlattices Microstruct.* *46*, 84–89.
- Drebes, G. (1974). *Marines Phytoplankton: eine Auswahl der Helgoländer Planktonalgen (Diatomeen, Peridineen)*.
- Drum, R.W., and Gordon, R. (2003). Star Trek replicators and diatom nanotechnology. *Trends Biotechnol.* *21*, 325–328.
- Dunstan, G.A., Volkman, J.K., Barrett, S.M., Leroi, J.-M., and Jeffrey, S.W. (1993). Essential polyunsaturated fatty acids from 14 species of diatom (Bacillariophyceae). *Phytochemistry* *35*, 155–161.
- Edgar, L.A., and Pickett-Heaps, J.D. (1983). The Mechanism of Diatom Locomotion. I. An Ultrastructural Study of the Motility Apparatus. *Proceedings of the Royal Society B: Biological Sciences* *218*, 331–343.
- Edgar, L.A., and Pickett-Heaps, J.D. (1984). VALVE MORPHOGENESIS IN THE PENNATE DIATOM NAVICULA CUSPIDATA1. *J. Phycol.* *20*, 47–61.
- Edlund, M.B., and Stoermer, E.F. (1997). ECOLOGICAL, EVOLUTIONARY, AND SYSTEMATIC SIGNIFICANCE OF DIATOM LIFE HISTORIES1. *J. Phycol.* *33*, 897–918.
- Fuhrmann, T., Landwehr, S., El Rharbi-Kucki, M., and Sumper, M. (2004). Diatoms as living photonic crystals. *Appl. Phys. B* *78*, 257–260.
- Garcia, A.P., and Buehler, M.J. (2010). Bioinspired nanoporous silicon provides great toughness at great deformability. *Comput. Mater. Sci.* *48*, 303–309.
- Gebeshuber, I.C., and Crawford, R.M. (2006). Micromechanics in biogenic hydrated silica: hinges and interlocking devices in diatoms. *Proc. Inst. Mech. Eng. Pt. J: J. Eng. Tribol.* *220*, 787–796.
- Gómez, F., and Souissi, S. (2010). THE DIATOMS *Odontella sinensis*, *Coscinodiscus wailesii* and *Thalassiosira punctigera* IN THE EUROPEAN ATLANTIC: RECENT INTRODUCTIONS OR OVERLOOKED IN THE PAST? *Fresenius Environ. Bull.* *19*, 1424–1433.
- Gordon, R., and Drum, R.W. (1994). The Chemical Basis of Diatom Morphogenesis. In *International Review of Cytology*, pp. 243–372.
- Gordon, R., Losic, D., Tiffany, M.A., Nagy, S.S., and Sterrenburg, F.A.S. (2009a). The Glass Menagerie: diatoms for novel applications in nanotechnology. *Trends Biotechnol.* *27*, 116–127.
- Gordon, R., Losic, D., Tiffany, M.A., Nagy, S.S., and Sterrenburg, F.A.S. (2009b). The Glass Menagerie: diatoms for novel applications in nanotechnology. *Trends Biotechnol.* *27*, 116–127.
- Greville, R.K. (1866). Descriptions of New and Rare Diatoms. Series XX. *Transactions of The Microscopical Society & Journal* *14*, 121–130.
- Gross, F., and Zeuthen, E. (1948). The Buoyancy of Plankton Diatoms: A Problem of Cell Physiology. *Proceedings of the Royal Society of London B: Biological Sciences* *135*, 382–389.

- Guiry, M.D. (2002). *Odontella chinensis* (Greville) Grunow (National University of Ireland, Galway: World-wide electronic publication).
- Guiry, M.D. (2011). Triceratiaceae (Schütt) Lemmermann, 1899. In: Guiry, M.D. & Guiry, G.M. (2016).
- Halse, G.R., and Syvertsen, E.E. (1996). Marine Diatoms. In *Identifying Marine Diatoms and Dinoflagellates*, pp. 5–385.
- Hamm, C.E., Merkel, R., Springer, O., Jurkojc, P., Maier, C., Prechtel, K., and Smetacek, V. (2003). Architecture and material properties of diatom shells provide effective mechanical protection. *Nature* 421, 841–843.
- Hendey, N.I. (1964). An Introductory Account of the Smaller Algae of British Coastal Waters. Part V. Bacillariophyceae (Diatoms). *Journal of the Marine Biological Association of the United Kingdom* 4, 1–317, Plates I – XLV.
- Hildebrand, M. (2006). 10 Silicic Acid Transport and its Control During Cell Wall Silicification in Diatoms. *Biom mineralization: Progress in Biology, Molecular Biology and Application*.
- Hildebrand, M., Volcani, B.E., Gassmann, W., and Schroeder, J.I. (1997). A gene family of silicon transporters. *Nature* 385, 688–689.
- Hildebrand, M., Dahlin, K., and Volcani, B.E. (1998). Characterization of a silicon transporter gene family in *Cylindrotheca fusiformis* : sequences, expression analysis, and identification of homologs in other diatoms. *Mol. Gen. Genet.* 260, 480–486.
- Hoppenrath, M., Elbrächter, M., and Drebes, G. (2009). *Marine Phytoplankton: Selected Microphytoplankton Species from the North Sea Around Helgoland and Sylt* (Stuttgart: E.Schweizerbart'sche Verlagsbuchhandlung (Nägele u. Obermiller)).
- Jantschke, A., Fischer, C., Hensel, R., Braun, H.-G., and Brunner, E. (2014). Directed assembly of nanoparticles to isolated diatom valves using the non-wetting characteristics after pyrolysis. *Nanoscale* 6, 11637–11645.
- Kieu, K., Li, C., Fang, Y., Cohoon, G., Herrera, O.D., Hildebrand, M., Sandhage, K.H., and Norwood, R.A. (2014). Structure-based optical filtering by the silica microshell of the centric marine diatom *Coscinodiscus wailesii*. *Opt. Express* 22, 15992–15999.
- Kim, S.-S., Pauly, T.R., and Pinnavaia, T.J. (2000a). Non-ionic surfactant assembly of ordered, very large pore molecular sieve silicas from water soluble silicates. *Chem. Commun.* 1661–1662.
- Kim, S.-S., Pauly, T.R., and Pinnavaia, T.J. (2000b). Non-ionic surfactant assembly of wormhole silica molecular sieves from water soluble silicates. *Chem. Commun.* 835–836.
- Kim, S.S., Karkamkar, A., Pinnavaia, T.J., Kruk, M., and Jaroniec, M. (2001). Synthesis and Characterization of Ordered, Very Large Pore MSU-H Silicas Assembled from Water-Soluble Silicates. *J. Phys. Chem. B* 105, 7663–7670.
- Kooistra, W.H., and Medlin, L.K. (1996). Evolution of the diatoms (Bacillariophyta). IV. A reconstruction of their age from small subunit rRNA coding regions and the fossil record. *Mol.*

Phylogenet. Evol. 6, 391–407.

Kröger, N., and Poulsen, N. (2008). Diatoms-from cell wall biogenesis to nanotechnology. *Annu. Rev. Genet.* 42, 83–107.

Lavigne, A.S., Ines, S., and Sar, E.A. (2015). Morphological, taxonomic and nomenclatural analysis of species of *Odontella*, *Trieres* and *Zygoceros* (Triceratiaceae, Bacillariophyta) from Anegada Bay (Province of Buenos Aires, Argentina). *Diatom Res.* 30, 307–331.

Lee, R.E. (2008). *Phycology* (Colorado State University: Cambridge University Press).

Lewin, J.C., Lewin, R.A., and Philpott, D.E. (1958). Observations on *Phaeodactylum tricornutum*. *J. Gen. Microbiol.* 18, 418–426.

Li, C.-W., and Volcani, B.E. (1985a). Studies on the biochemistry and fine structure of silica shell formation in diatoms X. Morphogenesis of the labiate process in centric diatoms. *Protoplasma* 124, 147–156.

Li, C.-W., and Volcani, B.E. (1985b). Studies on the biochemistry and fine structure of silica shell formation in diatoms IX. Sequential valve formation in a centric diatom, *Chaetoceros rostratum*. *Protoplasma* 124, 30–41.

Losic, D., Rosengarten, G., Mitchell, J.G., and Voelcker, N.H. (2006a). Pore architecture of diatom frustules: potential nanostructured membranes for molecular and particle separations. *J. Nanosci. Nanotechnol.* 6, 982–989.

Losic, D., Mitchell, J.G., and Voelcker, N.H. (2006b). Controlled Pore Structure Modification of Diatoms by Atomic Layer Deposition of TiO₂.

Losic, D., Mitchell, J.G., and Voelcker, N.H. (2009). Biomimetic Nanostructures: Diatomaceous Lessons in Nanotechnology and Advanced Materials (*Adv. Mater.* 29/2009). *Adv. Mater.* 21, NA – NA.

Macdonald, J.D. (1869). I.—On the structure of the Diatomaceous frustule, and its genetic cycle. *Annals and Magazine of Natural History* 3, 1–8.

Mann, S., and Perry, C.C. (1986). Structural aspects of biogenic silica. *Ciba Found. Symp.* 121, 40–58.

Medlin, L.K., and Kaczmarek, I. (2004). Evolution of the diatoms: V. Morphological and cytological support for the major clades and a taxonomic revision. *Phycologia* 43, 245–270.

Medlin, L., Kooistra, W.H.C.F., Gersonde, R., Sims, P.A., and Wellbrock, U. (1997a). Is the origin of diatoms related to the end-Permian mass extinction? *Nova Hedwigia* 65, 1–11.

Medlin, L.K., Crawford, R.M., and Andersen, R.A. (1986). Histochemical and ultrastructural evidence for the function of the labiate process in the movement of centric diatoms. *British Phycological Journal* 21, 297–301.

Medlin, L.K., Kooistra, W.H., Potter, D., Saunders, G.W., and Andersen, R.A. (1997b). Phylogenetic relationships of the “golden algae” (haptophytes, heterokont chromophytes) and their plastids. In *Plant Systematics and Evolution*, (Springer Vienna.), pp. 187–219.

- van de Meene, A.M.L., and Pickett-Heaps, J.D. (2002). VALVE MORPHOGENESIS IN THE CENTRIC DIATOM PROBOSCIA ALATA SUNDSTROM1. *J. Phycol.* 38, 351–363.
- Nandiyanto, A.B.D., Kim, S.-G., Iskandar, F., and Okuyama, K. (2009). Synthesis of spherical mesoporous silica nanoparticles with nanometer-size controllable pores and outer diameters. *Microporous Mesoporous Mater.* 120, 447–453.
- Nelson, D.M., Paul, T., Brzezinski, M.A., Aude, L., and Bernard, Q. (1995). Production and dissolution of biogenic silica in the ocean: Revised global estimates, comparison with regional data and relationship to biogenic sedimentation. *Global Biogeochem. Cycles* 9, 359–372.
- Ostenfeld, C.E.H. (1908). On the Immigration of *Biddulphia Sinensis* Grev. and Its Occurrence in the North Sea During 1903-1907, and on Its Use for the Study of the Direction and Rate of Flow of the Currents, Etc.
- Parambath, M., Hanley, Q.S., Martin-Martinez, F.J., Giesa, T., Buehler, M.J., and Perry, C.C. (2016). The nature of the silicophilic fluorescence of PDMPO. *Phys. Chem. Chem. Phys.* 18, 5938–5948.
- Perry, C.C. (2003). Silicification: How Organisms Capture and Mineralize Silica. *Rev. Mineral. Geochem.* 54, 291–327.
- Pfizer, E. (1869). Über den Bau und die Zellteilung der Diatomeen. *Bot. Ztg.* 27, 774–776.
- Pickett-Heaps, J., and Kowalski, S.E. (1981). Valve morphogenesis and the microtubule center of the diatom *Hantzschia amphioxys*. *Eur. J. Cell Biol.* 25, 150–170.
- Pickett-Heaps, J.D., Tippit, D.H., and Andreozzi, J.A. (1979). Cell division in the pennate diatom *Pinnularia*. IV. Valve morphogenesis. *Biologie Cellulaire*.
- Pickett-Heaps, J.D., Hill, D.R.A., and Richard, W. (1986). CELLULAR MOVEMENT IN THE CENTRIC DIATOM ODONTELLA SINENIS. *J. Phycol.* 22, 334–339.
- Pickett-Heaps, J.D., Schmid, A.M.M., and Edgar, L.A. (1990). The cell biology of diatom valve formation. 7, 1–168.
- Ross, R., Cox, E.J., Karayeva, N.I., Mann, D.G., Paddock, T.B.B., Simonsen, R., and Sims, P.A. (1979). An amended terminology for the siliceous components of the diatom cell. *Nova Hedwigia Beiheft*, 513–533.
- Round, F.E., Crawford, R.M., and Mann, D.G. (1990). *Diatoms: Biology and Morphology of the Genera* (Cambridge University Press).
- Royer, D.L. (2006). CO₂-forced climate thresholds during the Phanerozoic. *Geochim. Cosmochim. Acta* 70, 5665–5675.
- Schmid, A. (1980). Valve morphogenesis in diatoms: A pattern-related filamentous system in pennates and the effect of APM, colchicines and osmotic pressure. *Nova Hedwigia* 33, 811–847.
- Schmid, A.M. (1979). The development of structure in the shells of diatoms. *Nova Hedwigia* 64, 236.

- Schmid, A.-M.M. (1987). Morphogenetic Forces in Diatom Cell Wall Formation. In *Cytomechanics*, pp. 183–199.
- Schmid, A.-M.M. (1994). Aspects of morphogenesis and function of diatom cell walls with implications for taxonomy. *Protoplasma* *181*, 43–60.
- Schmid, A.-M.M. (2003). The evolution of the silicified diatom cell wall—revisited. *Diatom Res.* *18*, 191–195.
- Schmid, A.-M.M., and Schulz, D. (1979). Wall morphogenesis in diatoms: Deposition of silica by cytoplasmic vesicles. *Protoplasma* *100*, 267–288.
- Schmid, A.-M.M., and Volcani, B.E. (1983). WALL MORPHOGENESIS IN COSCINODISCUS WAILESII GRAN AND ANGST. I. VALVE MORPHOLOGY AND DEVELOPMENT OF ITS ARCHITECTURE1. *J. Phycol.* *19*, 387–402.
- Sims, P.A., Mann, D.G., and Medlin, L.K. (2006). Evolution of the diatoms: insights from fossil, biological and molecular data. *Phycologia* *45*, 361–402.
- Staats, N., Stal, L.J., de Winder, B., and Mur, L.R. (2000). Oxygenic photosynthesis as driving process in exopolysaccharide production of benthic diatoms. *Mar. Ecol. Prog. Ser.* *193*, 261–269.
- Sumper, M., and Brunner, E. (2006). Learning from Diatoms: Nature's Tools for the Production of Nanostructured Silica. *Adv. Funct. Mater.* *16*, 17–26.
- Sumper, M., and Brunner, E. (2008). Silica biomineralization in diatoms: the model organism *Thalassiosira pseudonana*. *ChemBiochem* *9*, 1187–1194.
- Sumper, M., Manfred, S., and Nils, K. (2004). Silica formation in diatoms: the function of long-chain polyamines and silaffins. *J. Mater. Chem.* *14*, 2059–2065.
- Tesson, B., and Hildebrand, M. (2010a). Extensive and intimate association of the cytoskeleton with forming silica in diatoms: control over patterning on the meso- and micro-scale. *PLoS One* *5*, e14300.
- Tesson, B., and Hildebrand, M. (2010b). Dynamics of silica cell wall morphogenesis in the diatom *Cyclotella cryptica*: substructure formation and the role of microfilaments. *J. Struct. Biol.* *169*, 62–74.
- Thamatrakoln, K., Kimberlee, T., Alverson, A.J., and Mark, H. (2006). COMPARATIVE SEQUENCE ANALYSIS OF DIATOM SILICON TRANSPORTERS: TOWARD A MECHANISTIC MODEL OF SILICON TRANSPORT. *J. Phycol.* *42*, 822–834.
- Theriot, E.C. (2010). A preliminary multigene phylogeny of the diatoms (Bacillariophyta): challenges for future research. *Plant Ecol. Evol.* *143*, 278–296.
- Tiffany, M.A. (2002). VALVE MORPHOGENESIS IN THE MARINE ARAPHID DIATOM *GEPHYRIA MEDIA* (BACILLARIOPHYCEAE). *Diatom Res.* *17*, 391–400.
- Tiffany, M.A. (2005). Valve development in the diatom family Asterolampraceae H. L. Smith 1872. *Micropaleontology* *51*, 217–258.

- Tiffany, M.A. (2008). VALVE DEVELOPMENT IN AULACODISCUS. *Diatom Res.* 23, 185–212.
- Tiffany, M.A. (2015). Valve and girdle band morphogenesis in the pseudocellate diatom species *Biddulphia biddulphiana* J.E. Smith (Boyer) and *Isthmia nervosa* Kütz. *Nova Hedwigia Beiheft* 144, 61–95.
- US Department of Commerce, NOAA, Earth System Research Laboratory (2005). ESRL Global Monitoring Division - Global Greenhouse Gas Reference Network.
- Van de Meene, A.M.L., and Pickett-Heaps, J.D. (2004). Valve morphogenesis in the centric diatom *Rhizosolenia setigera* (Bacillariophyceae, Centrales) and its taxonomic implications. *Eur. J. Phycol.* 39, 93–104.
- Vasani, R.B., Losic, D., Cavallaro, A., and Voelcker, N.H. (2015). Fabrication of stimulus-responsive diatom biosilica microcapsules for antibiotic drug delivery. *J. Mater. Chem. B Mater. Biol. Med.* 3, 4325–4329.
- Yang, W., Lopez, P.J., and Rosengarten, G. (2011). Diatoms: self assembled silica nanostructures, and templates for bio/chemical sensors and biomimetic membranes. *Analyst* 136, 42–53.
- Zhang, Y. (2012). Girdle Band Formation of *Odontella sinensis*. Master thesis. Faculty of Mathematics and Natural Sciences. Universität Bonn.
- Zyga, L. (2007). Microorganisms act as tiny machines in future MEMS devices.
- (1981). *Silicon and Siliceous Structures in Biological Systems* (Springer New York).

Part II. Frustule Morphogenesis

Fine frustule structures of *Odontella sinensis* has been reported in Chapter 1. Aspects of cytoskeletal dynamics have been revealed in Chapter 2 by looking at the structural changes of the cytoskeleton throughout the cell cycle. The information of the cytoskeleton function in silica morphogenesis shall now be complemented with observations on the behavior of the cytoskeleton in reaction to cytoskeletal inhibitors: Microtubules were inhibited by Oryzalin and Taxol (Chapter 3); actin filaments were inhibited by Jasplakinolide and Phalloidin (Chapter 3); myosins were inhibited by BDM, NEM and Blebbistatin (Appendix); calcium signaling pathway was interfered by calcium deficiency and calcium overdose (Appendix); the phosphorylation signal pathway was inhibited by Okadaic Acid and Calyculin A (Appendix).

Chapter 1

Fine Structure of the *Odontella* Frustule

Abstract

Fine structural aspects of the frustule of *Odontella sinensis* and its developmental stages is observed by scanning and transmission electron microscopy. The silica cell wall of *O. sinensis* consists of three differently patterned layers, i.e., the tectum (= roof: the outer layer facing the environment), trabeculae (= columns, connecting outer and inner layers), and the foraminal base layer. By the placement of the columns in hexagonal arrays a chambered pattern is created and each chamber has a single, large pore in the basal layer. This hexagonal chamber defines the unit structure of the frustule, termed areola. Beneath the silica, there is an organic layer acting as a transition zone between the cell wall and protoplast. In ultrathin sections observed in the transmission electron microscope, a fibrous structure is discovered for the first time in the lumen of the areola during its formation, which is proposed to play a role in the shaping of the areola chambers in the cell wall. As is typical for diatoms, the frustule components (valve and girdle bands) are prefabricated in a membranous compartment known as silica deposition vesicle (SDV). Formation of the siliceous cell wall inside the SDV starts with the virgae and continues growing inwards: under the virgae, triangular trabeculae project inwards, so that the areolae begin to be shaped; then spaces between virgae will be filled by silica forming a tectum, and embossing ridges appear at the inner side of the tectum; then followed by basal layer formation. The basal layer begins from the hexagonal frame surrounded trabeculae and close towards the center of hexagons until a roundish single central pore (foramen) reaches its size. This layer will be closed by an organic membrane when matured. Once the GB-SDV matured, the girdle band will be extruded and its serrated expansion gap will be open to adapt the new size. Connection way for overlapping zones between valve and girdle band are figured out in this chapter. Details of other fine structures are also presented: the pair of lips at the base of the labiate process and potential STV are recorded for the first time; functions of pores on the cell wall and on the face of the ocellus are also discussed in this

chapter. And finally, the head plate structure attracts our attention, which is considered to be two fused annuli.

1 Introduction

The siliceous frustule of diatoms exhibits a bewildering richness of fine structures including pore patterns, knobs, spines, marginal ridges, setae, labiate processes, ocelli, raphe slits and interlocking appendages and girdle elements (e.g., bands, segments, interlocking teeth). All of these structural elements of the frustule comprise phenotypic characteristics that have been extensively used in classical taxonomic implication, before the advent of molecular marker technique which are widely used in modern phylogeny (Ashworth et al., 2013; Kaczmarska et al., 2006; Sims et al., 2006).

The following aspects are introduced to give some important backgrounds on diatom fine structure morphogenesis and taxonomy. One of the most popular study object is the labiate process (LP) — a hollow spine-like projection on the valve protecting the cell from predators. In *Odontella sinensis*, the pair of LPs on each valve also have a simple interlocking function between adjacent cells in a cell filament. The labiate process is a special type of cell extension, because at maturity its lumen is not filled with cytoplasm as in the case of the setae, which are also long cell extensions found in diatoms such as *Chaetoceros* (Li and Volcani, 1985a). The adjective “labiate” is used because its connection to the inside of the frustule is sealed with two labia that form a slit. In their fine structure research on centric diatom species such as *Ditylum* (Li and Volcani, 1985b) and *Odontella* (Li and Volcani, 1985c), Li and Volcani illustrated that the base regions of LPs are the primary silicification sites of the valves in LP-decorated centric diatoms. According to their observation, the formation of the LP is under the control of labiate process apparatus (LPA), a fibrous, sometimes multilayered structure abutted to the cytoplasmic face of the inner silicalemma. From this region of the SDV the base plate of the LP forms first, and then the hollow shaft of the LP grows outwards. As the LP elongation relies on the apical growth, the LP siliceous wall begins as a base thin layer and then gradually becomes thicker radially. During this process, the plasma membrane doesn't fold into the tubular lumen (Li and Volcani, 1985c). Then the LPAs disappear after LPs maturation. Originally, Hasle has put forward the hypothesis that the LP is the phylogenetic predecessor of the raphe in pennate (Hasle, 1974). This was further supported by the finding that mucilage is secreted through the

LPs, which is the indirect cause of the subtle movement of living centrics (Medlin et al., 1986; Pickett-Heaps et al., 1986).

On the other hand, the fabrication of these fine structures on cell wall, which has yet not been fully understood, have raised researchers' curiosity on how these ornaments develop from the nano- to micro-scale.

In diatoms, silica is deposited in the silica deposition vesicle (SDV), where orthosilicic acids are accumulated during biomineralization. Silicic acid is transported into SDV and mixed with functional organic components within the SDV such as long chain polyamines and silaffins (Kröger and Poulsen, 2008), to create silica nanoparticles (Currie and Perry, 2007; Mann and Perry, 1986). Under laboratory conditions, such silica nanoparticles can self-assemble into a strikingly regular, porous layer of silica (Kröger and Poulsen, 2008; Sumper et al., 2004). However, formation of higher order structures is still challenging under laboratory condition.

Hence, the major question of interest in the biosilicification field is, what guiding factors in the natural process of silica frustule formation has confined the shape of the multiple silica layers and integrated them into a cell wall within the SDV. To this end, not only organic components are playing an important role, but cytoplasmic structures, such as spacer vesicles, organelles and cytoskeletal elements have been suspected to play roles as well (Borowitzka and Volcani, 1978; Chiappino and Volcani, 1977; Hildebrand and Wetherbee, 2003; van de Meene and Pickett-Heaps, 2002; Pickett-Heaps et al., 1990; Schmid, 1980, 1994; Schmid and Schulz, 1979; Schmid and Volcani, 1983; Van de Meene and Pickett-Heaps, 2004). In terms of the silica deposition source for the growing SDV, it comes from extracellular silicon (as silicic acid or silicate), which is then transported via silicon transporters (SITs) on plasma membrane into cytosol. The intracellular transportation of silicic acid is generally accepted by several possible mechanisms — through fusion with silicon transportation vesicles (STVs) (Schmid and Schulz, 1979), direct transportation through SITs, ionophore mediated diffusion and electrophoretic transportation via silicalemma (Thamatrakoln and Kustka, 2009). Eventually, a mature frustule cell parts appear to be made from ever repeating structural units, named as areolae, which merge into large scale ornaments in a regular fashion (Kröger and Poulsen, 2008; Kröger and Sumper, 1998; Sumper et al., 2004). And the blueprints for these patterns are likely species-specific (Willis et al., 2013).

These knowledges of fine structure construction and its morphogenesis process are usually contributed by SEM and TEM (Badour, 1968; Oey and Schnepf, 1970; Schmid, 1979, 1994; Schmid and Volcani, 1983; Tiffany, 2005, 2008, 2015). With the developmental technique of the

microscopy, atomic force microscopy (AFM) (Tesson and Hildebrand, 2010a, 2010b) and confocal microscopy (Annenkov et al., 2013; van de Meene and Pickett-Heaps, 2002; Van de Meene and Pickett-Heaps, 2004) are applied to complement the blur zone of cytoskeleton observation.

In this chapter, these traditional EM approaches have been employed and combined with one another to illustrate complicated fine structures of *Odontella sinensis*. Of this species, the overall frustule composition in different stages is reported by SEM. As the complement data, some fine structures are further illustrated by shadow imaging with TEM. Moreover, silica construction inside SDV are tracked by ultrathin sections analyzed by TEM to imply the silica deposition process of the cell wall.

2 Materials and Methods

2.1 Culturing

Colonies of *Odontella sinensis* were obtained in June and July 2011 from plankton catches routinely done by the staff of the Biological Marine Station Helgoland of the Alfred Wegener Institute. Cells were isolated manually under the binocular using a pipette, washed for several times in filtered seawater and kept at ambient temperature for several days to make sure that they were free of contamination. For cultivation, they were first transferred into f/2 medium (Guillard, 1975) mixed with seawater with a 1:4 volume ratio, then into a new mixture medium with a 1:3 ratio, and so forth into mixture medium with the descending volume of seawater to make the diatoms gradually adapted, and eventually into completely pure f/2 medium. The whole process persisted over a period of several days at a temperature of 16°C with a 12:12 h dark-light-cycle under 1000 lux cool white fluorescent light. A culture was started with 50 cells, which were cultured in a 60 x 15 mm plastic petri-dish with 10 to 15 ml of f/2 medium. Each culture contained cells at different phases of the cell cycle. After 3 to 4 days of unperturbed growth, the culture enters into an exponential growth phase, which takes 24 to 48 hours to double the population. Subsequent medium changes were made every week. Cells were usually harvested for experiments during the light period of the illumination cycle.

2.2 Fixation

Fixation was done at room temperature in three different ways:

1a. Simultaneous GA/Os Fixation: 1% glutardialdehyde (GA) in f/2 culture medium for 5 minutes, to which 4% osmium tetroxide (OsO_4) dissolved in distilled water was added to reach a final concentration of 0.1% OsO_4 . Fixation was continued in the mixture for another 15 minutes, before the fixative was replaced by distilled water.

1b. Simultaneous GA/Os Fixation: Same as above but 4% osmium tetroxide (OsO_4) was added until a final concentration of 2% OsO_4 was reached.

2. Sequential GA/Os Fixation: Cells were placed in 1% GA dissolved in f/2 culture medium for 15 minutes, followed by an f/2 medium wash for 5 minutes and subsequently post-fixed in 2% OsO_4 dissolved in distilled water for 15 minutes, before the fixative was replaced by distilled water.

Notably, identical results could be obtained by either fixation above.

3. Double-Aldehyde Fixation: 0.5% GA and 1.5% formaldehyde (FA) dissolved in actin-stabilizing buffer (ASB: 75 mM Pipes pH 6.8, 10 mM EGTA, 5 mM MgCl_2 , 50 mM KCl, 1% DMSO, pH adjusted to 7.1 by dropwise addition of KOH). FA was made by dissolving 20g paraformaldehyde powder in 100 ml distilled water. The suspension was heated to near 60°C , and mixed with solid KOH, until it turned clear, and eventually adjusted to pH 7.1 by dropwise addition of 1 mM NaOH. Additional 100 ml of phosphate-buffered saline (PBS: 0.14 M NaCl, 2.7 mM KCl, 6.5 mM $\text{Na}_2\text{HPO}_4 \times 2\text{H}_2\text{O}$, 1.5 mM KH_2PO_4 , adjusted to pH 7.4 by dropwise addition of KOH or HCl if required) was added resulting in a 10% PFA stock solution.

Cells were collected in a sterile, handmade polyethylene sieve (50 μm pore size, Fig. 1A), which was drained and transferred to a spot plate (Fig. 1 B & C), to submerge cells in 750 μl fixation solution for a minimum of 15 minutes. Then the sieve was drained and transferred to ASB in 2 to 3 spots, each of the washes lasted for 15 minutes.

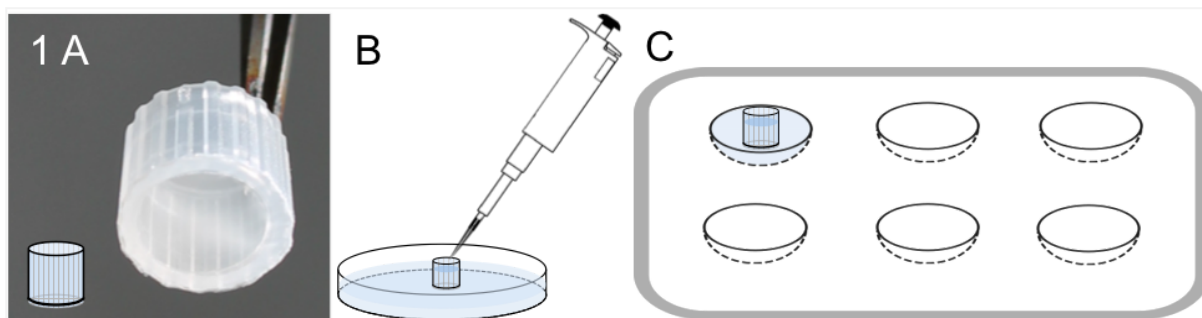


Fig. 1 Handling of cells. (A) Handmade sieve. (B) Cells were collected into the sieve by careful use of a 1000 µl automatic pipette. (C) A sieve placed in a spot plate for fixation and washing.

2.3 Preparations for Scanning Electron Microscopy (SEM)

2.3.1 Cell Treatments

In order to obtain views not only of the cell surface but also of internal cell structures in the SEM, post-fixation treatments were performed. These treatments gradually loosen frustule elements and slightly separate them from one another without destroying the structural context. Or alternatively, pre-fixation enzyme treatments were applied to separate and isolate frustule components entirely from one another. The harshest treatment involved acid hydrolysis to completely remove all organic material from the frustule elements.

2.3.1.1 Post-fixation Treatment — SDS Extraction

Method 1: AA - 5% SDS - CPD. Cells fixed by the double-aldehyde (AA) method were treated with 5% sodium dodecyl sulfate (SDS) dissolved in PBS for 24 hours in order to remove all detergent soluble material that was not crosslinked by the fixative. Subsequently the SDS sample was diluted with distilled water and the clean frustules were allowed to precipitate to the bottom of the glass container; the supernatant was removed and the washing step was repeated several times. The clean frustules were further processed by acetone dehydration and critical point drying (CPD) (see 2.3.2.2).

Method 2: AA - 3% SDS - freeze drying. Cells were fixed, extracted (but this time using only 3% SDS) and washed as described in Method 1 and then processed by freeze drying (see

2.3.2.3). Some freeze-dried samples were gently touched and torn open by adhesive tape to split open and remove cracked silica layers from the frustule surfaces. This should allow views into the internal substructure of the frustule wall.

Method 3: AA - 5% SDS - open flame incineration. Cells were fixed, extracted and washed as described in Method 1 but then processed by open flame incineration (see 2.3.2.4).

Method 4: GA/Os - 3% SDS - CPD. Cells were fixed by the sequential GA/Os method, then extracted with 3% SDS dissolved in PBS for 24 hours and further processed by washing and drying as described in Method 1.

Method 5: GA/Os - 3% SDS - open flame incineration. Cells were fixed by the sequential GA/Os method, then extracted with 3% SDS dissolved in PBS for 24 hours and further processed by washing and open flame incineration as described in Method 3.

2.3.1.2 Pre-fixation Treatment — Enzyme Digestion

Method 6: Chitinase digestion - AA - SDS - CPD. Live cells were treated with 0.25 µg/ml chitinase (Sigma C6137.25, *Streptomyces griseus*) dissolved in f/2 medium for 24 hours, followed by the double-aldehyde fixation. Subsequently, specimens were extracted by 3% SDS, washed and dried as described above (Method 1).

Method 7: Chitinase & proteinase K digestion - AA - SDS - CPD. Live cells were treated by a combination of 0.25µg/ml chitinase and 0.1 mg/ml proteinase K in f/2 medium for 24 hours, followed by the double-aldehyde fixation. Subsequently, specimens were extracted by 3% SDS, washed and dried as described above (Method 1).

2.3.1.3 Post-fixation Treatment — Acid Wash

Method 8: GA/Os - KW - CPD. Specimens obtained by the simultaneous GA/Os fixation method were transferred to “king’s water” (KW, aqua regia: a fresh mix of 37% HCl and 65% HNO₃ at a ratio of 3:1) in a tiny glass container for 5 minutes, heated at 50-60°C to improve extraction. The KW sample was then diluted with distilled water and the clean frustules were allowed to precipitate to the bottom of the glass container; supernatant was removed and

washing was repeated several times. The clean frustules were further processed by acetone dehydration and CPD.

Method 9: GA/Os - Proteinase K - SDS - KW - CPD. Live cells were first treated by the simultaneous GA/Os fixation, washed in f/2 followed by distilled water and then incubated in 0.1 mg/ml proteinase K for 24 hours. After a wash in distilled water they were further extracted in 3% SDS for 24 hours, washed again by distilled water and then incubated in KW for 5 minutes. Finally samples were washed in distilled water, dehydrated with acetone and CPD-dried.

2.3.2 Drying Methods

2.3.2.1. Acetone Dehydration. Specimens from the above treatments were subjected to sequential dehydration in an ascending series of acetone dilutions (30%, 50% 75%, 90%, 100%) for a minimum of 30 minutes each and kept in the last step for 15hrs before critical point drying (CPD).

2.3.2.2. Critical point drying (CPD). Specimens in acetone were transferred to the pressure chamber of a CPD 030 Critical Point Dryer (Bal-Tec). Acetone was replaced by liquid CO₂ (transitional fluid) and this was instantaneously evaporated by controlling pressure and temperature according to the manufacturer's instructions. The purpose of this method is to avoid turbulent liquid evaporation, which could damage microscopically small structures in the samples.

2.3.2.3. Freeze drying. Specimens in distilled water were subjected to freezing by the method of H.-J. Ensikat (Ensikat et al., 2010), which can be performed without professional freeze-dryer equipment. Briefly, a drop of the sample-suspension was transferred quickly (to avoid drying) onto a microscope glass slide, mounted into a “home-made cooling holder” equipped with a lid to protect the droplet, when the holder was immersed into liquid nitrogen. From the liquid nitrogen bath the sample holder with the frozen samples was quickly transferred onto the cooling stage in the specimen chamber of the SEM and subjected to a vacuum of 10⁻⁵ mB. When the vacuum was reached, the lid was removed to allow the frozen water to evaporate. Next, the glass slide with the samples was brought back to standard atmospheric pressure, removed from the cooling holder and mounted on a SEM specimen holder (aluminum stub).

2.3.2.4. Open flame incineration. Samples in distilled water were deposited on a glass slide, which was then carefully heated by the small pilot flame of a Bunsen burner at a temperature of above ca. 500°C. By this rather violent process, which can be monitored visually, all organic material is removed by thermal oxidation. Adhesions between frustule parts should be affected and it may also be expected that weaker structures will collapse onto each other.

2.3.3 Sputter Coating & SEM Observation

Dried specimens were manually placed on double adhesive tape (Tesafix), which was mounted on aluminum stubs. They were then sputter-coated with 20-30 nm gold in a Union SCD 040 sputter coater (Baltec). Gold coated specimens were viewed with a Cambridge Stereoscan S200 Scanning Electron Microscope (Cambridge, U.K.).

2.4 Preparations for Transmission Electron Microscopy (TEM)

2.4.1 Imaging of Ultra-thin Sections

Fixation, Dehydration and Resin Embedment: Live cells were fixed by 1% GA in f/2 culture for 10 minutes, to which 4% OsO₄ dissolved in distilled water was added to reach a final concentration of 1% OsO₄ for 25 minutes. Then samples were transferred to 2% OsO₄ in f/2, and finally washed by distilled water. Samples were dehydrated through an ascending acetone series up to 100% acetone, and then were carried through four steps of ascending resin infiltration made by mixing acetone with epoxy-resin (ERL4206, D.E.R. 736, NSA, S-1) according to Spurr's original protocol (Spurr, 1969). Specimens were kept at the 100% resin step overnight, before they were transferred to the front end of dried gelatin capsules. Afterwards, they were carefully filled up with fresh resin. The resin capsules were cured in an oven at 70°C for at least 7.5 hours. (Applied in section 3.2 except for Fig. 22 & Fig. 28C)

Fig. 22 A & a: Live cells were fixed by 1% GA in f/2 culture for 3-5 minutes, to which 4% OsO₄ dissolved in distilled water was added to reach a final concentration of 1% OsO₄ for 15 minutes. Then samples were dehydrated, embedded in resin in a same procedure above.

Fig. 22 B & C; Fig. 28C: Live cells were fixed by 1% GA in f/2 culture and kept in microwave (350 Watt, 60°C) for 3 minutes, and then awaited for minutes to cool down to room temperature. Then OsO₄ dissolved in distilled water was added to this mixing solution to reach a final concentration of 1% OsO₄ for 25 minutes. Then samples were transferred to the 2% OsO₄ in f/2 and kept at 4°C for 26 hours. Then samples were warmed up in room temperature for 2 hours before going through the same dehydration and the embedment in resin as above.

Ultrathin Sectioning and Post-staining: Pyramid cones were trimmed out of the tops of the resin blocks using a Reichert-Jung TM 60 trimmer and ultrathin sectioning was done on a Leica-Reichert Ultracut E ultramicrotome using a diamond knife. Silver to golden (ca. 70 nm) sections were spread with chloroform and picked up on polyvinyl formaldehyde (formvar) coated 200-mesh copper grids. They were then post-stained with 2% saturated uranyl-acetate dissolved in distilled water and subsequently with lead citrate according to Reynolds (Reynolds, 1963), briefly washed in 0.02 N NaOH and distilled water and finally dried overnight before use.

2.4.2 Shadow Imaging of Acid Cleaned Frustules

Cleaned frustules were prepared from double-aldehyde fixed cells by extraction with 5% SDS for 24 hours followed by KW wash for 10 minutes and further washing in distilled water. Frustules were pipetted from the precipitate (see 2.3.1.1, method 1) onto formvar coated 200 mesh copper grids. Grids were dried after excess liquid was drained off and then post-stained with 2% uranyl acetate. Images were taken by the TEM as described below. Essentially, identical results could be obtained, when the SDS extraction step was omitted.

2.4.3 TEM Observation

Images were taken with a LEO 912AB electron microscope using a high resolution CCD-Camera (Proscan HSC2) in combination with the image analysis software “analySIS” (Soft Imaging System, Münster).

2.5 Terminology

In this thesis, the popular terminology as established by leading authors in the field of diatom research is used (Perry, 2003; Pickett-Heaps et al., 1990; Ross et al., 1979; Round et al., 1990; Tiffany, 2015). In the following results section the SEM images of cells will be presented always in the same polar orientation, i.e. hypovalve pointing to the left, epivalve to the right.

2.6 Acknowledgement

Sample treatments were performed under the close guidance of Ursula Mettbach (IZMB). CPD drying, freeze drying and open flame incineration were done with extensive help from Hans-Jürgen Ensikat (NEES Institute of Plant Biodiversity). TEM and SEM images were taken together with Ursula Mettbach and Hans-Jürgen Ensikat, respectively. Use of the SEM facility of the Nees Institute was made possible by the courtesy of Prof. Dr. Maximilian Weigend.

3 Results

Frustule fine structure of *Odontella sinensis* was studied by scanning electron microscopy (SEM) and transmission electron microscopy (TEM) in combination with various preparation techniques.

3.1 Observations by SEM and TEM-Shadow Imaging

SEM is usually applied to observe upper or lower surface of samples in the field of cell biology. Thus a view into the inner construction of a cell requires preparations to break open the cell surface. To achieve this in the case of the diatoms, special pre- and post-fixation treatments were applied to gradually loosen and separate frustule components from one another. Among them were gentle treatments, which leave the cellular context largely intact, i.e., detergent extraction after fixation. But harsher treatments have also been employed to remove organic components by enzyme digestion either before or after fixation. In the latter case, fixation will certainly encumber enzyme action but may still be useful to remove macromolecules that have

not been properly fixed. Acid wash, on the other hand, is the harshest treatment, leaving behind empty frustules or even the plain silica frame of the individual valves or GBs. Another harsh post-fixation treatment was performed by cracking the silica wall open via freeze substitution and subsequent adhesive tape peeling, which removes scattered wall fragment from the dried samples. By such stepwise decomposition of the cell bodies and its component parts, more and more substructures were revealed even as down as into the details of areola substructure.

The shadow imaging by TEM uses thoroughly cleaned, acid-washed frustule parts flattened out on formvar-coated EM-grids. Other than in the SEM, we get a two-dimensional shadow cast of a three-dimensional object.

3.1.1 General Morphology of the Frustule

3.1.1.1 Frustule Compositions

The overall morphology of the *Odontella* frustule is best described in samples that have received gentle post-fixation-detergent extraction. Two morphotypes have been identified in the cell cultures, which are characterized by a width to length ratio of between 0.28 and 0.80 (W:L-ratio, based on Fig. 9 of (Zhang, 2012)). In fresh cultures obtained from auxospores the sturdy morphotype is very common (wide and short, e.g., Fig. 2; W:L-ratio = 0.5–0.8), whereas in old cultures the slender type predominates (narrow and long, e.g., Figs. 3, 4, & 5; W:L-ratio = 0.28–0.5).

Of a frustule, the smaller half (seen in all the following images on the left) is the hypotheca; the slightly bigger half on the right is the epitheca, which wraps outside around the hypotheca. The epitheca has the epivalve and two major girdle bands (eGB1 and eGB2) and sometimes plus a third narrow one termed eGB3 (e.g., Figs. 2b, 5a₁). The last GB of the epitheca is always sealed to the hypotheca by a small, band-like overlapping lace (sealing lace, Figs. 2b, 3B, 5a₁, 22E).

3.1.1.2 Young SDV beneath the Epitheca

Cells in Fig. 2 - Fig. 4 are arranged in the growing order of the frustule, which shows the cell develops from hGB1 to hGB2 during the interphase. By mild post-fixation SDS extraction, cells

are completely preserved, where the frustule parts are perfectly kept in place as in the live cell (Figs. 2A, 2B). While in some other cases, a part of the hypotheca has slipped out of the epitheca or it may even be that the epitheca has been cracked open (Fig. 2C, Fig. 3), revealing inner structures from underneath the frustule.

In Fig. 2C, a cell is depicted, where the hGB1 is developing. The distance, by which it has slipped out, is marked by a white arrow and the original position of the abvalvar edge of the epitheca on the hypothecal surface is marked by a stippled line. The brighter surface of the hypotheca, which had originally been hidden underneath the epitheca, appears abraded at the low magnification but turns out as coated with a regular brickstone-like pattern at higher magnification, indicating a young developmental stage of the underlying girdle band just shortly before fixation (further explanation see the legend of Fig. 14E).

Figure 3 shows a cell where the hGB2 is developing. A crack in the frustule occurred in the epitheca running from the abvalvar edge of eGB2 lengthwise through eGB1 and then bending up sharply along the edge of the epivalve, which allows a small fold of soft material protruding out. The brickstone pattern in the left half of this fold (Fig. 3B) identifies it as a young girdle band, the formation of which must be in progress, because the right half of the fold changes into a flake-like pattern, which help to identify this part of the fold as protoplasm with plastids. The protoplasm does not fall apart simply because it is being held together by aldehyde induced molecular cross-links created during fixation. Another interesting detail is that a piece of short stretch smooth surface at the beginning of hGB2 (arrow in Fig. 3C) has evaded destruction, which is interpreted as the remnant of membrane coat consisting of the plasma membrane and the upper silica lemma of the SDV (cp. Fig. 15F). As explained in the introduction, immature frustule structures, whose formation is still in progress, are enclosed in the silica deposition vesicle and this internal membrane compartment is covered by the plasma membrane.

The stage of Fig. 4A is later than Fig. 3. Plastids arranged along cytoplasmic strands can be seen as grey spindle-like profiles underneath hGB2. (Fig. 4a). Thanks to the enzyme digestion, the eGB2 was peeling apart to present a large piece of hGB2 under the epitheca.

The cell of Fig. 4B is in the same stage as Fig. 4A. But the same phenomenon occurred as in the case of Fig. 2C, that the soft immature hGB2 has slid forward from underneath the epitheca revealing the typical brickstone pattern of the immature girdle band in its surface. The eGB2 has become slightly opened at the long crack, and cytoplasm identified by the many plastid profiles has been squeezed out of the slit to some extent. Emergence of protoplasmic

content through frustule cracks is likely a post- rather than a pre-fixation artifact, because the cytoplasmic exudates are firmly held together. Would there be a forming hGB underneath eGB2 in this position, it would appear as a brickstone patterned surface in a similar way as seen in Fig. 2C.

Figure 4C shows a cell where the hypotheca is detached from the epitheca and a small gap is left between them. By enlarging the view through this gap (Fig. 4c₃) a delicate silica structure is spotted, which has the appearance of an incomplete brickstone pattern comparable to that of acid-washed immature valve parts (Fig. 17). Consequently this cell has undergone division and begun to produce daughter valves.

Even more extensive insights can be obtained, when the underneath part of hypotheca slid out a larger distance from of the epitheca. In Fig. 14A, the frustule displays an area devoid of plastidial profiles (red double headed arrow) in the region of eGB2, which was as large as the area of the hGB2 plus the adherent soft but fixation-stabilized cortical cytoplasm (white double headed arrow), indicating that this area of the cortical cytoplasm was ruptured and torn out from the epitheca, as it is known that well preserved protoplast by qualified fixation would display such profiles distributing evenly underneath the entire frustule (e.g., Fig. 3). The area devoid of plastids could conceivably happen at moments of solvent change due to the enormous volume of the vacuole. In the course of sample preparation, the first moment sensitive to osmotic imbalance would be the exchange of fixative against buffer. But the exchange of buffer against organic solvent or even the processes in the pressure chamber of the CPD could also produce local volume imbalances. In each of these cases the internal pressure might momentarily surpass the external pressure and cause the hypotheca to be pushed out. Additional SDS treatment would certainly promote this process by loosening the connections between hypotheca and epitheca. Much of the pressure imbalance was probably released by the slipping out of the hypotheca, so that the cell did not burst.

The fact that hGB2 was originally covered up by eGB2 in the live cell is again indicated by the abraded surface appearance of hGB2 (Figs. 14A & 14B), which comes from the brickstone pattern only visible at higher magnification (Figs. 14C, 14c). The small white arrows in Fig. 14c point at irregular deposits at the inner dark lumen. These deposits are interpreted as remnants of the membranous coating spanned over the silica frame in the SDV. The exposing process to explain this young silica is well described by two schemes (Figs. 14d & 14E) — one introduces the membrane-arrangement of SDV, while the other presents the membrane distribution on

virgae after rupturing — both of which are applicable to explain the situations of following images (Fig. 14E). Fig. 14D shows the abvalvar edge of hGB2 and the adjacent region of naked cytoplasm. The sharp border (marked by asterisks in Fig. 14D) can only be caused by a sharp shift in stiffness and cohesiveness at the abvalvar edge of hGB2.

In summary, these examples of views underneath the frustule cover reveal that each young SDV (hGB1, hGB2, HV) is always located during its formation beneath eGB2.

3.1.1.3 Porous Surface

Pores are visible on the frustule surfaces, which were treated by enzyme digestion plus SDS extraction (Figs. 4c₂, 5a₂, 12D), or SDS extraction alone (Figs. 9D, 9E). These pores are unexceptionally well visible in frustule surfaces that were acid washed (Figs. 6C, 7, 11c₂), because that removes organic material due to hydrolysis.

However, pores on girdle bands are always of one size (Figs. 5a₂, 6C, 7, 9E), while on valves there is an additional type of pores which are bigger, sporadically distributed among the smaller porelli (Figs. 4c₂, 9D, 11c₂, 12D). By measuring the dimension in the original file of Fig. 9D, which is in a higher resolution, the size of the porelli in either the girdle band or the valve is the same.

3.1.2 Structures of the Girdle Band

3.1.2.1 Expansion Gap

The structure of the girdle band seen in *Odontella sinensis* is neither of the closed nor the open type. Instead, it is an expandable type, which eventually gets sealed by a zip-lock mechanism. Each girdle band has two opposite edges serrated by complementary saw-like teeth, which interlock with each other. The gap that can occur between these edges is named here the “**expansion gap**” (Figs. 3C, 3E, Fig. 7).

It is obvious that the expansion gap opens more easily due to SDS extraction and mechanical impact, producing a long crack in the epitheca. This comes quite handy here, because it allows the observation of hypothecal structures, which would otherwise be hidden

beneath (Figs. 3C, 4A, 4B). In addition, the position of the future expansion gap in the immature girdle band seems to align underneath the already existing expansion gap of eGB2 (Figs. 4A, 4b). In some images it appears that the expansion gaps align along the entire frustule (Figs. 2A, 4A, 4C), but this may not always be the case.

In addition to the mechanical cracking (Figs. 3, 4B), the expansion gap is also opened more easily by chitinase treatment (Fig. 4A), or by double enzyme digestion resulting in an unfolding of the thecal wall (Fig. 8A), which suggests the presence of chitin as a sealing agent.

3.1.2.2 Edge Morphology of the Girdle Band

A closer look at girdle band fine structure was possible in cells prepared by GA/Os fixation, followed by subsequent extraction with SDS and final wash with acid (Method 9). During acid wash, all structural cohesiveness is suddenly released by rapid hydrolysis from the cell wall, which caused girdle bands to entirely flatten out (Fig. 6A). But sometimes, a girdle band curls its circumferential edges, so that it would shape in an open bracelet (Fig. 6B). Of the two circumferential edges, the abvalvar one is smooth (Fig. 6a1, red arrow) and the advalvar one is frayed (Fig. 6a2, yellow arrow). The short edges perpendicular to the circumferential edges, i.e., the edges armored with teeth, compose the expansion gap of the girdle band (Fig. 6a1 and 6a2, white arrow). The areola chambers cannot be seen in SEM when viewing from outside. However, the foramina would be presented, when looking from the inside (Fig. 6). Each foraminal pore is an entrance to an areola chamber but most time structural details inside the chamber are obscured, due to the fact that the gold coating would not reach that far into the cavity. Only in a few instances, the inner face of the tectum can be seen through the foramina and then small porelli become visible in the tectum wall (Fig. 6C).

As an alternative to SEM, acid-washed frustule can be observed by shadow imaging in the TEM, which in principle does not allow discriminating between inside and outside, because all object details are projected onto the same plane. However, due to the rolled up nature of the girdle band in this kind of preparation, the observation angle is mostly looking from inside towards outside.

The formation of the girdle band wall starts with the tectum. Parallel ribs of silica are formed first in the plane of the tectum along which the porelli are lined up (Fig. 7B₁), which is finally followed by the appearance of the bottom layer with the large foramina in it (Fig. 7B₂). The

edge of the expansion gap may develop from the short blunt wavy kind of teeth into long prominent sharp teeth, and the thin base rim also increases in its size when the girdle band grows older (Fig. 7C). The region of the frayed edge, which is the lace with binary teeth in the young stage, then further develops the embossed inner edges of the foramina and thickens the basement layer between the teeth, which get half way obscured (Fig. 7D). During the growing process, the foramina grow in from the chamber wall centripetally decreasing their sizes distinctly (Fig. 7E).

3.1.2.3 Orientation of the Girdle Band

Since a girdle band has two different circumferential edges, it is important to know its orientation, when it links up with the next girdle band. According to Fig. 5B and Fig. 9D, the abvalvar side is the smooth edge while the advalvar side is the frayed edge.

3.1.2.4 Organic Layer

The major effect of the double enzyme digestion and SDS extraction (Method 7) on frustule integrity is a weakening of the sealing function of the connecting lace, which secures the hypotheca in the embracement by the epitheca. When cells are observed in the binocular a few hours after enzyme treatment started, many cell develop a kink in the middle and the protoplast is beginning to squeeze out forming a bubble. After 24hrs, when cells were fixed, the majority of frustules were empty since protoplasts had liberated from the two separated thecae (data not shown). In the current protocol of pre-fixation enzyme treatment (Section 2.3.2.1), such empty frustules have been retrieved after fixation, whereas the protoplast bubbles got lost during handling.

Figure 8 shows a view into an opened frustule from such a preparation. An epithecal girdle band (eGB2) with the connecting lace at the abvalvar edge is seen on the left. To the right is the first girdle band (eGB1) which has become separated from eGB2 and further to the right is part of the epivalve, which is still firmly connected to eGB1. Higher magnification of the region, where a crack occurred at the advalvar edge of eGB2, shows small segments. The cracks through inner and outer levels of the frustule wall run slightly offset from each other, so that one can see against the inner face of the tectum with the embossed ridges standing out as a honeycomb

pattern (Fig. 8a₁). The inner face of the frustule wall appears smooth at this magnification. The next higher magnification reveals a regular pattern of dark, round profiles which represent the foraminal pores underneath a smooth layer of material (Fig. 8a₂). This layer is completely removed by acid wash as shown in Fig. 6, suggesting that the material of the layer is of organic nature.

The cell of Fig. 8B is also treated with Method 7 (chit-prot-AA-SDS-CPD), but its situation is more complex. The epitheca has remained intact and is completely open at the abvalvar side. Close-up 8b₁ is from the upper rim. The connecting lace is bent backwards so that an areola chamber pattern appears underneath. It is semi-transparent, which is unusual for a scanning EM image, but it can be explained by the fact that gold sputtering did not fully reach down to this object detail, so that absorption of electrons and emission of secondary electrons is about equally in dimension. Therefore this frustule element appears almost like a shadow image (cp. Fig. 7). What we are looking at, however, is not the epithelial girdle band, but an unexposed, immature hypothecal girdle band, probably hGB2, which was contained in the SDV. The reason for this assumption is that there is no sign of organic layer underneath the bottom layer (see also Figs. 8b₃ & 8b₄) and a frayed edge of the girdle band (like Fig. 7D) is clearly visible. Since the frayed edge is at the advalvar side of the GBs, this particular one can only be a hypothecal GB, which got clamped on the inside of eGB2 despite all the handling during the various preparation steps.

Figure 8b₃ shows the lower rim of the epithelial edge and here we see principally the same. The foramina are completely open and the edge of the hGB displays very fine teeth. The surface of this foraminal layer would be covered by an organic layer like Fig. 8A, if it were a mature epithelial girdle band.

3.1.3 Structures of the Valve

Exterior and interior surfaces of valves were observed by SEM (Figs. 9, 11, 12 & 13), and shadow imaging from interior of valves was obtained by TEM (Fig. 10).

The edge of a valve is also characterized by a smooth overlapping lace, which rests on top of the serrated advalvar edge of the first girdle band (Fig. 9D). The fine teeth of the frayed advalvar edge are just about visible underneath the detached connecting lace (Fig. 9D, asterisk). Shadow images by TEM in Fig. 10 present hexagonal areolae chambers of a

well-developed valve viewed from the interior (Figs. 10 C, E, F). The mature hexagonal pattern close to the valve edge becomes irregular (Fig. 10F), with a smooth region intercepting the hexagons and foramina at the edge (Figs. 10B, 10F). When the valve is young, its smooth edge is narrow, and the hexagons nearby are also irregularly arranged but without foramina (Fig. 10G).

At the front of the valve, there is a prominent elongated elliptical area (Figs. 11A, 12B) delineated by a sharp sculptured boundary (Figs. 12c₂, 12D), called “**head plate**” in this thesis. In the side view, it has the shape of a saddle (Fig. 10D). The head plate consists of two individual annuli (Figs. 11A, 12B), each of which is a elliptically slender circle (Figs. 11 B–D). In between the two annuli, there is an irregular mosaic pattern formed by the arrangement of the areolae (Figs. 11b, 11C).

At the outermost fringe of each annulus, there is a horn (ocellar protrusion) standing at each corner point of the valvar apical axis (Figs. 11B, 12A, 12E). The front surface of an ocellus is equipped with knobs scattered on a pore field (Figs. 12c₁ & 12e), but it is unclear whether the surface of the opposite horn has a matching surface structure.

Closely on the inner side of each horn, a spine-like labiate process (LP) extrudes from the head plate with a circular, thickened base (Figs. 11A, 11B, 11D, 12). LP and its base are completely devoid of areola patterns, instead they are either completely smooth or might be covered with tiny knobs (Fig. 11D). In a linear colony, cells connect to each other by the linkage between horns, and also by the mechanical interlocking of the LPs (Fig. 12A). Sometimes a full developed valvar dome bears short LPs facing to the observer (Fig. 12B & 12E). Notably, the arrangement of the two LPs on the valves of all samples, either of the epithecal or hypothecal valve, always follow the same centrosymmetric pattern as shown in Fig. 11A.

As described in section 3.1.1.3, bigger pores only appear on the valve surface. They scatter irregularly among the smaller porelli, which are aligning evenly along the ribs (Figs. 11b-D, 12D). This porous pattern on the surface is one of the characteristics of the valvar cell wall.

When looking from the interior side of the head plate, the two slender annuli can be recognized as two short sealing lines along the valvar apical axis, and between the two annulus-lines, the irregular patterned region again can be seen between the annuli (Figs. 13a, 13B, 13C). Two holes at each outermost side of the annulus-line are tunneling into the LP and

the horn, respectively (arrows in Fig. 13A). But the entrance to the LP is obstructed by a slit composed by two labia (Fig. 13c) whereas the entrance to the horn is open.

3.1.4 Development Stages of the Frustule

Girdle band formation and valve formation compose the frustule development stages, which occupy the major part of interphase of a cell cycle.

Knowing that each young SDV (hGB or HV) develops beneath the cover of eGB2 before its maturation (3.1.1.2), it is comprehensible that the membranous surface of the silica structure ruptures when it gets exposed from the epitheca. The rupture principle for the young silica structure is well described by Fig. 14E. By this artifact, the paralleling silica strips of hGB2 stand out clearly (Fig.15). This girdle band SDV was just beginning to form the virgae (the framework of the young tectum growing along the longitudinal axis) when being harvested. Due to the GA/Os fixation, which well preserves the soft protein-containing structures, the partially pulled out protoplast at the epitheca side reveals a smooth membrane with many very small lesions (Figs. 15C & 15c₂).

Virgae of the immature valve were also seen in SDS extracted samples, when the mother thecae separated from each other. After extraction, the prototype valve in the SDV was entirely exposed, revealing virgae constructing the valve framework (Fig. 16). Between this silicified region and the naked protoplast region there is a clear boundary, which is considered to be the growing frontier edge of silicification. The closer it gets to the frontier growing edge, the less silica is filled in between virgae (Figs. 17B, 17C) and the less vertical structures (areola chamber walls or columns) developing under the tectum (Fig. 17D). The rigidity of slender annulus is low and weak initially (Figs. 16B, 18a₂), because the inside of the young annulus is still open (arrow, Fig. 17a) even ribs have already spread over the head plate region.

The horns were first silicified by virgae; then the virgae would further develop into areolae (Figs. 16B, 18a₃); during this period, the ocellus is yet absent only foreshadowed by a depressed pit. Next, a wide tube forms, which appears open at the tip, but it could simply be an artifact due to the fact that the frontal face of the immature horn is very soft causing it to invaginate during preparation (see graphic sketch in Fig. 18a₃).

While most of the time the membranes covering the silica frame located inside the SDV collapse or rupture during the sample preparation for SEM (GA/Os-SDS-CPD) as shown above, sometimes exposed membranes in samples treated exactly the same evade this typical kind of destruction. As Fig. 18B proves, the membrane surface of an exposed daughter valve domain has remained almost intact, containing only smaller lesions. It can only be speculated, what the reason for this difference is. As is mentioned, the special construction of the diatom cell wall creates levels of nested micro-spaces, which might suffer more or less destruction as cells are subjected to rapid volume and pressure changes during the steps of preparation. Also, structural preservation by crosslinking fixative depends on the speed, with which the fixing agent enters the cell. These parameters act synergistically, so it could be under exceptionally favorable conditions, which caused the markedly high degree of structural preservation in the developing young daughter cell. The fact that such a result was rather the exception and not the rule and the presence of small bacteria-like structures in the size range of 0.5 to 1 μm suggest that this particular cell happened to have been open at the junction between hypotheca and epitheca already at the moment of fixation. This allowed rapid entry of the fixative with the effect that the covering plasma membrane in the young valve domains of the daughter cells was much better preserved than in cells tightly closed against the open by the frustule. Finding exactly this cell in the SEM may be considered pure chance, but on the other hand, it helps a lot in understanding the type of micro-rupture-artifacts occurring in the areas, where a forming frustule part is encountered. In many places of this sample the plasma membrane has suffered minor lesions, which look like the peeling of sunburned skin (arrows, Figs. 18B & 18b)

When the valve gets older, it will be deployed out of the cover of epitheca. However, during the handling, some samples would get an contraction at the boundary between the valve edge and the protoplast (Figs. 19A–19C); this may be due to the uneven rigidity at the two sides of the boundary. And lesions on the brickstone like cell wall may be remnants of silica lemma, suggesting the incompletely solid valve may probably still be wrapped in SDV when extruded out.

3.1.5 Substructures of the Cell Wall

A glimpse into the inner construction of the areola chambers is only possible when the frustule is observed by the TEM-shadow imaging method, which is made transparent in analogy with an x-ray reading. But then the 3-dimensional construction have to be reconstructed through the

2-dimensional imaging, unless the frustule is cracked open (Fig. 20). In order to make the cracking and splitting more regular, tearing of freeze dried samples with adhesive tape was attempted and it yielded superior results. The torn samples reveal that the matured silica cell wall is constructed by three layers — tectum, trabeculae and foraminal layer (Fig. 20). It is suggested from Fig. 17D that the building of the layers occurs sequentially, starting with the virgae, followed by the cross walls, space-filled tectum and concluded by the foraminal base layer (Fig. 17D).

The tectum is the exterior smooth layer with porelli laid aside hexagonal linear imprints (Figs. 5a₂, 20B), which are related to hexagonal embossed ridges or ridges on the interior face of the tectum (e.g., arrow pointing to an embossment in Fig. 20B). Each embossed ridge interlinks trabeculae that support areola chambers (Fig. 20C). Thus the trabecular layer the middle section of the cell wall. These trabeculae are hexagonally arranged triangular columns as can be seen from their triangular feet regularly placed on the tectum and the foraminal layer; each foramen is surrounded by six trabeculae (Figs. 20 A & D). The shape of trabeculae is either a triangular prism or a truncated triangular pyramid (Fig. 20B).

The foraminal layer at the bottom of the cell wall is porous, where foramina are arranged regularly. Notably, there is no embossed walls on this layer (Fig. 20C). In samples treated by acid washing and CPD drying without adhesive tape peeling, the foraminal layer looks smooth. Because the organic layer has been removed during acid washing and the bottom side only shows imprints of trabecular basal feet (Fig. 20E), the appearance of this layer is similar to that of Fig. 6a₂, so one could tell it is also facing to bottom side of the cell wall. Therefore, corners of the hexagons in Fig. 20E showing triangular imprints can stem from the trabecular feet attached on the other side.

The areolate chamber construction is outlined in a model summarizing the observations in the above experiments (Fig. 21A & B). Trabeculae may shape in either a prism or a frustum (i.e., the ratio of upper edge to lower edge length is 1: 1.5). Areola construction in the girdle band is different from that in the valve with respect to the middle section (Fig. 9E vs. Figs. 9D & 17D). In the former case the middle section comprises hexagonally placed trabeculae that serve as the major structural elements, whereas in the latter there are additional longer chamber walls (septal walls) filling in between trabeculae and gradually replacing them. The valve wall thus has two types of areolae: the wall of the boundary region is the same as in the girdle band (Fig. 21B), whereas that of the polar domain is like the model shown in Fig. 21C. In other words, from

the valvar edge towards the head plate, septal walls are getting longer until they grow into the full length as trabeculae on the internal side of the tectum, transiting from the model in Fig. 21B to Fig. 21C.

3.2 TEM

The classic use of TEM is to view sectioned samples. To achieve this, samples must be fixed, dehydrated and infiltrated with epoxy-resins. The epoxy-resin hardness is adjusted according to the properties of the specimens by properly mixing hardening and softening components. Diatoms are particularly challenging with respect to the optimal hardness of the resin, because their frustule is as hard as the glass knives routinely used for ultrathin sectioning. To avoid quick dulling of the knives, a diamond knife must be used. But still, the frustules in such sections cause all sorts of scratching and splintering artifacts, which are evident in almost all sections presented here. Often fragments of the frustule are simply ripped out of the section leaving holes behind, so that the output of good sections is really small. Despite these difficulties, cross sections, longitudinal sections and grazing sections are presented here. These sections observed with TEM yield useful structural information to gain some insight into the relationship between silica deposition and the molding by membrane compartments in the course of frustule morphogenesis.

3.2.1 Structures of the Mature Frustule

Cross sections through *Odontella* cells reveal that the cytoplasm is just a very narrow layer underneath the cell wall because volume of most cells is taken up by the central vacuole. The special, chambered substructure of the cell wall, which looks like the cross section through corrugated cardboard, can be seen at medium to high magnification (Fig. 22). In some lucky longitudinal sections, the overlap zone of two girdle bands has been encountered, which can be identified by the overlapping lip (Fig. 22E, comparable to the SEM image shown in Fig. 9D). The chamber substructure of the wall is impressively demonstrated in grazing sections (Figs. 23 & 28). The longitudinal section of the horn presents helically arranged porelli in the tectum at the neck, indicating the rotating growth of areolar chambers (Fig. 23A). In the consecutive section, which cuts through the same region at a somewhat deeper level, the hexagonal shape of the

areola chamber is revealed. And also, where the section goes through the bottom layer of the areolae, the central foramen with the septal walls is evident in each of the chambers (Figs. 23B & b). When cutting longitudinally through the base of the horn, it can be seen that the entrance from the cytoplasm of the main body into the horn is unobstructed (Fig. 23C). Interestingly, the areola chambers in the valve do not seem to contain the triangular columns in the corners of the hexagonally arranged septal walls (Fig. 23b) as compared to the cracked open walls of a girdle band viewed in the SEM (Fig. 20) and also the grazing sections of a girdle band viewed in the TEM (Fig. 28A). See also the model of Fig. 21C.

3.2.2 Young Cell Wall and Membrane Morphogenesis

The structure of the SDV is very interesting in *Odontella*. Initial stages, when the virgae of tectum layer is formed, are difficult to find. Fig. 24 (A,a) presents the profiles of such a stage in a longitudinal section. It is just the edge of an SDV appearing like a flat membrane sac abutted against the plasma membrane with a small piece of silica layer in it (Fig. 24A). Higher magnification of the SDV frontier reveals some dot and streak like structures which are in the size range of actin filaments.

Whenever silica structures occur in the ultrathin sections, they are characterized by increased electron contrast, meaning that they appear darker than the average cytoplasmic structures. Therefore it is reasonable to speculate that the small vesicles with a dark granular to mesh-like content, which are encountered in the cytoplasm (Fig. 24 B & C) could be the so called silica transport vesicles (STV), as has been postulated by Schmid and Schulz (Schmid and Schulz, 1979). Fusion of these vesicles with the SDV, however, has not been observed.

Stages of SDV maturation have been observed, which allow to reconstruct the stepwise assembly of the chambered girdle band wall. At the beginning, the initial silica deposition leads to the formation of the virgae (Figs. 25 c₁ & c₂, cp. Figs. 15, 17). The virgae can be recognized as small planar strips placed in a certainly regular distance to each other. They are best represented in Fig. 15 c₁. It appears that these strips are formed first, but then evaginations of the lower silica lemma occur (Fig. 25B) and expand vertically and these vertical sacs become filled with electron-dense silica deposits, which eventually take up the shape of the vertical columns (trabeculae). The exact geometry is often obscured due to the fact that a section is tilted out of the vertical plane, for instance in Fig. 25C. An example of a nice vertical profile of a

trabecula is seen in Fig. 26b (asterisk); this image represents an older stage of frustule formation, when chambers are beginning to emerge. Those trabeculae are sometimes absent, mainly because the cutting plane is across several chambers. It is evident at these older as well as younger stages that all silica deposits are closed in by the silica lemma.

When the tectum roof lumen between the trabeculae is filling (Fig. 26), a dense cluster of interwoven small fibres is positioned under each roof of the developing chamber. This is clearly seen in Fig. 25 c₁ and c₂ but also in Fig. 26a and b and in the grazing sections (Figs. 28 and 29). Since this is a novel structure, whose nature is obscure, the descriptive term “**fibrous balls**” will be used here and throughout this work. Their potential role will be addressed in the discussion. Following the formation of the columns, the areola base layer, where a large opening (foramen) of each chamber remains, is developed by a horizontal extension of the SDV. As a consequence, the base layer will be gradually closed (red arrows, Figs. 27A, 27D), leaving only foramina, which maintain contact between the inner lumen of the areolae and the deeper cytoplasm (Figs. 26, 28). Eventually, foramina will be sealed from outside by a hyaline organic layer (Figs. 8a₂, 9E).

And finally, after all these components being nicely assembled, the mature silica cell wall is extruded. In the course of this process, the upper silica lemma fuses with the plasma membrane; the lower silica lemma becomes the new plasma membrane. However, this process of extrusion has not been observed here in the ultrathin section, only one stage was encountered where the silica lemma is beginning to break down (Fig. 29C). When the new girdle band is placed on the protoplast surface, a fibrous organic layer of variable thickness sometimes uniform (FL, Figs. 29C, 31), sometimes stratified (Fig. 30C) appears between the cytoplasm and the cell wall. When exactly this layer is formed has not been clarified here, however there is one early appearance of apparently non-siliceous material between silica deposit and silica lemma (red arrows, Fig. 27A). It is unknown either why the cytoplasm disappears in chambers of mature cell wall, since the foramina is sealed by the organic layer, which should have prevented any leakage of the cytoplasm (Fig. 27D).

3.2.3 Fibrous Balls and Fibrous Layer

When cells within epoxy-resin were tilted against the sectioning plane during the cutting process in the microtome, so called “grazing sections” were produced. These kinds of sections have

been very informative to clarify the spatial arrangement of the two sets of girdle band that occur, when hGB1 or hGB2 are forming under the cover of eGB2 (Figs. 28-31).

In the grazing section from Fig. 28, the outer girdle band wall is divided into three layers: tectum, trabeculae and the areola base layer with foramina. Next comes a pale grey fibrous layer which represents the organic layer, but it may also include the plasma membrane plus the upper silica lemma, both of which have so little contrast that they cannot be recognized at this flat cutting angle. Underneath that pale grey layer, the virgae pattern of the tectum in the maturing girdle band appears in an unprecedented clear fashion (asterisks, Figs. 28a). Further inwards into the cell wall, several triangular profiles represent the forming trabeculae and parts of the embossed ridges erected between them. It is obvious that in this maturing cell wall, the foraminal base layer has not yet been formed, so that each of the areola chambers is open and filled with cytoplasm. In order to demonstrate more clearly that all of this complicated pattern of silica deposits is enclosed in the silica lemma, the SDV lumen is manually colored in cyan (Fig. 28a). All areola chambers in the forming girdle band wall contain a fibrous ball (Fig. 28a, and details see Fig. 29B).

Since the cutting angle is the same through the outer mature and the inner immature cell wall, the pattern inside the chamber can be nicely compared (Fig. 29A & B). In the older cell wall, its embossed ridges are absent likely due to the deeper cutting; and no cytoplasm are seen inside of the chamber.

In more vertical grazing sections (Figs. 29C, 30, 31), less silica faces are seen but the fibrous layer is much more evident. In Fig. 30 a longitudinal section is shown, cutting through an area of the cell where two older girdle bands overlap each other and the inner bands also seem to be mature and placed on the cell surface, which is made obvious by the prominent fibrous layer underneath. The region where this configuration would be encountered is the advalvar side of the epitheca at a moment when hGB2 has been completed and exposed on the cell surface.

Signs of wear and tear are seen in the outer girdle band of the epitheca (Fig. 31). Possibly due to the aging, both the tectum and the bottom layer have many small irregular lesions, whereas the younger girdle band below is more smooth and of higher electron contrast. The hyaline lids in the foramina of the older girdle band have become detached from the inner rim of the foramina (Fig 31B, red arrows) and they seem to be continuous with the underlying fibrous

layer. In this example, it is also evident that the fibrous organic layer appears in two locations: (1) between the outer and the inner girdle band; (2) beneath the inner girdle band.

3.2.4 Summary of the Cell Wall Growing Process

The development of the SDV involves spatially controlled growth of the silica lemma. This produces a molded membrane compartment continuously getting larger and more complicated. Deposition of silica occurs within the lumen of this compartment and is molded by its shape.

Firstly, the virgae of tectum grow horizontally within the initial flat sac (Figs. 15, 17, 25A, 25B & 32A). Then this cisterna will extend vertically at regular intervals, but its controlling mechanism remains obscure (Fig. 32B). Afterwards, silica deposits in these vertical lumens of the evaginations, within which will develop into trabeculae and this process is pretty strictly controlled in a same length and width (Fig. 32C). In this process, how the trabeculae shape triangularly and stay with a certain size is also obscure, but it does not seem to be controlled by the surrounding membrane.

Next, a fibrous ball appears in the middle of each chamber and it is positioned like a space holder propping up beneath the horizontal lumens of membrane compartment (Figs. 25C, 32D), when silica are filling in spaces between virgae to form a complete tectum (Figs. 26, 27B, 32E). It is a clear example that silica morphogenesis of the SDV does not entirely depend on the shape of the membrane compartment. When the tectum deposition has completed, erection of cross walls between the trabeculae are formed on the internal face of the tectum.

Later, the formation of the base layer, is again dominated by the horizontal of membrane evaginations, but whether and how the position and size of the pores (foramina) are controlled by the membranes, remains obscure (Figs. 25C, 28a, 29B, 32F, 32G).

Eventually, each foramen is closed by an hyaline lid, which may be related to the fibrous organic layer. (Figs. 27A, 32H). The mechanism behind the embossment of the foraminal pore rim is unknown. After maturation, the developed SDV would be exocytosed out of the plasma membrane (Figs. 27D, 32I).

4 Discussion

The micro-morphology and inner construction of diatoms has been studied for a long time with a variety of fine-structural techniques (Crawford et al., 2001; Gebeshuber and Crawford, 2006; Kucki, 2009; Li and Volcani, 1985b; van de Meene and Pickett-Heaps, 2002; Pickett-Heaps et al., 1979; Reimann et al., 1965; Schmid, 1994; Tesson and Hildebrand, 2010b; Tiffany, 2005). Particularly the ease, with which samples can be prepared from acid-treated frustule parts, to be viewed either by scanning or by transmission electron microscopy, has helped to produce a wealth of detailed fine-structural information (Borowitzka and Volcani, 1978; Reimann et al., 1965; Reynolds, 1963; Schmid and Volcani, 1983; Tyler et al., 2006). However, achieving a satisfactory structural preservation of both cytoplasm and silica frustule in the EM sample for the study of morphogenetic stages is still a challenge ((Chiappino and Volcani, 1977), see also Section 1 in Part III). The marine species *Odontella sinensis* has only rarely been in the focus of these kinds of studies (Li and Volcani, 1985b; Pickett-Heaps et al., 1986). The current work, therefore, makes a contribution to fill this gap by focusing on the ultrastructure of this diatom species through a unique combination of several structural methods, which allow the examination of prepared specimens by either scanning or transmission electron microscopy. The aim of combined methods was to provide a view not only of intact cells from the outside, but also of partially separated cell halves after various pretreatments. A further aim was to take a look into the inside of acid-cleaned frustules from mildly extracted cells, after their cytoplasm had been preserved by fixation. Next, the intention was to examine the inner construction of the frustule wall by cracking it open to reveal the structural details in the SEM (Miller, 1969) and also by taking advantage of the frustule's semi-transparency when viewed in the TEM. These approaches were rounded up by the study of the internal ultrastructure as it appears in ultrathin sections made at various sectioning planes through the cell.

4.1 Different Treatment Effects on Diatom Structures when Preparing Samples

The study of cell structure by SEM requires three steps of specimen preparation: fixation, dehydration, drying, further followed by the application of heavy metal coat (sputtering) (Pickett-Heaps et al., 1975; Schmid and Schulz, 1979; Schmid and Volcani, 1983; Tippit and

Pickett-Heaps, 1977; Tippit et al., 1975). The aim is to produce as few structural artifacts as possible through the first three steps, but usually specimens may still suffer a certain degree of deconstruction. As to the frustule wall of diatoms, its specific microarchitecture, which could be considered a system of nested micro-spaces, creates additional diffusion barriers during the course of specimen preparation, so the treated cells are likely to encounter destructive forces causing structural artifacts during sample preparation. Further, the close spatial association between “soft” materials such as membranes and “hard” materials such as silica structures could further aggravate the situation. The diffusion of the fixative could be impeded. Osmotic imbalance between the micro-spaces could occur and the exchange of aqueous against organic solvents and eventually the exchange of acetone against liquid CO₂ could create local pressure differences. The most likely source for violent effects on microstructure in a system of nested micro-spaces would probably be the process of critical point drying (CPD), even though this method was specifically designed to avoid turbulences (Williams and Clifford, 2000). Therefore, after testing several experimental parameters, the best solution of sample preparation was chosen in this study. The images obtained (e.g., Fig. 2) prove that reasonable structural preservation has been achieved.

4.1.1 Rationale for the Choice of Various Pretreatment Regimes

Since the surface of frustule might be impregnated and/or covered by organic materials such as glycoproteins and polysaccharides (van Heurck, 1896; Kröger and Poulsen, 2008; Kröger et al., 1994; Pickett-Heaps et al., 1990), possibly as well as lipids and phenolic components, it was tested, whether pre-fixation (enzyme digestion) and post-fixation (detergent or acid wash) treatments with “softening agents” might have an influence on the structural preservation of the cells. SDS was chosen as an agent that could potentially dissolve proteins, lipoproteins and lipids (Kashyap et al., 1980; Markwell et al., 1978; Schmid and Schulz, 1979). Next, proteinase K was tested as proteolytic agent (Takeichi and Kitamura, 2009) and finally chitinase was considered useful, because chitin has been reported to exist in diatoms. It may be secreted through special pores (Herth, 1979; Herth and Barthlott, 1979) or it may be present as organic components associated with the silica wall or even as component of the organic matrix inside the frustule wall (Brunner et al., 2009; Durkin et al., 2009). Since recently chitin was also discovered at the junctions between girdle bands (Cremer & Menzel unpublished), the use of chitinase appeared particularly promising.

4.1.2 Unique Effects of Various Pretreatments

4.1.2.1 Appearance of Enzyme-digested Samples Before Fixation

As it turned out, the double enzyme digested cells before fixation have their protoplasts more easily liberated from their frustules by weakening the connecting lace at the junction between epi- and hypotheca. In a matter of hours but before the fixation, cells would be separated into two frustule halves, resulting a protoplasmic free theca and an exposed live protoplast within the other theca. It is obvious that the turgor would release alongside the axial direction rather than circumferential direction. This axially opening of the frustule provides a good opportunity to glance at the internal wall of the empty theca; hence an organic layer with fibrous nature appearance is seen attaching on the wall (e.g., Fig. 8), otherwise this layer would be concealed by being covered with cytoplasm. This digestion is a mild treatment, suitable to reveal fragile organic structures of fresh samples.

In chitinase treatment, a milder treatment, a majority of cells appear to leak at the junction of the two thecae by affecting the sealing lace and the expansion gap. The lace appears torn so the two thecae got separated but a half of protoplast is still maintained in the open frustule (e.g., Fig. 4c₃). The expansion gap in the girdle band appears to spring open revealing structures on the surface of the protoplast (e.g., Fig. 4A). The common appearance of both cases is that the pressure from the turgor may act on the girth of the frustule, and this could partially reveal the structures under frustule but maintain the completion of the cell.

Since the degradation of proteinase K is always followed by the acid wash, the degradation effects on the frustule is still unknown, although theoretically proteinase K is known to degrade proteins by cleaving the peptide bonds.

4.1.2.2 The Appearance of Cells after the Post-fixation Treatments

After the fixation, the strongest extraction effect is achieved by the additional application of KW (king's water). The common phenomenon is that no matter what treatments were applied before, once cells were washed by KW, not only cytoplasm but also the organic layer would be completely removed, so that the intact frustule would be separated into individual components and sometimes the rolling girdle bands could even be unfolded, revealing the clearest silica

cell wall with pores (Figs. 7, 8, 11, 14, 17). However, the milder treatments — SDS extraction provides a good preservation for the intact frustule, which allows unexpected views on structures and their relative locations in the intact cell.

Given that membranes had been thoroughly fixed with both aldehydes and osmium, cells subjected to SDS extraction may suffer pressure differences acting mostly in axial direction at some point during preparation, which would push out the hypotheca from the epitheca for a certain distance without large scale breakage of the membranes. The distance by which the hypotheca would slide out, depended on the developmental stage of the cell. The consequence was that regions of the cytoplasm currently harboring an SDV would become exposed and often the cytoplasmic surface distal to the SDV could also be seen (e.g., Figs 14 & 15).

The physical principle behind this phenomenon are not entirely clear, except that one could think of a yield to internal pressure, possibly made by the enzyme degradation or extraction of material or structures involved in the sealing at the hypotheca-epitheca junction. If the affection on the sealing junction does not occur, the whole frustule would simply resist the internal pressure, which would intermittently build up, but subside once the exchange of solvents has equilibrated. Due to the petri-dish like construction of the diatom frustule and due to the fact that widening of the girth of the cell is prevented by the stability of the frustule case, which means a holding structure yields against internal pressure, the intermittently internal pressure driven process have to be exerted axially, forcing hypotheca sliding out of the epitheca.

In most cases, when the protoplast slides out of the frustule after SDS extraction, a rectangular brick stone like silica wall pattern emerges on the protoplasmic surface, which represents the immature areolate chambers or parallel stripes, if they are at the virgae stages (Fig. 15). But this young silica should be covered by two membranes — the plasma membrane on the outside and the upper silica lemma beneath the plasma membrane. In other regions of the protoplasmic surface, when the membrane was exposed, it appeared wavy but still perfectly well preserved by the fixation (e.g., Fig. 14). It is supposed that in places where an SDV with a developing frustule structure was lying underneath, the soft membrane once spanning over the grid of hard silica, got stretched and broke, even crumbled in those places, which were not supported by the silica frame underneath. It seems that this is an artifact induced by mechanical rupture during the critical drying step rather than created during the process of aqueous fixation.

4.2 Overall Architecture of the Frustule

The general aspects of frustule appearance of *Odontella sinensis* have been well known, such as the compressed oval of the apical plane, the prominent cone-like shape of the two opposite, apical valves with their two different kinds of appendages inserted at the ends of the oval, saddle-shaped head plate as well as the existence and overall shape of epithecal and hypothecal girdle bands inserted between the valves. The contribution of the current work to this field of diatom architecture concerns new details of the areolate frustule wall patterns, a clearer description of the annuli as integral parts of the head plate, and further insight into the interlocking structures of girdle bands including the role of a connecting lace between epitheca and hypotheca.

4.2.1 The Head Plate and the Annuli

In *O. sinensis*, the silicification of the valve cell wall begins from developing two initial SDVs, within either of which is a LP-base plate, before the completion of cytokinesis (Li and Volcani, 1985c). The term annulus goes back to the notion of a circular pattern center, which is the primary silicification site of valve morphogenesis in centrics (Pickett-Heaps et al., 1990; Round et al., 1990). In radial centrics, some species, like *Melosira*, develops their annulus in a circular loop (Round et al., 2007), but as to *Thalassiosira* or *Coscinodiscus*, the annulus develops into a roundish region with a distinct outline (Hoppenrath et al., 2007; Schmid and Schulz, 1979; Schmid and Volcani, 1983). In phylogenetically, related bipolar centrics which possess LPs (for the principle construction of a LP, see Fig. 5 in Part III) on their valves, annuli are developed differently: some genera with a prominent LP develop their annulus in a loop, with the LP originating from it, i.e. *Ditylum* (Li and Volcani, 1984, 1988), but as to genera with two LPs, i.e. *Odontella*, the morphology of the annulus is still poorly defined. Li and Volcani proposed there are two long parallel ribs at early valve development stage in *Odontella sinensis*. These ribs extend from both apical poles towards the middle of the head plate, where they're suspected to fuse with each other. They did not use explicitly the annulus concept, however, although they seemed suggesting these parallel ribs would eventually produce a single closed annulus (Li and Volcani, 1985b).

The current work, being rather different from the interpretation by Li and Volcani, shows that each LP of *Odontella sinensis* is associated with a compressed oval at its base along the apical

axis. Each oval is perceived as two parallel ribs of silica connected at both of their ends, which is best visible from the outside in acid cleaned valves (i.e., Fig. 11B) And they are well separated from each other by a region made of scrambled areolae in between (Fig. 11b, yellow stippled lines), preventing their possible fusion. Therefore, it is confirmed here that the head plate of *Odontella sinensis* possesses two individual annuli.

4.2.2 Interlocking Structures of the Girdle Bands

Girdle bands are the means of bipolar centrals to accommodate their growth in longitudinal direction (Zhang, 2012). It is shown here that the next (new) girdle band of the hypotheca is located underneath the last epithelial girdle band (eGB2), as long as it is being fabricated in the SDV (e.g., Fig. 3B). Only after its completion and exocytosis onto the cell surface, it is pushed forward to be placed in front of the last epithelial girdle band.

In different species, their girdle band shapes are diverse — the open band, the closed band, the half band and segments only (Tomas, 1997). In *Odontella*, a hybrid band between closed and open is found. As shown in the result section, acid-cleaned girdle bands completely unroll when being fixed on a support with their outer side facing down, whereas they recoil when lying on one of their circumferential sides (e.g., Fig. 6). This suggests that they have a certain intrinsic tension like an actuated spring, which brings the two open ends together and maintains a minimum slit between them. The slit between the opposite ends of girdle band can accommodate potential expansion in the girth of protoplast, which is thus termed it here “the expansion gap”. Interestingly, the opposite edges forming the expansion gap are armored with teeth, which is nicely demonstrated in the shadow images (Fig. 7). This teeth-like structure is to ensure girdle bands are well closed to avoid any potential leakage of cytoplasm; as is shown in SEM images of the cell surface of complete cells, they are in a tightly interlocked state (Fig. 3E). It is evident that the interlocked edges are additionally sealed by some inert material, which becomes distinct, when the underlying girdle band gets strained and the expansion gap eventually pulled apart as the pressure in the cell is raised (e.g., Fig. 2a₂). The presence of a sealing substance is further supported by the fact that girdle bands unfold more readily after pretreatment with chitinase or proteinase K, whereas in cells without such treatments the edges of expansion gap remain closed.

Considering the formation and deployment mode of an individual girdle band, it is clear that the girdle band must have a smallest possible diameter when being fabricated inside the SDV,

but it gets slightly expanded when being deployed on the cell surface. Because of this necessary expansion, subsequently, it should certainly be useful that the two edges are sealed by extendable structures — interlocking teeth, which can grow from short to long (Figs. 7C₁ & 7C₂), and this sealing way can offer a strong holding because of the interactive friction. The glue would eventually be secreted to the space between teeth, possibly after the exocytosis of the girdle band but before the axial expansion.

On the other hand, the securing circumferential stability between two adjacent girdle bands is also important. As the two girdle bands must stick firmly to each other at their circumferential edges in order to adapt for any bending or other forces acting along the longitudinal axis. Here again, apparently, their arrangement is well maintained. This situation is nicely captured in a rare SEM shot presented in Fig. 9D, where the smooth abvalvar edge of one girdle band is shown to overlap with the frayed advalvar edge of the adjacent girdle band. Fine structure of the frayed edge is shown in much better detail in the shadow images (Fig. 7) but also in the SEM images of acid-cleaned girdle bands (Fig. 6). The fact that this overlap zone is always closed, i.e., seen as a single line in almost all SEM views of complete cells shown in this work (Fig. 2), suggests that it must be tightly sealed. The increased surface area provided by the frayed edge suggests the presence of a sealing glue, having the same function as discussed above for the teeth at the expansion gap. It occurs in very rare cases that a fissure is seen, for instance, between eGB1 and eGB2 in SDS-treated cell (Fig. 2C). Much more often such lesions can be discovered in chitinase-treated cells, (e.g., Fig. 5 A & B), suggesting that chitin could be a component of such sealing material.

4.2.3 Connecting Lace

At the junction between epitheca and hypotheca, we see another sealing structure, termed here “the connecting lace” (e.g., Figs. 2, 3B, 4A). Apparently this structure is non-siliceous as suggested by its soft, folded appearance. It is much thinner than the frustule wall and often seen in a burst or ruptured state, whenever the cell halves were forced apart in the course of sample treatment. The connecting lace does not entirely dissolve after enzyme treatment, so its composition must be heterogeneous, but enzyme treatment does promote the artificial sliding-out process, which is addressed in Section 4.3 in further detail.

Little attention has been paid to this detail in diatoms by previous workers, although its presence must be considered as a necessity. Considering the deployment process of girdle

bands (exocytosis and axial expansion), its function is to exert a tight grip on the junction between epitheca and hypotheca and at the same time has some flexibility when necessary. On one hand the grip of the connecting lace must be tight enough to prevent breaking of the cell in the middle between the two thecae. This should include some protective properties to defend against predation, because this junction is a potential point of being attacked by predators, like dinoflagellates employing a feeding tube (peduncle,(Schnepf and Elbrächter, 1992)). On the other hand, in order to allow the axial expansion of the next girdle band, the grip of the connecting lace must be flexible and kept this way during expansion. Subsequently it must be tightened again, when the new girdle band has reached its final position. So the “sleeve” like wrapping of the lace appears to be a flexible solution to allow girdle band slippage.

The lace may be made of elastic organic material, which gets weakened by SDS and further degraded by proteinase K and chitinase. Or probably, the lace is made by thin silica but beneath it there are massive adhesive substances, which would be weakened by the degrading process. Once the chemical composition of the connecting lace is determined in future work, the question will be answered regarding how the grip of the sleeve is regulated.

During this physical clamping process of the lace, chitin might play a role and this role will be further explored in Chapter 2, as well as the roles of some other adhesive polysaccharide or protein. It is well known that diatoms produce and secrete adhesive organic polymers (Aumeier and Menzel, 2012; Brunner et al., 2009; Herth and Zugenmaier, 1977; Pickett-Heaps et al., 1986), so in principle the biochemical capability of producing a suitable material for the dynamic sealing purposes can come quite natural in *Odontella*.

4.2.4 Immature SDV Locating beneath eGB2

The SEM (Fig. 4A) has shown that a hypothecal girdle band is located beneath eGB2 made visible through peeling off part of the cell wall. The young GB presents a brick-stone patterned cell wall, suggesting its developing state and that it is in fact lying in an immature SDV. This discovery will be further proved by the double fluorescently stained samples presented in Chapter 2. In the case of a new girdle band, it can be concluded that the extrusion process, which in cell biological terms is the exocytosis of a massive structure (see Fig. 11 of (Schmid, 1987)), will also occur underneath the cover of eGB2, possibly followed by further maturation (i.e., impregnation with organic material at its circumferential edges or expansion gaps).

The clarification of relative position between immature SDV and the epithelial cell wall in the species of *Odontella* may probably reveal a general principle that could be applied to other diatom species. Thus, there are two points worth mentioning:

The first point is that the immature SDV has its fixed position for development, always beneath the last girdle band of the epitheca. Usually, the relative position of a new girdle band in a cell is always an obscure topic in diatom research. It is considered that when a SDV becomes mature, the silica would be extruded on the surface of the protoplast via exocytosis; this process is naturally considered to occur under the cover of the parental wall as long as the new silica connects to the end of hypotheca. Consequently, sometimes a young GB-SDV would be supposed to locate beneath the eGB1, which brings the illusion that the SDV location for each hGB can be different. However, the location of the immature SDV deserves a better attention. A critical evidence is the position of the nucleus, which always stays under the new girdle band (Zhang, 2012), and has never been observed moving beyond the middle region of the frustule towards the epitheca; thus, the overlapping zone can only be in the region of the last epithelial band (eGB2), rather than the second last (eGB1), otherwise the nucleus would not be located in the middle region of the cell.

The second point is about the deployment of a new girdle band. It has been long considered that the hGB is in a state of detaching from the abvalvar edge of the previous hGB before its exocytosis, which is the way how it is presented in graphic presentations (Fig. 2 of (Kröger and Poulsen, 2008)). However, in fact, a new hGB remains connected with the previous hGB during its development in the SDV (Figs. 2C, 3C; see also the model scheme in Fig. 17 of Chapter 2).

4.3 Internal Construction of the Frustule Cell Wall

Previous work by others (Li and Volcani, 1985c; Pickett-Heaps et al., 1986) has provided some insights into the fine structures of *Odontella sinensis*, but the cell wall construction has not been addressed specifically, thus the current study makes a major contribution by reporting on this point. Information on the cell wall construction process comes from three lines of experiments. The first stems from observations of incidentally occurring cracks in the SEM samples, and of intentionally forced cracks and subsequent splitting off of frustule layers. The second comprises details seen in shadow images of acid cleaned frustule parts; the third one comes from ultrathin

sections as well as acid cleaned frustule parts analyzed by TEM.

4.3.1 Cell Wall Construction Revealed by Cracked Open Samples

In most samples prepared for the observation in the SEM there is a certain portion of cells having been damaged. One recurrent phenomenon was that the entire middle part of the girdle bands would crack and collapse onto each other, whereas the valves usually show a stronger mechanical resistance and remain largely intact except that the LPs may break off (e.g., Fig. 9). The cracks in the girdle band walls provide an opportunity to see the cross section of the wall, which reveals their chamber-like structure and the placement of small pores in the tectum and large foraminal pores in the base layer. The difference between small and large pores could even serve as a landmark for the identification of inner and outer frustule faces.

Usually, the structural context can be maintained, if the wall is broken by perpendicular cracks (e.g., Fig. 9), whereas, many samples may get shattered and their structural context may then get lost, if the wall is damaged by removing outer layer (e.g., Fig. 20C). But regarding the latter case, there are exceptions. For example, the cell wall layer can be lifted off by teasing with adhesive tape, images of unprecedented clarity of this species have been obtained, showing that inner and outer layer of the cell wall are held together by hexagonally arranged triangular columns (termed “trabeculae”). Where the layers got separated from one another, the trabecular feet remained stuck to the upper side of the foraminal base layer. On the foraminal base layer, no chamber walls (embossed ridges and septal walls) appear to be erected between trabeculae (Fig. 20D). In contrast, the view from inside onto the underside of the tectum layer shows that embossed ridges outline each chamber in the form of a regular or long hexagon (Fig. 20C).

The SEM result has revealed that the areolate patterns on the girdle band and that on the valve are different: the former presents indistinct hexagonal imprints of areolae (e.g., Fig. 5a₂), whereas the latter presents rows of rectangular chambers (e.g., Fig. 11c₁). Shadow images of the arrays of areolate chambers may help to resolve this discrepancy (for further discussion of shadow imaging see Section 4.3.2). Here it becomes clear that long narrow stripes of silica overlap with the longer sides of the chambers, obscuring two of the six corners of the hexagon thus forming the shape of a rectangle (Fig. 17D). It would be desirable to see more of such detailed structural data not only from mature frustule walls but also from the stages of frustule development, but this information is not yet available from the current cracked samples.

4.3.2 Cell Wall Construction Revealed by Shadow Imaging

Silica structures cleaned of organic components by acid wash can be easily viewed in the TEM without further preparation, because they are stable in the electron beam and they scatter electrons, which is required for producing an image in the microscope (Reimer, 2013). This imaging method is termed “shadow imaging” in this study, even though the object information obtained by it contains more than just the object outline (shadow), because the electron contrast and hence the gradation of image details depends on the density of the silica deposition or else, the silica thickness of the sample in a particular area of the object. The only drawback is that, unlike the SEM images, three-dimensional object information is lost.

Significant progress has been made throughout the years by describing frustule fine structure with this method in various diatom species (e.g., Li & Volcani, 1985, Figs. 7-9; Drum 1963, Fig. 1; Oey & Schnepf 1970, Figs. 1 & 4) but not yet in *Odontella sinensis*. Here in this chapter, the view of previously unknown details on mature frustule wall structure, and also the view of cell wall in developmental stages, are provided. Very young stages, i.e., the virgae configuration (see below Section 4.3.3.2), have not been found, probably because they are too fragile to survive during sample preparation, but as soon as the tectum has become a confluent layer and chamber walls begin to become erected, the sample is stable to survive through preparation. It is a nice option now, to be able to compare the view of the inner side of the tectum (see Section 4.3.1 above, Figs. 20c₁, 20c₂) with the shadow image shown for instance in Fig. 7B₁. They are about exactly the same object detail. The former two images were created by removing the base layer, only showing the hexagonal embossed ridges (short chamber walls) on the internal face of the tectum. The latter was preserved without being torn by tape. Its shadow outlines hexagonal ridges and traces of the virgae on the external face of the tectum when viewing from inside (Fig. 7B₁). But the absence of foraminal pore indicates that this layer is at its young stage. Moreover, the foramen could be seen through the tectum via the method of shadow imaging in a mature frustule (Fig. 7B₂), which is an additional structure when compared to the tectum at the young stage with only virgae traces (Fig. 7B₁). This provides evidence for the existence of a developmental gradient from the outside inwards until the foraminal pores are shaped in the base layer. This is further supported by the appearance of cracked open walls in acid cleaned samples (e.g., Fig. 17D).

Prominently visible in the shadow images are the porelli in the tectum. The mechanism for

their placement remains unknown. It can only be stated on the basis of the shadow images, that it occurs most of the time at the rims of the initial virgae, i.e., at a fairly early stage of frustule morphogenesis (see discussion of molding, Section 4.3.3.2 below). They are also nicely depicted in acid cleaned frustule parts (mature frustule: Fig. 10, immature frustule: Fig. 17C). The fact that they are much less noticeable in SEM images of cells not subjected to acid cleaning or SDS extraction, suggests that the tectum porelli may get covered or even closed by organic material.

4.3.3 Frustule Structure and Morphogenesis Interpreted from Ultrathin Sections

By ultrathin sectioning, aspects of the internal organization of the frustule wall can be examined. The perpendicular cuts can be directly compared with the perpendicular cracks viewed with the SEM as discussed above (see Section 4.3.1). But in addition, grazing section can be obtained, which allow to see details that are otherwise concealed.

4.3.3.1 Structure of a Cell Wall Pattern Unit — the Areola Chamber

The fine structure analysis presented in the Results section has confirmed that in the apical valve region around the horn the trabeculae in the corners of the areolate chambers remain inconspicuous, whereas the long chamber walls termed “septal walls” are prominent. The chamber walls are completely closed, spanning between foraminal layer and tectum layer without interruption (Fig. 23B). It is suggested here that this type of construction applies to all areas of the valve. In the cell wall of the girdle bands, the chamber walls are shorter and termed “embossed ridges” as has been shown in the torn samples (see above Section 4.3.1 and Fig. 20). Trabeculae are the prominent structures between tectum and foraminal base layer in the cell wall from girdle band, as evidenced by the clearly visible typical triangular cross-section in Fig. 28A, where the embossed ridges are only seen as darker linear traces attached underneath the tectum layer. These different cell walls are depicted in the model shown in Fig. 21.

The transition between these differences is difficult to assess. Certainly, as in all diatom frustules, it can be assumed that the compromise between toughness and light-weight construction has governed the design of these constructions in *Odontella sinensis* as well.

Obviously, surfaces have a steeper curvature in the overall shape of the valve than in the girdle bands, for which the trabeculae architecture as in the girdle band may not be suitable. Besides, the interlocking between opposite valves in a chain of cells could mean a higher torsional load, which could be better compensated the chambered design of the valve wall. Whereas girdle bands may be subjected to uniform pressure, which may be better compensated by a phalanx of trabeculae. This is an interesting issue, especially in the light of thousands of diatom species displaying a dazzling diversity of structural designs, probably offering multiple solutions to the same mechanical problem (Gebeshuber and Crawford, 2006).

4.3.3.2 Organic Layer

In Section 3.1.2.4, the existence of an organic layer placed between the frustule wall and the protoplasmic surface has been proposed (i.e., Fig. 8 and 9E). This particular layer is indeed identified in many of the ultrathin sections through the cells. It is fibrous in nature, of variable thickness, sometimes composed of several layers and it appears to be continuous with the lid, which closes the foraminal pore (Fig. 8a₂). Sometimes, the lid appears to be a structure in its own right, not related to the fibrous layer (cross section: Figs. 25 B&C; grazing sections: Fig. 31B). How the lids are made has not been determined here, but it maybe that the fibrous layer gets compressed onto the opening of the foraminal pores.

The organic layer between silica frustule and protoplast has been described for many diatoms (Borowitzka and Volcani, 1978; Brunner et al., 2009; Crawford et al., 2001; Drum et al., 1966; Pickett-Heaps et al., 1990; Reimann et al., 1965; Schmid, 1980, 1986a, 1986b; Schmid and Burkhardt, 1984), but its composition remains to be clarified. It could be composed of polysaccharides, reminiscent to the plant or fungal cell wall. Pectin used to be considered as one of the components of the organic layer (Pickett-Heaps et al., 1990; Reimann et al., 1965). Another compound is supposed to be chitin, since it is not only found to be secreted as fibers through secretion pores (Herth, 1979; Herth and Barthlott, 1979), but also found localizing at this layer (Durkin et al., 2009). Like plant cells, diatoms can easily undergo plasmolysis (Pollock and Pickett-Heaps, 2005), which has also been observed during the current study (data not shown). This means the organic layer probably does not act as a stabilizing structure holding the protoplast in place at the inside of the frustule, i.e. by molecular bridges reaching through the membrane into the organic layer. Instead, one function of the organic layer might be to act as a mechanical buffer against the inner frustule surface. But it could be also that it has some filtering

function restricting the access of metabolites to the protoplasm, which would find little resistance by passing through the pores in the frustule wall. Since it is not known, when exactly the organic layer is produced, it remains to be seen, whether it is continuous with the sealing material at the junctions between frustule parts or whether it is added later as kind of a maturation process.

4.3.3.3 The Morphogenesis of the Silicalemma Lumen

Examination of ultrathin section in the TEM is the only method, with which the silicalemma of the SDV can be studied. The development of an SDV is thought to involve the fusion of STVs, which would offer silicic acids and membrane materials for silica deposition and silica lemma extension (Li and Volcani, 1984; Schmid, 2005; Schmid and Schulz, 1979). As shown here, small vesicles with an electron dense content are encountered in ultrathin sections of *Odontella* (Figs. 24B, 24C). These could potentially represent the STV population. But the occurrence of an electron-dense content alone is not a sufficient proof. Unfortunately, very early stages of SDV assembly, when masses of such vesicles are supposed to fuse (Schmid, 2005; Schmid and Schulz, 1979), have not been found here in the *Odontella* cytoplasm. As we know, the other two silicic acid importation ways (SITs and diffusion, see Introduction) may guarantee the material source of silica deposition, but the source of the silicalemma is still a mystery. Perhaps, like the growth of plasma membrane, silicalemma materials may come from the endomembrane system. And since the plasma membrane and the outer silicalemma are very close to each other, there is basically no distance between them, which is too narrow for vehicle-based transportation. If there is any vesicle fusion processes going on, it should be from the cytoplasm to the inner silicalemma, may be just at the advancing edge of the SDV. This remains to be seen.

It is, however, an established fact that the SDV is the membrane compartment within which the frustule components (valves and girdle bands) are fabricated into a single large piece (Müller, 2012; Reimann et al., 1966) and for each new frustule component a new SDV is formed. It is located right underneath the plasma membrane, grows synchronously with the frustule component that is formed inside of it, and eventually encircles and encloses a large portion of protoplasm. After the frustule component has been completed, it is brought onto the cell surface by the fusion of the outer silica lemma with the plasma membrane, while the inner silica lemma takes up the function of the new plasma membrane, because the old one has been destroyed in the fusion process. The remaining protoplast will reside within the space that is provided by the

new frustule component (Pickett-Heaps et al., 1990; Schmid, 1986a, 1986b).

Before the current work was started, nothing was known on fine-structural aspects of the SDV or the silicalemma, respectively, in *Odontella sinensis*. It is shown here that at the early stage of frustule formation, the SDV starts as a flat, continuous membrane cisterna, within which the virgae will appear. As has been shown in results (see Section 3.2.2), the virgae are flat ribs of silica with an irregularly undulating margin growing in the form of large arrays of regularly spaced parallel strands. This is nicely confirmed in grazing ultrathin sections (e.g., Fig. 28). This image also shows that virgae are still in the nascent state, when trabeculae and embossed ridges are beginning to be erected as has been discussed above (see Section 4.3.2). Somewhat behind the front of such an array of virgae cross-bridges are becoming inserted between the parallel strands, by which a regular grid of rectangular squares is created and at about that time, many small pores become inserted at the margins of the virgae. The positions of the pores in the early stages of virga formation are also demonstrated in acid cleaned valves (Fig. 17) and in shadow images of young valves (Fig. 10). They are supposed to be collateral products of the self-assembly process governed by the composition of low-molecular weight metabolites such as polyamines and silica-binding protein factors alongside with silicic acid (LCPA-silaffin matrix, (Kröger and Poulsen, 2008)), which is responsible for the size and the placement of pores in the plane of a silica layer (2-dimensional level).

In the diatom literature it has been stated that the formation of specific cell wall shapes could be based on a molding process by factors influencing the shape of the SDV and the resulting lumen in the SDV would then be filled out by silica deposition (Pickett-Heaps et al., 1990). Chambers surrounded by SDV lumen could be created by spacer vesicles, such as organelles or vesicles, so that exclusion areas would be formed, where no silica could be precipitated (Schmid, 1986b, 1994).

In *Odontella*, the SDV forms a flat, continuous membrane cisterna during the phase of virga formation. When virgae are seen in cross-section (Fig. 25c₂), no conspicuous indentations into the lumen of the SDV could be detected and no place holder organelles either. For the vertical developmental step of cell wall morphogenesis, which is considered as a 3-dimensional building process, the lower silica lemma forms finger-like evaginations downwards, within which the triangular trabeculae are going to develop and the interval distance between trabeculae is always the same. It could be envisioned that specific proteins embedded in the LCPA-matrix mark the extruding position of the vertical growth. Hence the silicalemma would be stretched vertically. However, how the regular hexagonal pattern and the length of the trabeculae is

determined is unknown. It might be again controlled by a specific factor in SDV.

Moreover, the formation of trabeculae under virgae before the completion of the tectum layer may have a physical reason. Recently, the Reverse Ostwald Ripening Mechanism has been reported (Huang et al., 2017), which demonstrates that the hexagonal pattern of foams could be auto-manipulated in the presence of hexagonally arranged pillars on the surface. Thus, it seems the first occurrence of trabeculae in the tectum lumen satisfies the condition for the reverse Ostwald ripening for silica acid to form into a framework, and this can be well supported by the appearance of a hexagonal network pattern composed by chamber walls (septal walls or embossed ridges) under the tectum. Nevertheless, this auto-manipulation process requires silicic acid created as liquid foams in the SDV. According to the recent knowledge, the three possible mechanism of silicic acid importing into the SDV – STV delivery, direct transportation through the silicalemma by SITs and ionophore mediated diffusion through the silicalemma (Hildebrand, 2006) – are unlikely able to create the bubble form of silicic acid in the SDV. Hence the assumption of the Reverse Ostwald Ripening Mechanism for silica self-assembly need to be further confirmed. On the other hand, to identify the development order of trabeculae is important if the auto-assembly of silica practically depends on this physical mechanism. Because the hexagonal silica frame is a popular cell wall structure among diatoms and interestingly, there are some species reported to build trabeculae first (4.2.3.4), so it is very likely that the formation of hexagonal silica patterns in diatoms follows this Reverse Ostwald principle. In addition, this mechanism, although it is assumed here in diatom cells, coincides with the theory of Helmcke that the foamy structure of areolae is a chemical process of the precipitation of silica, arising from the gas-vesicles (Helmcke, 1959). In other words, the gas, which may mix with silicic acid in the form of bubbles, likely appears in the early stage of the multiple wall formation, i.e., the tectum formation, because the internal side of the tectum has a hexagonal network pattern (Fig. 20C).

When the trabeculae formation has been done, the empty spaces between virgae in the horizontal tectum lumen of the SDV would be further filled by silica (Fig. 25). Coming back to the idea that space holder organelles may be involved in the positioning of the areola chambers, a population of fibrous balls has been discovered in the current study at the lower side of the SDV might be built by a unique assembly of cytoskeletal proteins (e.g., Fig. 25c₁), each of them occupying a small volume of cytoplasm, which gets surrounded by the evaginating silicalemma. This scenario ends, when the vertical evaginations have been filled by silica (Fig. 27). It is tempting to speculate that these fibrous balls act as a kind of space holder, in addition they

could have the function as a mechanical support to prevent the tectum from collapsing during silica deposition. This process, however, has not yet been captured by any images so far, so that it is left to future work to identify the nature of these fibrous balls and determine their function.

In the further development of the frustule, the trabecular feet wrapped by silicalemma extend and fuse thereby completing the foraminal base layer. But there is one unknown in this step regarding the open size control of each foramen, since there are no fibrous ball like structures are seen in EM at this stage. Next, the cytoplasmic content in the areolae retracts through the foramina towards the cell body. After that, the foramina get closed by the organic layer (e.g., Figs. 27D, 30B). But this must be tested in future work. A model summarizing the events during frustule morphogenesis is shown in Fig. 32.

5 References

- Annenkov, V.V., Basharina, T.N., Danilovtseva, E.N., and Grachev, M.A. (2013). Putative silicon transport vesicles in the cytoplasm of the diatom *Synedra acus* during surge uptake of silicon. *Protoplasma* 250, 1147–1155.
- Ashworth, M.P., Nakov, T., and Theriot, E.C. (2013). Revisiting Ross and Sims (1971): toward a molecular phylogeny of the Biddulphiaceae and Eupodisceaceae (Bacillariophyceae). *J. Phycol.* 49, 1207–1222.
- Aumeier, C., and Menzel, D. (2012). Secretion in the Diatoms. In *Secretions and Exudates in Biological Systems*, (Springer, Berlin, Heidelberg), pp. 221–250.
- Badour, S.S. (1968). Experimental separation of cell division and silica shell formation in *Cyclotella cryptica*. *Archiv Für Mikrobiologie* 62, 17–33.
- Borowitzka, M.A., and Volcani, B.E. (1978). THE POLYMORPHIC DIATOM PHAEODACTYLUM TRICORNUTUM: ULTRASTRUCTURE OF ITS MORPHOTYPES^{1,2}. *J. Phycol.* 14, 10–21.
- Brunner, E., Richthammer, P., Ehrlich, H., Paasch, S., Simon, P., Ueberlein, S., and van Pée, K.-H. (2009). Chitin-based organic networks: an integral part of cell wall biosilica in the diatom *Thalassiosira pseudonana*. *Angew. Chem. Int. Ed Engl.* 48, 9724–9727.
- Chiappino, M.L., and Volcani, B.E. (1977). Studies on the biochemistry and fine structure of silica shell formation in diatoms VII. Sequential cell wall development in the pennate *Navicula pelliculosa*. *Protoplasma* 93, 205–221.
- Crawford, S.A., Higgins, M.J., Mulvaney, P., and Wetherbee, R. (2001). NANOSTRUCTURE OF THE DIATOM FRUSTULE AS REVEALED BY ATOMIC FORCE AND SCANNING ELECTRON MICROSCOPY. *J. Phycol.* 37, 543–554.

- Currie, H.A., and Perry, C.C. (2007). Silica in plants: biological, biochemical and chemical studies. *Ann. Bot.* 100, 1383–1389.
- Drum, R.W., Stuart Pankratz, H., and Stoermer, E.F. (1966). Diatomeenschalen Im Elektronenmikroskopischen Bild: Electron microscopy of diatom cells.
- Durkin, C.A., Mock, T., and Armbrust, E.V. (2009). Chitin in diatoms and its association with the cell wall. *Eukaryot. Cell* 8, 1038–1050.
- Ensikat, H.J., Ditsche-Kuru, P., and Barthlott, W. (2010). Scanning electron microscopy of plant surfaces: simple but sophisticated methods for preparation and examination. In *Microscopy: Science, Technology, Applications and Education*, J.D. A. Mendez-Vilas, ed. (Formatex Research Center), pp. 248–255.
- Gebeshuber, I.C., and Crawford, R.M. (2006). Micromechanics in biogenic hydrated silica: Hinges and interlocking devices in diatoms. *Proc. Inst. Mech. Eng. Pt. J: J. Eng. Tribol.* 220, 787–796.
- Guillard, R.R.L. (1975). Culture of Phytoplankton for Feeding Marine Invertebrates. In *Culture of Marine Invertebrate Animals*, pp. 29–60.
- Hasle, G.R. (1974). The “mucilage pore” of pennate diatoms. *Nova Hedwigia Beiheft*, 167–194.
- Helmcke, J.G. (1959). Versuch einer Gestaltsanalyse an Diatomeenschalen/Attempt at a pattern analysis of diatom shells. *Recent Adv. Bot.* 1, 216–221.
- Herth, W. (1979). The site of β -chitin fibril formation in centric diatoms. II. The chitin-forming cytoplasmic structures. *J. Ultrastruct. Res.* 68, 16–27.
- Herth, W., and Barthlott, W. (1979). The site of beta-chitin fibril formation in centric diatoms. I. Pores and fibril formation. *J. Ultrastruct. Res.* 68, 6–15.
- Herth, W., and Zugenmaier, P. (1977). Ultrastructure of the chitin fibrils of the centric diatom *Cyclotella cryptica*. *J. Ultrastruct. Res.* 61, 230–239.
- van Heurck, H.F. (1896). *A Treatise on the Diatomaceae: Containing Introductory Remarks on the Structure, Life History, Collection, Cultivation and Preparation of Diatoms, and a Description and Figure Typical of Every Known Genus, as Well as a Description and Figure of Every Species Found in the North Sea and Countries Bordering It, Including Great Britain, Belgium, &c.*
- Hildebrand, M. (2006). 10. Silicic Acid Transport and Its Control During Cell Wall Silicification in Diatoms. In *From Biology to Biotechnology and Medical Application*, pp. 159–176.
- Hildebrand, M., and Wetherbee, R. (2003). Components and control of silicification in diatoms. *Prog. Mol. Subcell. Biol.* 33, 11–57.
- Hoppenrath, M., Beszteri, B., Drebes, G., Halliger, H., Van Beusekom, J.E.E., Janisch, S., and Wiltshire, K.H. (2007). Thalassiosiraspecies (Bacillariophyceae, Thalassiosirales) in the North Sea at Helgoland (German Bight) and Sylt (North Frisian Wadden Sea) – a first approach to assessing diversity. *Eur. J. Phycol.* 42, 271–288.
- Huang, Z., Su, M., Yang, Q., Li, Z., Chen, S., Li, Y., Zhou, X., Li, F., and Song, Y. (2017). A

general patterning approach by manipulating the evolution of two-dimensional liquid foams. *Nat. Commun.* **8**, 14110.

Kaczmarek, I., Irena, K., Margaret, B., Benoit, A.C., and Medlin, L.K. (2006). MOLECULAR PHYLOGENY OF SELECTED MEMBERS OF THE ORDER THALASSIOSIRALES (BACILLARIOPHYTA) AND EVOLUTION OF THE FULTOPOORTULA1. *J. Phycol.* **42**, 121–138.

Kashyap, M.L., Hynd, B.A., and Robinson, K. (1980). A rapid and simple method for measurement of total protein in very low density lipoproteins by the Lowry assay. *J. Lipid Res.* **21**, 491–495.

Kröger, N., and Poulsen, N. (2008). Diatoms-from cell wall biogenesis to nanotechnology. *Annu. Rev. Genet.* **42**, 83–107.

Kröger, N., and Sumper, M. (1998). Diatom cell wall proteins and the cell biology of silica biomineralization. *Protist* **149**, 213–219.

Kröger, N., Bergsdorf, C., and Sumper, M. (1994). A new calcium binding glycoprotein family constitutes a major diatom cell wall component. *EMBO J.* **13**, 4676.

Kucki, M. (2009). Biological Photonic Crystals: Diatoms: Dye Functionalization of Biological Silica Nanostructures.

Li, C.-W., and Volcani, B.E. (1984). Aspects of Silicification in Wall Morphogenesis of Diatoms. *Philos. Trans. R. Soc. Lond. B Biol. Sci.* **304**, 519–528.

Li, C.-W., and Volcani, B.E. (1985a). Studies on the biochemistry and fine structure of silica shell formation in diatoms IX. Sequential valve formation in a centric diatom, *Chaetoceros rostratum*. *Protoplasma* **124**, 30–41.

Li, C.-W., and Volcani, B.E. (1985b). Studies on the biochemistry and fine structure of silica shell formation in diatoms. *Protoplasma* **124**, 10–29.

Li, C.-W., and Volcani, B.E. (1985c). Studies on the biochemistry and fine structure of silica shell formation in diatoms X. Morphogenesis of the labiate process in centric diatoms. *Protoplasma* **124**, 147–156.

Li, C.-W., and Volcani, B.E. (1988). Aberrant valve formation in a centric diatom, *Ditylum brightwellii*. *Protoplasma* **145**, 1–6.

Mann, S., and Perry, C.C. (1986). Structural aspects of biogenic silica. *Ciba Found. Symp.* **121**, 40–58.

Markwell, M.A., Haas, S.M., Bieber, L.L., and Tolbert, N.E. (1978). A modification of the Lowry procedure to simplify protein determination in membrane and lipoprotein samples. *Anal. Biochem.* **87**, 206–210.

Medlin, L.K., Crawford, R.M., and Andersen, R.A. (1986). Histochemical and ultrastructural evidence for the function of the labiate process in the movement of centric diatoms. *British Phycological Journal* **21**, 297–301.

van de Meene, A.M.L., and Pickett-Heaps, J.D. (2002). VALVE MORPHOGENESIS IN THE

CENTRIC DIATOM PROBOSCIA ALATA SUNDSTROM1. *J. Phycol.* 38, 351–363.

Miller, U. (1969). Fossil Diatoms Under the Scanning Electron Microscope: A Preliminary Report.

Müller, W.E.G. (2012). *Silicon Biomineralization: Biology — Biochemistry — Molecular Biology — Biotechnology* (Springer Science & Business Media).

Oey, J.L., and Schnepf, E. (1970). Über die Auslösung der Valvenbildung bei der Diatomee *Cyclotella cryptica*. *Archiv Für Mikrobiologie* 71, 199–213.

Perry, C.C. (2003). Silicification: The Processes by Which Organisms Capture and Mineralize Silica. *Rev. Mineral. Geochem.* 54, 291–327.

Pickett-Heaps, J.D., McDonald, K.L., and Tippit, D.H. (1975). Cell division in the pennate diatom *Diatoma vulgare*. *Protoplasma* 86, 205–242.

Pickett-Heaps, J.D., Tippit, D.H., and Andreozzi, J.A. (1979). Cell division in the pennate diatom *Pinnularia*. V. Observations on live cells. *Biologie Cellulaire.* 35, 295–304.

Pickett-Heaps, J.D., Hill, D.R.A., and Wetherbee, R. (1986). CELLULAR MOVEMENT IN THE CENTRIC DIATOM *ODONTELLA SINENSIS*. *J. Phycol.* 22, 334–339.

Pickett-Heaps, J.D., Schmid, A.M.M., and Edgar, L.A. (1990). The cell biology of diatom valve formation. 7, 1–168.

Pollock, F.M., and Pickett-Heaps, J.D. (2005). Spatial determinants in morphogenesis: recovery from plasmolysis in the diatom *Ditylum*. *Cell Motil. Cytoskeleton* 60, 71–82.

Reimann, B.E., Lewin, J.C., and Volcani, B.E. (1965). STUDIES ON THE BIOCHEMISTRY AND FINE STRUCTURE OF SILICA SHELL FORMATION IN DIATOMS. I. THE STRUCTURE OF THE CELL WALL OF *CYLINDROTHECA FUSIFORMIS* REIMANN AND LEWIN. *J. Cell Biol.* 24, 39–55.

Reimann, B.E., Leivin, J.C., and Volcani, B.E. (1966). STUDIES ON THE BIOCHEMISTRY AND FINE STRUCTURE OF SILICA SHELL FORMATION IN DIATOMS. II. THE STRUCTURE OF THE CELL WALL OF *NAVICULA PELLICULOSA* (BRÉB.) HILSE. *J. Phycol.* 2, 74–84.

Reimer, L. (2013). *Transmission Electron Microscopy: Physics of Image Formation and Microanalysis* (Springer).

Reynolds, E.S. (1963). The use of lead citrate at high pH as an electron-opaque stain in electron microscopy. *J. Cell Biol.* 17, 208–212.

Ross, R., Cox, E.J., Karayeva, N.I., Mann, D.G., Paddock, T.B.B., Simonsen, R., and Sims, P.A. (1979). An amended terminology for the siliceous components of the diatom cell. *Nova Hedwigia Beiheft* 64.

Round, F.E., Crawford, R.M., and Mann, D.G. (1990). *The diatoms: biology and morphology of the genera*, ix, 747p. Cambridge University Press, 1990. Price £125.00. *J. Mar. Biol. Assoc. U. K.* 70, 924.

Round, F.E., Crawford, R.M., and Mann, D.G. (2007). *Diatoms: Biology and Morphology of the*

Genera (Cambridge University Press).

Schmid, A.M. (1979). The development of structure in the shells of diatoms. *Nova Hedwigia* 64, 236.

Schmid, A.M.M. (1980). Valve morphogenesis in diatoms : A pattern-related filamentous system in pennates and the effect of APM, colchicines and osmotic pressure. *Nova Hedwigia* 33, 811–847.

Schmid, A.M.M. (1986a). Organization and function of cell structures in diatoms and their morphogenesis. E. Richard. M, ed. (O. Koeltz, Koenigstein), pp. 271–292.

Schmid, A.M.M. (1986b). Wall morphogenesis in *Coscinodiscus wailesii* Gran et Angst. II. Cytoplasmic events of valve morphogenesis. E. Richard. M, ed. (O. Koeltz, Koenigstein), pp. 293–314.

Schmid, A.-M.M. (1987). Morphogenetic Forces in Diatom Cell Wall Formation. In *Cytomechanics*, pp. 183–199.

Schmid, A.-M.M. (1994). Aspects of morphogenesis and function of diatom cell walls with implications for taxonomy. *Protoplasma* 181, 43–60.

Schmid, A.-M.M. (2005). THE WALL & MEMBRANE SYSTEMS IN DIATOMS: COMMENT IN REPLY TO MEDLIN (2004). *Diatom Res.* 20, 211–216.

Schmid, A.M.M., and Burkhardt, B. (1984). Schalenmorphogenese in Diatomeen/Valve morphogenesis in diatoms. *Diatoms I, Shells in Nature and Technics Communications of inst.*, 300–317.

Schmid, A.-M.M., and Schulz, D. (1979). Wall morphogenesis in diatoms: Deposition of silica by cytoplasmic vesicles. *Protoplasma* 100, 267–288.

Schmid, A.-M.M., and Volcani, B.E. (1983). WALL MORPHOGENESIS IN COSCINODISCUS WAILESII GRAN AND ANGST. I. VALVE MORPHOLOGY AND DEVELOPMENT OF ITS ARCHITECTURE1. *J. Phycol.* 19, 387–402.

Schnepf, E., and Elbrächter, M. (1992). Nutritional strategies in dinoflagellates: A review with emphasis on cell biological aspects. *Eur. J. Protistol.* 28, 3–24.

Sims, P.A., Mann, D.G., and Medlin, L.K. (2006). Evolution of the diatoms: insights from fossil, biological and molecular data. *Phycologia* 45, 361–402.

Spurr, A.R. (1969). A low-viscosity epoxy resin embedding medium for electron microscopy. *J. Ultrastruct. Res.* 26, 31–43.

Sumper, M., Manfred, S., and Nils, K. (2004). Silica formation in diatoms: the function of long-chain polyamines and silaffins. *J. Mater. Chem.* 14, 2059–2065.

Takeichi, T., and Kitamura, O. (2009). Detection of diatom in formalin-fixed tissue by proteinase K digestion. *Forensic Sci. Int.* 190, 19–23.

Tesson, B., and Hildebrand, M. (2010a). Extensive and intimate association of the cytoskeleton with forming silica in diatoms: control over patterning on the meso- and micro-scale. *PLoS One*

5, e14300.

Tesson, B., and Hildebrand, M. (2010b). Dynamics of silica cell wall morphogenesis in the diatom *Cyclotella cryptica*: substructure formation and the role of microfilaments. *J. Struct. Biol.* **169**, 62–74.

Thamatrakoln, K., and Kustka, A.B. (2009). When to say when: can excessive drinking explain silicon uptake in diatoms? *Bioessays* **31**, 322–327.

Tiffany, M.A. (2005). Valve development in the diatom family Asterolampraceae H. L. Smith 1872. *Micropaleontology* **51**, 217–258.

Tiffany, M.A. (2008). VALVE DEVELOPMENT IN AULACODISCUS. *Diatom Res.* **23**, 185–212.

Tiffany, M.A. (2015). Valve and girdle band morphogenesis in the pseudocellate diatom species *Biddulphia biddulphiana* J.E. Smith (Boyer) and *Isthmia nervosa* Kütz. *Nova Hedwigia Beiheft* **144**, 61–95.

Tippit, D.H., and Pickett-Heaps, J.D. (1977). Mitosis in the pennate diatom *Surirella ovalis*. *J. Cell Biol.* **73**, 705–727.

Tippit, D.H., McDonald, K.L., and Pickett-Heaps, J.D. (1975). Cell division in the centric diatom *Melosira varian*. *Cytobiologie* **12**, 52–73.

Tomas, C.R. (1997). *Identifying Marine Phytoplankton* (Academic Press).

Tyler, J.J., Leng, M.J., and Sloane, H.J. (2006). The effects of organic removal treatment on the integrity of $\delta^{18}\text{O}$ measurements from biogenic silica. *J. Paleolimnol.* **37**, 491–497.

Van de Meene, A.M.L., and Pickett-Heaps, J.D. (2004). Valve morphogenesis in the centric diatom *Rhizosolenia setigera* (Bacillariophyceae, Centrales) and its taxonomic implications. *Eur. J. Phycol.* **39**, 93–104.

Williams, J.R., and Clifford, A.A. (2000). *Supercritical Fluid Methods and Protocols*.

Willis, L., Cox, E.J., and Duke, T. (2013). A simple probabilistic model of submicroscopic diatom morphogenesis. *J. R. Soc. Interface* **10**, 20130067.

Zhang, Y. (2012). Girdle Band Formation of *Odontella sinensis*. Master thesis. Faculty of Mathematics and Natural Sciences. Universität Bonn.

Chapter 2

Frustule Morphogenesis, Cell Cycle Activities and Cytoskeleton Dynamic

Abstract

A handy approach has been developed for the centric diatom *Odontella sinensis* to visualize newly made silica, microtubules and actin filaments in the same cell. The silica structures of the frustule have been live-stained by the fluorescent probes PDMPO and HCK-123 for various periods of time throughout the cell cycle to monitor the progression of frustule morphogenesis. After fixation of these fluorescently labelled cells, the cytoskeleton has been identified by immunofluorescence using antibodies directed against α -tubulin and actin. A perinuclear microtubule system and a complex actin cytoskeleton including axial bundles and a circumferential ring are described. The configuration of both, the microtubules and the actin bundles system go through dramatic stage-specific changes. A presumptive model at the intact cellular level is presented, interpreting the spatial relationship between the actin ring and the developing SDV. In addition with the dynamics of microtubules, another model is presented, interpreting the features and intracellular dynamics of the cytoskeleton in conjunction with frustule morphogenesis. In addition, chitin staining data are presented, which helps to interpret the anchoring of the actin ring at a specific intracellular location.

1 Introduction

1.1 The Composition of the Diatom Cytoskeleton

The cytoskeleton is a feature common to all eukaryotic cells, although there are differences between animals, plants, fungi and protists (Baskin, 2015; Schliwa, 1986). For instance, actin filaments and microtubules are found in both animals and plants, whereas intermediate

filaments (IFs) are found in vertebrates as well as lower animals, perhaps also in some plants, fungi and some unicellular organisms (Menzel, 1993; Traub, 2012), but have not yet been reported in diatoms, although the host ancestor of diatoms, a heterokont flagellate, which should be considered a primitive protist might have had some ancestral forms of coiled-coil proteins related to subunits of IFs, which then could have persisted in the extant diatoms, or there might be emerging vimentin-like coiled coil proteins or possibly lamins in some of the present types of protists, but all of this is yet controversial (Preisner et al., 2018). A similar situation applies to septins as well as to the microtubule-based motor protein dynein, but it should be mentioned, that homologous genes for septin (Yamazaki et al., 2013) as well as genes coding for dynein are present in diatoms (Wickstead and Gull, 2007).

The status of the cytoskeleton on the whole is less clear in protist groups, i.e. *Rhizaria* and *Excavata* (Dawson and Paredez, 2013). One of the protist groups, the *Chromalveolata*, to which heterokonts (synonymous of "*Stramenopiles*", including diatoms), *Haptophytes* and *Cryptophytes* belong, is a large and diverse assemblage of organisms (Andersen, 2004). The cytoskeleton composition in these subgroups are largely unexplored except for fine structural studies, where microtubules have often been encountered and studied in some detail (e.g., (Yamagishi and Kawai, 2012). The same goes for diatoms, which have arisen from a secondary symbiosis between a heterokont unicellular predator and a unicellular red alga (Nozaki, 2005). It is reasonable to speculate that the heterokont heritage should leave its mark on the characteristics of the diatom cytoskeleton, and some of this is beginning to emerge, although we are far from understanding it (Aumeier et al., 2015).

1.2 Current Background on the General Architecture and Function of the Diatom Cytoskeleton

Since the past decades, frustule structure and the cytoskeleton in different diatom species have been reported by observations largely using light microscopy, SEM, TEM (Badour, 1968; Oey and Schnepf, 1970; Schmid, 1979a, 1994; Schmid and Volcani, 1983; Tiffany, 2005, 2008, 2015), AFM (Tesson and Hildebrand, 2010a, 2010b) or confocal microscopy (Annenkov et al., 2013; van de Meene and Pickett-Heaps, 2002; Van de Meene and Pickett-Heaps, 2004). These

studies can be divided into two main groups — (1) function of cytoskeletal architectures with respect to mitosis and cytokinesis and (2) with respect to SDV¹ development at interphase.

(1) It is well known that microtubules radially converge onto a microtubule center (MC, this term is specifically used for the MTOC in diatoms) on top of the interphase nucleus. When entering mitosis, the MC will be replaced by a pair of polar complexes (PCs), which then will get separated from one another by an extending palisade of microtubules forming in between, becoming the central spindle (Pickett-Heaps and Tippit, 1978). Such an operation system of microtubules during the cell cycle is obviously different to that in other types of cells, like animals, yeasts and higher plants (De Martino et al., 2009). It is remarkable that while structure and function of the mitotic spindle in diatoms has been addressed extensively in the past (Pickett-Heaps 1998 and literature cited therein), there is a big gap with respect to cytokinesis. Although it has been reported several times in the past that cytokinesis is a furrowing (Pickett-Heaps et al., 1984, Pickett-Heaps 1991), and there is a long held opinion that actin is involved in the contractile process (Pickett-Heaps et al., 1990), there had been no proof until now (see results of this chapter) for the presence of actin in the cleavage furrow.

(2) At interphase, the cytoskeleton has been long considered to be involved in silicon transportation and according to that concept the intracellular source of silicic acid for silica deposition in the SDV may come from silicon transport vesicles (STVs) (Schmid and Schulz, 1979). However, more recently the direct membrane transport via silicon transporters (SITs), ionophore-mediated diffusion or electrophoretic transportation across the silicalemma has been brought into the discussion (Thamatrakoln and Kustka, 2009). Different to the last three recent modes, if the STV transportation is adopted by the cell, between the donor and acceptor compartments, cytoskeletal tracks and motor proteins should be required to transport the STVs. As to this aspect, microtubules were once suggested to be involved in silicon-transport (Gordon and Drum, 1994; Schmid, 1980), but microtubule-inhibitions proved that silicification can occur without the presence of microtubules (Schmid, 1994; Schmid et al., 1996; Wordeman et al., 1986). Since the other transportation ways may occur in the cell at the meanwhile, the microtubule inhibition cannot prove whether microtubules are responsible for the STV-transportation. Hence, the way of STV transportation in diatoms still require a further exploration.

¹ The silicification in the diatoms occurs at interphase, taking place in an organelle named silica deposition vesicle (SDV), where orthosilicic acid is deposited into silica nanobeads.

A different consideration is that the cytoskeleton may be involved in frustule morphogenesis at meso- and microscale, since silica particles generated on the nanoscale from silicic acid mixed with the organic matrix within the SDV (Currie and Perry, 2007; Kröger and Poulsen, 2008; Mann and Perry, 1986) do not themselves control the species-specific ornamentation of the frustule. Since microtubules appear to be closely attached to SDVs, they have been suggested to affect the pattern formation of the valve for instance by mediating the localization of the raphe (Schmid, 1979b, 1980, 2003), the labiate processes (LPs, sharp hollow spines, (Crawford and Schmid, 1986; Schmid, 1984a, 1984b; Tesson and Hildebrand, 2010a)), or the central positioning of the valve SDV (Tesson and Hildebrand, 2010a). Microtubules have also been suggested to shape the SDV into a flat membrane cisterna (Pickett-Heaps et al., 1988), such as those seen in the growing setae of *Chaetoceros* (Li and Volcani, 1985a; Pickett-Heaps et al., 1990), the growing proboscis of *Proboscia* (Fig. 4, (van de Meene and Pickett-Heaps, 2002)) or alongside the emerging raphe of raphid diatoms (Pickett-Heaps et al., 1979a, 1988). However, the elongation of the long narrow labiate processes and some other types of spines do not require microtubules (Crawford and Schmid, 1986; Pickett-Heaps et al., 1990; Schmid, 1984a). As to the actin cytoskeleton, its cellular localization is quite different from that of microtubules. One of the common actin structures of diatoms is the actin ring. In the EM observations, an actin filament bundle, shown in cross section as a group of dots, has firstly been reported to be located alongside the edge of the valve-SDV in the pennate diatom *Pinnularia*, although this has only casually been describe alongside with many other fine structural details (Pickett-Heaps et al., 1979a). The same has been subsequently reported in some other pennate and centric diatoms (Edgar and Pickett-Heaps, 1984; Pickett-Heaps et al., 1990; Schmid, 1980), but its composition was as yet uncertain. By using fluorochrome-conjugated phalloidin- or phalloidin-labelling, van de Meene & Pickett-Heaps (van de Meene and Pickett-Heaps, 2002; Van de Meene and Pickett-Heaps, 2004) as well as Tesson & Hildebrand (Tesson and Hildebrand, 2010a, 2010b) visualized the ring at the valve SDV edge in 4 centric and one pennate species, which confirmed that the composition of the ring is made of actin. All of these evidences explain the actin ring is a feature typical for the diatom valve morphogenesis (for the functional significance of this finding see Chapter 3). Whether the ring plays a role in expanding and shaping the SDV (Pickett-Heaps et al., 1990, 1979a; Tesson and Hildebrand, 2010a) is still open to conjecture. The other actin structures are the radial array of actin filaments around the nucleus and the cortical actin network: Both of them are present in the plane of the valve-SDV best demonstrated in *Coscinodiscus* (because this species is always oriented to the observer in valve view); the radial array has been

suggested to be involved in mediating the formation of ribs in the valve (Tesson and Hildebrand, 2010a, 2010b), while the network has been supposed to shape the SDV before the silica deposition occurs and stabilize it until the completion of silica deposition (Tesson and Hildebrand, 2010b).

In general, it is clear that some features of the cytoskeleton have been described in different diatom species at some detail, however, very little is known at the system level on the relationship between the actual process of cell morphogenesis and the cytoskeleton in a complete cell cycle.

1.3 Observing Frustule Structures and Cytoskeleton of *O. sinensis* by Fluorescence Microscopy

The frustule structures of *O. sinensis* have occasionally been studied, focusing on the growing process of LPs observed by EM (Li and Volcani, 1985b; Pickett-Heaps et al., 1990). Further fine structure details of the frustule at interphase have been observed in the current work (see Chapter 1). However, cytoskeleton structures are often not well preserved in TEM samples and their 3-D distribution is difficult to judge from single sectioning planes. Therefore, to observe the complete cytoskeleton architecture, it would be best to employ methods, which allow to image specifically labelled structures within the intact cell.

One of the most modern approaches would be the gene transformation technology using GFP-fusion constructs, which can visualize specific structures in live cells (see for instance (Mathur, 2007)). However, so far this is not a routine approach in diatoms, because it requires knowledge of the sequence of useful protein candidates for fusion with GFP, and this has been successful only in a few cases of proteins (e.g., cingulin) resident in the frustule (Kröger and Poulsen, 2008). Or by chance heterologous gene transformation works using highly conserved gene sequences of cytoskeletal proteins derived from foreign organisms such as the actin-probe “lifeact” (Aumeier et al., 2015). In the present study, such approaches had not been available yet, therefore a combination of traditional fluorescent labeling techniques has been applied.

1.3.1 Silica Probes

With the discovery of the usefulness of silica probes in live-staining of the diatom frustule, new tools have become available to study frustule morphogenesis. These probes can simply be dissolved in the culture medium and applied for desired periods of time to cover specific phases or the entire cell cycle.

Agents called LysoSensor and LysoTracker, originally used as fluorescent pH indicators, are able to selectively accumulate in acidic organelles, e.g., the animal lysosomes, though their retention mechanism is not clear (Life Technologies Corporation, 2013). In the field of diatom research, the agent "lysosensor yellow/blue DND-160" (which is also known as PDMPO) and the agent "lysotracker yellow HCK-123" are used as fluorescent probes to detect newly made silica (Desclés et al., 2008; Kucki, 2009; Martínez et al., 2014; Parambath et al., 2016). Other fluorescent probes for silica staining have also been applied: i.e., Rhodamins (Kucki, 2009; Kucki and Fuhrmann-Lieker, 2012; Li et al., 1989) can stain developing silica, but they have problems in accumulating effectively and dissolving in aqueous solution. FITC-silane (Desclés et al., 2008) not only stains silica but also extracellular organic matrix. Whereas, the agent NBD-N2 (Annenkov et al., 2013) has similar labelling properties as lysosensors, but has not become as popular.

As a representative of the silica probes, PDMPO has also been applied to track silica in other cell types, such as a lower vascular land plants — fern (Law and Exley, 2011), the marine protist — *Radiolaria* (Ogone et al., 2009). Its functional character in tracking silica in diatoms has been studied a lot. When the PDMPO concentration in the culture is at 1 μM , the visible fluorescence in developing silica of *Navicula salinarum* will emerge in about 20 minutes, which then will become stronger as the incubation time takes longer, until the silicification process is terminated (Hazelaar et al., 2005). The fluorescent stain can remain in the silica even after the frustule component has been released from the SDV (Hazelaar et al., 2005) and such staining of the silica even survives double aldehyde fixation (Zhang, 2012), but the stain in the organelle lumen (e.g., vacuoles, which also accumulate PDMPO because of their acidic content) cannot (Shimizu et al., 2001a). The retention mechanism of PDMPO in silica has been suggested to involve binding to undissociated Si-OH residues, which is the physical state of the developing silica deposits in the acidic SDV of living cells (Parambath et al., 2016). PDMPO exhibits both dual-excitation and dual-emission spectral peaks depending on the pH (the PDMPO stain exhibits yellow fluorescence in acidic organelles, whereas it is blue in less acidic organelles). In

diatoms, these two peaks combine resulting in the turquoise/green fluorescence, whereas HCK-123 does not exhibit the dual emission spectrum but simply fluoresces in a yellow/golden color.

In the past, numerous ornamentations of valves and shapes of girdle bands have been described and this is still in the focus of modern research (Chen et al., 2010; Ferrara et al., 2016), but research on the insertion mechanism of girdle bands during diatom growth has not yet been reported. Girdle band insertion has come into focus for the first time in my recent work (see Fig. 10, Zhang, 2012), where I applied PDMPO to living cells of *Odontella*. The study showed that silica deposition starts from a narrow ring, which then continues to grow in the longitudinal axial direction until reaching to the same size as other bands; the new band has always been in a row with the other hypothecal bands since its growth initiation. But using a single type of lysosensor dye one sometimes cannot identify, whether a girdle band in full size is of hypothecal or epithecal origin. Therefore, employing two different fluorescent agents allow to clarify the sequential order of the silica deposition and the relative spatial position of girdle bands between the two thecae of the diatom frustule.

Whether or not fluorescent silica probes possibly interfere with the intensity, quality or the fabrication timing of frustule morphogenesis, which may lead to the retardation or aberrance of the cell cycle, when compared with those of unstained cells, is not known. The data obtained here indicate that frustule morphogenesis proceeds normal in the presence of the fluorescent probes.

1.3.2 Double Immunolabeling in Lysosensor Stained Cells of *O. sinensis*

In the recent work (Zhang, 2012), the entire cell cycle of *O. sinensis* has been time-lapse-recorded by inverted light microscopy, which helped to define the consecutive order of stages but without visualizing the developing SDV, the nucleus and the cytoskeleton.

Tesson and Hildebrand (Tesson and Hildebrand, 2010a, 2010b) have followed a similar idea using *Coscinodiscus*, *Cyclotella* and *Surirella*, but in a different way. They were using lysosensor staining and combined this either with anti-tubulin immunolabeling of microtubules or with phalloidin-fluorochrome labelling of F-actin, but they did not combine all three. Phalloidin labelling of F-actin has been employed in several previous studies by van de Meene and Pickett-Heaps (van de Meene and Pickett-Heaps, 2002; Van de Meene and Pickett-Heaps,

2004), but also by Poulsen and coworkers (Poulsen et al., 1999) with limited success, because it stained only the most prominent actin structures and the spatial resolution was low. The other disadvantage was, that phallotoxin labelling and tubulin-immunolabeling could not be combined.

In preliminary experiments the most suitable heterologous antibodies against alpha tubulin and actin were identified (Aumeier, 2014; Polinski, 2012; Zhang, 2012, 2013), which in the present work are used together and in combination with lysosensor staining and DNA-staining. In this way, the structural correlation among SDV development, nuclear stage and the cytoskeleton can be studied in greater details that was impossible in the past.

1.3.3 Chitin Probes

Chitin, a group of amino-polysaccharides (N-acetylglucosamine in β -1,4-linkage), has been found in many diatom species either by structural, biochemical or biophysical evidence (Brunner et al., 2009; Imai et al., 2003; McLachlan et al., 1965; Morin et al., 1986; Tesson et al., 2008).

It is also known for a long time that centric diatoms, in order to increase the buoyancy (Herth, 1979; Herth and Barthlott, 1979; Herth and Zugenmaier, 1977; McLachlan et al., 1965), can secrete chitin fibrils through pores by the action of chitin synthase localized in the plasma membrane (Blackwell et al., 1967; Herth, 1978; Herth et al., 1986). These pores that specifically secrete chitin are strutted processes (Hasle, 1968) (also called fulcra (Ross and Sims, 1972)). Whereas, other pores like labiate processes (Hasle, 1972) (also called rimoprotula (Ross and Sims, 1972)), ocellate elevations (also called horns), pseudo-raphes (only in araphid diatoms), and raphes (only in raphid diatoms) are reported to secrete mucilage. The mucilage is secreted as adhesive pads between sibling cells, as stalks to anchor cells at a place (see the review in section 4.1 from (Pickett-Heaps et al., 1990)), or as adhesive nanofibres for the cell gliding motility. Therefore, one should distinguish the difference between chitin and mucilage and their secreting structures or secreting locations.

Genes of chitin synthase enzymes have been studied in the diatom *Thalassiosira pseudonana* revealing synthase members with regular domain structure but also some unusual members, i.e., chimeric forms of chitin synthase, which are composed by an N-terminal myosin head facing inside of the cell and the enzymatic synthase domain facing outside (Durkin et al., 2009). It is possible that the myosin head has a function in intracellular trafficking of chitin synthase but it could also have to do with positioning the enzyme in a specific domain of the

plasma membrane, i.e. right underneath a secretory pore. Similar chitin-myosin chimeric forms exist also in fungi (Tsuizaki et al., 2009), yeast, sponges (Ehrlich et al., 2010a, 2010b), bivalve mollusks and other invertebrates (Mulisch, 1993; Schönitzer et al., 2011; Takeshita et al., 2002).

In *O. sinensis*, many mucilage vesicles have been found to aggregate at the cytoplasmic side of the labiate processes (LPs) and some in the lumen of the horns, but only the LPs are found to secrete mucilage, which can be specifically stained by Alcian Blue (Pickett-Heaps et al., 1986). But as suggested by Pickett-Heaps and co-worker (Pickett-Heaps et al., 1990), LPs and horns should not be the structures to secrete chitin.

In the previous chapter, based on effects of chitinase or chitinase-protease K treatment, chitin is suggested to be the sealing materials between junctions of frustule components. Besides, in the recent work (Zhang, 2012), chitin was also shown to be a component spreading in the space between the inner wall of the frustule and the plasma membrane in *Odontella* (but absent in LPs), and it was also prominent at the junctions between frustule components, based on Calcofluor White staining, thus supporting the role as a sealing material. However, this staining substance is not entirely specific, because it binds to all beta-hydroxy-linked polysaccharides (Herburger and Holzinger, 2016; Rasconi et al., 2009). In order to determine, whether the Calcofluor signal is caused by chitin, a more specific histochemical agent should be employed.

To this end a fluorochrome-conjugated wheat germ agglutinin (WGA), which is highly specific for chitin (Herburger and Holzinger, 2016; Rasconi et al., 2009) was used as a probe to confirm this finding and narrow it down to the identification of chitin as the major responsible polysaccharide. This may not exclude the presence of other polysaccharides or glycoproteins, although there is no data available for that in *Odontella*, except the general information that the capability is well known in all diatoms for the secretion of all sorts of polysaccharides and adhesive organic materials (Aumeier and Menzel, 2012).

2. Materials and Methods

2.1 Culturing

Cells were cultured in the condition that described in Section 2 of Chapter 1.

2.2 Fluorescent Staining on SDV

2.2.1 Single Silica Probe Staining in Live Cell

According to tests, the minimum of the final concentration of PDMPO (1 mM stock solution mixed in DMSO, LysoSensor Yellow/Blue DND-160, $C_{20}H_{22}N_4O_3$, Invitrogen, UK) in *Odontella sinensis* is 0.5 μM ; otherwise (e.g., 0.25 μM , data not shown), the staining pattern of the silica structure looks like patches. PDMPO were dissolved in 10 ml f/2 culture medium to yield a final concentration of 0.5 μM ; alternatively, HCK-123 (1 mM stock solution mixed in DMSO, Yellow-HCK-123, $C_{16}H_{24}N_6O_4$, Life Technologies, UK) were applied in the 10 ml f/2 culture to also reach a final concentration of 0.5 μM . Cells were collected from an exponentially growing culture and then incubated in PDMPO medium or HCK-123 medium, which then were placed at 16°C culture room conditions under 700 lux cool white fluorescent light for photoperiods varying between 12 and 12 h. The exact incubation regime will be indicated in the figure legends. Collected cells using the hand-made sieve (Fig. 1 in Chapter 1). The sieve with cells were fixed by the double-aldehyde solution (Section 2.2 of Chapter 1), optionally followed by the step of immunolabeling (Section 2.4), and then stained by 0.5 μM DAPI.

2.2.2 Consecutive Staining by Two Different Probes in Live Cell

HCK-123 was applied in the 10 ml f/2 culture medium to reach a final concentration of 0.5 μM ; then the culture incubated in the same condition described above (e.g. 73.5 h). Collected cells using the hand-made sieve and transferred the sieve to a new f/2 medium for washing (e.g., 0.5 hour). The sieve was then transferred to the medium with 0.5 μM PDMPO for a short period (e.g., 3 hours, referring to the minimum girdle band fabrication time is 1 h 20 min in Fig. 3 of

Chapter 1, data from (Zhang, 2012)). Subsequently fixed, mounted and observed cells as described above.

2.2.3 WGA Staining in Fixed Cell

Double-aldehyde fixed cells were washed by ASB and stained by WGA-Tetramethylrhodamine conjugate 1.0 mg/ml (WGA powder dissolved in distilled water) for 30 minutes.

2.3 Double-Aldehyde Fixation

Stained cells were fixed in a mixture of glutaraldehyde and formaldehyde as described in Section 2.2 of Chapter 1.

2.4 Cytoskeleton Immunolabeling

2.4.1 Single Indirect Immunolabeling (Method 1)

Double-aldehyde fixed cells deposited in a handmade sieve (Fig. 1 in Chapter 1) were placed in the depression of a spot plate containing 750 μ l ASB buffer (actin-stabilizing buffer: 75 mM Pipes pH 6.8, 10 mM EGTA, 5 mM $MgCl_2$, 50 mM KCl, 1% DMSO, pH adjusted to 7.1 by dropwise addition of KOH) for 5 mins. They were then carried to the reducing solution, which is freshly prepared by dissolving $NaBH_4$ in ASB (1 mg / 1 ml), for 2 x 15 minutes. After a 3 x 15 min wash in ASB, cells were permeabilized (50 mM Glycine, 1% Triton x-100, 1% BSA, 1 drop of gelatin fish, all dissolved in ASB) for 2 hours. After another 3 x 15 min ASB wash, cell were subjected to a double blocking solution (1% BSA in PBS solution, 0.1% Gelatine fish). After a wash in PBS (phosphate-buffered saline: 0.14 M NaCl, 2.7 mM KCl, 6.5 mM $Na_2HPO_4 \times 2H_2O$, 1.5 mM KH_2PO_4 , adjusted to pH 7.4 by dropwise addition of KOH or HCl if required), the sieve with the extracted cells was placed in the primary antibody solution (Table 1a/b/c). During the antibody incubation, the spot plate was maintained in a wet box at 37°C for 2 hours. After a 4 x 15 min wash in PBS, the sieve with cells was incubated with the secondary antibody (Table 1a/b/c) under the same condition as described above. After another PBS wash (3 x 30 min),

cells were stained with 0.5 μ M DAPI dissolved in PBS for 10 minutes, then followed by a PBS wash and further processed for confocal microscopy (Section 2.5).

Table 1a. Single Indirect Immunofluorescence for Actin (Method 1a)

Step		Type	Diluted in "1% BSA in PBS" in the ratio of
1	Primary Antibody	Goat polyclonal IgG, Anti-actin (C-11): sc-1615 (SANTA CRUZ BIOTECHNOLOGY)	1:100
2	Secondary Antibody	Donkey anti-goat polyclonal IgG conjugated with Alexa-Fluor 568 / Alexa-Fluor 488 (Invitrogen)	1:100
3	DNA Staining	DAPI (Invitrogen) dissolved in PBS, reaches at 0.5 μ M. Stain cells for 10 minutes.	

Table 1b. Single Indirect Immunofluorescence for Actin (Method 1b)

Step		Type	Diluted in "1% BSA in PBS" in the ratio of
1	Primary Antibody	Mouse monoclonal IgM, anti-alpha-actin N350 (Amersham Pharmacia / Life Science)	1:100
2	Secondary Antibody	Goat / Rabbit anti-mouse IgM conjugated with Alexa-Fluor 488 (Invitrogen)	1:100

Table 1c. Single Indirect Immunofluorescence for Tubulin (Method 1c)

Step		Type	Diluted in "1% BSA in PBS" in the ratio of
1	Primary Antibody	Mouse monoclonal IgG3, Anti-Tyrosine Tubulin TUB-1A2 (Sigma)	1:100
2	Secondary Antibody	Goat anti mouse polyclonal IgG conjugated with Alexa-Fluor 488 (Invitrogen)	1:100
3	DNA Staining	DAPI (Invitrogen) dissolved in PBS, reaches at 0.5 μ M. Stain cells for 10 minutes.	

2.4.2 Double Indirect Immunolabeling: a Mixture of 1st Antibodies plus a Mixture of 2nd Antibodies (Method 2)

Cells were processed as described in most of the steps except for the antibody incubation steps were done differently. After the PBS wash, the sieve with cells was placed in a mixture of two primary antibodies (Table 2) and incubated for 2 h at 37°C, followed by a 4 x 15 min wash in PBS, and then placed in the mixture of two secondary antibodies. Two different combinations of primary antibodies were employed, requiring the use of matching secondary antibodies (see Table 2). The information of which combination was used in a given experiment will be provided in the legends to the figures.

Table 2. Double Indirect Immunolabeling for Method 2

Step		Type	Diluted in "1% BSA in PBS" in the ratio of
1	Primary Antibodies (Mixture)	Mouse monoclonal IgG1, Anti-actin mAbGEa: MA1-744 (Thermo Scientific)	1:100
		Rat monoclonal IgG2a, Anti-tubulin antibody YL1/2: ab6160 (abcam)	
2	Secondary Antibodies (Mixture)	Goat anti mouse polyclonal IgG conjugated with Alexa-Fluor 568 (Invitrogen)	1:100
		Goat anti rat polyclonal IgG conjugated with Alexa-Fluor 488 (Invitrogen)	
3	DNA Staining	DAPI (Invitrogen) dissolved in PBS, reaches at 0.5 µM. Stain cells for 10 minutes.	

2.4.3 Double Indirect Immunolabeling: A Mixture of 1st Antibodies Followed by the Separate Label of Each 2nd Antibodies (Method 3)

Cells were processed as described in most of the steps except for the antibody incubation steps were done differently. After the PBS wash, the sieve with cells was placed in a mixture of two primary antibodies (Table 3) and incubated for 2 h at 37°C, followed by a 4 x 15 min wash in PBS. Then the sieve with cells was placed in the secondary antibody solution for actin, followed by a PBS wash; again, it was placed in the secondary antibody solution for tubulin.

Table 3. Double Indirect Immunolabeling for Method 3

Step	Chemical	Type	Diluted in "1% BSA in PBS" in the ratio of
1	Primary Antibodies (Mixture)	Goat polyclonal IgG, Anti-actin (C-11): sc-1615 (SANTA CRUZ BIOTECHNOLOGY)	1:100
		Mouse monoclonal tubulin IgG3, Anti-Tyrosine Tubulin TUB-1A2 (Sigma)	
2	Secondary Antibodies (Individual)	Donkey anti-goat polyclonal IgG conjugated with Alexa-Fluor 568 (Invitrogen)	1:100
3		Goat anti mouse polyclonal IgG conjugated with Alexa-Fluor 488 (Invitrogen)	1:100
4	DNA Staining	DAPI (Invitrogen) dissolved in PBS, reaches at 0.5 µM. Stain cells for 10 minutes.	

2.5 Confocal Microscopy

2.5.1 Preparing Mounted Samples

Subsequently, cells treated by methods subscribed above were placed in anti-bleach mounting medium (dissolve 100 mg p-phenylenediamine in 10 ml PBS which is adjusted by 2M Tris pH=8.0 until pH7.4; mix with 90 ml glycerin; result in a 100 ml solution) and sealed in glass slides.

2.5.2 Imaging

Samples were observed by confocal microscopy and according to the different fluorescences made by different treatments; different detection settings were applied for imaging. The sequential scanning mode was adapted to avoid the interference between different fluorescent detections. Image stacks called Z- projections were stepwisely taken in a certain depth (usually between 0.5 and 1 μm), which then would be overlaid into one image by the Fluoview 1000 software.

2.5.2.1. PDMPO-DAPI stained sample from Section 2.2.1 was excited with 405 nm Diode laser (excitation dichroics: DM405/488), the emission wavelength firstly passed through a dichroic and barrier filter SDM490, separating the blue fluorescence of DAPI between 420 and 480 nm. Then the emission wavelength passed through a filter SDM560, separating the green fluorescence of PDMPO below 560 nm. The rest wavelength was reflected by mirror and the autofluorescence of chlorophyll was detected by Dichroics and Barrier filters BA655-755, recording the wavelength in the range between 570 and 650 nm.

2.5.2.2. PDMPO-HCK stained sample from Section 2.2.2 was excited with the 405 nm Diode laser and the 488 nm Argon Gas laser (excitation dichroics: DM405/488/543/635), the emission wavelength excited by the 405 nm laser passed through a dichroic and barrier filter SDM510, separating the green fluorescence of PDMPO between 430 nm to 510 nm. Then the emission wavelength excited by the 488 nm laser passed through a filter SDM640, separating the yellow

fluorescence of HCK-123 below 640 nm. The emission wavelength excited by the 635 nm laser was reflected by mirror and the autofluorescence of chlorophyll was detected by Dichroics and Barrier filters BA655-755, recording the wavelength at 664 nm.

2.5.2.3. Alexa-Fluor 488 - DAPI sample (Method 1), was excited with the 405 nm Diode laser and the 488 nm Argon Gas laser (excitation dichroics: DM405/488/543/635), the emission wavelength passed through a dichroic and barrier filter SDM490, separating the blue fluorescence of DAPI between 420 and 480 nm. The emission wavelength excited by 488 nm laser pass through a SDM640, separating the green fluorescence of Alexa-Fluor 488 between 520 – 590 nm. The emission wavelength excited by the 635 nm laser was reflected by mirror and the autofluorescence of chlorophyll was detected by Dichroics and Barrier filters BA655-755, recording the wavelength in the range at 664 nm.

2.5.2.4. PDMPO (Section 2.2.1) - Alexa-Fluor 488 sample (Method 1), was excited with the 405 nm Diode laser and the 488 nm Argon Gas laser (excitation dichroics: DM405/488), the emission wavelength passed through a filter SDM490, separating the green fluorescence of PDMPO below 490 nm. The emission wavelength of Alexa-Fluor 488 excited by the 488 nm Argon Gas laser was reflected by mirror, recording the wavelength between 500 – 600 nm. Notably, if the immunolabeled cytoskeletal object is actin, the green fluorescence of Alexa-flour 488 will be adjusted to the red color.

2.5.2.5. The lysosensor setting and the cytoskeleton setting were employed to observe PDMPO (Section 2.2.1) – double immunolabeled – DAPI sample (Section 2.4.2/ 2.4.3), revealing either SDV or cytoskeletons of the same cell, because all of the 5 emission wavelengths could not completely be presented by the 4 detection channels.

(1) In lysosensor channel, fluorescence of DAPI, PDMPO and chlorophyll were detected, by the same way of Section 2.5.2.1.

(2) In cytoskeleton channel, DAPI, actin and tubulin were detected: the sample was excited with the 405 nm Diode laser, the 543 nm Diode laser and the 488 nm Argon Gas laser (excitation dichroics: DM405/488/543/635), the emission wavelength passed through a filter

SDM490, separating the blue fluorescence of DAPI below 490 nm. The emission wavelength excited by 488 nm laser pass through a SDM560, separating the green fluorescence of Alexa-Fluor 488 between 506 – 536 nm. The emission wavelength excited by the 543 nm Diode laser are reflected by mirror and the Alexa-Fluor 568 was detected by Dichroics and Barrier filters BA565-660, recording the wavelength at 603 nm.

2.5.2.6. HCK-123 (Section 2.2.1) – double immunolabeled – DAPI sample (Section 2.4.2/ 2.4.3), was excited with the 405 nm Diode laser, the 543 nm Diode laser and the 488 nm Argon Gas laser (excitation dichroics: DM405/488/543/635), the emission wavelength passed through a filter SDM490, separating the blue fluorescence of DAPI below 490 nm. The emission wavelength excited by 488 nm laser pass through a SDM560, separating the green fluorescence of HCK-123 and Alexa-Fluor 488 between 500 – 530 nm. The emission wavelength excited by the 543 nm Diode laser are reflected by mirror and the Alexa-Fluor 568 was detected by Dichroics and Barrier filters BA565-660, recording the wavelength at 603 nm.

3. Results

3.1 Interphase: Morphogenesis of SDV and Cytoskeleton

3.1.1 The SDV Develops under the Cover of the Last Epithelial Girdle Band

By consecutive lysosensor staining (Method 2.2.2) as applied in this study HCK-123 was used first in order to mark several silica components of the frustule by yellow fluorescence; then the samples were washed in culture medium and PDMPO was applied next in order to mark the most recently developed silica component by green fluorescence. In the figures 1 – 3, the incubation schedules of the two silica probes are depicted as indicator bars in the upper right hand corner of the images. The HCK-period was always at least 45 hours to make sure that one complete cell cycle is covered. The second incubation was trying to cover the time needed for the fabrication of at least one silica component (either valve or girdle band).

In figure 1A, the hypovalve (HV) and the first hypothecal girdle band (hGB1) of the cell are stained by HCK and the second hypothecal girdle band (hGB2) is stained by PDMPO. It is

important to point out that this hypothetical girdle band develops under the cover of the unstained epitheca, i.e. the last epithelial girdle band (eGB2). It is difficult to see the epithelial wall here, because by this treatment it remains unstained. But contrast enhancement makes it visible (Figs. 1a & 1b, see also Fig. 2b₃).

In Fig. 1B, a pair of recently divided daughter cells lies within the frustule casing of the mother cell. It is a typical phenomenon that the epivalve remains unstained, because it is inherited from the previous generation, before the start of fluorochrome incubation. Both fluorochromes are shown simultaneous in this figure causing an overlap of the signal, but by blanking out the HCK signal (Fig. 1C) it emerges that the PDMPO staining is only present on the daughter HVs and since the signal is weak (except for the LPs, see below) it suggests that the switch from HCK to PDMPO occurred somewhere in the period from cytokinesis to daughter hypovalve morphogenesis, when silica deposition is just starting inside the valve SDVs. The fact that the LPs are prominently stained with PDMPO shows that this structure is made first before silica deposition spreads over the rest of the valve surface. It is obvious that the hypovalve of the right hand daughter cell comes to lie underneath the cover of eGB2. Since the left hand daughter cell undergoes a polarity switch, i.e., the mother hypotheca becomes the daughter epitheca, the HV of left daughter is nominally also placed underneath the cover of eGB2. This genuine feature of the diatom development process is illustrated in Fig. 1D. It demonstrates that the period of HCK-treatment (= 120 h) covers three generations. During the first generation (grandmother) the two girdle bands labelled here eGB1 and eGB2 were made, in the next generation (mother) the entire left hand theca was made, labelled here HV, hGB1 and hGB2, and in the third generation the new daughter HVs are beginning to be formed.

In Fig. 2A a daughter cell twin pair is shown within the frustule of the mother, which has only two generations covered by HCK treatment (= 73.5 h). Since the daughter hypovalves are sharply stained by HCK (Fig. 2a₁) and in addition also stained by PDMPO (Fig. 2a₂), it can be concluded that the switch from HCK to PDMPO occurred in the course of hypovalve fabrication and that the washing period (= 0.5 h) is too short to keep the two fluorochromes separated, which proves that valve formation requires more than half an hour. Again, the previous statement is supported that the new valve SDV is developing under the cover of eGB2.

The same is true for the position of the first hypothetical girdle band SDV (hGB1-SDV), i.e. it also develops underneath eGB1. As clearly demonstrated in the figures 2B, b₁, b₂, b₃, the developmental stage of the cell shown here is somewhat more advanced as compared with the

right hand cell of Fig. 2A, in the sense that this cell has completed valve morphogenesis and is now engaging in the formation of hGB1. For that to happen, the valve needs to be pushed out from the epitheca to make room (see Discussion 4.1.1). The fact that hGB1 is completely covered by eGB2 is almost impossible to see by looking at the complete image stack (Fig. 2B). The only indication of the overlap between the two silica components comes from the observation that both fluorochromes appear at the same location. However, if this view is resolved in the z-direction by looking at a median optical plane, it becomes clear that both eGB2 and to a certain extent also hGB1 are stained with HCK, whereas hGB1 is additionally and strongly stained just by PDMPO (Fig. 2b₃). The fact that both fluorochromes are present in the hGB1 compartment does not affect this assessment. It is due to the short washing step as mentioned above.

After completion of hGB1, the next hypothetical girdle band (hGB2) is again made in the same place underneath eGB2, which again requires an axial expansion step to make room for the new girdle band (see Discussion 4.1.1).

In Fig. 3A a cell is shown at this developmental stage. HCK incubation covers the development from eGB2 (which was hGB2 in the mother generation) to hGB2 of the daughter generation as judged from the distribution of the yellow fluorescence (Fig. 3a₁). So the treatment covers two generations. PDMPO fluorescence is exclusively found in hGB2, which indicates that this is the latest silica component. And this girdle band is located underneath eGB2.

Usually, the SDV is always growing under the cover of the last epithelial girdle band. And this conclusion supports the findings reported in Chapter 1 that "each young SDV (hGB1, hGB2, HV) is always located during its formation beneath eGB2" (Section 3.1.1.2 in Chapter 1). Notably, the SDV is sometimes developed under the cover of eGB1. It occurs when there is only one epithelial girdle band, which has occasionally been observed in Fig. 3B, the formation of hGB2 takes place under the cover of this single epithelial girdle band.

3.1.2 Chitin Plays a Role in Sealing between Silica Frustule Components

Wheat Germ Agglutinin (WGA) is applied to visualize chitin distribution in the diatom cell wall. Strong stains appear at the edges of the latest girdle band, when the newly made girdle band has not been extruded out (Figs. 4A – 4D) or at the middle axials of the frustule when the hGB2

has been extruded out (Figs. 4E & 4F). The former suggests the chitin is secreted at the beginning and the ending of the new girdle band development; the latter suggests the chitin is secreted at the edges of both thecae. In general, the chitin secretion is active to glue the latest changed region to adhere the silica components together.

3.1.3 Distribution of Microtubules and Microfilaments at Interphase

The microtubule system in *Odontella* tightly correlating with the nucleus, consists of delicate radially organized microtubule center, a larger radial array, and thick root bundles. There are no isolated MTs elsewhere in the cell. The orientation of the root may be transverse (Fig. 5A) or axial (Fig. 5B). The curved apex in Fig. 5A as opposed to the square apex in Fig. 5B is caused by the fact that the cell has rotated around the longitudinal axis during mounting on the microscope slide (see sketches of the axes in Figs. 5a and 5b). A clearer view of the perinuclear microtubules and the MC-associated microtubules is seen in Figs. 5C & 5D. The microtubules of the MC are always straight and short forming V-shaped sectors grouping around a center, whereas the perinuclear microtubules attach all over the surface of the nucleus and extend far out into the cytoplasm (Fig. 5C). In most cases, the MC looks like a hollow circular structure (Fig. 5D), which could mean that the inner side of the MC is not filled with any other substance or just because TUB1A2 does not bind to it.

The distribution of microfilaments in the cell is different. Because even though there is a greater number of MTs converging onto the nucleus, many of the microfilaments are not and appear everywhere throughout the protoplast (Fig. 5E). A prominent actin ring — a loop of actin cable consisted by microfilaments — forms a straight line along the girth of the cell (Figs. 5E & 5F). In the apical regions, microfilaments will accumulate in a prominent curved shape (Fig. 5G), the ends of which converge on to the LP base plates but no microfilaments appear inside the LPs (Figs. 5G & 5H).

The perinuclear microtubules, generally speaking, have no direct connection with the actin ring, but they do co-align with radial F-actin cables suggesting some kind of physical interaction (e.g., Fig. 6a₁).

3.1.4 The Spatial Relationship of the SDV with the Cytoskeleton

By co-localization with the SDV, it is shown here in Fig. 6A that the actin ring is aligning along the edge of the developing girdle band. In valve view, the radially distributing microtubules are facing to one side of this girdle wall forming an umbrella shaped cortical domain, while the microtubular root is facing to its opposite side (Fig. 6a₂). Aldehyde-fixed cell may sometime get split in half at the junction between epitheca and hypotheca gives rise to some unspecific staining patterns. Figs. 6B & 6C show such an example, where the two halves are just slightly separated from one another. It can be clearly seen, where they have originally been connected to each other. On the surface of the hypotheca edge a stretch of unspecifically stained surface indicates the presence of a sticky coating which has bound the green fluorescent secondary antibody. Part of the sticky coating was ripped out and held back on the opposite side on the epithelial edge (stippled circle). Due to this clear structural relationship this green, unspecific staining cannot be mistaken for PDMPO-staining (compare with Fig. 6C).

3.2 From Late Interphase to Anaphase: Development of the Spindle and the Occurrence of the Cytokinetic Actin Ring

The major part of interphase is dedicated to axial cell growth involving the formation of two hypothecal girdle bands. During this period the nucleus remains stationary at the position, where these girdle bands develop. The typical microtubule system at this stage consists of the MC visible on the surface of the nucleus by the short MT bundles radially arranged around the circular center and a large number of perinuclear microtubules (Fig. 7A). When the frustule has fully expanded after the last hypothecal girdle band (usually hGB2) has become extruded from the cover of eGB2, the cell is ready to divide. The nucleus is located at the geometrical middle of the cell, which would be exactly at the overlapping region between the edges of epitheca and hypotheca. Therefore the actin ring at the abvalvar edge of hGB2 (or if fabricated: hGB3) is always seen to the epithelial side of the nucleus (Figs. 7B & 7b). First sign of transiting into the mitotic phase is indicated by the appearance of a striated rod-like structure directly adjacent to the MC on the face of the nucleus. This structure is the precursor of the polar complex (PC) (Fig. 7B), which will eventually develop the polar plates and further mature into the spindle. Then, as the PC precursor grows longer and bigger (Fig. 7C), a thick actin filament bundle, which is in fact the initial cytokinetic actin ring, appears oriented roughly parallel to the precursor

(Fig. 8A). The PC precursor continues to mature by becoming more prominent and thicker and the cytokinetic actin ring also becomes wider (Fig. 8B). Notably, until this stage the microtubule root still exists (Fig. 8b). But then when the precursor becomes a pair of mature PCs, which is when the two polar plates are separating (Figs. 8C, 9A). At this stage, the cytokinetic actin ring has further increased in the width, whereas the GB-actin ring becomes inconspicuous (Fig. 8C), and the GB-actin ring is not visible, indicating that it has become depolymerized. The microtubule root also disappears at this stage. Meanwhile, the nucleolus is still present. Since chromosomes condense only afterwards, it suggests the cell stage belongs to late interphase, which can be named "preprophase" in the diatom cell cycle (Pickett-Heaps et al., 1975, 1979b).

Then the pair of polar plates expand and begin to form the mitotic spindle by growth of the microtubules between them (Fig. 9B). Chromosomes are not visualized here but should be condensed, base on the reference of the cell of Fig. 21E in Chapter 3 that its PC is also in a same morphology and the DAPI stained chromosomes suggest the cell is at prophase.

At metaphase chromosomes are arranged around the spindle in a dumbbell shaped cloud (Fig. 9C₁ & C₂); the two polar plates are further pushed away from each other by extension of the thick column of central microtubules. Some microtubules can be seen outside the core region of the spindle radiating out of the polar plates from opposite sides and some of them have not yet attach to chromosomes (arrows in Fig. 9C₁). Short astral microtubules are also visible (red arrows in Fig. 9C₁ & 9C₂). Notably, except for the cytokinetic actin ring and the remnant of the girdle band actin ring, not further labelled actin is visible in the cytoplasm (Fig. 9c).

At anaphase, kinetochore microtubules become very prominent and polar plates show a tendency of rounding indicating that the polar structure is beginning to degrade (Figs. 9D & 9E). Chromosomes are divided into two clouds (Figs. 9e & 9f). The cytokinetic actin ring is still maintained right above of the spindle (Figs. 9E & 9F).

3.3 From Telophase to Cytokinesis: Formation of the Horn Bundles, Reappearance of the MC and Constriction of the Cytokinetic Actin Ring

At telophase, the two chromosomal clouds are separated by the elongating central spindle microtubules (Fig. 10a), since the cytokinetic actin ring locates right above the central microtubules occluding the fluorescent signal from the labelled microtubules in the overlap region. Two new microtubule-forming regions appear on the central telophase spindle close to each daughter nucleus (Fig. 10A). The new microtubules form prominent bundles, which grow out along the cytokinetic actin ring (Fig. 10B). At this stage the MCs reappear on the surface of the daughter nuclei .

Later, either horn bundle would eventually extend to the full length which equals to one half of the girth (Fig. 10b₁); at this stage, the two MCs are prominently located on the nuclear surface near the insertion point of the central spindle microtubule bundles (Fig. 10B). The round smooth contours of the daughter chromosomal clouds indicate that reconstruction of the nuclear envelopes is in progress (Figs. 10b₂ & 10b₃).

And it is noted that the cytokinesis of *O. sinensis* has initiated at anaphase when small, unobtrusive cytokinetic pulses appear, but the successful cleavage proceeds from middle telophase (see Fig. 2E, (Zhang, 2012), when the microtubule horn bundles and nuclear envelope have been developed (the latter is based on the visible condensed chromosomes, see Figs. 10c₂, 10c₃). When the cleavage begins, the two microtubular horn bundles are maintained at the same place and the cytokinetic actin ring constricts in between them thus cleaving the protoplast into two parts (Fig. 10C). At this stage, chromosomes begin to decondense (Figs. 10c₂ & 10c₃).

As the constriction proceeds, either the cytokinetic actin ring may break the central spindle (Fig. 11C), or before being broken, the spindle may extend very long and thin (Fig. 11A); Meanwhile, both MCs connect to their respective microtubule horn bundles (Figs. 11A & 11a). At this late cytokinesis stage, both nuclei are showing stages of chromosomal decondensation (Figs. 11B₁ – B₅) and reappearance of nucleoli (Fig. 11G₁ & G₂).

It is notable that the microtubules from the horn bundle are all clearly connected with the MC (Fig. 11C & 11E). At the same time the actin cytoskeleton is reorganizing into a system of

filament cables alongside the microtubule horn bundles (Figs. 11c, 11e) defining the domain of the future head plate (Fig. 11F). Obviously, the presence of LPs is earlier than that of horns (Figs. 11F, 12B). In the next stage of valve morphogenesis, this system of filaments develop an actin ring, which will serve as the demarcation of the advancing edge of the valve SDV (see Fig. 13 C, F & G).

Fig. 11E shows a stage slightly more advanced than that in Fig. 11C, because the central spindle microtubular remnants have disappeared and the actin ring has reached to both ends of the horn bundle. Besides, on each tip of the microtubule horn bundles, there is a prominent patch of actin recognized by red immunofluorescence of anti-actin C11 (Fig. 11e), which is then hardly seen when the actin ring is located away (Fig. 13C). Thus it is likely that the actin patch is a part of the actin ring. Although the biological function of the actin patch is obscure so far, it is then found to involve in horn morphogenesis (see Part III. General Discussion). Comparing Fig.11e (cytoskeleton channel) and Fig. 11F (PDMPO-channel), a very young stage of LP-formation can be recognized. Starting from the strongly stained base plate a short, hollow LP shaft is extending outwards and a faint silica trace can be spotted running from the base plate towards the nucleus on the surface of the head domain (Fig. 11F). This is also the earliest observable stage of silica deposition in the head plate domain of the future valve (initial pattern center, see the developing process in Discussion 4.4.2).

3.4 Post-cytokinetic Phase (Early Interphase): Valve Morphogenesis involving the Valvar SDV and the Cytoskeleton

The post-cytokinetic phase begins at the stage, when the DNA of the daughter nucleus decondensed (e.g. Figs. 11G₁ & 11G₂) and at this stage the horn bundle is still straight. Later, the distal ends of the horn bundles curve serving as scaffolds of the horns and the subdistal regions bulge to become the supporting scaffold for the LP bases (Fig. 12A). PDMPO stains these regions revealing a regular pattern of parallel silica ribs coming off a central rib, which runs exactly along the microtubule horn bundles (Figs. 12A & 12B). Then microtubules of the horn bundles, which are originally connect with the MC (Fig. 11E) begin to detach and pass by the MC (Figs. 12C₁ – 12C₃), which seems to be an early transitional stage in the development of the radial perinuclear microtubule system (Figs. 13A₁ – 13B₂).

When horns have been completely silicified, the microtubule horn bundles disappear and the microtubule system transforms completely into a radial, perinuclear microtubule array defining the dome shaped valve domain (Figs. 13C – 13E). Typically, some of radially extending microtubules co-align with microfilament bundles (Fig. 13C, compare Fig. 13c₁ and Fig. 13c₂). The leading edge of the valve SDV is demarcated by the actin ring which moves down along the slope of the valve domain (Figs. 13D & 13E). When the dome region of the valve has developed, the MC will turn to face the girdle wall and the radial microtubules will turn to the same direction as well (Fig. 13E). Notably, these microtubules would not extend far away from the actin ring which is the demarcation sign of the valve-SDV edge.

4. Discussion

Countless microscopic studies have been made through past decades on the morphology of diatoms (Round et al., 2007). This is because sculpturing of the valves is quite easily observable in the light microscope, even though the diatom frustule, made of silica, is a translucent structure. It turned out to be more difficult to study the morphogenesis process of the valves and determine the positioning and fate of girdle bands by light microscopy. As mentioned in the introduction, silica probes like PDMPO and HCK-123 (Hazelaar et al., 2005; Parambath et al., 2016) have been introduced and recently used as interesting new tools to improve the identification of these frustule components (Annenkov et al., 2010; Desclés et al., 2008; Shimizu et al., 2001b; Zhang, 2012; Znachor and Nedoma, 2008). While this has meant a progress in diatom morphogenesis studies, even better would be a sequential application of the two silica probes, namely HCK-123 and PDMPO, which have different fluorescent properties. The expectation was that they may get consecutively incorporated into two different frustule parts in the same cell (Method 2.2.2), which is what mostly happened, although there were staining patterns, which did not conform to that expectation. In the current study, this approach has been applied for the first time in the field of diatom research. In addition a second level of complexity is added by simultaneously marking cytoskeletal proteins such as actin and tubulin with yet another set of fluorochrome labels by using a double immunolabeling procedure in combination with the silica probes. Frustule staining with silica probes happens, when the cells are alive undergoing their growth and morphogenesis, whereas cytoskeleton labelling occurs after double aldehyde fixation of the lysosensor stained cells.

4.1 Interphase

4.1.1 GB-SDV Development and the Mode of Frustule Elongation

The SDV development has been studied in the past mostly by fine structural analysis (Chiappino and Volcani, 1977; Schmid, 1979a, 1980; Tiffany, 2002) and the current work is also making a contribution on this level (see Chapter 1). However, the anchorage of the developing SDV (especially the SDV of the girdle bands, GB-SDV) and the deployment of the recently made silica structure onto the protoplast surface are still obscure and how these processes are linked with cell elongation is not well understood. As to the GB-SDV, it has recently been suggested by Scheffel and coworker (Scheffel et al., 2011) for the centric species *Thalassiosira pseudonana* that somehow the cell makes room between epi- and hypotheca exposing cytoplasmic surface for the insertion of the new girdle band.

Here it is shown that the insertion does not involve the open exposure of cytoplasmic surface and that it is not a simple one step process but a sequence of events linked to axial expansion, so that any new frustule component of the daughter generation is made and deployed under the cover of the mother frustule, nominally the last epithecal girdle band (usually eGB2, Fig. 1B).

The first step in daughter morphogenesis is the development and deployment of the valve at the apical pole, which happens right after division, when the daughter twin cell pair is completely enclosed by the casing of the mother frustule (Fig. 1B). Next steps involve axial expansion, which will lead to the breakage of the mother frustule at the joint between the two thecae and the formation and deployment of the first hypothecal girdle band of the daughters (hGB1). For explaining these next steps two alternatives models may be considered. In both models a ring of actin filaments in the cortical cytoplasm running around the girth of the cell plays an important but different role:

Model 1 (Fig. 14): Axial expansion sets in, after the hypovalve has been completed, which moves it out from underneath the epitheca, and places it in front by establishing a new joint with the epithecal edge. This is followed by the development of hGB1 within the SDV under the cover of eGB2 by expanding the abvalvar edge of SDV (abvalvar side = side facing away from the hypovalve), which is the side, where the actin ring is found. So the advancing edge of a girdle

band moves towards the epivalve (yellow horizontal arrows in Fig. 14) and the actin ring is always attaching to the front and moving with it, thereby functioning as a mobile demarcation for the SDV membrane, and preventing the advancing edge of the SDV from meandering. At the completion of the GB, the actin ring has reached the position of the joint between eGB1 and eGB2 (vertical arrow) and subsequently exocytosis of hGB1 occurs underneath the cover of eGB2, which is followed by axial cell expansion, moving hGB1 out from underneath the epitheca (horizontal double arrow). The actin ring moves with it and thus the ring returns back to its original start point at the abvalvar edge of eGB2. Next the same process repeats: a new SDV is created, within which hGB2 is made. The advancing edge of the SDV together with the actin ring move until they again reach the junction between eGB1 and eGB2. hGB2 is deployed and a final phase of axial expansion moves it out from underneath the epitheca.

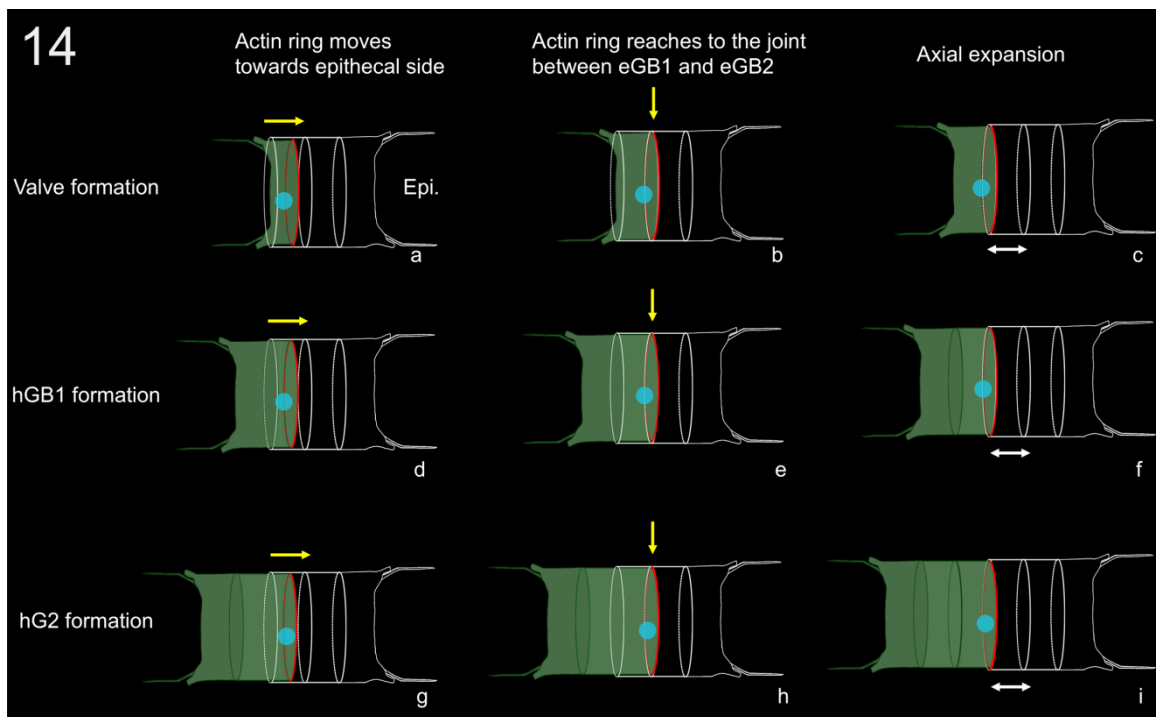


Fig. 14 Simplified illustration of model 1. The order of the cell stages are marked by alphabet.

Model 2 (Fig. 15): In the course of hypovalve formation the advancing edge moves away from the apex (yellow horizontal arrow), same as in model 1. After the completion of the daughter hypovalve (a-c), the valve-SDV edge has reached the joint between eGB1 and eGB2 (yellow vertical arrow) and the valve gets deployed. A new SDV will be added in front of the edge of the hypovalve, which will become the hGB1 (d-f). The abvalvar edge of the new SDV, as well as the

accompanying actin ring, remain fixed and regularly coincide with the same joint (vertical arrow). In this model, the actin ring functions as a bumper to keep the abvalvar side of the SDV-cylinder from moving, so that the girdle band grows towards the hypothecal side (GB's advalvar side). This requires the axial cell elongation to occur concomitantly with the expansion of the SDV. Then the formation of hGB2 (g-h) follows by the same procedure as that of hGB1.

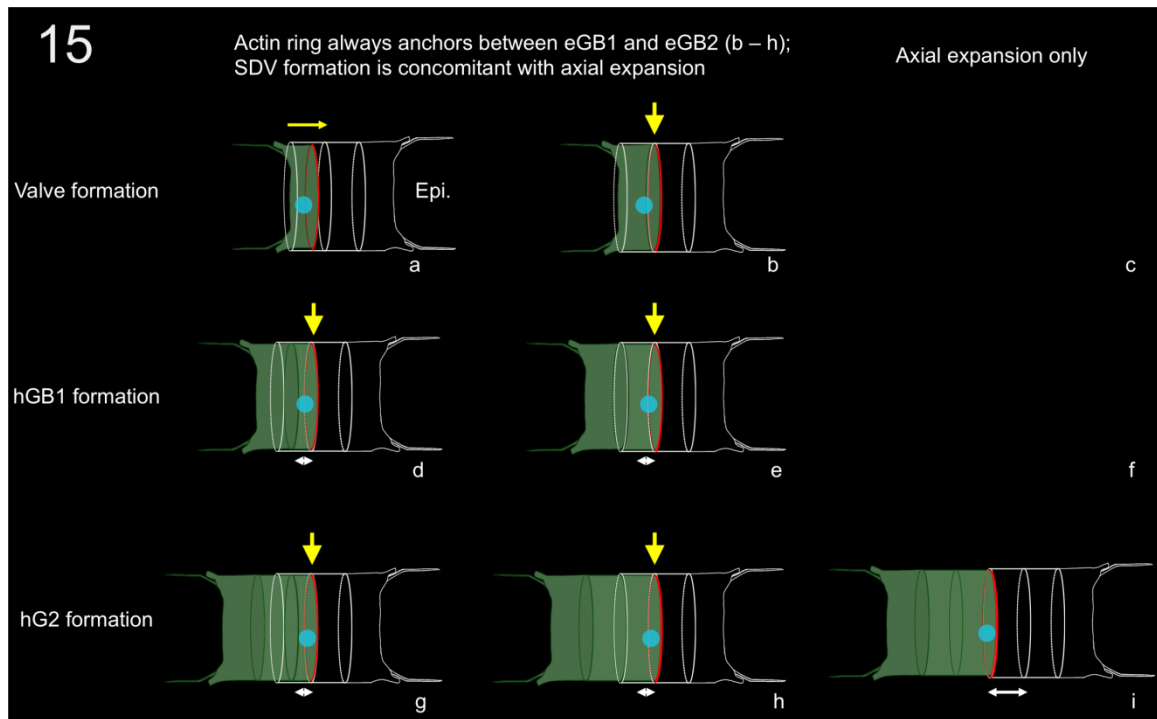


Fig. 15a Simplified illustration of model 2. The order of the cell stages is marked by alphabet. Comparing to Fig. 14, the stage 'c' and 'f' are missing, because the axial elongation at these stages is usually concomitant with the SDV expansion except step 'i'. The hypovalve development process here (step 'a') is the same as that in model 1 (step 'a' of Fig. 14); both of them eventually reach to the joint between eGB1 and eGB2.

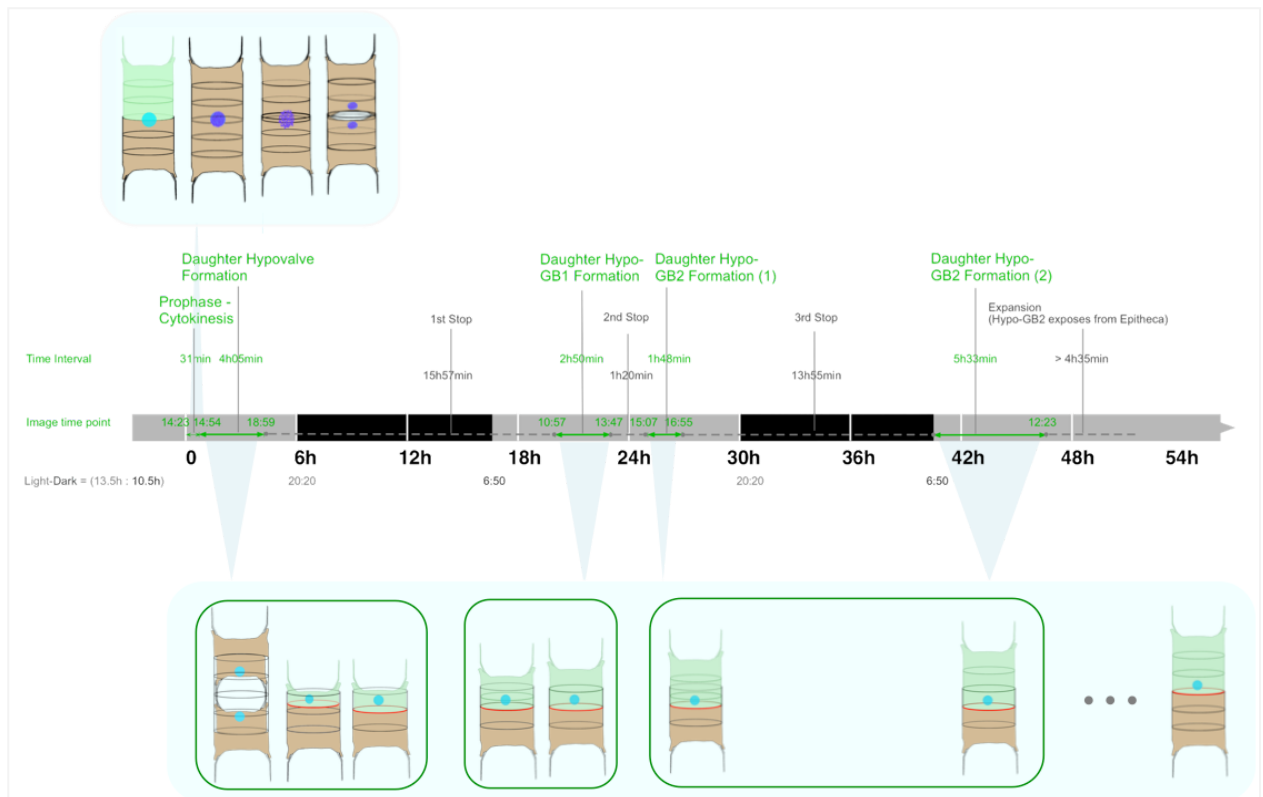


Fig. 15b Re-explaining the summary scheme from the general introduction (see Fig. 3 in Part I) of the vegetative developmental cycle of *O. sinensis*. The difference is that cell elongation is accompanied by the SDV development. Duration of silica fabrication and the cell elongation are illustrated along the time scale bar according to a live observation recorded by the time-lapse movie (Zhang, 2012). Actin ring is shown in red; nucleus is shown in blue, and nuclei of mitotic stages are shown in darker blue. Mother frustule is transparent, exposing the protoplast in khaki-grey. Green theca represents hypotheca. Solid green frames indicate the silicification states, when new frustule components form in an SDV. The periods marked by "Stop" means that cell elongation pauses.

Model 2 (Fig. 15b) is clearly favored here. This preference comes from the fact that in all samples screened in the course of this study, a developed hypovalve has never been found outside the cover of the epitheca, unless the hGB1 had been made. This means the fabrication of hGB1 is required for moving out the new valve from underneath the epitheca. In addition, this model nicely conforms with the observations made on the actin cytoskeleton that the actin ring is always found located at the site of the joint between eGB1 and eGB2 (see the yellow arrow in Fig. 15a), which means that within the SDV, the matured region of the silica cell wall is pushed towards the hypothecal side, when the deposition of silica is occurring at the opposite end of the SDV. So the advancing edge moves towards the hypovalve and the actin ring is fixed in

position. And therefore, based on this model, for example, the explanation of the time-lapse data given in my master thesis ((Zhang, 2012), see Fig. 3 in Part I, based on the logic of Model 1), has to be changed in the sense that SDV development and cell elongation do not occur one after the other but simultaneously (see Fig. 15b, based on the logic of Model 2).

The pushing force for axial expansion growth could come from two sources. It could mainly come from a step-up in turgor pressure, but in addition it could be helped by the molecular pushing force of silica deposition in the SDV. But it should be noted that hGB2 does not have a next SDV developing behind it, when it is axially sliding out, so the latter will not help in this case. As shown below, the construction of the cytoskeleton during interphase cell expansion suggests that the modulation of stretch and tension between the two opposite cell poles could be of importance to finely tune axial expansion.

4.1.2 Configuration of the Interphase Cytoskeleton

As detailed in the introduction of this chapter, the cytoskeleton of diatoms is mainly composed by actin filaments and microtubules. Therefore, cytoskeletal configuration of *O. sinensis* at interphase can be divided into two basic parts — the actin and the microtubule system.

4.1.2.1 The Interphase Microfilament System

In detail, the actin cytoskeleton consists of (1) the actin ring, (2) a transcellular actin cable system, (3) a perinuclear actin filament system co-aligned with the perinuclear microtubules and (4) a cortical actin filament network.

(1) As mentioned below, the actin ring that was formed at an early stage of valve morphogenesis, grows until it reaches the dimension of cell girth and is subsequently present throughout interphase. It disappears, when the cell prepares for mitosis and cytokinesis. Its function as a bumper has been detailed above.

(2) The actin cable system consists of 4 branches of actin cables, each of which is anchored in the protruding lips of the four LPs (labiate processes, see Fig. 13c in Chapter 1). These cables reach out from there into the cytoplasm, where they splice into a network.

(3) The perinuclear actin system consists of filaments associated by collateral alignment with perinuclear microtubules. This system is linked up with the actin cables anchored at the labiae of the LPs and it is difficult to decide, whether it is an independent system or just a subdomain of the general cytoplasmic actin system.

(4) There is a cortical network of actin filaments, which may be considered a peripheral domain of the main cytoplasmic network.

4.1.2.2 The Actin Ring

It has been suggested that the actin ring synchronously enlarges its loop to peripherally demarcate the edge of the outwardly extending valvar SDV (van de Meene and Pickett-Heaps, 2002; Pickett-Heaps et al., 1990; Tesson and Hildebrand, 2010a, 2010b; Van de Meene and Pickett-Heaps, 2004). Tesson and Hildebrand speculated that the actin ring may stabilize the valvar silicalemma until the completion of silica deposition (Tesson and Hildebrand, 2010b). However, the behavior of the actin ring in the course of valve morphogenesis has not been studied so far and whether or not this might also be of significance for GB-SDV development has not been known. The results shown in this chapter are the first to reveal that after completion of the valve the actin ring will be continually involved in the GB-SDV formation, based on the observation on *Odontella sinensis*. And it is proposed that the dynamic activity of the actin ring during valve formation is different from that during girdle band formation. In the latter it is fixed in position but in the former it moves (see Model in Fig. 15a).

In *Odontella sinensis*, the actin ring originates at the edge of the head plate (e.g., Fig. 11C) and then it appears to be hooked onto (e.g., Fig. 11E) the two distal tips of the microtubule horn bundles (see below); then the ring expands to adapt to the size of the cell girth, which places it in the outermost cortex underneath the plasma membrane and then it moves from the hypothecal pole downwards, i.e., in the direction away from the hypothecal cell pole (Fig. 13C) until valve silicification is completed. However, next, in the course of girdle band formation, which follows the valve formation, the same actin ring remains stationary underneath the joint between eGB1 and eGB2 (as explained in the chitin model, see the grey arrow in Fig. 17). This means, it acts as a bumper for the abvalvar edge of the GB-SDV, so that the pushing force of polarized silica deposition at this edge of the SDV drives SDV expansion on the opposite end,

i.e., directed towards the hypothecal side. Such a fixation mode could be a universal principle in all diatoms.

This raises the interesting question, as to how the actin ring recognizes and anchors at this location at the joint between eGB1 and eGB2 (see the yellow arrow in Fig. 15) before girdle band formation begins. Obviously the actin ring moves down from the slope of the apical domain during the valve morphogenesis, which is consistent with the idea of it functioning as a demarcation for the SDV to help it maintain a straight circumference. When the ring arrives at the joint between eGB1 and eGB2, the only conceivable way of making it become stationary is to establish a physical connection across the plasma membrane between inside and outside. Assuming the presence of anchor sites in the organic matrix of the mother frustule, one could argue that transmembrane proteins attached to the actin ring on the cytoplasmic side could reach out to these extracellular anchor sites, thus possibly serve as such physical connections. However, while nothing is known yet on any of these potential transmembrane proteins, there is a much easier explanation involving chitin as an organic linker component (see below section 4.1.3).

4.1.2.3 The Microtubule Cytoskeleton

The microtubule cytoskeleton in *Odontella sinensis* consists of the nucleus-associated MC (microtubule center), microtubules converging on the MC, and in addition other perinuclear microtubules as well as the microtubule roots, which are thick bundles of microtubules reaching from the nucleus towards the opposite cortex region. This configuration of the cytoskeleton provides the structural basis for nuclear positioning, and for the mechanism of axial expansion growth (see the tension equilibrium model, Fig. 16) as well as the correct placement of girdle bands in *Odontella*. Its functional aspects are described and will be interpreted in the following section.

The MC is a special form of MTOC typical for the interphase MT-cytoskeleton in diatoms. Other than MTOCs in plant cells (Shimamura et al., 2004), it is a structural entity, which is even identifiable in a good light microscope (see Pickett-Heaps et al., 1984 confirming Robert Lauterborn's original work in 1896).

The shape of the MC may vary among different diatom species. In EM observations, the MC of the pennate diatom *Surirella* (Pickett-Heaps, 1991; Pickett-Heaps et al., 1984; Tippit and

Pickett-Heaps, 1977) and that of the centric diatom *Melosira* (Tippit et al., 1975) appear as a globule. Whereas in *Pinnularia*, the MC appears as a filled or a hollow circle (Pickett-Heaps et al., 1979a). This difference may be due to the sectioning angle through the diatom sample. In *Odontella sinensis*, the MC structure appears like a hollow circle after fluorescent immunolabeling. But in the absence of additional fine structural evidence the question, whether or not it may be filled by a spherical structure remains unresolved. The hollow appearance in the tubulin immunofluorescence images simply means that there is no tubulin present in the middle of the MC.

In the traditional view, the MC is the only nucleation site of all MTs (Crawford, 1973; Drum, 1966; Pickett-Heaps et al., 1990). But from the tubulin immunofluorescence images obtained in the present study, it is clear that MTs form a cage around the nucleus and that the MC in *Odontella* is a distinctive organelle independent of the MT-cage associating with the nuclear surface, onto which only some of the microtubules converge (e.g., Figs. 5C, 7A). Apparently, most of the radial perinuclear MT-system anchors on the nuclear surface, where a variable number of discrete focal points are often observed (e.g., Figs. 5C, 7A–C). These might be subordinate MTOCs. This implies the MC of *O. sinensis* is just one of the nucleation sites among the others on the nuclear surface. But it is not clear in this chapter, whether this interpretation is true. Clearly one observation made in the current study is at variance with this interpretation, showing that after Phalloidin treatment, the MC can be entirely removed from the nucleus, and meanwhile almost no other MTs remain associated with the nuclear surface (see Figs. 40C, 41 in Chapter 3), suggesting that under these conditions the MC is the only microtubule center (see Discussion 4.4.3.3 in Chapter 3).

It should be noted that the MC may not always be the only configuration pattern of microtubules among diatoms as suggested by the pattern found in some centric diatoms such as *Lithodesmium* and *Mediophyxis*, where the entire nuclear surface is covered by a network of microtubules organized in regular focal points without a distinct dominating center (see Figs. 1 – 4 in the Appendix).

In the young *Odontella* daughter cell, the MC sits at the apex of the hypovalve domain on top of the nucleus. Microtubules radiate from the nucleus forming the typical umbrella type of array, where the valve is forming. When the nucleus moves away from the apex, the microtubule umbrella will move with it spreading underneath a partial area of the cylindrical GB-SDV (covering at least one half of the cell's girth), within which the girdle bands are fabricated. So in

both cases microtubules coincide with the position of the SDV. In the case of the valve this co-distribution is very close and the same has been reported for the radial centric species *Coscinodiscus wailesii* (Tesson & Hildebrand, 2010). In case of the girdle band, the situation is less clear. As to whether interphase MTs may or may not influence the GB-SDV shape will further be discussed in Chapter 3.

4.1.2.4 The Spatial Relationship among Cytoskeleton, Nucleus and the SDV

As suggested by the co-aligning configuration between microfilaments and microtubules in Fig. 6a₁, it is likely that these two types of cytoskeleton have a physical interaction. In most eukaryotic organisms, interactions between them are a common feature (Basu and Chang, 2007; Dugina et al., 2016; Goode et al., 2000; Mohan and John, 2015; Pacheco and Gallo, 2016), which can either be mediated by cross-linking proteins or by motor proteins (see also (Collings, 2008) for the situation in plants), so it may also be the case in diatoms.

Based on the observation in live or fixed cells, the nucleus, microtubules, actin ring and the GB-SDV, are always configured together in the same position during girdle band morphogenesis and growth. And this strict interdependency is similar in the stage of valve morphogenesis only in the aspect of the geometry, but how the elements are positioned to each other, is different. The two key elements in understanding the mid-interphase mechanics of tension generation are the anchoring of the actin cables at the base labiae of LPs and the association between microtubules and radial actin filaments (Result 3.1.3).

The mechanism underlying the behavior of the actin ring is more difficult to interpret. It is a consistent observation in this study that the nucleus with its perinuclear MT-system is always located on the advalvar side of the actin ring (facing the hypovalve). This is the position, where the most recent girdle band is being assembled in the SDV. This could be taken as an indication that the microtubule system somehow binds along the cytoplasmic face of the SDV's silicalemma. However, there were only a few examples in the data suggesting a co-alignment of some sort between microtubules and girdle band SDV (e.g., Fig. 2D), so on the whole this was not convincing enough. The same goes for the possibility of a direct interaction between the microtubule system and the actin ring. It may happen sometimes, but in general it can be excluded as a regular situation.

Yet, on the other hand, there were always examples of co-alignment between perinuclear microtubules and actin filaments. Since these microtubules tie into the cytoplasmic actin filament network, which in turn is anchored at the LP-labiae of both opposite sides, the idea suggests itself that the nucleus is suspended in this network and that nuclear position depends on the tension between the opposite poles of the actin network. This gives rise to the tension equilibrium hypothesis formulated in Fig. 16.

In order for such a mechanism to function properly, the actin ring must somehow be anchored at a fixed position as described above. The way how this could be achieved, is laid out in the next section.

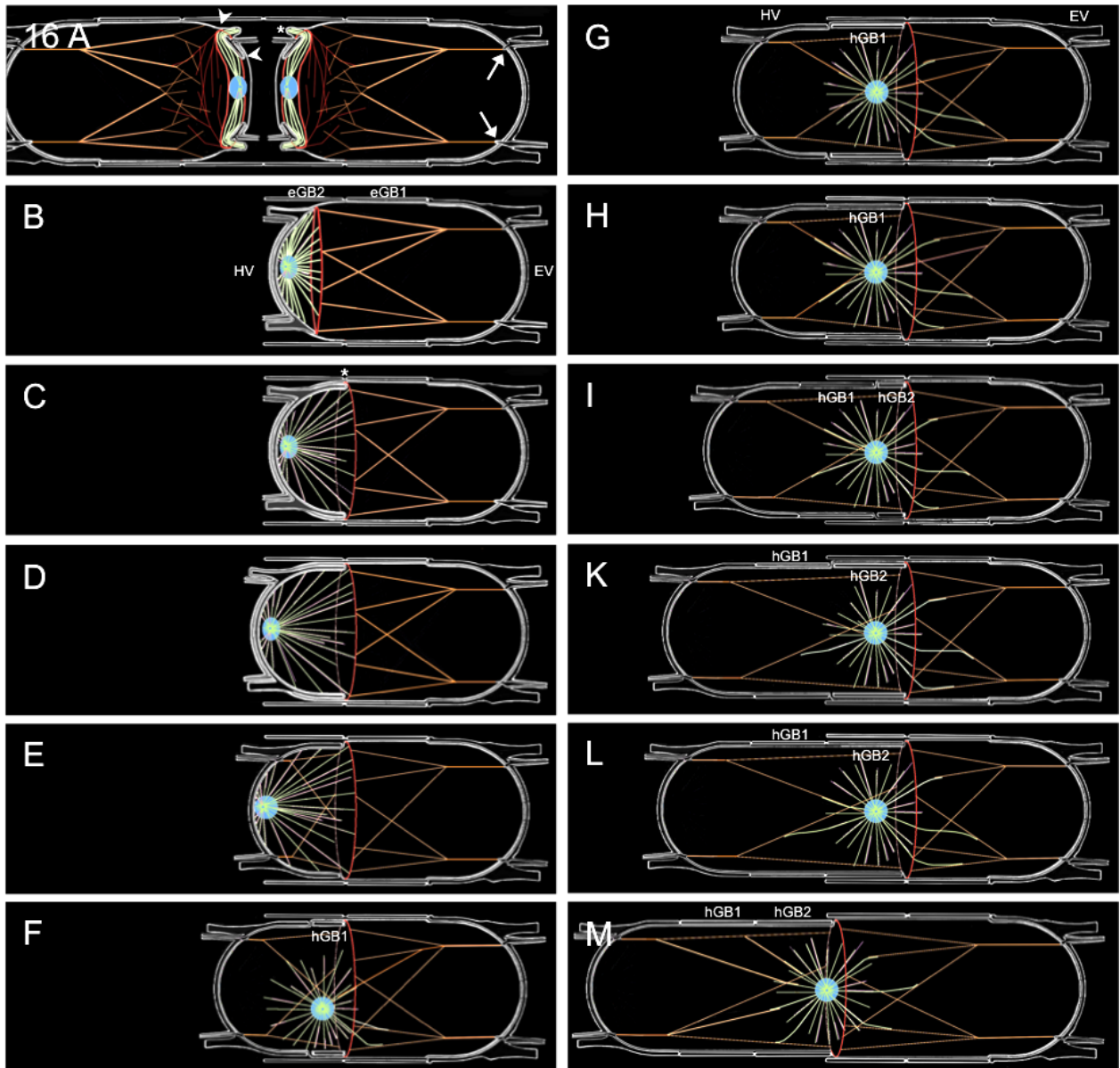


Fig. 16 Tension equilibrium model of cytoskeleton dynamics in *O. sinensis* cell morphogenesis.

A-M. Component images of the animation (presented in the Appendix) showing schematic views of daughter cell development in girdle view, looking through from the surface into the depth of the cell. Silica frustule components are framed with white lines, membranes are light grey, microtubules - green, actin - red, and nucleus - blue. LPs (labiate processes) are truncated, horns are represented as contours instead of cross-sectional views.

A. Post-cytokinetic daughter twin cell pair at horn bundle stage within the confinement of the mother frustule. Formation of spine bases (i.e. labiae at the LP base) within the initial SDVs (e.g., in the left cell, the SDV is between the arrowheads) is in progress and spines are emerging. Cytoplasm is beginning to protrude at the ends of the horn bundles (asterisk shown in the right cell), a ring of actin filaments assembles around the horn bundles defining the future head plate domain. Loose connection of the actin ring with the actin bundles system of the epitheca is provided by a network of fine actin filaments. The

actin cytoskeleton of the epitheca merges into two major bundles anchored at the inner labiate of the labiate processes of the valve (e.g., arrows in the right cell). The cortical actin network, which is present throughout the cell, is omitted for clarity.

B. The perinuclear microtubule system has transformed into a radial array underneath the hypovalve SDV, which was established by the fusion of the two initial SDVs. The actin ring marks the advancing edge of the SDV, which expands downward the apical dome. Left daughter has been omitted. EV – Epivalve, HV – Hypo valve, eGB1, eGB2 – girdle bands of the mother frustule.

C. The advancing edge of the hypovalve SDV has reached the position at the joint (asterisk) between eGB1 and eGB2, where it gets anchored.

D. The slope of the valve is further extending within the valve SDV, but now extension is pushing against the stationary actin ring so that the daughter cell pole gets moved outwards against the sibling cell. This is the moment, when the mother frustule breaks at the joint between epitheca and hypotheca (not shown).

E. Deployment of the hypovalve onto the protoplast surface of the apical cell pole. At this stage the actin cytoskeleton gets anchored at the inner labiae of the hypothecal labiate processes (LPs). This establishes a connection with the actin ring and with the actin cytoskeleton in the opposite half of the cell.

F. The SDV of the first hypothecal girdle band (hGB1) has emerged and expands away from the actin ring so that the hypovalve gets pushed out from underneath the epitheca. Since the nucleus has become suspended between the two cell poles by the association of the perinuclear microtubules with the actin filament system, it does not stay in the apical cell pole, but moves closer to the middle of the cell.

G. As the formation of hGB1 is nearing completion, the hypothecal cell pole is now further extruded from the epitheca. In the process of cell expansion the actin cytoskeleton in the hypothecal half softens allowing it to get stretched, whereas it maintains tension in the epithelial half, so that the nucleus is kept in the middle position.

H. Deployment of hGB1 on the protoplast surface underneath the cover of eGB2.

I. The SDV of the second hypothecal girdle band (hGB2) has emerged and begins to expand away from the stationary actin ring towards the hypothecal cell pole. This causes the hypotheca to further slide out from underneath the epitheca. As the cell expands in axial direction, the hypothecal actin system softens again and further proliferates, the nucleus remains suspended between the two opposite actin filament systems but stays at the left of the actin ring. The actin ring continues to act as a bumper thus securing the position of SDV edge.

K. In the process of hGB2 formation axial expansion continues. The actin cytoskeleton in the hypothecal half gets further stretched, whereas in the epithelial half the actin cytoskeleton maintains tension so that the nucleus is kept in the middle position.

L. hGB2 gets deployed to the surface of the protoplast underneath the cover or eGB2.

M. After the final phase of axial expansion, the actin cytoskeleton on the left side pulls tight until an equilibrium of tension forces is reached between the two opposite actin systems keeping the nucleus in the middle. The actin ring has lost connection with the external anchor points at the joint between eGB1 and eGB2 and has been taken along with the edge of the outward moving hGB2. Next, the cytokinetic ring will develop slightly offset towards the left, in the geometrical middle of the cell exactly over the

nucleus (not shown). Alternatively a small hGB3 forms and is located under the edge of epitheca (see Section 4.2.3.3.1).

4.1.3 Involvement of Chitin in Controlling Axial Cell Expansion

As detailed in the introduction of this chapter, the presence of chitin in the diatom frustule is undisputed. In order to investigate the potential link between chitin and the cytoskeleton in the centric species *Odontella sinensis*, fluorochrome-conjugated WGA was used as a specific probe for chitin. The pattern of WGA staining (Fig. 4) confirms that it is indeed chitin at the junctions between all frustule components, most strongly at the junction between epi- and hypotheca. This has independently been demonstrated by the recent study of Moritz Cremer (Cremer, 2013). The location of this label was definitely not inside the protoplast. This finding allows to further explore the hypothesis of axial expansion growth, because it provides a clue for the kind of mechanism that might stop expansion, otherwise the cell would fall apart. Also, the presence of chitin at the junctions between girdle bands provides an explanation for how the cell determines the location of the actin ring and the initial site of the GB-SDV, which is associated with the actin ring.

It should be undisputed that there is only axial expansion in diatoms, no circumferential expansion, because the latter is physically restricted by the cylindrical silica casing (frustule). Axial expansion, however, is principally not restricted by the frustule. The only restricting elements are the adhesive joints or laces acting as a braking device between girdle bands, preferentially the larger sleeve between the two thecal halves (see SEM images in Chapter 1, Figs. 4c₃ & 5a₁). If these would be missing, frustule components would become pushed apart and separated from each other by turgor pressure. This would inevitably cause a liberation of the protoplast from the frustule. In fact, this separation can be experimentally invoked by applying protein- and chitin- degrading enzymes to live diatoms. As has been shown in preliminary experiments, such a treatment causes the liberation of protoplasts depending on enzyme concentration and incubation time (not shown, see also (Cremer, 2013)). This confirms the suggestion made in Chapter 1 that the adhesive sleeve, observed by SEM at the joint between the thecae contains chitin together with some proteinaceous materials. The edges of girdle bands apparently also have chitin associated with them. One could then envision a scenario, where the sliding out of a freshly deployed girdle band promoted by turgor pressure, would come to a halt, when the two chitin laces, one on the epithecal edge and the other at the

hypothecal girdle band edge, come into contact with each other. Hydrogen bondages but also potential bridging proteins and other polysaccharides capable of forming cross-links could potentially be involved in the linking mechanism. Whether subsequent down-regulation of turgor pressure and/or up-regulation of cytoskeleton-based tension returns the cell to normal, is an additional assumption. This scenario should be testable by experiments in future research.

The question, where the chitin comes from inside the cell, has not been experimentally clarified in the current study. However, recently published information gives a clue and also helps to understand, how the actin ring could be maintained at a fixed position. Diatoms obviously possess chitin synthases and it has already been shown that chitin fibers originate from transmembrane protein complexes in the plasma membrane, an example of that is the centric diatom *Cyclotella* (Herth, 1978; Herth et al., 1986). And indeed, most chitin genes in the centric diatom species *Thalassiosira* code for proteins that feature a transmembrane domain (Durkin et al., 2009). Two of these genes even code for chimeric proteins with a myosin motor domain on the N-terminus, whereas the chitin synthase domain is located on the extracellular C-terminus. This opens the possibility that these special isoforms of chitin synthase, which incidentally have similar members in filamentous fungi (Tsuizaki et al., 2009), can form a physical link between the actin ring on the inside of the cell and the chitin polymer networks outside of it, as long as they are enzymatically engaged (see also Part III. General Discussion, Section 4.2.1).

Taken this information together with the data obtained in the current thesis, the following mechanism could be envisioned to explain, how the cell could be able to specifically predefine the location of the GB-SDV initiation site and how the cell regulates, in a controlled fashion, the axial expansion without the frustule falling apart.

Instrumental to this mechanism is the joint region between eGB1 and eGB2. As mentioned in the previous section (4.1.2.1), this is the location, where the actin ring, coming down from the hypovalve domain in front of the advancing valve SDV edge, is trapped most likely involving hydrogen bondages between the chitin at the advancing edge of SDV and the chitin at the girdle band junction. From this point on in the development, the actin ring remains stationary at this location, because of the actin ring associated chimeric chitin synthase molecules. Eventually, however chitin ceases or is inhibited by regulatory processes so that no physical links exist anymore between the extracellular chitin and the plasma membrane-inserted enzyme

molecules. This should be the prerequisite to allow the actin ring move forward with the deployed last GB (hGB2) during the final phase of axial cell expansion (see Fig. 17).

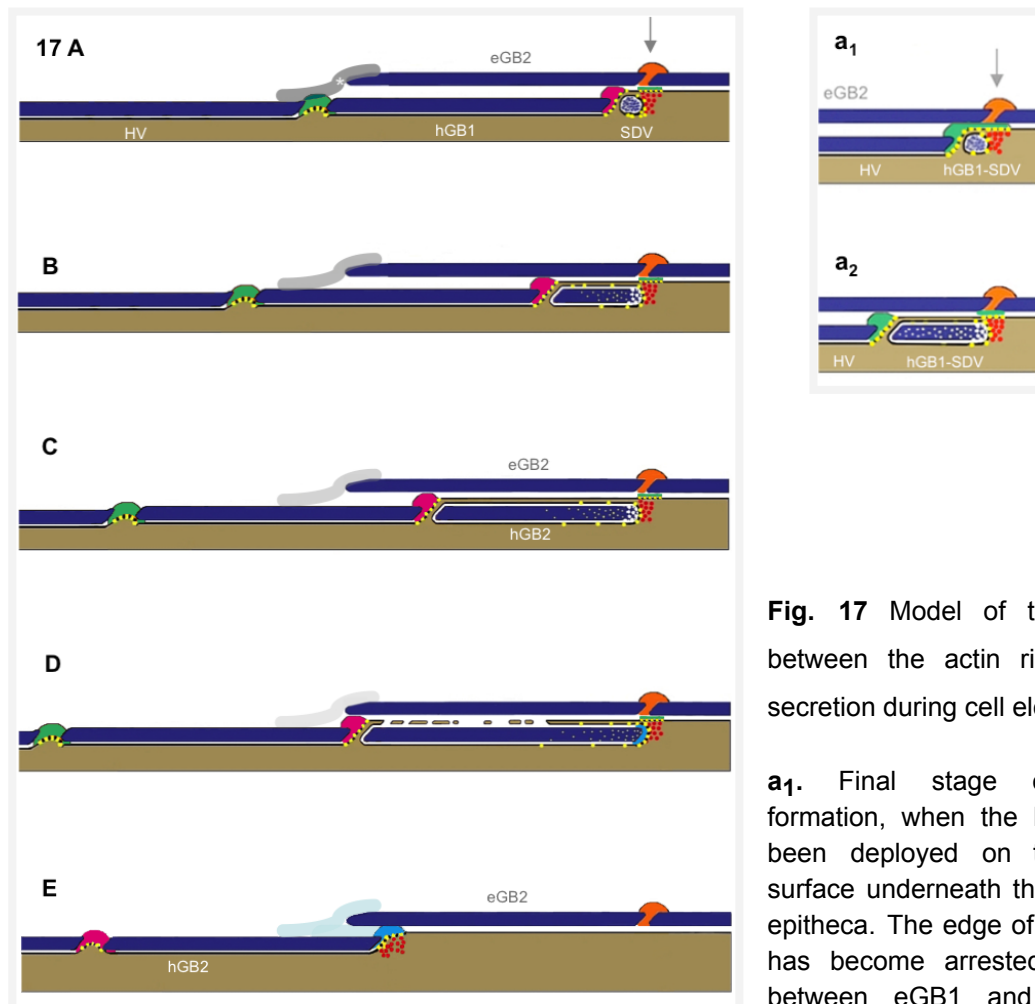


Fig. 17 Model of the interaction between the actin ring and chitin secretion during cell elongation.

a₁. Final stage of hypovalve formation, when the hypovalve has been deployed on the protoplast surface underneath the cover of the epitheca. The edge of the hypovalve has become arrested at the joint between eGB1 and eGB2 (grey arrow). Chitin-synthases (yellow

dots) originally inserted into the SDV membrane, now fused into the plasma membrane, continue to secrete chitin (green) into the space underneath the epitheca thus forming a physical connection between the edge of the hypovalve and the chitin cushion at the joint region (chitin anchor). The N-terminal myosin head domain of the chimeric chitin synthases attaches to the underlying actin ring (red dots). This fixes the position of the actin ring and consequently the abvalvar edge of the SDV of the first girdle band is also fixed in position.

a₂. By expansion growth of the hGB1-SDV the hypovalve is beginning to be pushed out from underneath eGB2. Fresh membrane material is becoming inserted into the plasma membrane area thus diluting out the number of chitin synthase molecules. This causes the break of the chitin cushion (green) into a small portion remaining at the original position at the joint between eGB1 and eGB2 (orange) and a larger portion moving with the edge of HV.

A. HV has been fully pushed out from underneath the cover of eGB2; hGB1 is completely fabricated and deployed underneath the cover of eGB2; the initial hGB2-SDV is inserted under the junction between eGB2 and eGB1 (grey arrow) and secured there by the original chitin-anchor (green).

The sleeve between the epi- and hypotheca (white asterisk) is a chitin-containing bandage originating from the mother cell. It may function as a friction brake pad counteracting axial expansion forces.

B. The abvalvar edge of the SDV is further secured by the actin ring, which remains in its original position, whereas the advalvar edge extends towards hGB1, which is getting pushed out from underneath the cover of the epitheca. The sleeve may suffer abrasion while sliding over the surface of the hypotheca during axial expansion.

C. Growth of SDV continues, chitin (white sprinkles within the blue-colored silica) gets woven into the matrix of the growing girdle band (hGB2), which is still underneath the cover of eGB2.

D. Fusion of the upper silica lemma with the plasma membrane during exocytosis of fully matured hGB2. Chitin-synthase localized along the interface between actin ring and silica lemma, now becoming the new PM. There it secretes a fresh cushion of chitin (sky-blue) at the abvalvar edge of hGB2. The sleeve is in a transparent grey, as it may get consumed by further abrasion.

E. Further expansion growth pushes the fully deployed hGB2 out from underneath eGB2, but the epitheca still slightly overlaps with the hypotheca. After shut down of chitin synthase activity plus extra forces from the cytoskeletal interaction, the actin ring detaches from its previous location and moves with the abvalvar edge of hGB2. The actin ring gets degraded at the onset of mitosis. The edges of hGB2 and eGB2 come in contact with each other by means of the chitin-containing sticky material (blue cushion) thus establishing the new junction between epi- and hypotheca. Aqua color of the sleeve indicates freshly secreted chitin-containing adhesive material. [How exactly the shut-down of chitin synthase is regulated and an additional force is exerted by the cytoskeleton is to be experimentally addressed in the future.]

Note: Chitin-containing adhesive material – orange & green (old), magenta (younger) and sky-blue (fresh) “cushions”; chitinase – yellow, chitin – white dots; actin ring – red dots.

4.2 Mitosis

4.2.1 Transformation of Mitotic Structures: MC, PC and Spindle

The MC (microtubule center) will disappear at the transition from interphase to mitosis, when spindle poles form. It has been suggested that the MCs of the daughter generation derive from the PCs (polar complexes) of the mother's mitotic spindle (Tippit and Pickett-Heaps, 1977). Earlier observations on *Melosira* (centric), *Diatoma* (pennate) and *Pinnularia* (pennate) have even suggested that the MC in turn is associated with the initiation of PCs (Pickett-Heaps et al., 1975, 1978; Tippit and Pickett-Heaps, 1977; Tippit et al., 1975). For example, in *Surirella ovalis* (Tippit and Pickett-Heaps, 1977), the early PCs get initiated at late interphase/preprophase as a conspicuous, sandwich-like multilayered structure near the MC, and then continue to grow

longer to become the mature PCs. When the cell enters into early prophase, the central spindle appears as a dense palisade of MTs between the two PCs; this is about the stage, when the MC disappears, which is still some time before metaphase.

In the current study of *O. sinensis*, a PC precursor (the initial form of PCs) is also found to locate beside the MC at preprophase. But whether it derived from the disassembling MC, as suggested to be the case in other species by Pickett-Heaps (Pickett-Heaps, 1991) or whether the MC just interacts with the PC-formation, is not clear. Then the MC soon disappears before mitosis and the precursor will transform into mature PCs, which involves elongation and increase density and complexity of the PC structure. At prophase, the *Odontella* PCs separate and a dense palisade of microtubules develops as described above between them, forming the central spindle as they further separate. At late telophase before the completion of cytokinesis, the new MC will reappear in each daughter of *O. sinensis*. Similar situation has been reported in the pennate *Surirella*, which suggests that new MCs derive from the PCs (Tippit & Pickett-Heaps, 1977). In *Odontella*, the MC may also derive from the PCs, however, the situation is more complicated due to the presence of the MT horn bundles.

4.2.2 Origin of the MT-Horn Bundles at Late Mitosis

In *Odontella*, the horn bundles are formed at late telophase from two additional MTOCs (they are termed here: hb-MTOCs), which are unique and have not been described in any diatom before. These sites form close to the ends of the telophase central spindle. Their origin is unknown, but one possibility is that they are hitherto unknown derivatives of the PCs (further speculation see Part III. General Discussion, Section 3.2). Each hb-MTOC gives rise to a pair of horn bundles. Each pair radiates out as narrow fans into two opposite directions. This can be seen in control cells (Fig. 10A of this chapter) and even better in Taxol-treated cells (Figs. 22d₁, 22d₂ of Chapter 3). Next the microtubule fans tighten into bundles and these bundles grow longer on both sides alongside the cytokinetic actin ring, which continues to straddle the middle of the telophase spindle (see below). The two opposite arms of the horn bundles merge at a slightly later stage into the MC, which can be visually distinguished in the immunofluorescent images (Fig. 11). No matter whether the hb-MTOC has fused with the MC, or they have interlocked together or one has replaced the other, this phenomenon could be taken as an indication that the hb-MTOC and the MC both originated from the same source at telophase,

meaning both types of centers are from the PCs and now as the horn bundles merge back on the MC, they become reunited. At least, it is safe to assume that both of them have MT-organizing properties. So, in summary, it appears that the transformation of the PC into the MC, which in other diatoms (i.e., *Surirella*, (Tippit and Pickett-Heaps, 1977)) occurs in one smooth process, is separated into a series of steps in *Odontella*, due to the formation of the unique horn bundles.

4.2.3 The Development of the Cytokinetic Ring

4.2.3.1 Proof of Actin in the Cytokinetic Ring

Unlike the situation in other organisms, which divide by the generation of a phragmoplast as in higher plants (Otegui et al., 2005) or by a phycoplast as in some green algae (Hoek et al., 1995; Raven et al., 2005), diatoms undergo cytokinesis by furrowing similar to animal cells (Pickett-Heaps and Spurck, 1982; Schmid and Volcani, 1983; Wordeman, 1992). It has always been inferred from the appearance of the cleavage furrow that a cytokinetic actin ring must be operating in diatoms (Cohn et al., 1989; Pickett-Heaps and Spurck, 1982; Wordeman and Cande, 1990). However, a direct experimental proof for this interpretation has not been provided so far. In *Odontella*, the cytokinetic ring can be strongly labeled with actin-specific antibodies that were generated against animal actin, e.g., MA1-744 or C11 (see Material and Methods, Section 2.4), indicating that it is composed of F-actin. And probably the cytokinetic actin ring in *Odontella* is also associated with myosins and a number of associated proteins, like that in animal cells.

4.2.3.2 The Timing of Setting up the Cytokinetic Ring

The localization mechanism of the cytokinetic actin ring of animal cells is still under debate, although it is postulated to rely on the spindle and/or on the astral microtubules (von Dassow, 2009; Maddox and Oegema, 2003). However, the determination of the cleavage plane position in diatoms has been assumed to be under the control of cortical determinants before mitosis rather than by the location of the nucleus, based on a microtubule interruption-recovery experiments on the centric diatom *Stephanopyxis turris* (Wordeman, 1992). It was found that the nucleus became displaced from the middle of the cell as a result of inhibition by the microtubule

depolymerizing drug Nocodazol; however, when the inhibitor had been washed away, the nucleus that formed a normal mitotic spindle inside was still displaced, but surprisingly the cleavage furrow appeared at the middle girth, suggesting the displaced spindle and nucleus, cannot affect the position of the division plane (Wordeman, 1992). This disagrees with the long-held notion by Schmid that the nucleus and the MTs take effect in the location of the cleavage furrow, which was drawn from experiments on the nuclear positioning of *Coscinodiscus wailesii*, as well as *Cerataulina bergonii*, some *Rhizosolenia spp.*, *Chaetoceros didymus*, *Stephanopyxis turris*, *Ditylum brightwelli*, whose nucleus was always positioned at the middle girth, when the cell was preparing for mitosis (Schmid and Volcani, 1983). No matter what the initiation mechanism is, however, the common point of both views is that the determination of the division plane is before mitosis.

In the current study on *Odontella sinensis*, a cytokinetic actin ring is found to be initiated and established at late interphase/ preprophase, which is in agreement with Wordeman, as well as Schmid & Volcani. Two observations have been made with regard to the cytokinetic actin ring formation, which are important and unique. The first is that the cytokinetic ring forms, when the obsolete, old GB-actin ring is still present; the second is that the cytokinetic actin ring is associated with the pair of PCs from their earliest stages on and then remains associated with the developing spindle throughout mitosis such that the cytokinetic ring crosses over the spindle axis at right angles. These two observations naturally give rise to the question, whether the location of the cytokinetic actin ring correlates with the position of the GB-actin ring or with the PC precursor at the equator (further discussion see Discussion 4.2.3.3.2).

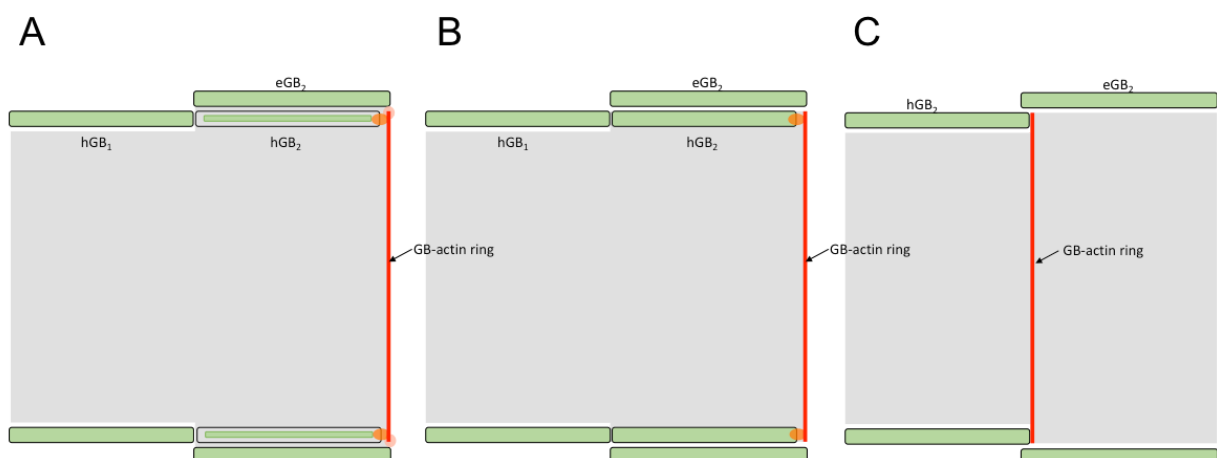
4.2.3.3 The Initiation of the Assembly of the Cytokinetic Actin Ring

4.2.3.3.1 The Role of the GB-Actin Ring

The spatial correlation of the cytokinetic ring in the state of assembly with the GB-actin ring in the state of disassembly prompts several more questions. For instance, how can a cell recruit assembly components for one actin ring to a specific site in the cell, when nearby a seemingly similar actin ring is becoming disassembled at the same time. A simple answer could be that, while both rings contain F-actin, they might still be very different. For one, the molecular components other than actin in the rings may not at all be the same. For instance the GB-actin ring might have a supplement of actin-cross-linking proteins plus proteins functioning as linkers

to the plasma membrane and silica lemma, but either much less myosin motor molecules or different types of it and on the whole, the F-actin polymers could be very long and arranged in a parallel collinear fashion. The cytokinetic actin ring, on the other hand, could be made of short, antiparallel actin filaments held together by cross-bridging bipolar myosin filaments, which is also the typical feature for cleavage furrows of animal (von Dassow, 2009) and yeast (Wu et al., 2006), together with other typical components such as formins (Kovar et al., 2003), septins (Joo et al., 2005), anillins (Piekny and Glotzer, 2008). Such potential molecular differences could, after all, make it possible that the construction of one kind of ring could run temporally and spatially in parallel and side by side with the deconstruction of the other ring.

The second question is why and how a GB-actin ring gets detached from its original anchor site and follows with the abvalvar edge of the last hGB to come to a position near the geometrical middle of the cell. The answer to the question is not known, but it is conceivable that the last population of chitin synthase molecules responsible for secreting chitin into the SDV just before silicalemma fusing with the plasma membrane, maintain contact with the abvalvar edge of hGB2 via its chitin polymers (see above Section 4.1.2.2 and the step “E” of the model in Fig. 17), whereas the older population of chitin synthases has ceased its enzymatic activity as dictated by its half-life-time so that the connection to the joint between eGB1 and eGB2 is weakened. This idea is supported by the finding that the narrow hGB3, which is sometimes observed at the junction between hypo- and epitheca, never forms at the joint between eGB2 and eGB1 but always near the geometrical middle of the cell (see the off-set model suggested in Fig. 17-2 below).



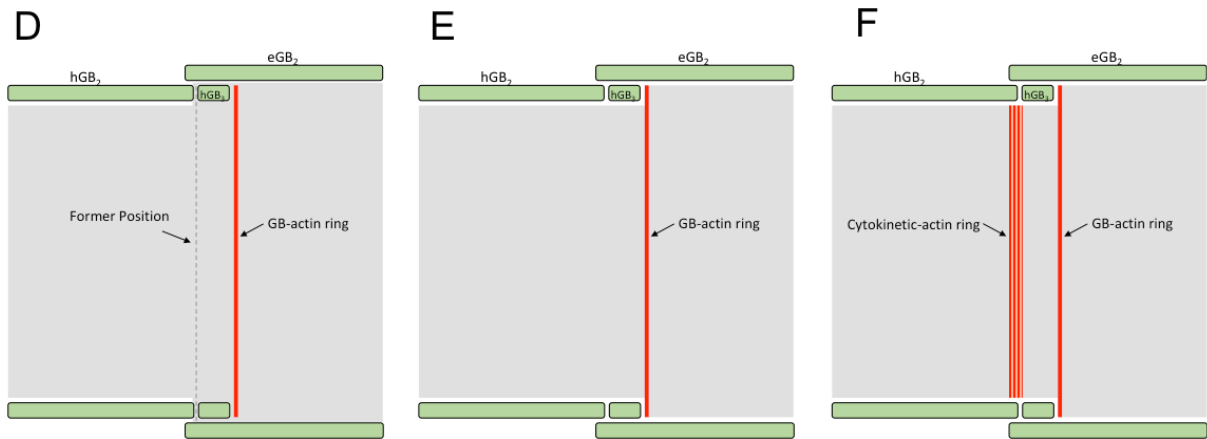


Fig. 17-2 The off-set model.

This would also answer the question, how the cell manages to maintain a constant close spatial relationship between the two actin rings, the GB-actin ring being always slightly offset the geometrical middle of the cell, usually a distance of 10 μm . The solution for this question could be found in the tension equilibrium mechanics and the frustule construction. At the end of interphase, tension generated by the two opposite sets of actin networks is proposed to reach equilibrium (see Fig. 15), which would result in placing the nucleus in the geometrical middle of the cell. Since hypotheca and epitheca slightly overlap, i.e., a small strip of hGB2 is still under the cover of eGB2, or the narrow hGB3 is made at this location (as shown in the model above), it will result in an equally small offset between the cytokinetic actin ring in the geometrical middle of the cell (the broad red band in the step 'F') and the GB-actin ring at the abvalvar edge of hGB2, so the latter is always located at the epithelial side of the cytokinetic actin ring (small red line in steps 'A' – 'F'). So following this reasoning, the GB-actin ring most likely does not function as a landmark for the placement of the cytokinetic actin ring, but the two rings are placed by two unrelated mechanisms close to each other.

4.2.3.3.2 The Role of the PC Precursor

It has been long appreciated that in many cell types, the division plane of a cell is established by a signal chain starting from the central spindle at anaphase, which acts as a molecular mark in the cell cortex for the recruitment of actin and other components relevant for furrow ingression (Chircop, 2014; Miller, 2011; Piekny et al., 2005). Based on the finding that *O. sinensis* develops

its contractile ring at late interphase/ preprophase and probably be ready at prophase (Fig. 8), the intuitive evidence is raised against the traditional view that the contractile ring assembly is regulated by anaphase spindle. And this is consistent with the speculation by Wordeman that the division plane of the centric diatom *S. turris* is determined prior to mitosis (Wordeman et al., 1986).

At prophase, one can see the thin actin ring at the equator extending on top of the PC precursor; then the ring becomes thicker, while the PC precursor transforms into a spindle in the following stages of the cell cycle. This close, spatial correlation suggests that the PC precursor may play a role in the assembly and the positioning the cytokinetic actin ring.

Potentially, microtubules coming off the PC structure (PC precursor and PCs) could serve as kind of a guidance, however, they run only a short distance alongside the developing ring, which should not be sufficient in guiding the growing ring around the entire circumference (e.g., Fig. 8a₂). So there must yet be something else that shapes the ring. The solution might reside in the dynamic properties of the cortical actin network. There is probably little axially directed tension left at this stage, because the axial actin cytoskeleton with its four branches of actin cables anchoring at the bases of LPs has largely disappeared in mitotic cells. Assuming the activation of regulatory factors promoting gradual, weak contraction of the cortical actin network in the middle of the cell and the presence of the right complement of actin binding proteins and motors (Ayscough, 1998; Nagaoka et al., 1995; Piekny and Glotzer, 2008), a circumferential actin belt would inevitably condense even without the involvement of PC precursor or PCs. However, such a shaping process still cannot guarantee the ring being placed exactly along the geometrical middle of the cell and between the two daughter nuclei. This could be the role of the PC precursor acting as a physical marker for the ring to form at the desired position (equator) across the prospective spindle. This way of positioning the cytokinetic actin ring follows the paradigm in animal cells (Miller, 2011) and fission yeast (Almonacid et al., 2009; Daga and Chang, 2005; Pollard, 2010; Tolic-Nørrelykke et al., 2005), saying that the spindle exerts a short range control on the position of the contractile ring. If however, the nucleus is removed far from the prospective division site, as in the above case of Nocodazole treatment, the cytokinetic actin ring can form autonomously (Wordeman et al., 1986).

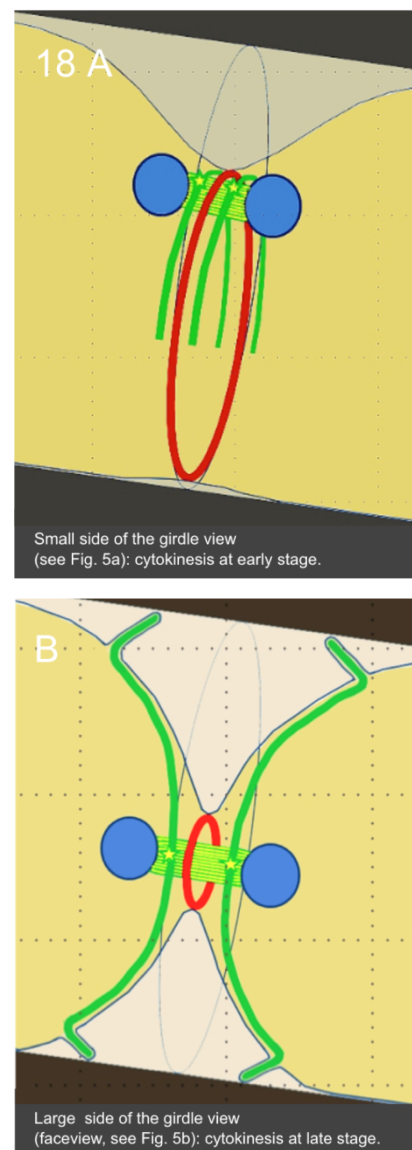
In *O. sinensis*, the assembly of the cytokinetic actin ring is complete at about anaphase, when the cytokinesis will be initiated, which is similar to the situation in animal cells (Fededa and Gerlich, 2012). The cytokinetic actin ring appears as a ribbon and assuming that it consists of

many units of actin filaments, one would expect that it increases in size as it constricts. However, since this is not the case, it suggests that it undergoes continuous reshaping by which the number of F-actin units gets simultaneously reduced in the same way as for example in fission yeast (Pollard and Wu, 2010).

4.3 Localization of Horn Bundles during Cytokinesis

As the cytokinetic actin ring is assuming its final pre-constriction shape, horn bundles lining up alongside take the ring into the middle between them (see Fig. 10B). When the constriction initiates at around anaphase, the dividing nucleus is still located in the cell cortex on the large face of the oval division plane (e.g., Fig. 10b₁). When focusing with the microscope into the cell at the position of the nucleus, the cytokinetic actin ring comes first into focus, followed right after it by the spindle without any empty space between them, so it is clear that the ring presses onto the spindle. This also implies that the constriction begins at the large face of the protoplast. When looking through the small face of the oval cross-section (which in practical terms is not possible because the cell is always oriented with the large face towards the observer), one would see that the elongated horn bundles sit on the slopes of the incipient furrow, while the furrow cuts through between them, as if they would aid in the cleavage process, i.e. by mechanically stabilizing the slopes on both sides of the cut (Fig. 18A).

Later, the constriction further moves the spindle further down into the middle of the cell, so that the future daughter nuclei come to lie almost exactly at the center of the division plane, and the horn bundles run exactly along the major axis of the plane, acting like a clamp, which secures the position of the division configuration (Fig. 18B). This could involve anchoring the distal ends of the horn bundles onto the inner cell wall of



the mother frustule at the vertex of the major axis of the oval division plane. The presence of anchorage points at the immature horns has also been postulated by Pickett-Heaps (1990). The possible nature of this anchorage will be further discussed in the Section 3.4.2.4 of Part III. General Discussion.

The daughter nuclei and the elongated central telophase spindle as well as the horn bundles are still stably configuring together, which maintain their relative positions inside the cleavage furrow, until the central telophase spindle either breaks or tapers out at the end of cytokinesis. In this configuration, the role of the horn bundles is obvious — to control the position of the late telophase structures and to make sure they will be correctly positioned for the next steps in post-cytokinetic apical domain morphogenesis.

4.4 Post-cytokinetic Valve Morphogenesis

4.4.1 Silicification of the LPs

In diatoms, the silicification of the valve initiates at the "primary silicification site", which is where the initial SDV is located. In *O. sinensis*, two of these sites form, one on either side of the nucleus, where the horn bundles slightly bulge out, before they sharply bend their ends forward to shape the actual horn (ocellar protrusion). At the primary silicification site, a base plate is created first as the future anchorage of the LP (labiate process) in the frustule and next the initial SDV stretches to form the slit-like annulus (Li and Volcani, 1985a; Pickett-Heaps et al., 1990). Not much more is known about the primary silicification sites in *Odontella*. In principle, however, they are similar to that in the centric diatom *Ditylum* that has only one LP, which initiates from the centrically positioned round SDV on top of the valve domain. In their fine structure studies, Li and Volcani report on the earliest identification of these sites by the appearance of the so called "labiate process forming apparatus" (LPA), which is a local membrane associated differentiation of the silica lemma. The LPA first gives rise to the base plate wrapped within the SDV. From the base plate, a hollow tube, made of a dense silica wall, grows out, whose inner and outer side is completely wrapped by the silica lemma (Li and Volcani, 1985a); through the base plate, the tube opens towards the inside by a slit with embossed rims like a pair of lips, the labiae (Li & Volcani 1975), which better explains, why the term "labiate process" has been chosen to describe this spiny extension of the frustule (see also the sketch in Fig. 5 of Section 3.3.1 in Part III). But the discovery of the LPs so far has only been

limited in the description of the morphology, which does not give a hint as to how these structures are guided to develop.

As shown in the current result of *O. sinensis*, the silica fluorescence of the LPs at different morphological stages is well present, but cytoskeleton signals are hard to be seen. Only in some case, very dim fluorescence of actin could be recognized in the LPs (e.g., Figs. 13 A₁ – B₂), but yet the possibility of background fluorescence cannot be ruled out. As it is known that, different to horns, there is obviously no cytoplasm within LPs and its silica surface is smooth rather than the areola chamber pattern seen in the silica casing of the horns, implying the LP elongation is mainly based on silica precipitation by self-assembly rather than guided by a cytoskeletal scaffold. A clear difference between the LPs and the rest of the frustule has been observed earlier (Zhang, 2012), showing that the entire frustule including the horns could be fluorescently stained by Calcofluor White, whereas only the LPs remained unstained, indicating the presence of beta-hydroxy-linked polysaccharides in the organic layer (see introduction of this chapter), which obviously is missing from the LPs. This significant difference may be exploited in future taxonomic research to distinguish ocellar protrusions/elevations from LPs.

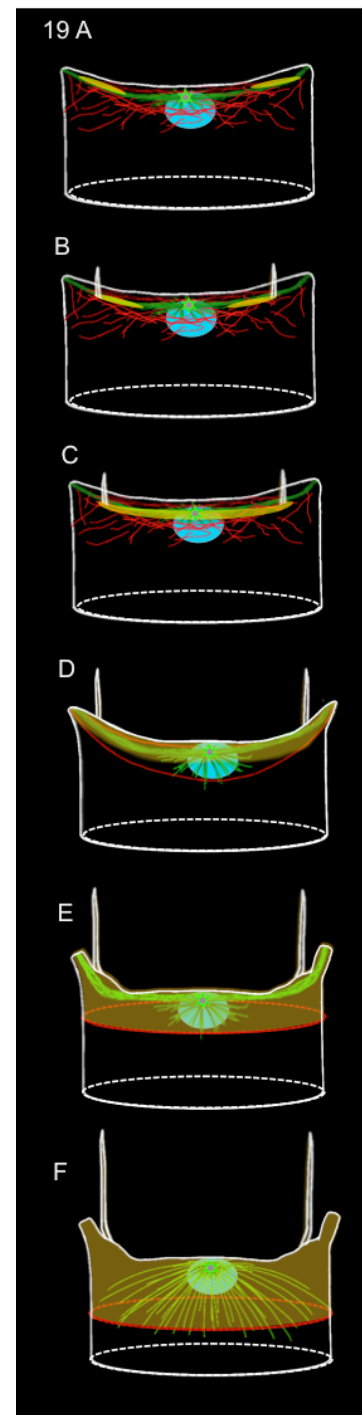
4.4.2 Formation of the Head Plate

Cytoskeletal guidance is certainly involved in the sculpturing of the valve head plate. As discussed above, two primary silicification sites are formed in *Odontella* before the completion of cytokinesis. And after cytokinesis, these two sites are speculated to fuse together to form the apical region of the valve (named "head plate" here, (Li and Volcani, 1985a)). The early TEM study on *O. sinensis* shows that before the completion of cytokinesis, the initial SDV at each side of the head plate region is found to be situated on top of the labiate process apparatus (LPA, a structure related to the LP initiation) (Li and Volcani, 1985b), which means the primary silicification site is determined by the LP initiation site. But since the actin ring only occurs after cytokinesis, it suggests the location of the silicification site is not related to the actin ring. Unfortunately, there is no striking structural clue to answer how LPs come to be initiated at exactly this cell location. And in combine with the current observation that an initial SDV presents in each of the newly divided daughter cell (Fig. 11C), although the PDMPO staining cannot well present the location of initial SDV, the spatial relationship between the initial SDV and the cytoskeleton is assumed by presenting in Fig. 19A. When the formation of the LP shaft is well in progress, additional fine silica deposition can first be detected extending from the base

plate proximally towards the head plate center in the form of two narrow stripes, one on each side (Fig. 19B). These stripes are interpreted here as the compressed annuli in the state of their formation. The term “annulus” has originally been assigned to the circular silica pattern center in the very early stages of silica deposition in the valve-SDV of many radially symmetrical centric diatoms (Li and Volcani, 1985a). The compressed slit shape of the annuli as well as the duplication in number occurring in *Odontella* may be regarded a derived geometrical variation of this original pattern. Other derived geometries of the head plate are triangular (*Lithodesmium*), polygon-shaped (*Asterolampra*). Then silica deposition along the slit will cause the formation of a fine strip lining the contours of the annuli. The closure process at the open end of each annulus is very hard to catch, but it does close and after that, the formation of vertical silica ribs coming off the strips starts simultaneously for both annular slits. This will bring about the two SDVs from the primary silicification sites fusing together, which will eventually give rise to the head plate with an embossed ridge around (Figs. 19 A – D). Then the combined valve SDV extends around the contours of the head domain and around the predefined horn protrusion and finally extends to the end of the valve dome (Figs. 19E & 19F, see also Section 3.4.2.1 in Part III).

The microtubule configuration of the horn bundle undergoes some subtle changes at the time, when the annuli appear, although these are very difficult to pin down. It may best be described as a partial splicing of the microtubule bundles in the region between the position of the LP base plates and the nucleus (e.g., Fig. 11e). This suggests a function of microtubules in the spacing of the annular slit, but there is little more that can be said here so far. And more evidence on the cytoskeletal involvement in annulus formation will be provided in Chapter 3.

Interestingly, the head plate of the valve is armored by a sharply edged ridge, which conspicuously separates it from the smooth slope of the dome (see Fig.11A in Chapter 1) and



the question is, how this is made. The following idea might be helpful to explain the mechanism: Silica morphogenesis in the SDV naturally depends on the supply of materials, but it should also depend on cytoskeleton molding the contour of the silicella. Because if one assumes that the silicification can run in an auto-regulatory fashion inside the SDV, when no other guiding mechanisms are put in place, the SDV would expand centripetally along with the increment of the silica deposits at the stage, which turns out to be a correct idea as experimentally proven in Chapter 3 (Fig. 7A). Since the sharp edge circles the head plate region between the two horns, it is likely that the head plate SDV extending between the horns would become stalled by the actin ring, which is hooked onto the tips of the horn bundles. At this stage, the actin ring that is also anchored in the plasma membrane may have acquired a certain inner stability due to extensive bundling of actin filaments and should be capable of generating some tensional force. This would bring the approaching valve SDV to a transitional halt or at least a slow-down of its peripheral expansion. Stalled by the actin ring, new silica deposits cannot be added at the margin and also can not evade down the bottom of the SDV, but addition of silica can evade up the top area, where the SDV is not reinforced. This naturally gives rise the fabrication of an embossed silica edge around the entire head domain.

This assumption may also be applicable to explain the existence of another embossment which often (not always) runs around the bottom ridge of the valve (SEM images and also shadow images, see Figs. 2a₁, 4c₁, 9D in Chapter 1), as if another phase of stalling had happened right before termination of valve morphogenesis: As we know, after the development of horns, the horn bundles will splice apart and spread, giving rise to a dome shaped radial perinuclear microtubule system encircled by an actin ring performing a very smoothly orchestrated circumferential widening, which provides a moving border for the expanding valve-SDV. To achieve this, one can assume that the actin ring may yield by increasing its diameter (by increasing the length of individual actin filaments) in order to reduce tensional strength. At some point the diameter of the mother frustule dictates the maximum diameter of the daughter valve. Growth of the valve continues and is probably driven from that point on by the silica assembly pressure curtailed by the confining actin ring, until the prospective anchorage site of the actin ring is reached. The termination signal for this process is yet unknown, but it needs to be delivered, when the advancing edge of the valve SDV eventually reaches the junction between eGB1 and eGB2 (see Fig. 17 and Discussion 4.1.3), it might have to do with chitin.

4.4.3 Bending of the Microtubule Horn Bundles

A unique feature of the horn bundle stage is that the distal ends of the bundles become curved outwards, extruding towards the opposite sister cell thereby a local cytoplasmic protuberance is formed, which is to become the ocellate elevation (horn). It has been suggested that the partial retraction of the daughter apex is an integral part in the post-cytokinetic morphogenesis (Pickett-Heaps et al., 1990), which would leave some room for a hypothesis, i.e., that the horn bundles get passively bent forward, once their distal ends have arrived at the cell margins and begin to further push outwards, because the cell apex is retracting backwards simultaneously (see the video #1 from my master thesis (Zhang, 2012), in the Appendix).

But beyond the involvement of cytoplasmic retraction, an alternative mechanism might be considered. It is based on the observation that the curving of horn tips is remotely reminiscent to the bending of the axoneme in a flagellum (Wargo and Smith, 2003) in that it may involve asymmetric parallel sliding of microtubules, i.e., the ones in the outside bend slide further than the ones in the inner bow of the curved bundle. As in the flagellar axoneme, sliding translates into bending, because the distal microtubule ends are firmly connected with each other. This, however, is only a speculation, unless one would be able to specifically address the potential MT-dependent motor proteins, which should be dyneins, if one takes the axoneme as the paradigm (Warner and Mitchell, 1981).

The other aspect that may also be considered is that the front face of the horn remains uncovered with silica for some time (see Fig. 12B, also see Fig. 18a₃ in Chapter 1) and this retardation is probably related to the fact that the pattern of the prospective ocellar plate² is different to that of cylindrical wall of the horn. This case also calls for a mechanism to regulate the silicification of the horn closure.

Combining both aspects, it is reasonable to assume that the diffuse actin patch recognized by anti-actin C11 at the tip of the horn (Fig. 11e) takes action at this state. It may be functional as follows: First, the actin patch can stabilize the tip of the forward-bending horn bundles, which therefore would prevent the random bending behavior of the bundles. Second, the actin patch prevents the valve-SDV margin from quickly closing the front face of a horn and further may be

² Ocellar plate is armored with knobs and perforated by small pores, which may serve a special function related to cell-to-cell contact between neighboring cells with in a chain of cells.

instrumental in the construction of the porous pattern of the ocellar plate, which is typically present at this location (see Fig. 12e in Chapter 1); then the patch connects the valve actin ring when the expanding ring reach to it (Fig. 11e of Chapter 2) and halt the ring there until the head plate formation completes. Traces of the actin patch are still present during splicing and spreading of the microtubule horn bundles, but they become undetectable, when the actin ring at the advancing valve edge has moved away (Fig. 13C of Chapter 2, see also the model presented in Fig. 10 of Part III).

4.5 Developmental Road Map

1. Interphase — The mature cell of *O. sinensis* is equipped with four girdle bands. Two girdle bands and a valve are inherited from the mother cell and serve as epitheca components. A new hypovalve and two more girdle bands are formed by the daughter and serve as hypotheca elements. The nucleus is located right under the forming SDV, which is usually located under the cover of eGB2. The valve-actin ring grows from small to the circumference of the cell, moving from the apical domain of the daughter protoplast to the joint between eGB1 and eGB2. From that stage onwards it serves as GB-actin ring. It remains placed between eGB1 and eGB2, at the growing front of the SDV and serves as a bumper. A microtubule center (MC) always appears on the nuclear surface during this period. Microtubules do not appear to play a role in the shaping of girdle bands, but may be important for nuclear positioning. Microtubules and actin filaments cooperate to maintain the tension equilibrium of the cell. The hGB1 is pushed out from underneath the cover of eGB2, when hGB2 is fabricated in the next GB-SDV, whereas hGB2 is moved out from underneath eGB2 by axial expansion, i.e., without another SDV in the same size coming after it. When the cell reaches full length by extruding the silica components of hypotheca, interphase is almost completed.

2. Preprophase — It is a period close to the end of interphase but right before mitosis. The MC disappears and is replaced by the precursor of the polar complex (PC) which will then develop into a pair of mature PCs. Meanwhile, the cytokinetic actin ring is assembled next to the existing GB-actin ring. When the cytokinetic actin ring have become exactly positioned across the developing spindle which is derived from PCs, mitosis will proceed.

3. Mitosis — Chromosomes get segregated and move towards the two spindle poles. Close to each daughter nucleus MT-horn-bundles grow outwards from the central spindle toward the

co-vertices of the cellular cross section alongside the surface of inner cell wall. Next, the MC reappears on the surface of each daughter nucleus. Starting at anaphase, cytokinesis occurs by constriction of the cytokinetic ring.

4. Post-cytokinetic phase — Horn bundles set the bipolar symmetry of the valvar head plate, from which two labiate processes (LPs) grow. There is a spatial correlation between the LPs and the horn bundles in the sense that they develop from the surface of the horn bundles, where the bundle is slightly bulging out. A new actin ring begins to form at the edge of the head plate. The MT-horn-bundles bend sharply at their distal ends thus forming a cytoplasmic protrusion, which serves as a mold for horn development. Then the actin ring moves with the expanding front of the valve SDV; in the meantime, the radial, perinuclear MT-system establishes a dome coinciding with the growing valve-SDV (Fig.9).

A summary of the developmental stages is described in the figure below. And the roadmap of the morphogenesis during the cell cycle is attached in the following page.

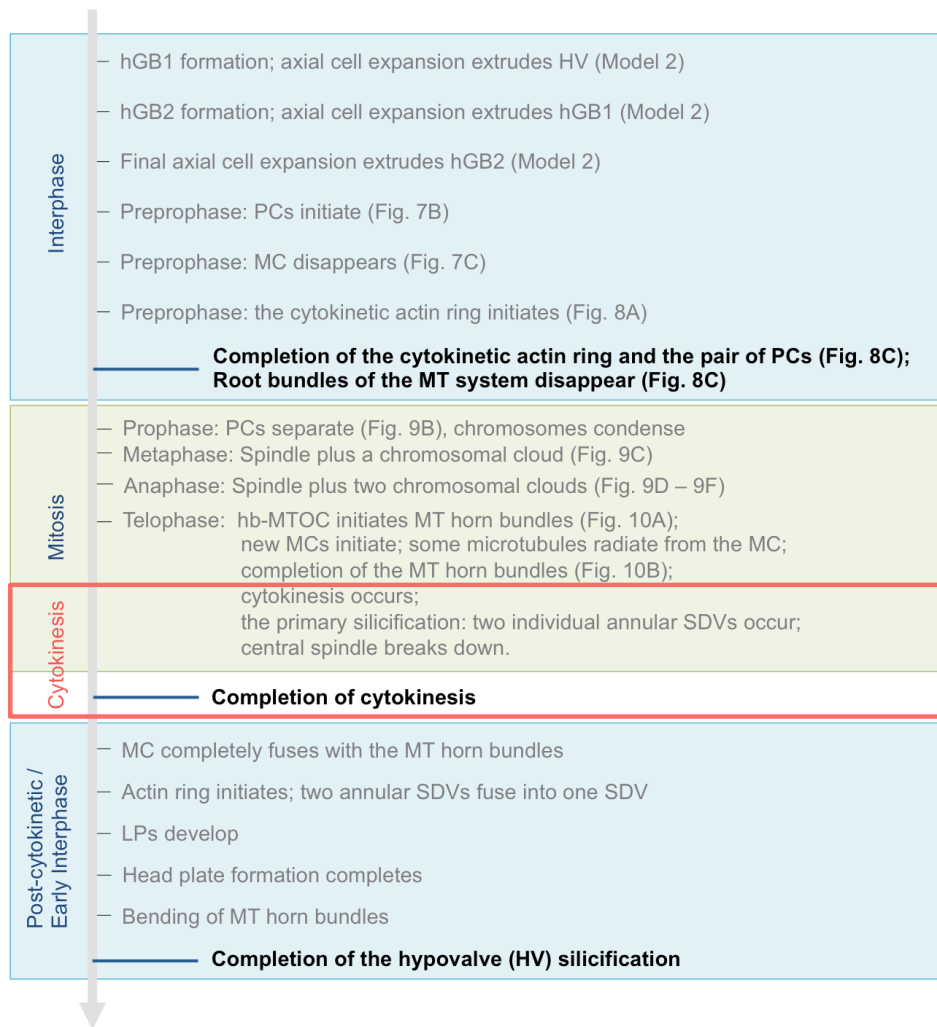
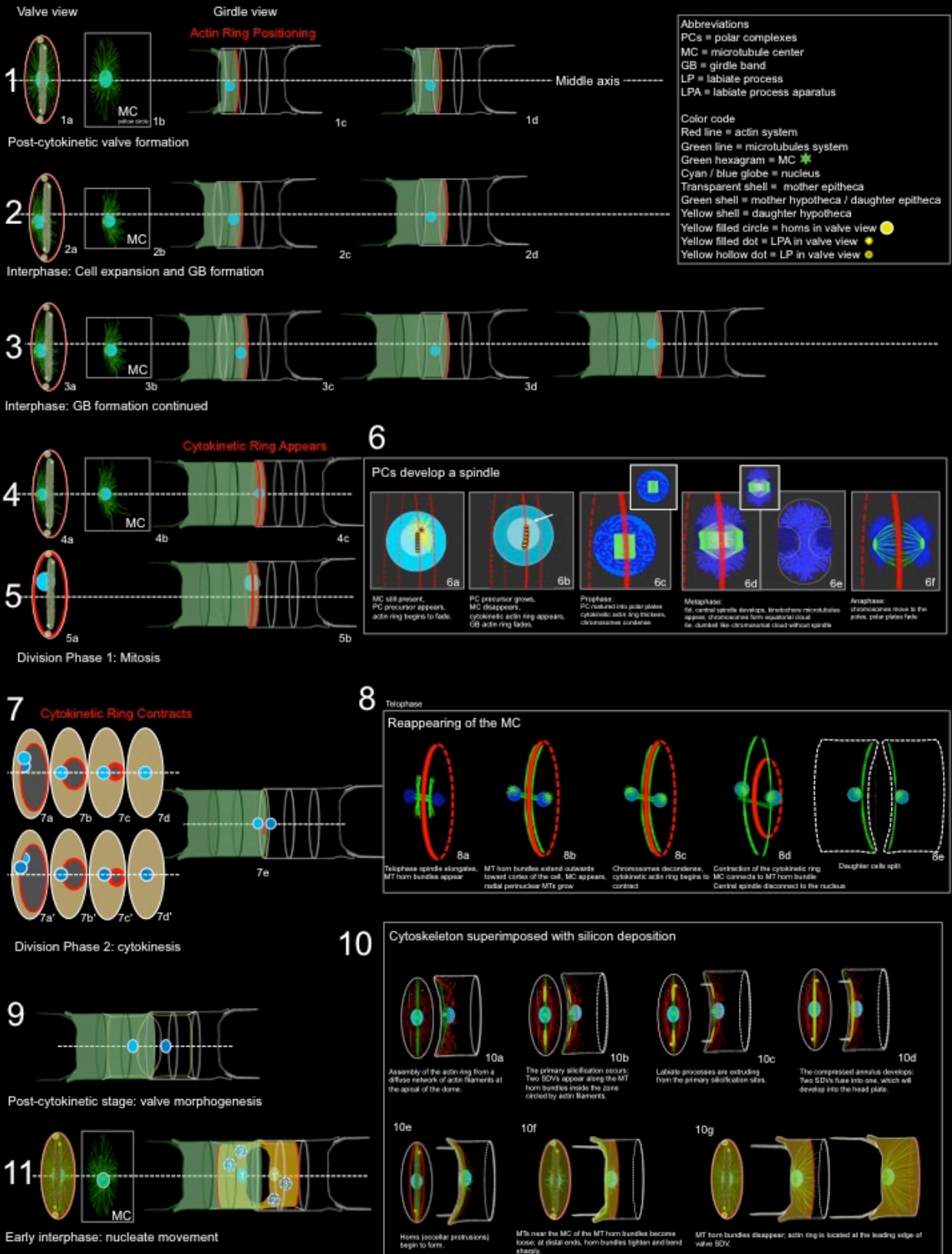


Fig. 20 Summary of the special morphogenetic activities of cytoskeleton in *O. sinensis*.

Roadmap of Morphogenesis in *O. sinensis*



5 References

- Almonacid, M., Moseley, J.B., Janvove, J., Mayeux, A., Fraisiert, V., Nurse, P., and Paoletti, A. (2009). Spatial control of cytokinesis by Cdr2 kinase and Mid1/anillin nuclear export. *Curr. Biol.* **19**, 961–966.
- Andersen, R.A. (2004). Biology and systematics of heterokont and haptophyte algae. *Am. J. Bot.* **91**, 1508–1522.
- Annenkov, V.V., Danilovtseva, E.N., Zelinskiy, S.N., Basharina, T.N., Safonova, T.A., Korneva, E.S., Likhoshway, Y.V., and Grachev, M.A. (2010). Novel fluorescent dyes based on oligopropylamines for the in vivo staining of eukaryotic unicellular algae. *Anal. Biochem.* **407**, 44–51.
- Annenkov, V.V., Basharina, T.N., Danilovtseva, E.N., and Grachev, M.A. (2013). Putative silicon transport vesicles in the cytoplasm of the diatom *Synedra acus* during surge uptake of silicon. *Protoplasma* **250**, 1147–1155.
- Aumeier, C. (2014). *The Cytoskeleton of Diatoms Structural and Genomic Analysis*. Doktorgrades. Bonn University.
- Aumeier, C., and Menzel, D. (2012). Secretion in the Diatoms. In *Secretions and Exudates in Biological Systems*, (Springer, Berlin, Heidelberg), pp. 221–250.
- Aumeier, C., Polinski, E., and Menzel, D. (2015). Actin, actin-related proteins and profilin in diatoms: a comparative genomic analysis. *Mar. Genomics* **23**, 133–142.
- Ayscough, K.R. (1998). In vivo functions of actin-binding proteins. *Curr. Opin. Cell Biol.* **10**, 102–111.
- Badour, S.S. (1968). Experimental separation of cell division and silica shell formation in *Cyclotella cryptica*. *Archiv Für Mikrobiologie* **62**, 17–33.
- Baskin, T.I. (2015). The Cytoskeleton. In *Biochemistry and Molecular Biology of Plants*, B.B. Buchanan, W. Gruissem, and R.L. Jones, eds. (John Wiley & Sons), pp. 191–238.
- Basu, R., and Chang, F. (2007). Shaping the actin cytoskeleton using microtubule tips. *Curr. Opin. Cell Biol.* **19**, 88–94.
- Blackwell, J., Parker, K.D., and Rudall, K.M. (1967). Chitin fibres of the diatoms *Thalassiosira fluviatilis* and *Cyclotella cryptica*. *J. Mol. Biol.* **28**, 383–385.
- Brunner, E., Richthammer, P., Ehrlich, H., Paasch, S., Simon, P., Ueberlein, S., and van Pée, K.-H. (2009). Chitin-based organic networks: an integral part of cell wall biosilica in the diatom *Thalassiosira pseudonana*. *Angew. Chem. Int. Ed.* **48**, 9724–9727.
- Chen, X., Ostadi, H., and Jiang, K. (2010). Three-dimensional surface reconstruction of diatomaceous frustules. *Anal. Biochem.* **403**, 63–66.
- Chiappino, M.L., and Volcani, B.E. (1977). Studies on the biochemistry and fine structure of

- silica shell formation in diatoms VII. Sequential cell wall development in the pennate *Navicula pelliculosa*. *Protoplasma* **93**, 205–221.
- Chircop, M. (2014). Rho GTPases as regulators of mitosis and cytokinesis in mammalian cells. *Small GTPases* **5**.
- Cohn, S.A., Nash, J., and Pickett-Heaps, J.D. (1989). The effect of drugs on diatom valve morphogenesis. *Protoplasma* **149**, 130–143.
- Collings, D.A. (2008). Crossed-Wires: Interactions and Cross-Talk Between the Microtubule and Microfilament Networks in Plants. In *Plant Microtubules*, (Springer, Berlin, Heidelberg), pp. 47–79.
- Crawford, R.M. (1973). The protoplasmic ultrastructure of the vegetative cell of *Melosira varians* CA Agardh. *J. Phycol.*
- Crawford, R.M., and Schmid, A.M. (1986). Ultrastructure of silica deposition in diatoms. *Biom mineralization in Lower Plants and Animals* **30**, 291–314.
- Cremer, T.M. (2013). Untersuchung der organischen Matrix in der Frustel von *Odontella sinensis*. Bachelor. Rheinische Friedrich Wilhelms University, Bonn.
- Currie, H.A., and Perry, C.C. (2007). Silica in plants: biological, biochemical and chemical studies. *Ann. Bot.* **100**, 1383–1389.
- Daga, R.R., and Chang, F. (2005). Dynamic positioning of the fission yeast cell division plane. *Proc. Natl. Acad. Sci. U. S. A.* **102**, 8228–8232.
- von Dassow, G. (2009). Concurrent cues for cytokinetic furrow induction in animal cells. *Trends Cell Biol.* **19**, 165–173.
- Dawson, S.C., and Paredez, A.R. (2013). Alternative cytoskeletal landscapes: cytoskeletal novelty and evolution in basal excavate protists. *Curr. Opin. Cell Biol.* **25**, 134–141.
- De Martino, A., Amato, A., and Bowler, C. (2009). Mitosis in diatoms: rediscovering an old model for cell division. *Bioessays* **31**, 874–884.
- Desclés, J., Vartanian, M., El Harrak, A., Quinet, M., Bremond, N., Sapriel, G., Bibette, J., and Lopez, P.J. (2008). New tools for labeling silica in living diatoms. *New Phytol.* **177**, 822–829.
- Drum, R.W. (1966). Electron microscopy of paired Golgi structures in the diatom *Pinnularia nobilis*. *J. Ultrastruct. Res.* **15**, 100–107.
- Dugina, V., Alieva, I., Khromova, N., Kireev, I., Gunning, P.W., and Kopnin, P. (2016). Interaction of microtubules with the actin cytoskeleton via cross-talk of EB1-containing +TIPs and γ -actin in epithelial cells. *Oncotarget* **7**, 72699–72715.
- Durkin, C.A., Mock, T., and Armbrust, E.V. (2009). Chitin in diatoms and its association with the cell wall. *Eukaryot. Cell* **8**, 1038–1050.
- Edgar, L.A., and Pickett-Heaps, J.D. (1984). VALVE MORPHOGENESIS IN THE PENNATE DIATOM *NAVICULA CUSPIDATA*1. *J. Phycol.* **20**, 47–61.

- Ehrlich, H., Deutzmann, R., Brunner, E., Cappellini, E., Koon, H., Solazzo, C., Yang, Y., Ashford, D., Thomas-Oates, J., Lubeck, M., et al. (2010a). Mineralization of the metre-long biosilica structures of glass sponges is templated on hydroxylated collagen. *Nat. Chem.* *2*, 1084–1088.
- Ehrlich, H., Demadis, K.D., Pokrovsky, O.S., and Koutsoukos, P.G. (2010b). Modern views on desilicification: biosilica and abiotic silica dissolution in natural and artificial environments. *Chem. Rev.* *110*, 4656–4689.
- Fededa, J.P., and Gerlich, D.W. (2012). Molecular control of animal cell cytokinesis. *Nat. Cell Biol.* *14*, 440–447.
- Ferrara, M.A., De Tommasi, E., Coppola, G., De Stefano, L., Rea, I., and Dardano, P. (2016). Diatom Valve Three-Dimensional Representation: A New Imaging Method Based on Combined Microscopies. *Int. J. Mol. Sci.* *17*.
- Goode, B.L., Drubin, D.G., and Barnes, G. (2000). Functional cooperation between the microtubule and actin cytoskeletons. *Curr. Opin. Cell Biol.* *12*, 63–71.
- Gordon, R., and Drum, R.W. (1994). The Chemical Basis of Diatom Morphogenesis††Dedicated to the memory of Judith Georgia Colburn, botanist, and her love for plants. In *International Review of Cytology*, R. Gordon, ed. (Academic Press), pp. 243–372.
- Hasle, G.R. (1968). The valve processes of the centric diatom genus *Thalassiosira*. *Nytt Mag. Bot.* *15*, 193–201.
- Hasle, G.R. (1972). Two types of valve processes in centric diatoms. *Nova Hedwigia* *1972*, 39.
- Hazelaar, S., Van Der Strate, H.J., Gieskes, W.W.C., and Vrieling, E.G. (2005). Monitoring rapid valve formation in the pennate diatom *Navicula salinarum* (Bacillariophyceae). *J. Phycol.* *41*, 354–358.
- Herburger, K., and Holzinger, A. (2016). Aniline blue and Calcofluor white staining of callose and cellulose in the streptophyte green algae *Zygnema* and *Klebsormidium*. *Bio Protoc* *6*.
- Herth, W. (1978). A special chitin-fibril-synthesizing apparatus in the centric diatom *Cyclotella*. *Naturwissenschaften* *65*, 260–261.
- Herth, W. (1979). The site of beta-chitin fibril formation in centric diatoms. II. The chitin-forming cytoplasmic structures. *J. Ultrastruct. Res.* *68*, 16–27.
- Herth, W., and Barthlott, W. (1979). The site of beta-chitin fibril formation in centric diatoms. I. Pores and fibril formation. *J. Ultrastruct. Res.* *68*, 6–15.
- Herth, W., and Zugenmaier, P. (1977). Ultrastructure of the chitin fibrils of the centric diatom *Cyclotella cryptica*. *J. Ultrastruct. Res.* *61*, 230–239.
- Herth, W., Mulisch, M., and Zugenmaier, P. (1986). Comparison of Chitin Fibril Structure and Assembly in Three Unicellular Organisms. In *Chitin in Nature and Technology*, (Springer, Boston, MA), pp. 107–120.
- Hoek, C., Mann, D., and Jahns, H.M. (1995). *Algae: An Introduction to Phycology* (Cambridge University Press).

- Imai, T., Watanabe, T., Yui, T., and Sugiyama, J. (2003). The directionality of chitin biosynthesis: a revisit. *Biochem. J* 374, 755–760.
- Joo, E., Tsang, C.W., and Trimble, W.S. (2005). Septins: traffic control at the cytokinesis intersection. *Traffic* 6, 626–634.
- Kovar, D.R., Kuhn, J.R., Tichy, A.L., and Pollard, T.D. (2003). The fission yeast cytokinesis formin Cdc12p is a barbed end actin filament capping protein gated by profilin. *J. Cell Biol.* 161, 875–887.
- Kröger, N., and Poulsen, N. (2008). Diatoms—From Cell Wall Biogenesis to Nanotechnology. *Annu. Rev. Genet.* 42, 83–107.
- Kucki, M. (2009). Biological Photonic Crystals: Diatoms: Dye Functionalization of Biological Silica Nanostructures.
- Kucki, M., and Fuhrmann-Lieker, T. (2012). Staining diatoms with rhodamine dyes: control of emission colour in photonic biocomposites. *J. R. Soc. Interface* 9, 727–733.
- Law, C., and Exley, C. (2011). New insight into silica deposition in horsetail (*Equisetum arvense*). *BMC Plant Biol.* 11, 112.
- Li, C.-W., and Volcani, B.E. (1985a). Studies on the biochemistry and fine structure of silica shell formation in diatoms. *Protoplasma* 124, 10–29.
- Li, C.-W., and Volcani, B.E. (1985b). Studies on the biochemistry and fine structure of silica shell formation in diatoms X. Morphogenesis of the labiate process in centric diatoms. *Protoplasma* 124, 147–156.
- Li, C.W., Chu, S., and Lee, M. (1989). Characterizing the silica deposition vesicle of diatoms. *Protoplasma*.
- Life Technologies Corporation (2013). LysoTracker® and LysoSensor™ Probes (Molecular Probes by Life Technologies).
- Maddox, A.S., and Oegema, K. (2003). Deconstructing cytokinesis. *Nat. Cell Biol.* 5, 773–776.
- Mann, S., and Perry, C.C. (1986). Structural aspects of biogenic silica. *Ciba Found. Symp.* 121, 40–58.
- Martínez, R.A., Isari, S., and Calbet, A. (2014). Use of live, fluorescently-labeled algae for measuring microzooplankton grazing in natural communities. *J. Exp. Mar. Bio. Ecol.* 457, 59–70.
- Mathur, J. (2007). The illuminated plant cell. *Trends Plant Sci.* 12, 506–513.
- McLachlan, J., McInnes, A.G., and Falk, M. (1965). STUDIES ON THE CHITAN (CHITIN: POLY-N-ACETYLGLUCOSAMINE) FIBERS OF THE DIATOM THALASSIOSIRA FLUVIATILIS HUSTEDT: I PRODUCTION AND ISOLATION OF CHITAN FIBERS. *Can. J. Bot.* 43, 707–713.
- van de Meene, A.M.L., and Pickett-Heaps, J.D. (2002). VALVE MORPHOGENESIS IN THE CENTRIC DIATOM PROBOSCIA ALATA SUNDSTROM1. *J. Phycol.* 38, 351–363.

- Menzel, D. (1993). Chasing coiled coils: intermediate filaments in plants. *Plant Biol.*
- Miller, A.L. (2011). The contractile ring. *Curr. Biol.* *21*, R976–R978.
- Mohan, R., and John, A. (2015). Microtubule-associated proteins as direct crosslinkers of actin filaments and microtubules. *IUBMB Life* *67*, 395–403.
- Morin, L.G., Smucker, R.A., and Herth, W. (1986). Effects of two chitin synthesis inhibitors on *Thalassiosira fluviatilis* and *Cyclotella cryptica*. *FEMS Microbiol. Lett.* *37*, 263–268.
- Mulisch, M. (1993). Chitin in protistan organisms: Distribution, synthesis and deposition. *Eur. J. Protistol.* *29*, 1–18.
- Nagaoka, R., Abe, H., Kusano, K., and Obinata, T. (1995). Concentration of cofilin, a small actin-binding protein, at the cleavage furrow during cytokinesis. *Cell Motil. Cytoskeleton* *30*, 1–7.
- Nozaki, H. (2005). A new scenario of plastid evolution: plastid primary endosymbiosis before the divergence of the “Plantae,” emended. *J. Plant Res.* *118*, 247–255.
- Oey, J.L., and Schnepf, E. (1970). Über die Auslösung der Valvenbildung bei der Diatomee *Cyclotella cryptica*. *Archiv Für Mikrobiologie* *71*, 199–213.
- Ogane, K., Tuji, A., Suzuki, N., Kurihara, T., and Matsuoka, A. (2009). First application of PDMPO to examine silicification in polycystine *Radiolaria*. *Plankton Benthos Res.* *4*, 89–94.
- Otegui, M.S., Verbrugghe, K.J., and Skop, A.R. (2005). Midbodies and phragmoplasts: analogous structures involved in cytokinesis. *Trends Cell Biol.* *15*, 404–413.
- Pacheco, A., and Gallo, G. (2016). Actin filament-microtubule interactions in axon initiation and branching. *Brain Res. Bull.* *126*, 300–310.
- Parambath, M., Hanley, Q.S., Martin-Martinez, F.J., Giesa, T., Buehler, M.J., and Perry, C.C. (2016). The nature of the silicophilic fluorescence of PDMPO. *Phys. Chem. Chem. Phys.* *18*, 5938–5948.
- Pickett-Heaps, J. (1991). Cell Division in Diatoms. In *International Review of Cytology*, K.W. Jeon, and M. Friedlander, eds. (Academic Press), pp. 63–108.
- Pickett-Heaps, J.D., and Spurck, T.P. (1982). Studies on kinetochore function in mitosis. I. The effects of colchicine and cytochalasin on mitosis in the diatom *Hantzschia amphioxys*. *Eur. J. Cell Biol.* *28*, 77–82.
- Pickett-Heaps, J.D., and Tippit, D.H. (1978). The diatom spindle in perspective. *Cell* *14*, 455–467.
- Pickett-Heaps, J., Schmid, A.-M.M., and Edgar, L.A. (1990). The cell biology of diatom valve formation. *Progress in Phycological Research* *7*, 1–168. pls. 1–101.
- Pickett-Heaps, J.D., McDonald, K.L., and Tippit, D.H. (1975). Cell division in the pennate diatom *Diatoma vulgare*. *Protoplasma* *86*, 205–242.
- Pickett-Heaps, J.D., Tippit, D.H., and Andreozzi, J.A. (1978). Cell division in the pennate diatom

- Pinnularia. I. Early stages in mitosis. *Biologie Cellulaire* 33.
- Pickett-Heaps, J.D., Tippit, D.H., and Andreozzi, J.A. (1979a). Cell division in the pennate diatom Pinnularia. IV. Valve morphogenesis. *Biologie Cellulaire*.
- Pickett-Heaps, J.D., Tippit, D.H., and Andreozzi, J.A. (1979b). Cell division in the pennate diatom Pinnularia. V. Observations on live cells. *Biologie Cellulaire* 35.
- Pickett-Heaps, J.D., Schmid, A.-M.M., and Tippit, D.H. (1984). Cell division in diatoms. *Protoplasma* 120, 132–154.
- Pickett-Heaps, J.D., Hill, D.R.A., and Wetherbee, R. (1986). CELLULAR MOVEMENT IN THE CENTRIC DIATOM ODONTELLA SINENSIS 1. *J. Phycol.* 22, 334–339.
- Pickett-Heaps, J.D., Cohn, S., Schmid, A.-M.M., and Tippit, D.H. (1988). VALVE MORPHOGENESIS IN SURIRELLA (BACILLARIOPHYCEAE) 1. *J. Phycol.* 24, 35–49.
- Piekny, A.J., and Glotzer, M. (2008). Anillin is a scaffold protein that links RhoA, actin, and myosin during cytokinesis. *Curr. Biol.* 18, 30–36.
- Piekny, A., Werner, M., and Glotzer, M. (2005). Cytokinesis: welcome to the Rho zone. *Trends Cell Biol.* 15, 651–658.
- Polinski, E. (2012). Immunfluoreszenzmikroskopische Untersuchung des Aktinzytoskeletts in der Kieselalge *Odontella sinensis*. Einfluss von Aktin-depolymerisierenden Agentien. Bachelorarbeit. Bonn University.
- Pollard, T.D. (2010). Mechanics of cytokinesis in eukaryotes. *Curr. Opin. Cell Biol.* 22, 50–56.
- Pollard, T.D., and Wu, J.-Q. (2010). Understanding cytokinesis: lessons from fission yeast. *Nat. Rev. Mol. Cell Biol.* 11, 149–155.
- Poulsen, N.C., Spector, I., Spurck, T.P., Schultz, T.F., and Wetherbee, R. (1999). Diatom gliding is the result of an actin-myosin motility system. *Cell Motil. Cytoskeleton* 44, 23–33.
- Preisner, H., Habicht, J., Garg, S.G., and Gould, S.B. (2018). Intermediate filament protein evolution and protists. *Cytoskeleton* 75, 231–243.
- Rasconi, S., Jobard, M., Jouve, L., and Sime-Ngando, T. (2009). Use of calcofluor white for detection, identification, and quantification of phytoplanktonic fungal parasites. *Appl. Environ. Microbiol.* 75, 2545–2553.
- Raven, P.H., Evert, R.F., and Eichhorn, S.E. (2005). *Biology of plants* (Macmillan).
- Ross, R., and Sims, P.A. (1972). The fine structure of the frustule in centric diatoms: A suggested terminology. *British Phycological Journal* 7, 139–163.
- Round, F.E., Crawford, R.M., and Mann, D.G. (2007). *Diatoms: Biology and Morphology of the Genera* (Cambridge University Press).
- Scheffel, A., Poulsen, N., Shian, S., and Kröger, N. (2011). Nanopatterned protein microrings from a diatom that direct silica morphogenesis. *Proc. Natl. Acad. Sci. U. S. A.* 108, 3175–3180.

- Schliwa, M. (1986). *The Cytoskeleton: An Introductory Survey* (Wien, New York: Springer Press).
- Schmid, A.M. (1979a). The development of structure in the shells of diatoms. *Nova Hedwigia* **64**, 236.
- Schmid, A.-M. (1984a). Tricornate spines in *Thalassiosira eccentrica* as a result of valve-modelling.
- Schmid, A.-M. (1984b). Wall morphogenesis in *Thalassiosira eccentrica*: Comparison of auxospore formation and the effect of MT-inhibitors.
- Schmid, A.-M.M. (1979b). Influence of environmental factors on the development of the valve in diatoms. *Protoplasma* **99**, 99–115.
- Schmid, A.M.M. (1980). Valve morphogenesis in diatoms : A pattern-related filamentous system in pennates and the effect of APM, colchicines and osmotic pressure. *Nova Hedwigia* **33**, 811–847.
- Schmid, A.-M.M. (1994). Aspects of morphogenesis and function of diatom cell walls with implications for taxonomy. In *The Protistan Cell Surface*, R. Wetherbee, J.D. Pickett-Heaps, and R.A. Andersen, eds. (Vienna: Springer Vienna), pp. 43–60.
- Schmid, A.-M.M. (2003). The evolution of the silicified diatom cell wall—revisited. *Diatom Res.* **18**, 191–195.
- Schmid, A.-M.M., and Schulz, D. (1979). Wall morphogenesis in diatoms: Deposition of silica by cytoplasmic vesicles. *Protoplasma* **100**, 267–288.
- Schmid, A.-M.M., and Volcani, B.E. (1983). Wall morphogenesis in *Coscinodiscus wailesii* Gran and Angst. I. Valve morphology and development of its architecture. *J. Phycol.* **19**, 387–402.
- Schmid, A.-M.M., Eberwein, R.K., and Hesse, M. (1996). Pattern morphogenesis in cell walls of diatoms and pollen grains: a comparison. *Protoplasma* **193**, 144–173.
- Schönitzer, V., Eichner, N., Clausen-Schaumann, H., and Weiss, I.M. (2011). Transmembrane myosin chitin synthase involved in mollusc shell formation produced in *Dictyostelium* is active. *Biochem. Biophys. Res. Commun.* **415**, 586–590.
- Shimamura, M., Brown, R.C., Lemmon, B.E., Akashi, T., Mizuno, K., Nishihara, N., Tomizawa, K.-I., Yoshimoto, K., Deguchi, H., Hosoya, H., et al. (2004). Gamma-tubulin in basal land plants: characterization, localization, and implication in the evolution of acentriolar microtubule organizing centers. *Plant Cell* **16**, 45–59.
- Shimizu, K., Del Amo, Y., Brzezinski, M.A., Stucky, G.D., and Morse, D.E. (2001a). A novel fluorescent silica tracer for biological silicification studies. *Chem. Biol.* **8**, 1051–1060.
- Shimizu, K., Del Amo, Y., Brzezinski, M.A., Stucky, G.D., and Morse, D.E. (2001b). A novel fluorescent silica tracer for biological silicification studies. *Chem. Biol.* **8**, 1051–1060.
- Takeshita, N., Ohta, A., and Horiuchi, H. (2002). *csmA*, a gene encoding a class V chitin synthase with a myosin motor-like domain of *Aspergillus nidulans*, is translated as a single polypeptide and regulated in response to osmotic conditions. *Biochem. Biophys. Res. Commun.*

298, 103–109.

Tesson, B., and Hildebrand, M. (2010a). Extensive and intimate association of the cytoskeleton with forming silica in diatoms: control over patterning on the meso- and micro-scale. *PLoS One* 5, e14300.

Tesson, B., and Hildebrand, M. (2010b). Dynamics of silica cell wall morphogenesis in the diatom *Cyclotella cryptica*: substructure formation and the role of microfilaments. *J. Struct. Biol.* 169, 62–74.

Tesson, B., Masse, S., Laurent, G., Maquet, J., Livage, J., Martin-Jézéquel, V., and Coradin, T. (2008). Contribution of multi-nuclear solid state NMR to the characterization of the *Thalassiosira pseudonana* diatom cell wall. *Anal. Bioanal. Chem.* 390, 1889–1898.

Thamatrakoln, K., and Kustka, A.B. (2009). When to say when: can excessive drinking explain silicon uptake in diatoms? *Bioessays* 31, 322–327.

Tiffany, M.A. (2002). VALVE MORPHOGENESIS IN THE MARINE ARAPHID DIATOM *GEPHYRIA MEDIA* (BACILLARIOPHYCEAE). *Diatom Res.* 17, 391–400.

Tiffany, M.A. (2005). Valve development in the diatom family Asterolampraceae H. L. Smith 1872. *Micropaleontology* 51, 217–258.

Tiffany, M.A. (2008). VALVE DEVELOPMENT IN *AULACODISCUS*. *Diatom Res.* 23, 185–212.

Tiffany, M.A. (2015). Valve and girdle band morphogenesis in the pseudocellate diatom species *Biddulphia biddulphiana* JESmith (Boyer) and *Isthmia nervosa* Kutz. *Nova Hedwigia* 61–95.

Tippit, D.H., and Pickett-Heaps, J.D. (1977). Mitosis in the pennate diatom *Surirella ovalis*. *J. Cell Biol.* 73, 705–727.

Tippit, D.H., McDonald, K.L., and Pickett-Heaps, J.D. (1975). Cell division in the centric diatom *Melosira varians* [Algae]. *Cytobiologie*.

Tolic-Nørrelykke, I.M., Sacconi, L., Stringari, C., Raabe, I., and Pavone, F.S. (2005). Nuclear and Division-Plane Positioning Revealed by Optical Micromanipulation. *Curr. Biol.* 15, 1212–1216.

Traub, P. (2012). *Intermediate Filaments: A Review* (Springer Science & Business Media).

Tsuizaki, M., Takeshita, N., Ohta, A., and Horiuchi, H. (2009). Myosin motor-like domain of the class VI chitin synthase CsmB is essential to its functions in *Aspergillus nidulans*. *Biosci. Biotechnol. Biochem.* 73, 1163–1167.

Van de Meene, A.M.L., and Pickett-Heaps, J.D. (2004). Valve morphogenesis in the centric diatom *Rhizosolenia setigera* (Bacillariophyceae, Centrales) and its taxonomic implications. *Eur. J. Phycol.* 39, 93–104.

Wargo, M.J., and Smith, E.F. (2003). Asymmetry of the central apparatus defines the location of active microtubule sliding in *Chlamydomonas* flagella. *Proc. Natl. Acad. Sci. U. S. A.* 100, 137–142.

Warner, F.D., and Mitchell, D.R. (1981). Polarity of dynein-microtubule interactions in vitro:

- cross-bridging between parallel and antiparallel microtubules. *J. Cell Biol.* **89**, 35–44.
- Wickstead, B., and Gull, K. (2007). Dyneins across eukaryotes: a comparative genomic analysis. *Traffic* **8**, 1708–1721.
- Wordeman, L. (1992). THE MITOTIC SPINDLE AND CELL CYCLE. *The Cytoskeleton of the Algae* **39**.
- Wordeman, L., and Cande, W.Z. (1990). Cytokinesis by furrowing in diatoms. *Ann. N. Y. Acad. Sci.* **582**, 252–259.
- Wordeman, L., McDonald, K.L., and Cande, W.Z. (1986). The distribution of cytoplasmic microtubules throughout the cell cycle of the centric diatom *Stephanopyxis turris*: their role in nuclear migration and positioning the mitotic spindle during cytokinesis. *J. Cell Biol.* **102**, 1688–1698.
- Wu, J.-Q., Sirotkin, V., Kovar, D.R., Lord, M., Beltzner, C.C., Kuhn, J.R., and Pollard, T.D. (2006). Assembly of the cytokinetic contractile ring from a broad band of nodes in fission yeast. *J. Cell Biol.* **174**, 391–402.
- Yamagishi, T., and Kawai, H. (2012). Cytoskeleton organization during the cell cycle in two stramenopile microalgae, *Ochromonas danica* (Chrysophyceae) and *Heterosigma akashiwo* (Raphidophyceae), with special reference to F-actin organization and its role in cytokinesis. *Protist* **163**, 686–700.
- Yamazaki, T., Owari, S., Ota, S., Sumiya, N., Yamamoto, M., Watanabe, K., Nagumo, T., Miyamura, S., and Kawano, S. (2013). Localization and evolution of septins in algae. *Plant J.* **74**, 605–614.
- Zhang, Y. (2012). Girdle Band Formation of *Odontella sinensis*. Master thesis. Faculty of Mathematics and Natural Sciences. Bonn University.
- Zhang, Y. (2013). Double Indirect Immunolabeling for the cytoskeleton of *Odontella sinensis*.
- Znachor, P., and Nedoma, J. (2008). APPLICATION OF THE PDMPO TECHNIQUE IN STUDYING SILICA DEPOSITION IN NATURAL POPULATIONS OF *FRAGILARIA CROTONENSIS* (BACILLARIOPHYCEAE) AT DIFFERENT DEPTHS IN A EUTROPHIC RESERVOIR(1). *J. Phycol.* **44**, 518–525.

Chapter 3

Cytoskeletal Dynamics in Consecutive Stages of Frustule Morphogenesis Challenged by Inhibitors

1 Introduction

As it has been introduced in section 1.3.2 of Chapter 2, many suggestions have been made so far on the involvement of microtubule cytoskeleton and actin cytoskeleton in the course of silica deposition and in the valve morphogenesis.

Although many fine structural evidences of coalignment between silica and cytoskeleton have been reported in control cells (Pickett-Heaps et al., 1990; Schmid, 1984, 2003), examinations of the cytoskeleton role mostly come from the work in combination with pharmacological inhibitors (Pickett-Heaps and Spurck, 1982; Schmid, 1980; Schmid and Volcani, 1983; Wordeman, 1992). The reason for applying this approach rather than silencing a certain cytoskeleton protein is that the knowledge of cytoskeleton gene sequences in the diatom is limited (only the genomes of centric diatom *Thalassiosira pseudonana* and the pennate diatom *Phaeodactylum tricorutum* are completely known (Vardi et al., 2008)) and the first gene modification on cytoskeleton (GFP labelled actin in live cell) has only been achieved recently (Aumeier et al., 2015), so there is no convenient molecular technique could be applied to *Odontella sinensis*, and the inhibition here is to use the traditional way.

1.1 The Inhibition of the Microtubule System

In Chapter 2, it was shown, that microtubules can be clearly visualized by immunofluorescence in *O. sinensis* and several other diatoms (e.g., see images plates Figs. 7.1 – 7.13 in Appendix). Therefore, it has become possible to monitor the reaction of the MT-cytoskeleton to microtubule

inhibitors (Dostál and Libusová, 2014). Of the several potent agents, which had been tested in preliminary experiments such as Colchicine, Nocodazole, Vinblastine, Amiprophos-methyl and Oryzalin, the latter has been chosen as the major pharmacological agent, because its interference with microtubule function in diatoms turned out to be reliable, reproducible and reversible (Mettbach & Menzel, unpublished). Its specificity was as high in diatoms as it was reported for the plant MT-cytoskeleton (Bajer and Molè-Bajer, 1986), whereas Colchicine had a much lesser effect.

While Oryzalin causes a break-down of the microtubule cytoskeleton, Taxol could be employed to achieve the opposite, i.e., stabilize microtubules (Bokros et al., 1993). Therefore this inhibitor was applied to *Odontella*, however, as presented below, the effects have been more subtle than expected.

Obviously, MT-binding proteins and MT-dependent motor proteins such as kinesin and dynein, are of great importance for microtubule function in the cell. However, nothing is known on these proteins and there were no suitable experimental approaches at reach to address their function in the diatoms. Neither are there specific antibodies available, nor has a sufficiently specific pharmacological agent been reported, which could interfere with microtubule-associated proteins (MAPs) or microtubule-based motors. Hence, these aspects had to be left aside for the time being.

1.2 The Inhibition of Actin Cytoskeleton

In my previous work ((Zhang, 2012) master thesis) the effect of Latrunculin A, as well as Jasplakinolide, as inhibitors of the actin cytoskeleton have already been initially investigated, I will further concentrate here on Jasplakinolide, which has originally been isolated from the marine sponge *Jaspis johnstoni* (Crews et al., 1986). This inhibitor has dramatic effects on the animal and the plant actin cytoskeleton (Bubb et al., 1994; Holzinger and Blaas, 2016; Sawitzky et al., 1999) and since it has turned out in preliminary experiments (Mettbach & Menzel, unpublished) to have similarly dramatic effects on diatoms, it was chosen here as the major pharmacological tool to interfere with the functions of the actin cytoskeleton in correlation with frustule morphogenesis. Since the major effect of this inhibitor is a massive breakdown and restructuring the actin cytoskeleton, it was of interest to see, what happens in the opposite case, when the actin cytoskeleton was protected against destruction. Therefore, the fungal

Phalloidin, Phalloidin (Holzinger and Blaas, 2016; Wehland et al., 1977; Wieland, 1987), was used with the intention to provoke over-stabilization of the actin cytoskeleton.

2 Materials and Methods

Cells were cultured and harvested as described in section 2.1 of Chapter 1. In general, they were treated by different inhibitors in the presence or absence of lysosensors PDMPO or HCK-123 to monitor frustule morphogenesis. Inhibitor treatment was stopped by double-aldehyde fixation (see Section 2.2 of Chapter 1). Then cells were subjected to immunofluorescence labelling (see Section 2 of Chapter 2), and finally stained with 1 μ M DAPI for 10 minutes. In the end, cells were mounted on slides.

2.1 Oryzalin

2.1.1 Short-term Incubations

2.1.1.1 Incubation only with Inhibitor. Cells were incubated in 1 μ M Oryzalin dissolved in f/2 medium for 60, 80 or 120 minutes, respectively. They were fixed, subsequently treated by immunofluorescence labelling of microtubules (TUB-1A2). Eventually, cells were stained by DAPI and mounted on slides.

2.1.1.2 Recovery Incubation. Cells treated by 1 μ M Oryzalin for 120 minutes were transferred to pure f/2 medium for 1, 2 or 4 hours. Then they were fixed, subsequently treated by immunofluorescence labelling of microtubules (TUB-1A2). Eventually, cells were stained by DAPI and mounted on slides.

2.1.1.3 Control and Inhibition in the Presence of Lysosensor. Cells were firstly stained by PDMPO for 2 hours, followed by 2-, 4- or 6-hour recovering period in pure f/2 medium; then cells were inhibited by 0.5 or 1 μ M Oryzalin in the presence of 0.5 μ M PDMPO. Afterward, cells were fixed. Alternatively, either microtubules (TUB-1A2) or microfilaments (C-11) were labelled by immunofluorescence. Eventually, cells were stained with DAPI and mounted on slides.

2.1.2 Long-term Incubations

2.1.2.1 “2+48 h” Inhibition. Lysosensor (PDMPO or HCK-123 in 0.5 μM) was absent in the first 2 hours of inhibition (0.5 or 1 μM Oryzalin), then present in the following 48 hours. Afterward, cells were fixed, double immuno-labelled (using Method 2/3 of Chapter 2), stained with DAPI and subsequently mounted on slides.

2.1.2.2 Simultaneous Inhibition (Inhibition in the Presence of Lysosensor). Lysosensor was presented in the whole 24- or 48-hour-inhibition (0.5 or 1 μM Oryzalin). Afterward, cells were fixed, either followed by double immunolabeling (using either method 2/3, see Table 2/3 of Chapter 2) or by no labelling at all. Eventually, cells were stained with DAPI and mounted on slides.

2.1.2.3 Confocal Microscopy. Cells after various treatments as described above were observed by confocal microscopy (for product information and setting details, refer to Section 2.5 of Chapter 2).

2.1.2.4 Time-lapse Photography. Cells were incubated with inhibitor (0.5, 1, 2, or 5 μM Oryzalin) in a μ -Dish (petri-dish with a gas permeable foil bottom, lumix, Sarstedt) which was mounted on the stage of an inverted microscope. The live observation was proceeded in a dark cool room with a dark:light cycle in 12 : 12h under 700 –1000 lux cool white fluorescent light. The light source for viewing the field of the inverted microscope was adjusted to almost darkness as perceived by naked eye. A high resolution CCD-Camera was adopted to capture a shot at regular time intervals and these shots are then recorded by the Visitron Meta-View programme (VISITRON Systems GMBH, Puchheim). These images were eventually edited into a video using Image J (imagej.nih.gov/ij/). Alternatively, a Canon EOS 1100D camera was used to capture static images; the auto-shooting was conducted by a timer remote controller TC-C1.

2.2 Taxol

Lysosensor (PDMPO in 0.5 μM) was present over the whole 24-hour inhibition period (1, 10, 100 μM Taxol). Afterward, cells were fixed and subsequently double immunolabeled (using either method 2/3 of Chapter 2). Eventually, cells were stained with DAPI and mounted on slides.

2.3 Jasplakinolide

2.3.1 2+48 Inhibition. Lysosensor (PDMPO or HCK-123 in 0.5 μM) was absent in the first 2 hours of inhibition (0.25, 0.5 or 1 μM Jasplakinolide), then present in the following 48 hours. Afterward, cells were fixed and subsequently double immuno-labelled (using either method 2/3 of Chapter 2). Eventually, cells were stained by DAPI and mounted on slides.

2.3.2 Time-lapse Photography. Same preparation procedure as Section 2.1.2.4.

2.4 Phalloidin

2.4.1 Short-term: Simultaneous Inhibition (Inhibition in the Presence of Lysosensor). Cells were incubated in 0.5 or 1 μM Phalloidin plus PDMPO dissolved in f/2 medium for 2 hours. Then they were fixed and immuno-labelled (double labelling – method 2 of Chapter 2; single labelling – tubulin::TUB-1A2). Eventually, cells were stained by DAPI and mounted on slides.

2.4.2 Long-term: 2+50 Inhibition. Lysosensor (PDMPO in 0.5 μM) was absent in the first 2 hours of inhibition (0.5 μM Phalloidin), then present in the following 50 hours. Afterward, cells were fixed and double immunolabeled (double labeling – method 2 of Chapter 2; single labelling – tubulin::TUB-1A2). Eventually, cells were stained by DAPI and mounted on slides.

3 Results

1. Microtubule Inhibition – Oryzalin & Taxol

As mentioned in the Introduction, the inhibition mechanisms of Oryzalin and Taxol are different. Oryzalin inhibits the polymerization of MTs by binding to free tubulin dimers so microtubules would be eventually depolymerized under continuing natural hydrolysis (treadmilling balance is disturbed); whereas Taxol prevents microtubule catastrophe by binding to GDP-bound tubulin in microtubule so that microtubules become over-stabilized even GTP hydrolysis occurs. In this section, the effects of short-term and long-term applications of Oryzalin (1–2 h and 50 h) and the effects of Taxol application for a medium period (24 h) on *Odontella* cells are described.

3.1 Oryzalin

Live cultures incubated with Oryzalin in different concentrations (0.5 μM , 1 μM , 2 μM , or 5 μM) have been observed by time-lapse photography (Method 2.1.2.4). The concentration at 1 μM has been chosen as a reference level, which was then further tested by three different short-term treatments to examine the effect on microtubules. Based on the results obtained, the Oryzalin at 0.5 μM and 1 μM was applied for the long-term inhibition. The confocal microscopy observation turns out that the biosynthetic herbicide Oryzalin effectively caused a fragmentation of microtubules at 1 μM within 50 min and 80 min at 0.5 μM , thus to guarantee the complete depolymerization of MTs, the complete inhibition would begin to take effect after 120 min (Section 3.1.1.1). So one should be careful to distinguishing the difference between results coming from different inhibition manners: In the “2+48h” inhibition (Section 2.1.2.1), all PDMPO stained silica were made during the full inhibition stage (i.e., after 2 hours since the start of inhibition), whereas in the simultaneous inhibition (Method 2.1.2.2), some silica may still be made in the initial inhibition stage (i.e., within the first 2-hour inhibition).

3.1.1 Setting the Incubation Parameters by Tests of Short-term Treatment

Short-term inhibition was applied to determine the effective concentration of Oryzalin and the

time needed that would lead to complete depolymerization of microtubules (3.1.1.1). At the same time, it was also important to examine the cell capability to recover, i.e., the performance of microtubules to restore integrity on removal of the agent. Therefore, microtubule recovery experiment was conducted to evaluate proper toxic concentrations of the agent (3.1.1.2). To these ends, short-term inhibitions were designed to examine silica morphogenesis under both “control” and “inhibiting” conditions on the same cell to determine whether a shift in morphogenetic activity occurred (3.1.1.3). In summary, the lysosensor co-incubation experiments were conducted in three different variants: (1) Inhibitor was applied for different time periods to determine the ideal treatment time; (2) Additional washes were applied for different durations following the inhibition to observe cell recovery; (3) Lysosensor was first applied for a small duration with the intention of monitoring normal frustule morphogenesis, and then inhibition proceeded for the same duration with an intermittent wash. Most experiments were followed by immunolabeling the cytoskeleton.

3.1.1.1 Effects of Short-term Treatment on Post-cytokinetic Cells

As normal morphogenesis unfolds in control cells, the nucleus relocates slowly from the pole of the young hypovalve, down to the side of the cell, and moves further along the side towards the center of the cell, where it remains more or less stationary through three consecutive axial expansions until mitosis sets in (see Fig. 3 of Part. I Generation Introduction). This normal mode of morphogenesis was observed to change into an erratic type of movement by time-lapse microphotography when microtubule inhibition was taking effect. The lowest effective concentration of Oryzalin was 0.5 μM , as determined by this method, and it took about 80 min before a change in nuclear behavior could be recorded. At a concentration of 1 μM , it took only 43–48 min, and at 5 μM , it took 30 min. Under such inhibition, the nucleus may reach the middle of the cell, but more often, the mitosis will not take place. Axial expansion, however, remains entirely unaffected. Besides, the longitudinal growth of the cell seems to be promoted causing a longer shape than the normal.

Moreover, if a cell was transferred from the 1 μM Oryzalin (inhibited at hGB1 phase for 58 minutes) into fresh inhibitor-free medium, it would consequently expand (time-lapse video not shown). After the removal of Oryzalin for 5 hours, the mitosis set in, followed by cytokinesis. The daughter valves, however, formed by these new daughter cells remained aberrant, without

horns and spines. It takes another cell cycle for the daughter cells to produce ordinary hypovalves. Thus, for the labelling experiments described below, a maximum concentration of 1 μ M Oryzalin, or an even lower one, is preferred.

Figure 1 presents the inhibition by 1 μ M Oryzalin under confocal microscopy observation. After treatment for 60 or 80 minutes, the thick horn bundle of microtubules was not yet fully depolymerized, though it has shown clear disruption, preventing the cell from leaving the post cytokinetic phase (Figs. 1A, 1B). The radial, perinuclear microtubules are almost absent in the cell of mid-interphase, leaving only the microtubule center (MC, green arrow of Figs. 1D₁, 1D₂) on top of the nucleus, after 60- or 80-minute inhibition. The 80-minute inhibition depolymerized spindle microtubules, leaving only bare polar complexes (PC) showing as two flat plates (Figs. 1D₃, 1D₄). When inhibition is prolonged to 120 minutes, not only radially perinuclear microtubules are absent (Fig. 1E), but also the horn bundle of microtubules is profoundly deconstructed (Figs. 1C, 1c). According to these results, to guarantee the complete inhibition, concentrations of 0.5 μ M and 1 μ M Oryzalin were applied to cells for at least 2 hours.

3.1.1.2 Recovery following Short-term Treatment on Post-cytokinetic Cells

Post-cytokinetic cells, after 1-hour recovering following a 2-hour treatment with 1 μ M Oryzalin (Figs. 2A & 2B showing two different cells), have certainly shown reorganization of horn bundle (cp. Fig. 1C), but a fully continuous array of horn bundle of microtubules remained to be rebuilt. As a result the two horns are aberrantly slim. Figure 2C shows another cell which recovered for 2 hours after the removal of Oryzalin. The perinuclear microtubules are nicely radiating from the MC, indicating a rigorous state of recovery. Though not exactly identical, the state of the MT system at the end of the 2-hour inhibition is supposed to be somehow comparable as that in Fig. 1E. Still, in the epitheca a few MT-needles and MT-speckles are visible, likely a sustained legacy of the inhibition. In Fig. 2D, a cell at the middle of interphase is shown, which is 4 hours after the removal of Oryzalin. This cell has recovered to a state nearly perfectly normal. The cell shown in Fig. 2E is again after only 2 hours of recovery but in a much later stage of the cell cycle, presumably at pre-prophase. This can be deduced from the structure on the nuclear surface, which looks like a somewhat deranged spindle precursor. In summary, the main message here is that the short-term (2-hour) inhibition effect is entirely reversible.

However, the recovery experiment following inhibitions of a longer term has not yet be

performed, but the toxicity of 2 μM Oryzalin at a longer exposure time of 50.5 hours seems to be tolerated (see Fig. 12).

3.1.1.3 Staining under Control and Short-term Inhibition on a Same Cell at Mid-interphase

The major activities of mid-interphase cells are formation of girdle bands and their exocytosis and the axial expansion. The latter two steps are termed “deployment” here. In order to study the short-term inhibition effects during girdle band formation, protocols with specified schedule linked with girdle band developing activity have been applied, i.e., initial treatment for 2 hours with PDMPO alone (control step), then washing in f/2-medium for 4 or 6 hours (wash step), followed by co-incubating with PDMPO plus 1 μM or 0.5 μM Oryzalin (inhibition step). The time lengths in this schedule were based on the observation (see Fig. 3 of Part I. General Introduction) that morphogenesis of either girdle band takes 1.3–7.5 hours and its deployment takes ~2 hours. Therefore, this treatment schedule (Section 2.1.1.3), including the period of the control and inhibition step, should be suitable to cover the period for both the fabrication and at least one girdle band deployment (8–10 hours).

As shown in Fig. 3, the results confirm the expectations. Initially, girdle band formation proceeded normally during the control step, as clearly made visible by the PDMPO stains, but began to become aberrant, when the next girdle band developed during the inhibition step. Both modes of morphogenesis, i.e., the control (normal) form and the aberrant form, can be conveniently compared in the same cell. The pattern from the control incubation step is the regular honeycomb-pattern in the left girdle band (Fig. 3a₁), whereas the inhibition step produced a smaller girdle band with a prominent streak-like pattern (Figs. 3A, 3a₁) consisting of arrays of parallel, unconnected virgae (Fig. 3a₂). This latter pattern in shorter form can be found in normal cells in the early phase of the girdle band formation (e.g., Fig. 15c₁ of Chapter 1), but such a long streak form has never been captured by either SEM or confocal microscopy. The width of each streak gradually diminishes and then streaks abruptly fade into a somewhat uniform, dimly stained layer, which ends with a smooth edge (arrows in Figs. 3a₂ & 3a₃). Notably, there is a small dark gap between the first and the second girdle band in this example. This gap may be caused by two reasons: (1) the deployment of the control hGB1 took less than 4 hours; (2) the early stage of the inhibition step covers the beginning silicification of the hGB2. But referring to Fig. 3 of Part I, the control hGB1 expansion takes about 2 hours, even though

the exocytosis time is unknown; if plus the 1.3-hour-formation period of the hGB1, which may contain the time of exocytosis, the sum up time is 3.3 h, which still could be covered by the 4-hour-wash, so the occurrence of the gap may because of the first reason.

Whereas, in the next example of Fig. 3B, which also presents the regular and the aberrant smaller girdle band side by side, there is no trace of a gap even though the wash lasted for 6 hours. But this is still reasonable, because an axial expansion period may have taken more than 4 hours. The difference is that here in the control girdle band, the expansion gap (white arrow Fig. 3b) is seen, because it happens to be captured in the image stack, whereas it was not present in the image stack of the cell shown in Fig. 3A. In additional, the zone with the streak pattern in the aberrant girdle band here is smaller and the streaks are less clearly delineated. They are best seen in the lower right hand corner of the image Fig. 3b.

Unlike in Fig. 3A and 3B, there is only one (abnormal) girdle band showing up in Fig. 3C. The hexagonal areolate pattern has some slight irregularity at the advalvar side of this girdle band and gradually deteriorates when reaching the abvalvar side. This suggests the operation timeline began when the hGB1 was being deployed, so there would be no control girdle band being stained (when deposition is done, PDMPO staining does not take effect). On the other hand, the big region of slightly irregular areolate pattern on the advalvar side implies that the inhibition began to take effect when silica deposition was proceeding, i.e., the silica deposition started before the end of the wash step. As the inhibition step began, silica deposition would be disturbed in the meanwhile stained by PDMPO, presenting irregular honey-comb areolate pattern on the advalvar side. (This implies on the left side of the stained cell wall shown here might be an area with regular areolate pattern, which is invisible here simply because it has not been stained in the wash step.) Whereas the abvalvar side, which is delimited by the first actin ring, shows the streak pattern, suggesting that Oryzalin inhibition took a prominent effect.

Regarding cytoskeleton morphogenesis, the concentration of Oryzalin and duration of treatment are sufficient to depolymerize the microtubules of radial, perinuclear MT arrays, one typical configuration of the MT system for this phase of the cell cycle. In Figs. 3B & 3b, anti-tubulin TUB-1A2 was applied to show the morphology of the MT system. Except for intensely immunostained needles and speckles scattered in the cytoplasm and an equally strongly stained rim around the nucleus, there are no microtubules present in the cell. The speckles are interpreted as paracrystal aggregates of tubulin. In Fig. 3C, the immuno-labelling was performed with the anti-actin N350 to present what happened to the actin filaments after

microtubules have been destroyed by short-term inhibition. In this cell, surprisingly, rather than only one actin ring found in control cells (see Chapter 2), there is a second, equally prominent actin ring in front of the first ring. The ca. 8 μm wide zone between the two actin rings has no identifiable PDMPO fluorescence pattern. Though this cell is the only actin-labelled sample with a developing girdle band at inhibition step, such multiple actin ring arrangement is rare because it does not happen in long-term inhibited cells at interphase (Figs. 8A–8D). So it is hard to explain why this occasional situation occurred, but at least it shows that microtubule depolymerization by short-term treatment with Oryzalin does not destroy or remove the actin ring from the developing frontier edge of every frustule component.

Sometimes, the cellular activities of mid-interphase may miss the first two steps of the operation (control step + wash step). For instance, Fig. 4A shows a pair of daughter cells, but only one of them is nucleated, one typical outcome under Oryzalin inhibition (more results could be seen in Section 3.1.2.1). This indicates the inhibition started before the mitosis. The hGB3 of this mother frustule has PDMPO signals, which may be made in the first two or only in the third step(s) of the treatment, but this is of no importance. What deserves our attention here is that a cell treated by short-term inhibition could present the same result as those treated by long-term inhibition (e.g., Figs. 4C, 4D, 5 – 7).

3.1.2 Cells after Long-term Inhibition

The long-term treatment covers about 48–50 hours which matches duration of the cell cycle in control cells. Two different treatment schedules have been applied: “2+48 h” inhibition (Method 2.1.2.1) and simultaneous inhibition (Method 2.1.2.2).

The “2+48 inhibition” means that cells were subjected to the culture medium with Oryzalin for 2 hours prior to the presence of PDMPO for 48 hours. As has been shown in previous tests (q.v. Section 3.1.1.1), microtubules could be completely depolymerized within 2 hours by 0.5 μM or 1 μM Oryzalin, so any PDMPO-stained silica appearing in the cell means they are made in the absence of microtubules.

In the simultaneous inhibition, both Oryzalin and PDMPO are added in the culture at the same time, so that PDMPO can simultaneously present the gradient changes of silica deposition with the gradually enhanced inhibition. With 1 μM Oryzalin, the complete inhibition period is

scheduled for 2 hours (see short-term effects of Section 3.1.1.1). But to identify the cellular activity after the 2-hour complete inhibition, it is required to estimate the consumed time of the previous activities. For example, the divided mother cell (Figs. 7B, 7C) treated by simultaneous inhibition, has developed and deployed its girdle band before division, which consumed at least 3 hours ($n>2$, refer to the control data from Fig. 3 of Part I. General Introduction), thus the non-mitosis protoplasmic division occurred in the complete inhibition stage.

3.1.2.1 Cells at Post-cytokinetic Stage — Cell Division without Preceding Mitosis

The common phenomenon of the 0.5 μM and 1 μM Oryzalin inhibitions is the occurrence of cell division in the absence of mitosis (Figs. 4–7). The nucleus of these cells often appears in the state of interphase or of prophase because of the absence of spindle, but it is likely that their DNA have duplicated at S-phase, because in normal cells protoplasmic division begins at telophase. Even though it has not been experimentally verified in this study, the visible increased size of the nucleus in some extreme cases supports this assumption (see the giant nucleus in Figs. 5 & 6 of the Appendix). These mother protoplast dividing without preceding mitosis inevitably produces unequal offsprings — one with a nucleus and the other without, as exactly what is shown in these figures. Immunolabeling of such inhibited cells with PDMPO stains are devoid of microtubules in both the nucleated as well as the anucleate daughter cell³ leaving only needle-shaped or irregularly shaped tubulin crystallines in protoplast (Figs. 4C, 5D, 6B, 6D, 6F). In the lysosensor channel, both daughter cells present PDMPO staining on their daughter hypovalve poles, which means that silicification can occur to form valvar SDVs in the absence of microtubules. But these hypovalves bear neither horns nor spines, only leaving several aberrant annuli (Figs. 4D, 5A, 5B, 5E, 6A, 6C, 6E, 7A). Usually, the anucleate cells bear a smaller silicified domain on the valve (Figs. 4D, 5E, 6C, 6E, 7B, 7C) and sometimes contain a big amount of lipid droplets (bright red dots) spreading in the whole protoplast (Fig. 4D).

When taking a closer look at these aberrantly assembled annuli, they appear in either a closed or an open ring-like configuration (Figs. 4d₁, 5a₁, 5b₁, 5b₂, 5e₁), and each of them is radially surrounded by blocks of regular streaks (Figs. 4d₂, 5a₂, 5e₂). Silica streaks at younger stage have less cross connections in between and should therefore be equivalent to the virgae

³ Neither the term “cell” nor the term “protoplast” would be correct for describing the state of the anucleate cytoplasmic portion divided off from the single nucleate mother cell. However, for simplicity, this division product is termed here the “anucleate daughter cell”.

(Fig. 5a₂). The area enclosed by the annuli appear either empty or may be filled by a thin silica layer perforated by pores whose diameter is larger than those of areola. This porous region is often accompanied with several silica knots (bright dots of Fig. 6c). Sometimes there is an extremely bright PDMPO signal in the area enclosed by an annulus, which comes from an aberrant LP base plate (Fig. 5e₂).

The actin immunolabeling has not been regularly documented in these abnormally divided cells. One lucky shot (Fig. 5C), however, proves that actin filaments are still quite abundant, though arranged in an irregular loop in the shrunken protoplast, which reflects the existence of the actin ring in the disrupted cell.

One extreme case that occur in long-term inhibitions is that a mother cell may divide into one nucleated cell (with a giant nucleus) and several anucleate cells (see Figs. 5 & 6 in the Appendix). These anucleate cells probably come from the continuous division of the nucleated cell, based on the knowledge proved by the cell in Fig. 12. On one hand, these daughter cells suggest the cytokinesis can repeatedly occur in the nucleate cell even though MTs have been removed. On the other hand, the giant nucleus suggests the DNA of nucleus must have replicated before every division. Analogically, those divided cells mentioned above (Figs. 4–7) may also have replicated their DNA before the division. Their cell cycle arouses our curiosity and see further discussion in Section 4.1.6.1.

3.1.2.2 Cells at Late-interphase — before Transition to Mitosis

Many cells (>50%, according to incomplete statistics) inhibited by 1 μ M Oryzalin for the schedule of "2+48h" that captured at interphase are devoid of PDMPO stained silica and their actin-ring locates at the abvalvar side the hGB2, which means the complete inhibition began from the stage when hGB2 has just been developed (Fig. 8 A–D). Usually, the axial expansion should follow to extrude the new hGB2 out of the eGB2 cover, but here the actin ring is locating beneath the advalvar edge of eGB2. This means no expansion has been performed and cells must have paused at this stage for at least 48 hours. The needle-like MT-crystallines in protoplast and the displaced nucleus away from the equatorial plane indicate microtubules have been completely depolymerized. And it seems these inhibited cells might have been paused at late interphase and retarded the transition to mitosis. Sometimes, the head plates of interrupted hypoalves are in normal shapes (e.g., Figs. 8E, 8F).

However, in a milder inhibition with 0.5 μM Oryzalin, cells can develop silica. For an extreme example which is encountered by chance (Figs. 8G–8H), a cell may arrange its actin ring chaotically when microtubules have been completely broken down into crystallines. However, silica is still able to be deposited inside the region that demarcated by the actin ring. From the morphology of the silica, it likely consists of two girdle bands. Moreover, that pieces of MT-crystallines co-aligning with actin filaments gives a hint that microtubules may physically interact with the actin ring. Another example looks more regular is a cell with a PDMPO stained hGB2 (Figs. 9B & 9C), whose complete inhibition begins from the hGB2 formation stage. In protoplast, MT-crystallines and the displaced nucleus again indicate the MT-system has completely depolymerized. The thick actin ring at the abvalvar side of the hGB2 could be mistaken for the GB-actin-ring; however, it is not, because a remnant of the abvalvar actin ring can be seen as a weak trace (white arrow in Fig. 9a), so this should be an cytokinetic ring at young stage. As we known from Chapter 2, the cytokinetic ring will be prepared before entering prophase, which means cells without MT-system still can transit towards mitosis.

3.1.2.3 Cells at Cytokinetic Stage — Morphology of Cytokinetic Actin Ring

In control cells, after the last hGB has been made and deployed on the cell surface, cells proceed into mitosis immediately followed by cytokinesis. The most eye-catching cytoskeletal structure seen in *Odontella* is the complex formed by the telophase spindle which locates right beneath the cytokinetic actin ring. However, this complex is entirely absent in Oryzalin-treated cells.

In Fig. 10, the nucleus of each cell has managed to condense the chromosomes, but due to lacking the support from MTs which have been removed by inhibition, it is displaced and cannot associate with the contractile ring at the equatorial plane. The only difference between the cells in Fig. 10C and 10E is the morphology of the contractile ring. The former has a flabby shape and the latter is contracting. Note the position of the nucleus, which shows that the cleavage furrow has just passed by its side (Figs. 10B, 10C). Notably, the cell in Fig. 10E has a cleavage furrow induced by the contraction of cytokinetic actin ring. And given the knowledge that the cytokinetic ring contracts at telophase, so this cells must have entered to this stage, even though other typical assorting signs like the horn bundle and telophase spindle are missing due to the loss of microtubules.

3.1.2.4 Repetitive Constricting Pulses during Cytokinesis

Cell division without a preceding mitosis differs in three aspects from normal cytokinesis in control cells (Fig. 11): (1) repeated attempts of constriction occurs at the equatorial plane; (2) positioning of the nucleus is unpredictable; (3) entry into protoplasmic division is retarded. The entire process of repeated attempts of cytokinesis between the first attempt and the completion of cell division may take up to 3 hours.

In control cells (light blue trace in Fig. 11A), the duration of cytokinesis is about 25 minutes, which is almost equal to the last successful attempt of the constriction in the Oryzalin-treated cell. The alignment of the spindle in control cells is perpendicular to the direction of constriction as shown in Fig. 11V (see also Figs. 8 – 10 in Chapter 2). The wave crests of the pulses (lower y-value means stronger constriction) are always close to 5, which indicates that the ingression at this degree is a critical point for division.

The situation captured in Fig. 12 is the same as that shown in Fig. 11, except that it shows a cell, which has already passed through an Oryzalin-induced protoplasmic division before. It resulted in a nucleated daughter cell, seen here on the left, and an anucleate daughter cell to the right. The nucleated daughter first went through a phase of axial expansion growth, which implies new girdle bands are made and deployed on the cell surface and then in frame C of Fig. 12. The first attempt of constriction occurred at a position near the nucleus which is located only slightly off the equatorial plane. Three further attempts had followed, before the division was successful. The unequal sizes of the two progenies come from the slightly misaligned division plane.

Some of the microtubule inhibition experiments have been performed using Colchicine instead of Oryzalin. The effective concentration of Colchicine was about 200 times higher than that of Oryzalin but the principle action was quite comparable to that of Oryzalin (Fig. 13). The whole activity of cytokinetic pulsing is much longer than that of Oryzalin, which takes 260 minutes. And the complete division counting from the last pulse is longer as well, lasting 125 minutes. Comparable to the Oryzalin inhibition (red arrows, Fig. 11 C – F), the cell treated with Colchicine also exhibited some local contractions before establishing the cleavage furrow (arrows, Fig. 13 E – G). What these time-lapse series also show, is the remarkable phenomenon that the major constriction, which eventually divides the cell, can occur roughly at the equator of

the protoplast, whereas the nucleus is misplaced far away to the side.

3.1.2.5 Formation of Lateral Frustule Components

Almost all cells inhibited for 48 – 50 hours with 0.5 μM Oryzalin failed to undergo mitosis, and about half of them (a quarter of them at 1 μM Oryzalin) went through some form of protoplasmic division as described in the above section (3.1.2.4). A quarter of them (about a half when 1 μM) failed to divide, pausing at the end of interphase without the formation of cytokinetic ring, i.e., Fig. 8. The rest cells are undivided and contain only one nucleus as well, but they have a minor constriction in the middle of the cell indicates that cytokinesis was attempted but then was aborted (Figs. 14, 15). Interestingly, after the failure of division, valve morphogenesis commenced in the subsequent daughter cell cycle in conjunction with axial cell expansion, so that the shape of the new daughter valves is molded according to the available surface area. This creates a convoluted fabric consisting of two fused, completely aberrant pancake-like domains, termed “lateral valve complex”, which wraps around the girth of the cell. In some case (Fig. 17), the undivided cell has two nuclei and its daughter hypovalves are partially connected at the apical site of the dividing poles wrapping around the deep cleavage furrow, termed “partially connected valves” cell joining together.

3.1.2.5.1 Formation of the Lateral Valve Complex: Inhibition Starting from Interphase

A very early stage of the lateral valve complex is shown in cells treated with Oryzalin and simultaneously stained with PDMPO for 24 hours (Fig. 14A). The well-developed girdle bands of the mother hypotheca (hGB1m, hGB2m and a narrow hGB3m) suggest that the cell has been challenged by the inhibitor at early interphase, when hGB1m was formed. Interestingly, the formation of none of these girdle bands suffered much of a perturbation. Only the hGB3 is atypically faint. This could mark the moment, when inhibition took effect and, sure enough, mitosis and cytokinesis failed completely. At the moment of fixation the cell was captured in a stage when the fabrication of the lateral valve complex was still going on. This can be concluded from the fact that the complex is as yet entirely encased by the mother frustule. The large areas of the lateral valve complex are probably still enclosed by the SDV, though they are well visible. Two separate pattern centers (annulus regions) can be recognized by the radial arrays of areola

streaks around them (Fig. 14A, stippled boxes). The annular region to the left of the nucleus is split into two separate annuli, with one forming a circle having an irregular LP base plate in it, and the other having an open finger-like structure (Fig. 14a₁). The second annular region (to the upper right of the nucleus) looks like two fingers fused together at their distal open ends (Fig. 14 a2). Each annulus region is actually the center of a daughter valve domain, and the overlapping boundary (arrows) between the two domains can be seen in Fig. 14a₁ (arrows). At higher magnification, the area enclosed by the annular rim turns out to be covered by a silica layer perforated by many densely packed pores (Figs. 14a₂, 14a₃), which are larger in size than the areolae.

A typical shape of lateral valve formation is shown in Figs. 14 B & C, after a cell had been treated with 0.5 μ M Oryzalin and simultaneously stained with PDMPO for 48 hours. This effect is strikingly different from the aberrant, individual daughter valves formed during short-term inhibition (Fig. 5). The lateral valve complex is made of two aberrant daughter valves adjoining together in a crooked fashion. Horns are missing on the lateral valves, but abnormal annuli (sealed or hollow openings, Fig. 14b₁, 14b₂), radially patterned rows of areolae near the annulus (Fig. 14c) and abortive and deformed spines (Fig. 14C) are present. In some cases, large islands with radial silica patterns around a prominently stained center may be formed (Fig. 14b₁). The streaks at the margin of these islands are similar to the streaks occurring in girdle bands of Oryzalin-treated cells (Fig. 3a₂), which were thought to be virgae, and therefore they are likely to be virgae as well. The bright fluorescent region at the center is a sealed annulus. Start of inhibition can be determined by the appearance of the first PDMPO-stained structure. This is a narrow silica band around the equatorial plane of the mother cell (Figs. 14B, 14C, white arrows), representing the hGB3 (arrows), which suggests that the initial inhibition began at the stage right before the transition into mitosis or even earlier (axial expansion period of the hGB2).

The other typical shape of the lateral valve complex is shown in cells (Fig. 15) either treated with 0.5 or 1 μ M Oryzalin. The complex is completely smooth without any accessories like annuli, horns or spines. The PDMPO-stained hypothecal girdle bands of the mother frustule indicate the cell has begun to be inhibited at the phase when the first hGB was made.

3.1.2.5.2 Formation of Lateral Girdle Band: Inhibition Starting from Interphase

In normal daughter cells, girdle bands are made after the valve formation. The same sequence

is observed in the daughter cell cycle of an Oryzalin-treated cell, even though neither mitosis nor cytokinesis has occurred. The cells shown in Fig. 15 are examples of such case. In the middle of these cells, the two fused lateral valves can be recognized and lateral girdle bands are arranging at both sides of the fused lateral valves. Notably, both first lateral girdle bands have a pointed end inserting into the curve between the two lateral valves (Fig. 15a).

Viewing the lateral valve complex in the SEM adds additional information, which helps to understand the mechanics of this process. In Fig. 16 three consecutive stages have been aligned with each other. The most revealing of these is the stage in the middle (Fig. 16B), when the two thecae of the mother have just become pushed apart by the new lateral valve complex inserted between them. It is obvious that this requires axial cell expansion to accommodate the aberrant valve complex on the cell surface. The inhibited cell from Fig. 16A would be the stage before cell expansion, resembling the situation seen in Fig. 14A, only that we cannot look here under the cover of the frustule. But inside this cell, the lateral valve complex is likely to be already assembled and deployed on the protoplast surface, waiting to get exposed by cell expansion. Because this cell is from the same batch as those in Figs. 16B & C, suggesting that it is just at an earlier stage than the latter two when being fixed. Fig. 16C shows a much older stage, when two lateral girdle bands have been added on both sides of the lateral valve complex, pushing the old thecal halves of the mother even further apart. This Oryzalin-driven aberration in the development creates cells of a monstrous length, which however still remain viable.

The open end of the cell in Fig. 16C & D provides the opportunity to take a closer look onto the inner surface of the girdle band (LGB2d). Since this cell has only been extracted with SDS after fixation (no enzyme treatment, no acid wash) one should expect to see the organic layer covering up the foraminal basal layer of the frustule wall. This is indeed the case, however, different from the situation described in Chapter 1 (Fig. 8a₂), the efficiency of gold sputtering is reduced here due to the remote location of this sample area. Hence, due to reduced details of the gold-sputtering object on the inner surface of the girdle band are dimmed, whereas other details of structures underneath shine through, i.e., the triangular columns in the middle layer of the frustule wall and the foraminal pores. This particular appearance of the image provides a rare opportunity to directly compare the frustule chamber structure in the SEM-view with a PDMPO dye image obtained by confocal microscopy of a girdle band from a short-term Oryzalin treatment (Figs. 16d₂ & d₃). It shows that the principal construction of the areola chamber is not disturbed by Oryzalin and at the same time it attests to the fidelity of confocal fluorescent

imaging down to the sub-micrometer scale. The regular frustule architecture seen here after long-term Oryzalin treatment is at variance to the disturbances by the same concentration reported above in cells subjected to short-term treatment (see Fig. 3). This aspect will be addressed in the Discussion 4.1.4.

3.1.2.5.3 Partially Connected Valves: Inhibition at Mid-cytokinesis

The other typical type of aberrant valve is shown in Fig. 17A, that the morphology of the two lateral valves, like siamese twins, are similar to two individual mature valves that are partially connecting together at their apical sites. A unique elliptical head plate in a mature shape like control is shared at the middle of the adjoining valves; an LP is extruding from the head plate while an abortive horn (circle) is standing outside of this area (Fig. 17a). The immunolabeling with tubulin antibody (Fig. 17B) visualizes a completely destroyed microtubule system with MT-fragments surrounding the nuclear surface. The half fused lateral valves and the two complete chromatin nuclei suggest the cell was inhibited at midway of cytokinesis and the mitosis had been completed. It differs to that of the cells with lateral valve complex (3.1.2.5.1), which was inhibited starting from the interphase.

3.1.3 Inhibitory Phenotypes of Long-term Inhibition with Oryzalin

In general, the cellular morphologies resulting from long-term treatments with different concentrations of Oryzalin (including "24h", "48h" and "2+48h" inhibitions, see section 2.1.2), can be categorized into 5 basic inhibitory phenotypes (Table 1). It should be noted that in the "2+48h" schedule silica components are all made, when all MTs are gone, whereas in the simultaneous inhibition schedule ("24h", "48h") cells may initially contain normal silica components before the inhibitor comes into full effect. Given that cells had not been synchronized⁴, cells within a batch were at different developmental stages, when the inhibition began. But this will not bring troubles to trace back the developing process of each cell, because the sequence of stages throughout the cell cycle during normal development is well understood

⁴ The cellular synchronization has not been applied in the current study, because standard methods such as pretreatment with germanium or silica starvation (Darley and Volcani, 1971; Eppley, 1977), may disturb the cell cycle or modify the effects of drug inhibition.

(see Chapter 2), so that the starting point of the inhibition can often be reconstructed. To better understand how these different morphologies have developed, these different inhibitory phenotypes are further illustrated in a timeline scheme marking the inhibition schedule and the cell cycle (Fig. 18), which also allows to determine the effects of Oryzalin inhibitions resulting from different concentrations that begin at the same developmental stage.

In the "2+48 h" inhibition schedule (Method 2.1.2.1), the culture at 0.5 μ M Oryzalin has produced more inhibitory phenotypes than the culture at 1 μ M. The former consists of subtype #1b, basic type #2, subtype #3a, #3b and basic type 5; the latter only consists of type #1 (except the subtype #1b).


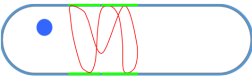
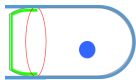
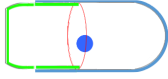
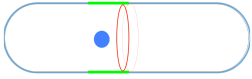
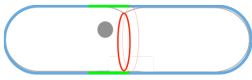
In the 0.5 μ M Oryzalin treated group, subtype #1b is the only exception that the cell stays at the interphase of the mother cell cycle (see Fig. 18-1b), because the actin ring arrangement was affected when the ring lost the mechanical interaction with MTs, leading to the ring fail in directing the SDV in a normal shape and thus the cell cannot enter into the next step (i.e., expanding the cell to expose hGB2). But in usual, the actin ring, like that in the rest of inhibitory phenotypes, is able to maintain ring shape and cells can go beyond the mother interphase, after the loss of MTs. Further, the morphology of the cytokinetic actin ring and the valve- or GB-actin ring for the daughter generation are normal as well, suggesting the actin system can operate independently. On the other hand, in the 0.5 μ M Oryzalin batch, except phenotype #1b, the remaining types of cells had all assembled a cytokinetic actin ring in the midline and were able to constrict the cytoplasm, no matter when the inhibition took effects: (1) the phenotype #5 was inhibited midway of cytokinesis, meaning the inhibition began after the positioning of the cytokinetic ring; (2) the rest of the phenotypes (basic type #2, basic type #5, subtype #3a and #3b) were inhibited before mitosis suggested by the single nucleus, but normal constriction could still occur and even some of the cells could complete the division (i.e., subtype #3a & #3b). This suggests the loss of MT system will not prevent the cell from entering into the next step of the cell cycle, and further suggests the actin system is the main operation system of the cell cycle. Lastly, one interesting phenomenon is that cases, where both daughter cells are nucleated under this inhibiting concentration, have never been observed, although mitosis-inhibited but protoplast-divided cells (Figs. 11 – 13) or cytokinesis-inhibited but nuclear-divided cells (Fig. 17) have been found.

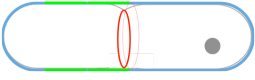
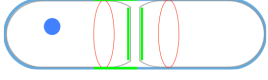
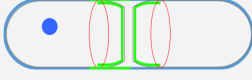
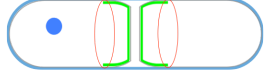



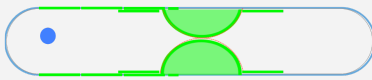

The inhibition impact is obvious, when the concentration of Oryzalin reaches 1 μ M in the "2+48 h" inhibition schedule — lots of cells were arrested at interphase of the mother cycle

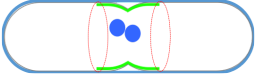
(phenotype #1a, #1c, #1d), which means the cell cycle was interrupted. However, in the simultaneous inhibition schedule ("24 h", "48 h"), the occurrence of sibling protoplasts, one of which is nucleated and the other of which is anucleate (subtype #3a), as well as the undivided mother cells with a lateral valve complex plus lateral girdle bands (subtype #4c), suggest that the cell cycle was actually not blocked. By tracing back the time point when division occurred and lateral valves were formed (see subtype #3a and 4c in Table 1), the inhibition of 1 μ M Oryzalin had already taken effect for more than two hours. So it is strange that after the two hour-pre-inhibition⁵ of the "2+48 h" inhibition, only cells of type #1 arrested in the cell cycle are found, without seeing other possible phenotypes like type #3 and #4, which had achieved cell division or the formation of lateral valves. Perhaps, percentage of both cases in the "2+48 h" batch was too low to be found and the sample number may not have been big enough, because the simultaneous inhibition and live observations reveal that cell division can still occur after 2 hours, when the concentration of Oryzalin reaches 2 μ M (Fig. 12) and even up to 5 μ M (see video series #2 of Appendix).

⁵ The complete reduction of microtubule system takes the minimum 2 hours in 1 μ M Oryzalin.

Table 1. Morphological types of Oryzalin-treated cells from different long-term inhibitions.

Basic Types	Subtypes	0.5 μ M	1 μ M
1	1a	Not found	 <p>2+48 (Figs. 8 A – D) (>50% of the population in the whole "2+48 h" batch, by incomplete statistic)</p>
	1b	 <p>2+48 (Figs. 8 G – H) (Only one case observed so far, takes about 1/1000)</p>	Not found
	1c	Not found	 <p>2+48 (Fig. 8E) (hypo valve is normal, rare)</p>
	1d	Not found	 <p>2+48 (Fig. 8F) (hypo valve and the new GB are normal, rare)</p>
2	2a	 <p>2+48 (Fig. 9)</p>	Not found
	2b ₁	 <p>2+48 (Figs. 10 A – B, 10 E – F)</p>	Not found
	2b ₂		

		 <p>2+48 (Figs. 10 C – D)</p> <p>* Type 2 takes up 45 %, by incomplete statistic</p>	Not found
3	3a	 <p>2+48 (Figs. 6 E – F) (horns and LPs are devoid)</p>	 <p>24 (Fig. 7C), 48 (Fig. 7B) (horns and LPs are devoid)</p>
	3b	 <p>2+48 (Figs. 4 C – D, 5, 6 A – D)</p> <p>* Subtype #3a & #3b take up 45 %, by incomplete statistic</p>	Not found
	3c	 <p>48 (Fig. 12J)</p>	 <p>*50.5+2.5 (2 μM: Fig. 12A–I, the last 2.5 h is detected by the time-lapse photography)</p>
4	4a	 <p>24 (Fig. 14A)</p>	Not found
	4b	 <p>48 (Fig. 14 B – C)</p>	Not found
	4c1	 <p>48 (Fig. 15 A – B)</p>	 <p>48 (Fig. 15 C – D)</p>
	4c2	Not found	 <p>48 (data not shown)</p>

5	 <p>2+48 (Fig. 17)</p> <p>* Type 5 takes up <10 %, by incomplete statistic</p>	Not found
---	--	-----------

* Cells performing cytokinetic pulses in live observation are recorded to be treated by “50.5+2.5” hours (cells were inhibited by Oryzalin for the 50.5 hours before recording, and then they were recorded by time-lapse observation in the following 2.5 hours).

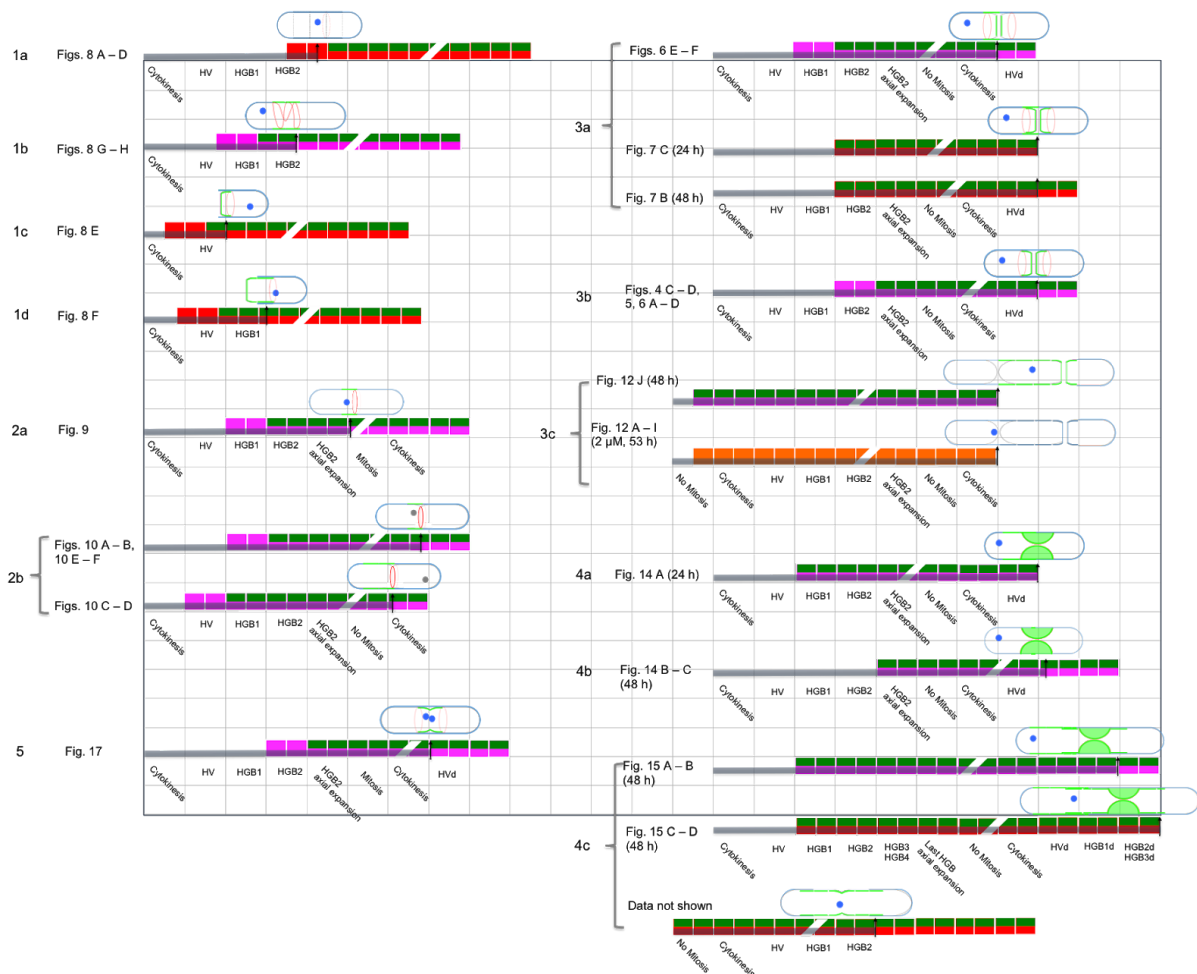


Fig.18 Frustule morphogenesis under different concentrations of Oryzalin (for a high resolution version of this figure see Appendix). Cells have been treated by different long-term inhibition schedules (“24 h”, “48 h”, “2+48 h”, depicted as a line of squares) differing by the starting points of the inhibition and by the concentration of Oryzalin. One square represents 1 hour, square colors represent the concentration of Oryzalin: magenta – 0.5 μ M, red – 1 μ M, orange – 2 μ M respectively; green represents the presence of

PDMPO. Not all of the cell activities take the same amount of time, but for convenience of the comparison the timeline representing the average duration of stages is placed underneath. The time elapsed between two developmental stage is omitted. Abbreviations: HV – hypovalve, HGB1 – hypothecal girdle band 1 (of the mother generation), HGB2 – hypothecal girdle band 2 (of the mother generation), HGB1d – hypothecal girdle band 1 of the daughter generation.

3.2 Taxol

Taxol was applied at concentrations of 1, 10, and 100 μM to the culture for 24 hours. It was always co-incubated with PDMPO. At each concentration obvious effects of inhibition have been observed. Cells were captured at almost all stages of the cell cycle, except for the metaphase and anaphase that were rarely seen (data not shown).

3.2.1 Inhibition at Interphase

Taxol-inhibited cells at interphase were observed in the batch treated with the 100 μM Taxol. Cells in Fig. 19 were developing their valves when the inhibition began. The first cell (Figs. 19A & 19B) has failed to complete its valve, with the actin ring being located far from the silica edge. Whereas the latter two cells (Figs. 19 C–F) have reached the stage of hGB1 formation before the end of inhibition. The new girdle band has not yet been deployed out of the eGB2 cover and the actin ring is located off the abvalvar edge of the recent hGB1. It might have been caused by the strong interaction between the over-stabilized perinuclear microtubules and those long actin bundles anchoring at the LP base plate region. Those perinuclear microtubules radiating towards the epithelial side bind to the long actin bundles; the nucleus, the cytoplasmic cortex nearby, as well as the actin ring seem being pulled out from their original places. Apparently, perinuclear microtubules and those long actin bundles can be conceived as an interconnected network, as they are physically interacting with each other. In normal cells, the same type of interaction should also occur in control cells, except that the interaction between the perinuclear microtubules and the actin anchor bundles is weaker, because the microtubules have the flexibility to grow or shrink; the consequence is that the nucleus and the cortex nearby closely follow the actin ring, which is aligning with the abvalvar edge of the developing girdle band. The cytoskeleton morphology like Figs. 19C–F is rarely captured in control cells, because dynamic change of the MT in normal cells is very fast, and the movement of the nucleus and the actin ring is accompanied by the timely axial expansion. However, it can be easily captured in Taxol-inhibited cells because although the axial expansion is blocked, the shifting of the nucleus and the actin ring continues.

The cell shown in Fig. 20 is a contrary case that the actin ring lags behind the abvalvar edge of hGB2. Here the perinuclear microtubules are radiating towards the hypothecal side and

binding to the long actin bundles, therefore the nucleus with the microtubule system and the nearby cortex as well as the actin ring shifted back to the middle of the hGB2. And the oval shape of the nucleus aligns along the longitudinal axis, indicating a high degree of tension acting on the nuclear surface. It is unclear how this has occurred but beyond the actin ring, there are a complete hGB2 and a region with irregularly deposited silica (aberrant hGB3). These two girdle bands are covered by eGB2 and eGB1, respectively, indicating that the axial expansion after the formation of hGB2 was inhibited. Perhaps the efficient inhibition occurred earlier, possibly at the moment when the hGB2 was almost completed, and then the axial expansion and the hGB3 fabrication were strongly interfered by Taxol. This is supported by the fact that the abvalvar edge of the hGB2 is not smoothly straight and the silica deposition of hGB3 was unevenly accumulated into the fragmented regions under the cover of eGB1, with the nucleus not being located right beneath.

Common characteristics of cells inhibited at interphase are summarized as follow, even though not all these characteristics exhibit in all cells: (1) the actin ring is misaligned with the silica edge (Figs. 19, 20); (2) the last silica is incomplete (Figs. 19A, 19B, 20); (3) the axial expansion is lacking in all cells (Figs. 19C–F, 20). The configuration of the SDV, actin ring and the nucleus in these cells is contradictory to the knowledge we learned from control cells (see Chapter 2). It shows that after the axial expansion, the silica deposition occurs to develop a new girdle band under the cover of eGB2, with the nucleus being located right beneath; the actin ring always demarcates the abvalvar edge of the most recent girdle band either before or after the axial expansion.

3.2.2 Inhibition at Preprophase and Prophase

In control cells, the prominent feature of the preprophase is the presence of the polar complex (PC) precursor, and for the prophase is the presence of the mature polar complex.

Here, cells were treated by the Taxol at a concentration of 10 μ M for 24 hours. The PC precursor of Fig. 21b₁ appears as a thin layer before the assembly of the cytokinetic actin ring, indicating it is at the early preprophase. Then it thickens when the young cytokinetic ring appears on top of it (Fig. 21b₂, arrow). The fabrication of the entire hypotheca looks quite normal. However, the two girdle bands are located beneath the cover of eGB1 and eGB2. This means the cell has not taken any axial expansion after the hypovalve had been deployed out of

the eGB2 cover. It suggests that the effective inhibition at least took place when the hGB1 was completed. In control cells, the nucleus and the actin ring are placed at the abvalvar side of the hGB2 (i.e., in the middle region of the frustule). However, here due to the lack of axial expansion, their relative position to epitheca is weird that they are at the advalvar side of the eGB1. It is a pity that the sample of Fig. 21b₁ does not show a later stage and the sample of Fig. 21b₂ has lost its epitheca, so whether the cell like Fig. 21b₁ could produce a cytokinetic ring right above the initial PC but close to the GB-actin ring at the advalvar side of eGB1 is unknown.

Later, when the precursor has developed into a mature PC appearing as a thick bi-layer and the cytokinetic ring has matured as well (like a thick band), the nucleus has entered prophase (Fig. 21 C₁–C₆). This morphogenesis process of the polar complex proceeds the same way as in control cells, which seems not being influenced by Taxol. Likewise, the maturation process of the cytokinetic ring does not seem to be affected by Taxol either at this concentration. The only difference is that the MT roots still appear when the PC matures, which would not occur in control cells.

3.2.3 Inhibition at Telophase

Cells at earlier stages of mitosis than telophase are rarely captured under Taxol inhibition. Although the cell in Fig. 22 had been inhibited from valve formation onwards by 100 µM Taxol for 24 hours, the nucleus went through mitosis and eventually entered telophase. The characteristics of the telophase spindle are similar as in control cells, although the spindle appears more prominently labelled, which reflects a larger amount of microtubules (Fig. 22). However, the telophase spindle has a much higher chance to be encountered in the Taxol-treated samples than in control batches. It suggests that the retention time has been much longer, i.e., although being not entirely blocked, the process is substantially retarded.

3.2.4 Inhibition in the Course of Cytokinesis

Maybe owing to the long retention time of microtubules in Taxol treated cells, the nicest snapshots of various stages ranging from telophase through cytokinesis to the early stages of daughter cell development. For instance, one of these lucky shots is shown in Fig. 23, where the

cytokinetic actin ring is constricted down to a small thick circle being penetrated by the late telophase spindle. The cytoskeletal features revealed by these images are similar to control cells, except that at each stage the microtubules appear extremely well preserved and strongly labelled. Several structural aspects can be seen very clearly. The central spindle are turned away and exposed like that in control (Figs. 23b₁, b₂). In the stage before this (mid-telophase, Fig. 22), two new convergent sites for additional microtubules are formed on both sides of the central spindle. From these convergent sites two arrays of microtubules grow out and elongate along the arc of the cytokinetic actin ring. These arrays will eventually transform into the horn bundles. However, the MC at this stage has not yet associated with the horn bundle. In the case where cytokinesis is completed, the telophase spindle has been cleaved in the middle but failed to completely disassemble due to the Taxol effect (Fig. 23d₁). The central spindle no longer extends neither reduces to be thin; the two daughter protoplasts are closely facing to each other and obviously have failed to contract backward. By the way, as is also present in other phases, the silica pattern of girdle bands do not clearly show areola pattern but present a fine texture (Fig. 23c).

3.2.5 Inhibition at Post-cytokinetic Phase

The high labelling intensity of the microtubule horn bundles is exceptional. This is also likely a Taxol effect, and suggests that the next developmental step might also be affected, due to a delay or stagnation in bundle disassembly. This stage was observed in the batch treated by 1 and 10 μM Taxol, in the example of Fig. 24. The mother cell has developed its hGB1 and hGB2 in the presence of 1 μM Taxol, then passed through mitosis and cytokinesis and entered the post-cytokinetic phase in the course of 24 hours. As in control cells, an MC is visible on top of each daughter nucleus; thick branches of horn bundles connect from both sides to the MC and run along the valvar apical axis into the horns. At the most distal ends of the horn bundles, however, a unique difference to control cells is found (Fig. 24b₁, d₁, f₁) — an overshooting of the horn bundle has extended beyond the end of the horn; the full length of the horn bundle cannot fit into the available space. This is likely due to the excessive MT growth, as a result the horn bundle poked through the weakest point at the tip of the horn. Since these cell were perfectly viable until the point of fixation, it may be conservative to assume that, there was some membrane sealing around this extended tip.

II Actin Inhibition – Jasplakinolide & Phalloidin

The actin inhibition mechanisms of Jasplakinolide (JAS) and Phalloidin are different. The former prevents the elongation of actin filament by binding to G-actin, while the latter prevents the filament depolymerization by binding to interfaces of monomers in F-actin. In this section, the effects of JAS applications for long term (2 + 48 h) and the effects of Phalloidin application for both short (2 h) and long terms (2 + 48 h) on *Odontella* cells are described.

3.3 Jasplakinolide

Cells were treated by the “2+48 inhibition” with 0.25, 0.5 or 1 μM JAS, aiming to examine whether cells would proceed throughout the cell cycle when the actin system is reduced. When the concentration of JAS reaches 1 μM , the silica deposition tends to be severely blocked. In the meanwhile, the treatment with 1 μM JAS for long term observed by time-lapse photography, reveals that inhibited cells cannot axially expand anymore.

3.3.1 Inhibition at Interphase of the Mother Generation

Interphase cells inhibited by 0.25 μM JAS are still able to produce new silica (visualized by lysosensor) and the morphology of which is always normal (Fig. 26). As to the actin system of these cells, except for the visible actin ring, other microfilaments are barely visible and small actin clusters are found dispersing throughout the protoplast. Nevertheless, the morphology of MT-system looks normal and the nucleus is located beneath the recent silica as in control cells.

When JAS concentration reaches 0.5 μM , two cellular phenotypes arise — with (e.g., Fig. 27A) or without successful silicification (e.g., Fig. 27B). However, unfortunately, no corresponding cytoskeleton images were obtained for cells of Fig. 27A & Fig. 27B, due to the failure of immunolabeling.

Further, when JAS concentration reaches 1 μM (e.g., Figs. 27C & 27D), there is no silica in inhibited cells, which means the silicification has been completely blocked. As to their actin system, the actin ring becomes less conspicuous and the other remaining microfilaments are barely seen. Again, pieces of actin clusters are dispersing throughout the cell, especially accumulating around the ring. In fact, such actin clusters could be found merely after 3 hours inhibition (Fig. 27E). All these phenomena indicate that the inhibition with 1 μM JAS can remove almost all of microfilaments in a cell. On the other hand, the perinuclear microtubules are very long, much longer than those in normal cells. In addition, inhibition videos of 1 μM JAS recorded by time-lapse photography (Method 2.1.2.4), which are obtained in my master thesis (Zhang, 2012), all show axial expansion defect of the observed cell (see video #4 in the Appendix). So in brief, the strong depolymerization of microfilaments by 1 μM JAS inhibition will lead to the absences of the silicification and the axial expansion (see further Discussion 4.3.1.1).

In summary, in cells treated by JAS at 0.25 μM , the actin ring is slightly deconstructed but

clearly visible; in cells treated with higher concentrations, the actin ring is severely diminished and only fairly visible, often shown as only a thin trace. But it is unsure whether both types of the ring are just the remnant of the original ring or they are a reorganized one. And this question could be answered by following results that the actin ring (or actin ring trace) appears at the boundary of lateral valve complex or lateral girdle bands (Section 4.3.1). In all these cells, microtubules grow very long no matter what concentration is applied. Finally, by incomplete statistic (not shown), the change in the silicification behavior from low to high concentration is clear, proving that the population of cells with lysosensor stained silica decreases as the inhibitor concentration gets higher.

3.3.2 Inhibition until the Daughter Generation without Cell Division

Sometimes, inhibitions would encounter telophase and cytokinesis, so cells cannot divide as a consequence of the deconstruction of the cytokinetic ring. Their protoplasts are maintained in a complete unity containing one or two nuclei. Due to the constriction of the cytokinetic ring before its depolymerization, cleavage furrow is made and the new exposed protoplasmic region is often covered by lateral silica structures, which belong to the daughter generation.

As we learn from the control cell that the protoplasmic division of *O. sinensis* begins from telophase (Chapter 2), so microtubules with typical telophase characteristics (e.g., horn bundles) are expected to be seen in cytokinesis inhibited cells. However, the microtubules of these inhibited cells, as to their morphology and spatial location, are quite different to our expectation.

3.3.2.1 Silica Development of the Daughter Generation with Preceding Nuclear Division

Cytokinesis interrupted cells with two nuclei are reported in this section (Figs. 28–31, 33D, 33E). Based on the morphology of the lateral silica, they can be roughly classified into two phenotypes — cells with lateral valve complex and cells with partially connected lateral valves. Both phenotypes appear in batches treated by 0.25 μM JAS (Figs. 28–31), whereas only the latter type appears in batches treated by 0.5 and 1 μM JAS (Figs. 33D & 33E).

The first phenotype concerns with cells with initial lateral valve complex which occurred on a shallow cleavage furrow (Figs. 28, 29), and big pieces of actin clusters accumulating on the

furrow suggest the cytokinetic ring has been just deconstructed by JAS. In Fig. 28, the two nuclei are closely connected by a high density microtubule spot in between. Since they are at interphase, the central spindle of telophase must have been depolymerized and the spot should be two adjacent MCs. Straight and long microtubule horn bundles are not shown here, but are replaced by two portions of radial microtubules that are supposed to be derived from two straight horn bundles. Under careful observation, a dim trace of a curve actin ring could be seen (arrow in Fig. 28B), which looks like the demarcation of an initial lateral valve complex. This complex has no lysosensor signal, which means it has not yet been silicified. Besides, the lysosensor stain of the hGB2 (Fig. 28a₁) suggests the JAS inhibition begins from the interphase of the mother generation. The cell in Fig. 29 has a similar morphology — the two nuclei are closely connected and the lateral valve complex has not yet been silicified, except the actin ring is more prominent (arrows in Fig. 29C) and microtubules are diffusing radially from the horn bundles (bundles could be found, when viewing from the top of the lateral valve, see video #4 in Appendix). The two stained hGBs also indicate the cell was inhibited in the interphase of the mother generation. The stained girdle band(s) in these two cells suggest cells inhibited by 0.25 μ M JAS in the interphase are still able to enter the cytokinetic stage, even though the cytokinesis have been blocked in the mid-way.

The second phenotype is cells with partially connected valves covering the surface of the prominent cleavage furrow. This phenotype has several subtypes which are described as follow.

The first subtype is the lateral valves without horns and LPs, but when looking carefully, traces of annuli are found, which are typical signs of valves (Fig.30). The two connecting nuclei are not located at the middle plane of the cell any more but are placed aside. This time, the lateral valve is clearly visualized by the HCK-123 signal, suggesting silica has been well deposited on the exposed protoplasmic surface. In the cell of Fig. 30A, there is one big and one small nucleus, suggesting the uneven nuclear division has occurred. This means the nuclear division must have been interfered at anaphase, and the actin system may play a role in nuclear division (see Discussion 4.3.3). As to the cytoskeleton, microtubules are radially diffusing in the protoplast; small pieces of actin clusters are dispersing throughout the cell. The cell in Fig. 30B also has a similar morphology, which has two partially connected valves on the big cleavage furrow as well. Here, microtubules are not visible due to the poor immunolabeling but the trace of the actin ring at the edge of either valve is clearly seen even the actin system has been inhibited by JAS for a long time. Besides, the nuclear division of this cell is normal as can be deduced from the even size of the two daughter nuclei.

Sometimes, the partially connected lateral valves are found to have only horns, each of which is located on the apical point of either valve, partially resembling the prototype of normal valves (Figs. 31A & 31B). The HCK-123 signal of the mother hGB2 indicates the cell was inhibited in the interphase of the mother generation, while the HCK-123 signal of the lateral valves and lateral girdle bands (λ GBs) indicates the inhibition ended at the interphase of the daughter generation. The presence of lateral girdle bands suggest the inhibition is too mild, which failed to completely prevent the following cellular activities after the cytokinesis had been blocked at the mid-way. In the actin channel (Fig. 31A), it is surprising that each lateral girdle band has a trace of actin ring co-aligning at the abvalvar edge, which suggests the organization of actin has not been fully blocked by 0.25 μ M JAS. In this undivided cell, two connecting nuclei have been distributed to the right compartment of the cell, with four thick radiating microtubule bundles and hundreds of perinuclear microtubules. Since there are horns, we speculate microtubule horn bundles must have once appeared to support local cytoplasm during the horn silicification.

While in other cases, the partially connected lateral valves are found to have only LPs (Figs. 31C & 31D). Since these cells have two connected nuclei, the effective inhibition probably began after the nuclear division. And since except for the stained lateral valves, there is not any other lysosensor stained silica structure that is generated after cytokinesis, the effective inhibition of 0.5 or 1 μ M JAS probably took place at the midway of cytokinesis. In the meanwhile, the silicification of the valves was triggered to make valves because the cleavage furrow had reached to a certain extent (Discussion 4.1.5.4).

In summary, cells from the inhibition with 0.25 μ M JAS (Figs. 28, 29, 30, 31A) illustrate that such concentration is not sufficient to completely suppress the activity of the actin system, because the trace of actin ring at the growing frontier of the recent silica structure suggests the inhibited actin system can still develop F-actin at the growing frontier of the most recent silica. Whereas, cells from the inhibition with a higher concentration (Figs. 31C & 31D) do not show actin filaments because of the failure of immunolabeling, but we can examine the inhibitor effect by observing the indirect inhibition object — silicification state. Unlike the cell inhibited by 0.25 μ M in Fig. 31A which have not only lateral valves but also lateral girdle bands, these two cells inhibited by 0.5 or 1 μ M JAS (Figs. 31C & 31D) have only lateral valves, which may be due to a more rapid and complete inhibition by a higher concentration. Thus, we infer that whatever the cellular phase occurs under either high inhibition, cell activities would be quickly suppressed so that the cell might be “frozen” in that phase. In other words, if cells of Figs. 31 C&D had been

inhibited from interphase as the cell of Fig. 31A, they would pause at interphase, rather than develop until the cytokinesis and the lateral phase as in Fig. 31A.

3.3.2.2 Silica Development of the Daughter Generation without Preceding Nuclear Division

Cells with with one nucleus and a cleavage furrow are found in batches of 0.25 and 0.5 μM inhibitions. Their furrows are covered by valvar silica, which are usually decorated by LPs (Figs. 32, 33A–33C). The appearance of the cleavage furrow suggests the cytokinetic ring has been made and the constriction has occurred before the deconstruction of the cytokinetic ring. According to the curve gradient of the lateral valves, these cells could be classified into two phenotypes.

The first phenotype has a lateral valve complex covering the shallow saddle of the cleavage furrow (Figs. 32, 33B). The cell in Fig. 32 is inhibited by 0.25 μM JAS. Its lateral valve complex has four LPs at the furrow and annuli are surrounding at their base plates. Either end of the complex is followed by one lateral girdle band whose abvalvar edge is co-aligned with a trace of the actin ring (Fig. 32D), even though almost all microfilaments in the protoplast are depolymerized into actin clusters. The perinuclear microtubules and the prominent MC on top of the nucleus exhibits the typical morphology of interphase. The cell of Fig. 33B inhibited by 0.5 μM JAS has a similar lateral complex. Between the two domains of LP-base plates, there are two embossed rims (arrows, Fig. 33B), which are considered as the ridges of two fused annuli.

The second phenotype is characterized by two partially connected lateral valves covering the surface of the deep cleavage furrow (Figs. 33A, 33C₁&C₂). The most typical shape is the cell of Fig. 33C₁, which is from the batch of 0.5 μM inhibition, that the furrow silica is clearly composed by two apical hypovalves. In cytoskeleton channel, even though the immunolabeling is poor, an MC and radial perinuclear microtubules are well visualized, showing the typical morphology of interphase (Fig. 33C₂). In a more extreme case, i.e., the cell of Fig. 33A from the batch of 0.25 μM inhibition, the lateral valves have a sharp curve at the middle because of the deep cleavage furrow. Pieces of actin clusters are close to the two edges of the lateral valves. This time, no LPs but only PDMPO bright spots are seen which are probably LP base plates.

In brief, batches respectively inhibited by 0.25 and 0.5 μM JAS are not obviously different in terms of the cell phenotype. The first common point is both batches have both phenotypes.

However, we have never found either type is shown in the batch of 1 μM inhibition. It seems the silica deposition could still occur when microfilaments are not severely inhibited (Discussion 4.3.1). The second common point is that most these daughter valves do not have any horns, suggesting the disfunction of microtubule horn bundles during the horn development. The last common point is that the nucleus cannot divide, which implies the nuclear division may rely on some facilities related to the actin system (Discussion 4.3.3).

3.3.3 Inhibition until the Daughter Generation with Cell Division

In the batch of 0.25 μM inhibition, cells influenced from the late interphase are usually paused at the halfway of cytokinesis. Nevertheless, there are still some escapees having successfully divided into individual daughter cells. There are some common characteristics of these daughter cells: (1) horns are absent; (2) the head plate is perfectly placed at the center of the valve domain but it is aberrant, because it is composed by two anamorphic annuli; (3) the formation of hypovalve is aborted; (4) it is very likely that there are pieces of actin clusters accumulating at the edge of each abortive valve, even though only the actin of Fig. 34B is well immuno-labelled to present actin signals.

Between the cells in Fig. 34A and Fig. 34B, there are two differences. One simple difference is the latter has long LPs extending from the the two apical point of the head plate. The reason for the occurrence of the LPs is unknown, but their development seems to rely on the microtubule horn bundles during cytokinesis (Discussion 4.1.3). The second difference is the start point of the inhibition. The stained hGB2 of the mother cell in Fig. 34A indicates it was at least inhibited from the hGB2 developing stage. Apparently, this cell was inhibited earlier than the mother cell in Fig. 34B. Because the latter cell has not any lysosensor stains on its mother frustule, and only the daughter hypovalves are stained. As we know, the first 2 hours inhibition excluding lysosensor is apparently longer than the 31 minutes of mitotic and cytokinetic phase (Fig. 3, Part I), so this cell was also inhibited from the late interphase.

The most attractive but confusing point in this section is why the mother cell of Fig. 34 (i.e. phenotype #4, Table 2) could still completely divide even though the cell has been inhibited from the late interphase. Because, as reported above, cells inhibited from later interphase with the same inhibitor concentration can also end up as undivided mother cells being covered with various types of lateral valve complex (i.e., phenotype #5 & #6, Table 2). Here, the completion of cytokinesis may be due to the incomplete deconstruction of the cytokinetic ring. Besides,

although we have seen a deep cleavage furrow in the cell of Fig. 33A, we have never seen the asymmetrical division occurs, which produces one nucleated and one anucleate daughter cell.

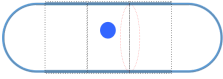
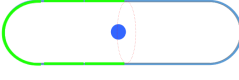
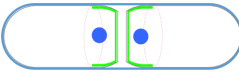
Moreover, the absence of horns arouses our curiosity, as we know their development are regulated by microtubule horn bundles, which should not be affected by the JAS inhibition (see Part III. General Discussion).

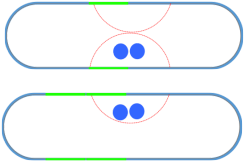
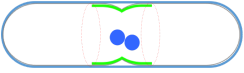
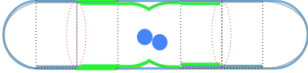

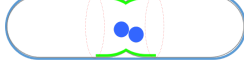
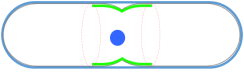
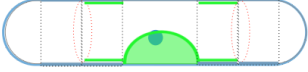
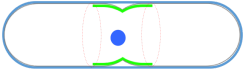

3.3.4 Inhibitory Phenotypes of Long-term Inhibition with JAS

The cellular morphologies resulting from the treatment with different JAS concentrations of the “2+48h” inhibition schedule, can be categorized into 5 basic inhibitory phenotypes (Table 2). Given that cells had not been synchronized⁶, they should be in a different developmental stage when the inhibition began. To learn the effects of JAS inhibitions resulting from different concentrations that begin at the same developmental stage, the starting point of the inhibition are reconstructed (Fig. 35-1)

⁶ See explanation in Section 4.1.2.

Table 2. Morphological types of JAS-treated cells from “2+48 inhibition”.

Basic types	Subtypes	0.25 μM	0.5 μM	1 μM
1	1a 1b	No effect	 Fig. 27B	 (Not shown)  Figs. 27C, 27D By visual inspection, about 70% of basic type #1 in the culture.
2	2a 2b 2c	 Fig. 26A  Fig. 26C	 Fig. 27A	Not found
3	3a 3b	 Fig. 34A  Fig. 34B	Not found	Not found

4	<p>4a</p> <p>4b</p> <p>4c</p>	 <p>Figs. 28, 29</p>  <p>Fig. 30</p>  <p>Fig. 31A–B</p>	 <p>Fig. 31C</p>	 <p>Fig. 31D</p> <p>By visual inspection, about 20% of this type in the culture.</p>
5	<p>5a</p> <p>5b</p> <p>5c</p>	 <p>Fig. 33A</p>  <p>Fig. 32</p>	 <p>Fig. 33C</p>  <p>Fig. 33B</p>	<p>Not found</p>

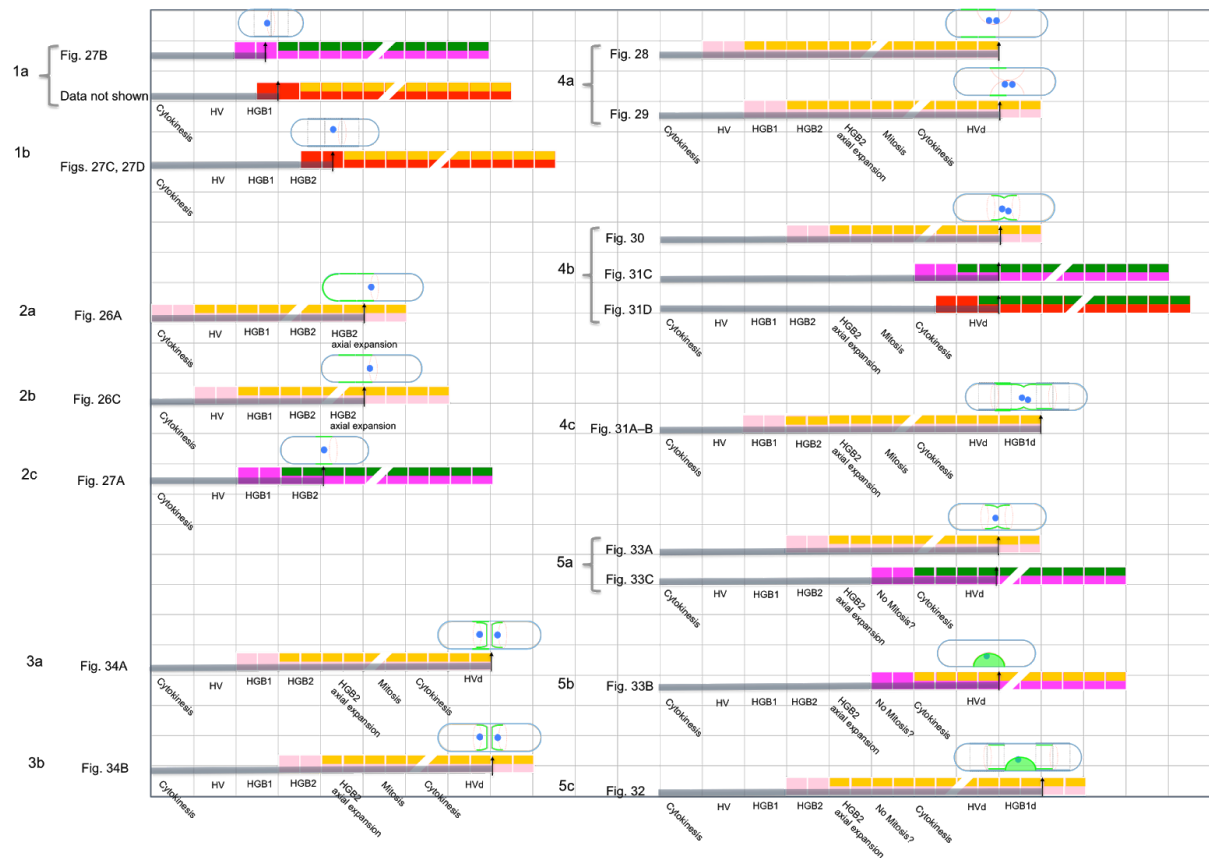


Fig.35-1 Frustule morphogenesis under different concentrations of JAS (for a high resolution version of this figure see Appendix). Cells have been treated by the same long-term schedule (“2+48 h”, depicted as a line of squares) differing by the starting points of the inhibition and by the concentration of JAS. One square represents 1 hour, square colors represent the concentration of JAS: pink – 0.25 μM , magenta – 0.5 μM , red – 1 μM respectively; green and yellow represent the presence of PDMPO and HCK-123, respectively. Not all of the cell activities take the same amount of time, but for convenience of the comparison the timeline representing the average duration of stages is placed underneath. And the time elapsed durations between two activities is omitted. Abbreviations: HV – hypocone valve, HGB1 – hypocone girdle band 1 (of the mother generation), HGB2 – hypocone girdle band 2 (of the mother generation), HGB1d – hypocone girdle band 1 of the daughter generation.

Treatment with JAS at a concentration of 0.25 μM causes the highest variability of inhibitory phenotypes (Table 2), except for the basic type #1, which stands for the complete inhibition. And cells which have completely divided (basic type #3) exclusively occur at such a mild inhibition. Since these cells are from the “2+48h” inhibition schedule, it means that all lysosensor-stained silica was fabricated, deployed on the cell surface and axially extruded from underneath eGB2 in the presence of the inhibitor and this indicates that the SDV formation and the axial expansion

were not effectively disabled at this concentration. The silica deposition and the axial expansion will, however, be inhibited as the concentration gets higher (see Discussion 4.3.1). One of the best examples is the inhibitory phenotype #2, which occurs at two concentrations (0.25 μ M and 0.5 μ M), whereby the treatment at the lower concentration generated more lysosensor stained silica structures during interphase than at the higher concentration. In addition, cells treated by this low concentration still can generate an actin ring at the abvalvar edge of the most recent SDV (e.g., Figs. 28, 29, 31, 32). Thus, in general, the inhibitor concentration is too mild to deconstruct the actin system completely, so cells could manage to proceed through the subsequent stages of the cell cycle.

When the inhibition of 0.25 μ M JAS acts on cytokinesis, some cells can continue to divide (basic type #3), while others fail to do so (basic type #4), corresponding to complete or partial protoplasmic cleavage. The different types of cleavage are caused by the different degree of actin deconstruction, which gives rise to different contractile properties in the meshwork of actin clusters. These cleavage types are a special feature of JAS inhibition, which are not typical for other actin inhibitors. For instance, if cells were inhibited by Latrunculin A, which directly prevents actin monomers from polymerization, no visible aggregates would be induced and therefore probably neither type of cleavage would occur.

In the case of basic type #5, the single nucleus of cells with lateral valves must contain duplicated DNA, because this is always concomitant with the appearance of the lateral valves (Oey and Schnepf, 1970). This indicates either the failure of nuclear division or the re-fusion of daughter nuclei, or the degeneration of one of the two daughter nuclei (see Discussion 4.3.3).

When the JAS concentration reaches 0.5 μ M, the inhibition becomes stronger, showing less inhibitory phenotypes. Some cells are incapable of producing any lysosensor stained silica structures (phenotype #1a), while others are still able to develop a girdle band but remaining under the cover of eGB2 (phenotype #2c). In both cases, the axial expansion is absent. The other phenotypes are cells equipped with only lateral valves, which suggests the beginning inhibition may range from S phase to midway cytokinesis (phenotype #4b, #5a and #5b). But lateral-valve cells inhibited from the middle of interphase as seen in the 0.25 μ M JAS treatment (i.e., phenotype #4a, #4c and #5c), whose mother girdle bands were stained by lysosensor, were no longer present in the batch of 0.5 μ M inhibition. Naturally, the phenotypes of cells equipped with only lateral valves occur at a higher frequency in this concentration than that in

0.25 μM . These aspects indicate that the when cells are inhibited from the middle of interphase would be blocked immediately by 0.5 μM JAS.

When the JAS concentration reaches 1 μM , the variety of inhibitory phenotypes is strikingly lower and has only two basic types remaining: (1) Basic type #1 are cells that neither are capable of axial expansion nor do they deposit any silica. It comes in two subtypes (#1a, #1b) depending on when the inhibition started in the cell cycle, i.e., the inhibition of subtype #1a starts from early interphase and #1b starts from mid-interphase. At any rate, the actin cytoskeleton was disrupted after the deployment of the recent hGB but before the axial cell expansion; all following stages of morphogenesis were swiftly interrupted, before lysosensor staining could occur in the following 48 hours. (2) Basic type #4 has only one subphenotype, which belongs to the type #4b. The reason why silica deposition is seen in the lateral valve complex is discussed (see Fig. 35-3).

In summary, the variety of inhibitory phenotypes is decided by three aspects: (1) The time point, when the inhibition begins from. (2) The concentration of the inhibitor, and (3) the sensitivity of the microfilament-based cell functions.

3.4 Phalloidin

Phalloidin at a concentration of 0.5 μM or 1 μM has been applied in two different treatments: short-term treatment — a 2-hour inhibition in the presence of the lysosensor PDMPO; long-term treatment — a 2-hour pre-inhibition with Phalloidin alone followed by a 50-hour inhibition in the presence of the lysosensor PDMPO (“2 + 50 h” inhibition). The idea was to examine, by short-term treatment, whether a momentary process can be completely inhibited; by long-term treatment, whether cells would be completely inhibited to pause at a stage or whether they are able to continue to the following steps of the cell cycle but performing abnormal behavior. It turns out that some inhibition effects on cytoskeleton and frustule morphogenesis are similar in both treatments, and that cells under long-term treatment would be blocked after valve formation or before cytokinesis.

3.4.1 Inhibition at the Post-cytokinetic (Valve-formation) Stage

Under short-term treatment, three phenotypes of inhibition were observed. A mild phenotype shows subtle effects on the formation of the annulus and the edge of a valve (Fig. 36). In normal development, two compressed oval annuli form on the head plate, originating from the bases of the LPs. Each annulus consists of straight narrow double lines extending from each apical site towards the middle of the head plate. But the two pairs of double lines extending from the opposite apical sites do not fuse in the middle. Instead, a field of perturbed areolae (i.e., yellow stipend area of Fig. 11b in Chapter 1) is inserted between them. It is found that in the Phalloidin cells subjected to short-term inhibition, the narrow double lines run up reaching even closer to the middle point of the head plate, the extending double lines are not yet fused into two individual annuli, and the middle region of the young head plate are still open (Fig. 36F), which suggests that development proceeds at a slower pace than in control, and such open ends have never been observed before. Although in this image it cannot be seen what the silica pattern is like in the center region of the head plate due to the high fluorescence background produced by the underlying nucleus, those parts that can be seen show a highly regular silica pattern as in control cells. This notion is also supported by the finding that in other Phalloidin-treated examples, silica patterns remain highly regular. But the only subtle difference to normal cells, is that the silica pattern becomes less distinct when moving further from the head plate and and

thus leads to a blurred advancing silica edge of the valve (Fig. 36). In this case, the actin ring seems locating far from the silica edge of the valve, whereas in control cells it is closely co-aligning at the growing edge of the valve. Hence, it seems the silica deposition density correlates to the actin ring location, i.e., the blurred edge of the valve is caused by the far location of the actin ring. A more severe inhibition of this phenotype is found in long-term treatment (Fig. 37 D&E), whose entire head plate is lack of PDMPO signals, although PDMPO had been present in the incubation for 50 hours.

In addition, a point should be noted that when the horns have been silicified, the radial dome of perinuclear microtubules is accompanied by two prominent branches of microtubule horn bundles. These bundles are long and straight and they should have been completely transformed into radial arrays at this stage if not inhibited (compare Fig. 36C with Fig. 13C in Chapter 2). In the actin fluorescent channel, shallow red fluorescent signals are found along the horn bundle. Despite whether these signals are unspecific stains, the actin patches on bundle tips are not visible at this stage.

The second phenotype shows a much more severe inhibition effect that the geometry of the head plate is heavily disturbed and the valve advancing edge is extremely abnormal (Fig. 37 A–C). As is known in normal cells, two compressed elliptical annuli comprise a head plate, the apical side of which is decorated with an LP and a horn. But this phenotype of inhibition shows a completely different scenario: there are four annuli exhibiting as roundish centers on each valve, and each apical side has one horn but not always an LP. The number of annular centers here is the double of the normal case, and these centers are formed in the vicinity of each other, but they do not combine into a meaningful valve shape. Consequently, this brings about the extremely abnormal valve edge (i.e., Fig. 37). The abnormal geometry of the head plate on the valve suggests an elongated development of an annulus, which should be related to the malfunction actin microfilaments under the Phalloidin inhibition.

The third phenotype is cells with completely aberrant valve (Figs. 37F, 39 A–D). The PDMPO signal of the abnormal valve could be seen, with abnormal annuli and no horns or LPs. The absence of horns and LPs implies that microtubule horn bundles have not been made because they are responsible for the formation of LPs and horns. The formation of microtubule horn bundles, in turn, might have been interfered when actin microfilaments are inhibited by Phalloidin. This means the inhibition process might have begun from telophase or even earlier. However, the completion of the cell division indicates the cytokinetic ring was able to complete the constriction in the end, possibly as a result of insufficient inhibition at cytokinetic stage. To

summarize, the initial inhibition occurring before the horn formation might have interfered with the assembly of microtubule horn bundle, and the following complete inhibition might have created an aberrant valve without horns or LPs. This will be further examined by the Fig. 41 A–E.

In both the long-term and short-term inhibition, there are some common features of silica morphology (Figs. 36A, 37A, 37E): (1) The valves at uncompleted stage are more often to be captured than in control cells, indicating the progression of valve morphogenesis has been slow down. (2) Sometimes, their tips of horns appear to be open, which suggests the closure of the tip with an ocellus relies on the shortening of F-actin.

3.4.2 Inhibition from Mid-Interphase to Prophase

Cells at the middle interphase or at prophase have been encountered in both short- and long-term inhibitions (Figs. 38–40). All of them have completed the transition from hypovalve formation to girdle band formation. Regarding the inhibitory stages, there are 4 phenotypes.

The first type is the cell shown in Fig. 38. Its PDMPO stained valve suggests the cell has been inhibited at least 2 hours before the valve formation. Thought it has developed a hypovalve, but the actin ring, which should be designated to sit at the valve edge, is located far away. And following the actin ring, the interphase nucleus and the radial microtubules (Fig. 38b₂) have been located away from the valve. Long actin bundles appear prominently in the cell and some of them seem to co-align with microtubules (Fig. 38b₃). The valve morphology looks normal, but there are not any traces to show silica is going to deposit in the area between the valve and the actin ring. Whether the girdle band formation has not yet occurred, which means the configured cytoskeleton is just been pulled out, or alternatively the GB-formation would not occurred due to the inhibition, is unclear.

The second phenotype is shown in Fig. 39 A–D The cell has a completely aberrant valve that is without any horns and LPs, and a malformed girdle band which exhibits wavy edges. The actin ring is missing and long actin bundles are not aligning with the abvalvar edge of the girdle band (Fig. 39a). Microtubules are very long, co-aligning with actin bundles. The interphase nucleus has been pulled out from the cover of the recently made girdle band.

The third phenotype is the inhibited cell who successfully developed a girdle band (Figs. 40A, 40B). Here the morphology of the girdle band looks normal; the abvalvar edge is

co-aligned with an actin ring. The cytoskeleton arrangement is like that in control cells except the two long actin bundles originating from the bases of the LPs. This may be because the cell has been inhibited for only 2 hours and the complete inhibition has not yet taken effect.

The last phenotype is cells with abnormally radial microtubules which are converging all microtubules only on the MC or the PC precursor (Figs. 40 C–D, 41). The radial configuration of cytoskeleton has two subtypes. The first subtype is shown in Fig. 40 C–D, the cell has no PDMPO stained silica but a weak trace of actin ring is seen (yellow arrow, Figs. 40c₁, c₂, c₄) and since the MC there is a PC precursor, one would expect the inhibition may have begun from the initiation of PC precursor. Long microtubules are emerging from the PC precursor, co-aligning with long actin bundles, which are extending from base plates of LPs.

However, the inhibition began from a similar time point (after hGB2 formation) may not bring the same result. For instance, in the cell of Fig. 40F, perinuclear microtubules are emerging from the surface of the nucleus, with a PC-precursor-like structure dominating on top of the nucleus. However, its actin ring is thick and its location suggests it is a cytokinetic actin ring rather than a thin GB-actin ring which should be seen on the edge of the hypotheca. However, in control, a cytokinetic ring will not appear when the PC is thin and young (Fig. 40f₁, note the linear shaped MT-structure) and the ring only be visible when the PC precursor becomes thicker and more matured. This may be because its thickness is promoted by the Phalloidin.

On the other hand, it is frequently observed that one or both LP base plate positions inside the epivalve serve as anchor (focal) points for the actin cytoskeleton in Phalloidin-treated cells (e.g., Figs. 40 B&C). In the majority of images, this particular detail is presented to the observer in perfect girdle view, so it is attractive to see how this configuration looks like in a valve view with a rare chance. Here in Fig. 39 F&f, the cells are presented in a tilted valve view, showing that several microfilaments form a circle around the position of the spine base.

The second subtype is shown in Fig. 41. After the application of Phalloidin, a separation of the MC from the nuclear surface occurs and literally all microtubules, previously perceived as being perinuclear are now all only centered onto the MC, and none remain associated with the nuclear surface. This configuration appear in both short-term and long-term inhibitions, but they may have slight differences in other minor aspects: In the short-term inhibited cell Fig. 41A, there is not any PDMPO stains, but given that the hGB1 has been extruded from the cover of eGB2, the inhibition might have started when the cell completed the silicification of hGB1 or hGB2. In the long-term inhibited cell Fig. 41C, only the hypovalve, which looks normal, has been

stained in the 2nd stage of the inhibition (50-hour inhibition in the presence of PDMPO). This suggests the silicification was completely blocked after the valve completion, but it is abnormal that the nucleus is not located under the valve cover and has reached prophase. Although both cells were blocked from interphase and they have not yet fully expanded into the full length, their nuclei have still entered prophase, as is evident from their condensed chromosomes (Figs. 41b & 41c₂). These two cells do not have actin ring anymore but replaced by radial microfilament arrays. And the absence of the ring may be the reason why the silicification of the rest frustule components did not occur.

3.4.3 Inhibition on Prospective Cytokinesis

Cells inhibited from interphase have never found to be retarded at the midway of cytokinesis (Figs. 42, 43).

In Fig. 42, which has been inhibited since interphase and is eventually able to transit to metaphase in the presence of 0.5 μ M Phalloidin for 52 hours. This is supported by the fact that this cell has two PDMPO-stained hGBs and the dumbbell-shaped nucleus. Although the hGB2 has some subtle artifacts (Figs. 42b₁, b₂, b₃), the transition of the cell is successful, because the spindle has been assembled, and the cytokinetic actin ring has been formed, which is placed almost correctly over the middle of the spindle. Unfortunately, the actin ring is partially concealed behind the nonspecific fluorescence on the cell wall. However, we can manually trace the shape of the ring by going through the image stack. The result shows that one half of the ring has the right intensity and width and straightness, which is typical for a cytokinetic actin ring, whereas the other half, which is associated with the spindle, turns out thin and wavy, appearing like a flat band of the cytokinetic ring turns a quarter (Fig. 42a₅). And there must be a reason for the meandering path of the ring. It could either be caused by the post-fixed folding of the cytoplasm or widened by the Phalloidin treated actin filaments which have consequently developed a ring larger than the diameter of the cell. Luckily, this cytokinetic ring is not affected by a local invagination seen at the lower rim of the cell (arrow in Fig. 42B), which is located outside from the invagination (seen for instance in Fig. 42a₂). Even though the spindle looks quite normal, there is a long-term effect of Phalloidin on the spindle fibers to capture segregated chromosomes, because there is clearly one orphan chromosome being isolated from the chromosomal cloud (see circle in Fig. 42b₄).

Mitosis apparently can progress to the stage of telophase as shown in Fig. 43, which is the

last phenotype of the mitotic stage. The cytokinetic ring in this cell also shows some wavy feature and there is a local view of thinning because of the tilted angle. At this moment, this cell is not ready to constrict, because the two microtubule horn bundles have not yet completely developed. All aspects look largely normal. And it is a pity that no further cytokinetic stages based on this development have been discovered in other cells; otherwise, we can check whether cells are blocked at this stage and lost the ability to pass through the cytokinesis.

4. Discussion

4.1 Oryzalin

4.1.1 General Effects of Oryzalin

4.1.1.1 Dynamic of the Microtubule System under Inhibition

The biosynthetic herbicide Oryzalin depolymerizes microtubules of the diatom *Odontella sinensis* in a gradual fashion depending on the inhibitor concentration, treatment duration and also on the type of microtubule array in the cell. At interphase, there are two major types of microtubule arrays present in *Odontella* — the bundles (shown as root bundles at interphase or horn bundles from telophase to early interphase) and the radial, perinuclear array. The latter disappears faster than the former during Oryzalin treatment. This suggests a difference in the modes of dynamics, stabilization and interactions among the MT structures and also possibly in the interactions with the actin cytoskeleton or with membranes. The reason why the perinuclear MTs disappear faster is that they are very dynamic and they are single or only lightly bundled. They do not appear to converge primarily on the MC but on the entire nuclear surface (though this feature changes in the Phalloidin-treated cells, see Figs. 40C, 41A & 41D). The MT bundles on the other hand are more stable, because they are tightly packed, which suggests the presence of molecular cross-linkers, i.e. MAPs.

The MC is still detectable by immunostaining with tubulin antibodies after short-term treatment with Oryzalin, and it does not look much different from the control, since some short microtubules are almost always seen radiating from it (Figs. 1B, 1D₁), whereas the perinuclear MTs are much more sensitive. Still, there are always some crippled remnants of the MT-system after Oryzalin inhibition, either in the form of fragmented single filaments near the interphase nucleus (Fig. 1D₂), or a rim around the nucleus of dense material stained by anti-tubulin (Fig. 3B). This situation becomes more severe in long-term treatment — a thicker mesh of intensely stained material surrounds the entire nucleus, which looks like a cage (MT-cage, see Figs. 4C, 5C, 6F, 8, 9A). Often highly immuno-labeled material also occurs in the cytoplasm in the form of rod- or needle-like structures, when the perinuclear MTs and also the more stable horn bundles have completely disappeared.

The extreme resistance of the MT-cage could be explained on one hand that microtubules may cross-link to the nuclear surface possibly via MAPs, and on the other hand that the rods

and needles rather speak for an aberrant type of tubulin supramolecular architecture such as para-crystals. The phenomenon of inducing para-crystal is an effect known from Vinca alkaloids (Amos, 2011) and it has also occasionally been seen using Oryzalin, which in the case of higher plants suggested that this could be due to the excessive binding of MAP65 (Panteris et al., 2010). The formation of this material around the nucleus and in the cytoplasm is unprecedented in diatoms. The suggestion of MAPs is speculative, because their presence in diatoms is not yet known, but the least one could say is that the original microtubule arrays are broken down, because Oryzalin acts via binding to the free tubulin dimers, rendering them incompetent of polymerization (Hugdahl and Morejohn, 1993), and at the same time Oryzalin promotes the formation of persistent para-crystals, which do not show subunit turn-over.

The para-crystals that labeled by anti-tubulin often align with actin bundles (Fig. 8H). This is an interesting result, because it suggests a physical interaction between the two cytoskeleton elements. The physical interaction is also suggested from the displaced nucleus induced by Oryzalin (Figs. 8 – 10) and this is supported by the results of Phalloidin treatment (Figs. 40C, 41). These results support the tension-equilibrium model (see Chapter 2). Further, the binding occurs over the entire length of those needle like para-crystals, creating the parallel alignment along the actin cables. This could be interpreted in two ways. Either is the interaction achieved by MAPs or by actin-based motor proteins carrying microtubules as their cargo (such types of motor proteins are known from other organisms (D'Avino et al., 2008; Etienne-Manneville, 2004; Rodriguez et al., 2003; Woolner et al., 2008) and in this case, the interaction would be dynamic. Either way suggests that there is a high number of such proteins around in the diatom cell, and Oryzalin-inhibition leaves them without a useful function and deprives them of a target to bind to, so these proteins get bound to the needle like para-crystals and cause them to align along actin filaments.

The MC is present on top of the nucleus in control cells lasting from the early post-cytokinetic stage until the onset of prophase. The MC in the short-term Oryzalin-inhibited cells can also be found, except that the number of associated microtubules has been strongly reduced by Oryzalin. So it is clear that the MC is still capable of protecting short microtubules that are attached to it at an inhibition period of 2 hours. When the inhibition takes much longer, the MC will become almost invisible, because the entire nucleus is covered by the MT-remnant-cage, so the MC is hard to be identified. In normal prophase cells, the MC disappears naturally, while the spindle precursor appears (Tippit and Pickett-Heaps, 1977). This is also the case in the Oryzalin treated cells (Figs. 1D₃ & 1D₄), but now, the spindle precursor is

affected by the inhibitor, because its shape is dramatically changed. Instead of the layered, rod-like feature of the spindle precursor known from the control, two disc-like structures appear side by side on the nuclear surface upon Oryzalin-treatment, and this is a hitherto unknown phenomenon. The discs are diffusely stained with the tubulin antibody, showing a fuzzy edge, and they appear larger than the polar plates of normal cells. This can be interpreted to be that the polar plates have individually reoriented 90° from their narrow flank side to their large distal/front side with the planar association along the nuclear surface, which is a consequence of the separation of the polar plates after the depolymerization of the MTs that connected them. Internal structural organization in the polar plates themselves may also change, which could explain the increase in their size.

The Oryzalin-induced breakdown of the MT system has no immediate effect on the dome shape of the cell, when the treatment time is just 2 hours at the post-cytokinetic stage (early interphase). These cells survive perfectly, when the inhibitor is removed and they are even able to enter the next following developmental stage, e.g., the recovery of the early post-cytokinetic cell begins with the re-establishment of the former horn-bundles followed by the reappearance of the perinuclear MT-system (Fig. 2).

Differing from the normal case, where horn bundles merge on the MC, which should indicate that the MC has microtubule organizing property (see Chapter 2), during the recovery period, the horn bundles are not rebuilt from the MC, so that the MC appears to have no polymerization function at this stage. Alternatively, one could expect that the regrowth of microtubules could begin from the former ends of the horn bundles, where they formed the protoplasmic protrusions. This is because they potentially could be the places, where re-polymerization of microtubules could become enhanced by tubulin-binding proteins. However, instead, the horn-bundles re-appear over the entire transapical axis by a process that appears to involve the fusion of smaller bundle fragments (Figs. 2A & 2B). In that sense, re-formation occurs directly reverse to the Oryzalin-induced breakdown process, which caused the fragmentation (Fig. 1C).

What could be the reason for this genuine mode of reconstruction of the horn-bundles? In the normal development occurring in control cells, the formation of these horn-bundles proceeds from the hb-MTOCs of each daughter cell (e.g., Fig. 10A of Chapter 2). But these centers exist only, when the cell is at telophase and obviously they could not be regenerated at the post-cytokinetic stage. The fact that the MC is not the starting point for the reappearance of MT bundles after the wash-out of Oryzalin indicates that it does not have a stage-specific MTOC

property in the sense of rebuilding the previously destroyed structure. The only confusion is, which cell component carries the structural information to rebuild the horn bundles in the original position. This is unknown, but suggests that there are still molecular markers left at the original site of the apical membrane, which help to localize the rebuilding process to the correct positions.

Another aspect about the recovery from inhibition is that at the post-horn bundle stage, the overall re-appearance of perinuclear microtubules in cells recovering from Oryzalin is massive, almost overshooting, if compared to those of untreated cells. This suggests that tubulin synthesis is scaled-up in response to the disturbance of the dynamic equilibrium between the monomer and polymer states, which is a demonstration of how adaptable the tubulin biosynthetic machinery is in the diatoms.

4.1.1.2 Are Microtubules Required for the Silicic Acid Supply?

Microtubules could possibly transport vesicles that contain silica deposition materials (named “silicon transportation vesicle”, STV) to the SDV (Schmid, 1980; Schmid and Schulz, 1979), which is one of the silicon transportation ways suggested to occur in diatoms (see section 1.2 of Introduction of Chapter 2). Previous studies with other diatoms have shown that the silica deposition can still occur when MTs are absent after inhibitions (Schmid, 1994; Schmid et al., 1996; Wordeman et al., 1986), which agrees with the “2+48 h” result here: The extent of PDMPO staining reveals that cells of *O. sinensis* inhibited by Oryzalin are still able to develop silica structure throughout the developmental steps of the cell cycle, when microtubules are completely absent. This means that ample supplies of silicic acid have arrived in the SDV in the absence of microtubule based long distance STV transport. This result and the previous studies together suggest that the microtubule transportation is not the necessary way to supply silicic acids, if such a way really occurs in diatoms. Thus it naturally illustrates the necessity of the direct transportation to be responsible for the silicic acid import, which described in the recently emerging concept may have three different physical importing accesses on the silicalemma (Baeuerlein, 2004; Hildebrand et al., 1998; Thamtrakoln et al., 2006).

Returning back to the role of microtubules, how to know whether they are involved in transporting silicic acids or not? To answer this question, one should first eliminate the occurrence of the direct transportation in microtubule inhibited cells (Baeuerlein, 2004;

Hildebrand et al., 1998; Thamatrakoln et al., 2006), before applying lysosensor staining to examine whether the silica deposition can still occur or not.

4.1.1.3 Sometimes Silica Deposition is Inhibited

When considering these subtypes of #1 in the batch of "2+48 h" treated by 1 μ M Oryzalin (see Result 3.1.3), cells were not able to reach cytokinesis in the coming 48 hours, suggesting they eventually entered into the state of G0. And this result seems contradicting the suggestion above ("the loss of MT system will not prevent the cell from entering into the next step of the cell cycle"), because it implies the increase of Oryzalin concentration will increase the percentage amount of G0 cells. The explanation for this would be that the sharp increase of the tubulin pool will affect the homeostasis of intracellular calcium (Hertel et al., 1981; Thion et al., 1996) which is an important second messenger that triggers a cascade of events (Allen et al., 2008; Falciatore et al., 2000; Kröger et al., 1994; Vardi et al., 2006) that may trigger the checkpoint and eventually disturb the progression of the cell cycle that relies on calcium or calmodulin-dependent pathways (Kahl and Means, 2003). In the the simultaneous inhibition schedule, subtype #3a can be achieve in 24 hours which means this type from the 48-hour treated group may have also entered to the state of G0 after the first 24 hours. In brief, G0 cells would also be possible to appear in this inhibition mode, but it needs further careful observations to prove that.

4.1.1.4 Lateral Valves are Absent if the 2-hour Pre-Inhibition has been Applied

Lateral valves can also be found in the cells, which were not co-incubated with lysosensor (Figs. 16 B & C). This is also the case in the early study on *Cyclotella*, where lateral valves have been reported after the application of Colchicine instead of Oryzalin (Badour, 1968). This shows that both microtubule inhibitors have the same effect on the formation of lateral valves in undivided cells. However, it is interesting to note that in the "2+48" Oryzalin schedule lateral valves have never been observed (see Table 1 in Result 3.1.3). This could be because the sudden addition of lysosensor after the 2-hour Oryzalin pretreatment could reduce the Oryzalin inhibition effect, because the additional chemical may disturb the cytosolic acidic balance, cytosolic calcium transient or inhibitor affinity of the cell, either of which then interferes with the uptake of Oryzalin

and eventually affects cytokinesis. And this is one of the possibilities, even though it is not likely the major cause.

4.1.2 The Potential Role of MTs in the SDV Shaping and Functioning

4.1.2.1 Role in Girdle Band Morphogenesis

In general, the micropattern of girdle bands in long-term treated cells, resembles that of controls, but in short-term treated cells, there are some interesting differences between Oryzalin treated cells and control. To show this more clearly, the attempt was made in the experiment to separate normal morphogenesis occurring in the presence of PDMPO from the disturbed morphogenesis occurring in the presence of PDMPO plus Oryzalin by the insertion of a washing step in between. The expectation was that a larger unstained gap between the two activity states would result, if the washing step is longer. But the effect of the washing step was not as dramatic as anticipated, even when it was as long as four hours. This is because of the staining nature of PDMPO. It has been shown that the lysosensor can stain silica as long as it has undissociated Si-OH residues (Parambath et al., 2016), which is valid only in the lumen of the SDV. This means not only silica made during the inhibition period was stained by PDMPO, which was administered in the inhibition period, but also the region of silica made during the washing step, if it was in the same SDV. This explains why regions stained by PDMPO sit next to regions where silica was affected by inhibition even without a gap (e.g. Fig. 3B). But it is still possible to distinguish the silica parts coming from the two different incubation phases, because one can see a long girdle band with undisturbed silica pattern is made in the control incubation period, which is followed by a shorter girdle band with disturbed pattern, which comes from the Oryzalin incubation period (Fig. 3).

One point should be noted that the long-virgae-pattern appears in short-term inhibited cells (Fig. 3), but it has never been found in long-term inhibited cells, suggesting this is a temporary state of the silica deposition, because the gaps between them will inevitably be filled as autonomous silicification continues (see Chapter 1), whose silicic acid supply can be independent of microtubules (Section 4.1.1.2).

The question remains, how the short term disturbance with Oryzalin promotes the formation of virgae. Virgae are formed, when the SDV has the shape of a flat cisterna, which is in the region of the advancing edge, whereas the more elaborate pattern of the areolae is achieved by

three-dimensional folding of the inner silica lemma further away from the advancing edge (see the cell wall developing order in Chapter 1). In case that expansion of the SDV proceeds fast and uncontrolled, the two-dimensional area can expand faster and hence virgae formation can proceed faster. This virgae-pattern phenomenon points at a function of MTs as drag shoes, and it also suggests that the actin ring does not exert its demarcation function in a proper way on its own, but rather needs the collaboration with microtubules.

Even though each of the partners, microtubules and actin filaments, have genuine functions in their own rights, it is becoming a powerful, new concept in cytoskeleton research that they cooperate in many ways. Using neuronal morphogenesis, particularly the behaviour of the growth cone as a role model, Pacheco and Gallo (Pacheco and Gallo, 2016) describe several kinds of cooperations between microtubules and the actin cytoskeleton: the most interesting in the context of the current discussion are the lateral associations between microtubules and actin filaments bundles promoting mutual stabilization and the interaction of so called actin arcs with microtubules running perpendicular to them, which blocks their advance. The latter would come closest to the drag shoe hypothesis mentioned above for the function of microtubules in *Odontella*. It is then becoming an attractive hypothesis to be tested in future research that microtubules and actin filaments work together in the control of SDV expansion.

Hence, applying the drag shoe hypothesis into the tension equilibrium model of cytoskeleton dynamics (see Fig. 16 in Chapter 1), this phenomenon can be explained as follows: The axial expansion of the cell driven by turgor pressure loses the restriction by the tension system, when no microtubules can interact with the actin bundles, so the SDV expansion proceeds as fast as the axial expansion of the cell, and therefore the initial silica structure virgae grows faster. But inevitably the axial expansion of the cell will stop and so will do the SDV expansion, which allows the silica deposition to fill gaps between virgae if given enough time. And this is why the virgae pattern is missing in the long-term MT-inhibition.

In the tension equilibrium model, the axial expansion is based on parallel interactions between microtubules and actin filament bundles. So taking out the microtubules should throw the system out of balance. Indeed, particularly in the long term Oryzalin treatments cell tended to be double as long and girdle band tended to be double as wide as in control. But the data show that the cells did not over-expand to the extent that protoplast surfaces get exposed to the environment. The reasons for that may be the following: First, the holding power of the adhesive organic material (including chitin) at the joint between epitheca and hypotheca and at the joints

between girdle bands might always be stronger than the pushing force of turgor pressure, provided that the glue is not actively hydrolyzed by the cell (see Fig. 17 of Chapter 2). A second aspect is that an increase of internal pressure may invoke a response of the actin cytoskeleton. Pressure has been experimentally increased by placing whole plants into pressure chambers (Li, 2011) or by localized compression, i.e. by pressing a blunt microneedle against the wall (Hardham et al., 2008). In both experimental setups the reaction to the increasing pressure is an increase and bundling of actin filaments either throughout entire tissues (Li, 2011) or localized in the cytoplasm underneath the needle (Hardham et al., 2008).

Apart from these aspects, heavy perturbation of cell function could reside in a side effect of tubulin depolymerization, which is that an increase of the cytoplasmic tubulin subunit pool, for instance as a consequence of microtubule depolymerization, could have an effect on the calcium homeostasis. This is known from animal cells (Maldonado et al., 2010), where Colchicine induced free tubulin subunits affect the mitochondrial membrane potential, which in turn leads to a release of Ca^{2+} into the cytoplasm. Similarly in higher plants, it has been reported that the depolymerization of microtubules increases the level of cytosolic calcium by affecting Ca-channels in the plasma membrane (Thion et al., 1996). The increase of intracellular calcium could have a variety of effects on the actin cytoskeleton. For example, actin-severing proteins such as gelsolin could be activated, or the amount of tension could be enhanced by the activation of myosin (Hepler, 2016).

It should therefore not be surprising, if in the diatoms, the actin cytoskeleton suffers concomitant changes, which goes beyond the fact that the microtubules as the interacting cytoskeletal partners are missing. Unfortunately, the current data do not allow an in-depth analysis of the underlying processes.

4.1.2.2 Role of Microtubules in Valve Morphogenesis

Regardless when the inhibition begins and what the concentration of the inhibitor is, once a cell has passed through the cytokinetic stage, the cell may either be divided or undivided, resulting in two major types of the valve morphology: the single daughter hypovalve or the connected lateral valves.

When the inhibition begins before mitosis, nuclear division has been always inhibited, usually followed by a successful cytokinesis, giving rise to a nucleate and an anucleate daughter

cell, each of which has an aberrant valve (case 1, short term: Figs. 4–7; long term: Figs. 11–13). And occasionally, some divided daughter cells have normal valves (Figs. 8E & 8F), this is because of the staining nature of PDMPO, which can bind previously made silica if it is still wrapped in SDV. Therefore, the normal valves of Fig. 8E and 8F suggests the structures of the head plate region have developed before the 2-hour pre-inhibition takes effect and then lysosensor was added before the break down of SDV (see the inset 1c and 1d in Fig. 18).

But surprisingly, cytokinesis is sometimes inhibited, resulting in a cell with lateral valves containing only one nucleus (case 2, Figs. 14–15, see Section 4.1.3). On the other hand, when the inhibition begins midway of cytokinesis, the cell will not be able to divide and contain two daughter nuclei (case 5, Fig. 17 in Table 1). However, it has never been found an inhibitory phenotype that the mother cell divided into two daughter cells, each of which containing one daughter nucleus.

The valve formation at the post-cytokinetic stage is quite strongly affected by Oryzalin inhibition. In the following sections, emphasis will be placed on the analysis of the morphology of separated valves (case 1, Section 4.1.2.2.1) and of lateral valves (case 2, Section 4.1.2.2.2) that are produced under inhibition with Oryzalin.

4.1.2.2.1 Aberrant Morphology of Separated Valves

In case 1, the single nucleus is shifted away from the usual position and bears a cage of struts or needles stained by the tubulin antibodies (MT-cage), which are the only remains of the former MT-cytoskeleton.

The valve is often composed by a patchwork of disk-shaped silica islands and there are more than two per hypovalve. The islands are called "annular disks", since each has a round, single annulus in its middle and rows of areolate chambers radiating from it (e.g., Figs. 5, 14). The disks can be of different size, because they appear to expand up to the point, when they "collide" with a neighboring disk, which causes them to fuse (e.g., Fig. 5A). The morphology of each annular disk suggests that the silica deposition in the form of regular, radial rows starting from a circular pattern center (the annulus) is likely an autonomous, self-organizing process, which does not require microtubules. And this is different to the bipolar head plate in normal cells that contains two linearly compressed annuli, which are surrounded by an embossed rim. Besides, since the polymerization of microtubules has been inhibited after cytokinesis, horn

bundles do not form at all, leading to the absence of horns as well, and also the LPs as well as the head plate are missing, resulting in an aberrantly silicified valve, which indicates that the LP initiation site and the annular initiation site are just associated with each other coincidentally rather than the two structures comprising a morphogenetic unit. And this behavior is a good evidence for answering the long held question that whether the LP and the annulus should be treated separately (Pickett-Heaps et al., 1990).

The type of morphogenetic information required for correctly setting the number of annular disks per apical daughter cell domain remains a matter of speculation. Considering the fact that the cell cover of diatom auxospores is often made of scales (Idei et al., 2012), each of the annular disks may be interpreted as a large scale, which could mean that in the absence of microtubule bundles the cell falls back on an archetypal mode of scale formation. But it should be noted that the scales of auxospores do not fuse into one large unit before deployment. Each of them is deployed independently and after deployment they form an overlapping pattern outside of the cell (e.g., Fig. 9 C & D in (Idei et al., 2012)). Whereas here in the Oryzalin-treated cells, they do fuse together, because the SDVs fuse with each other before the deployment; confluent areolae patches are filled in between the annular disks. This morphology is consistent with the concept put forward here, that a closed actin ring confines the fused SDVs into one common structure functioning as a demarcation (see Fig. 5C, although it became deformed in the artificial damaged cell) on the top of the valve domain, preventing the islands from drifting away before fusion. Naturally, this conjecture can also be applied to all other cells which have formed one nucleate and one anucleate daughter as a consequence of Oryzalin treatment. One other aspect is that the internal silica pattern of the annular-disk SDVs shows a high proportion of virgae in their periphery instead of the normal rows of areolae, which could be due to the fast expansion of those SDV edges because the drag shoe function of microtubules is missing (see discussion above). This in turn may cause the faster expansion of the actin ring, which in normal cells would be restrained. Also the actin ring in control cells starts out as a compressed ellipse, but here the absence of horn bundles takes a more expanded morphology. Combining the two aspects, when the platform offered by the horn bundles and the boundary offered by the actin ring are both lost, the hypothetical seeding structures (primary silicification sites, *sensu* (Li and Volcani, 1985)) for the initiation of annular disks can be considered to be scattered around the disturbed apical dome of each daughter; otherwise in the undisturbed cell, they should be guided and correctly positioned along the horn bundles giving rise to the two annular SDVs of the head plate.

In comparison, valve morphogenesis in *Ditylum* starts out as a single, round annular SDV forming the base of the prospective LP, whereas the annular SDVs of *Odontella* get stretched along the horn bundles to adopt the typical compressed form (Li and Volcani, 1985) and later fuse into one complete piece of SDV held together by the demarcation of the actin ring.

Since the radial expansion of the valve SDV in other radial centrics has been postulated to be caused by microtubule-dependent motor proteins (Davis and Hildebrand, 2010) on the basis of the observation that microtubules run in a radial fashion, parallel to the radial rows of areolae (Davis and Hildebrand, 2010), it is not a far-fetched idea that shaping the SDVs into a linear figure in *Odontella* occurs by the action of motor proteins attached to the silica lemma surface of the SDV along the microtubule horn bundles. In Oryzalin treated cells, when microtubules are absent, the annuli remain round just as the ones in *Ditylum*, because there is apparently no spatial cue for them to orient in line and there is no motile system to stretch them.

Another interesting aspect is that, both daughter cells formed during Oryzalin treatment are able to produce silica on their apical dome; a small one in the anucleate daughter cell and a large one in the nucleate one. The explanation, why the anucleate daughter cell can still form silica structures in the apical domain, is based on the following two points: First, it is obvious that silicification can occur independent of microtubules (see Section 4.1.1.2). Second, it has been reported that the initial SDVs are formed before the completion of cytokinesis in *Odontella sinensis* (Li and Volcani, 1985). So, even for the anucleate daughter portion, the initial SDV will be set up before the completion of cytokinesis, but then cannot develop further due to the lack of morphogenetic information. The fact that several separate islands form suggests that the initial SDVs get multiplied and scrambled due to the forceful process of cytokinesis in the absence of any scaffolding function of the microtubule horn bundles (*see below Section 4.1.2.2.2). Genetically, those initial SDVs originate from the previous mother cell cycle but after cell division they require additional information from the daughter nuclei for their further development.

4.1.2.2.2 Lateral-Valve Formation Induced by Oryzalin

Lateral valves have been reported for the first time in *Cyclotella* cells (radial centric diatom) that were neither able to achieve mitosis nor cytokinesis as a result of inhibition by Colchicine or by the deficiency of Ca^{2+} or Mg^{2+} (Badour, 1968). Its formation, as well as the normal formation of

daughter valves, was suggested to depend on the DNA duplication, rather than depending on mitosis or cytoplasmic growth (Oey and Schnepf, 1970).

As to *Odontella*, lateral valves could be found in Oryzalin-treated cells that were not able to reach mitosis and cytokinesis (case 2, Fig. 14–15), or in cells that were blocked midway of cytokinesis (case 5, Fig. 17). Obviously, the abortion of cytokinesis is the side effect of the inhibition of the microtubule system. It may be because the depolymerization of microtubules affects the Ca-homeostasis (Section 4.1.2.1), which could further affect the course of cytokinesis as has been shown for animal cells (Chang and Lu, 2000).

Another point should be noted that lateral valves are not composed of clearly defined islands (annular scales). The reason for this may be that in the absence of cytokinesis there is no force acting on them so that they do not get scrambled (compare with Section 4.1.2.2.1, see asterisk mark in the text). This is even more prominent in the case 2 cells (lacking the remnant of aborted cleavage furrow, e.g. Fig. 17, for case 1 see Section 4.1.2.2.1), which are flat and smooth due to the fact that cytokinesis did not occur and hence did not disturb so much the geometry of the annular distribution along the cell surface. These lateral valves contain a big irregular empty space at the center region of each half domain of the lateral valve complex, which can be interpreted as a giant deformed annulus conceivably formed by the fusion of two initially separated annuli. But it is pity that the morphology of the actin ring is not documented here, because of the poor actin immunolabeling, so it is unknown, whether the entire lateral valve complex is surrounded by an actin ring, although this is strongly implied from all the other observations of post-cytokinetic valve morphogenesis.

Unlike the two giant flat pieces of annular disks just discussed for case 2 cells, the lateral valves in case 3 cells are more like two oppositely fused hemispherical cups. The trace of the head plate on the curved lateral valves with the decoration of an LP and a dwarf horn, suggests that the microtubule horn bundles were originally present but then disappeared due to the Oryzalin treatment. From the curvature in the middle of the lateral valves, one can speculate that cytokinesis was slowed down or remained incomplete and eventually became outpaced by the silicification process, which prevented any further constriction.

One interesting aspect of both cases is that given enough time, the lateral girdle bands are orderly generated on each side of the lateral valves, which suggests that the same principal bipolar organization is established in the uninucleate, undivided protoplast, as is present in two

normally divided daughter protoplasts. It also shows that microtubules are not required for the girdle band formation; neither the placement nor the function of the GB-actin rings.

4.1.3 Pulsing Cytokinesis

When microtubule inhibition by Oryzalin takes place before telophase in *Odontella*, the nucleus is not anymore anchored by microtubules and divided by the mitotic spindle, which subsequently brings about the failure of nuclear division and mislocation in the cell. These uninucleate cells may either bypass cytokinesis and continue to grow (Figs. 14–16), or proceed by cytokinesis generating one nucleated and one anucleate daughter cell (Figs. 4–7).

In the latter case, the cleavage furrow performs repeated pulses before the final constriction of the protoplast is achieved (Figs. 11 – 13), which is a hitherto newly observed phenomenon termed "pulsing cytokinesis". Beginning from the first pulse, this type of cytokinesis takes more than 1 hour, much longer than a normal one, which begins from anaphase and takes only about 15 minutes (Zhang, 2012).

4.1.3.1 Repetitive Pulses of Cytokinesis

In the example of Fig. 11, the furrow begins to develop above the nucleus, producing a small protoplasmic indentation, but then it retreats only to try again. Such a pulse repeats several times, which in the time lapse movies is perceived as a pulsing motion. Each time the furrow reaches to a similar depth (shown as a periodic limit point of troughs around the y-value 5 in the data graph), until it could break through to complete the cleavage. From the end of the interphase to the completion of the pulsing cytokinesis, under the 0.5 μM Oryzalin, the procedure costs more than 2 hours.

The pulsing cytokinesis also costs more than 2 hours, when the concentration of Oryzalin reaches 2 μM (Fig. 12) and even 5 μM (see Appendix video #2). In the case of Fig. 12, the data graph is composed by the shots captured at a lower frequency (5 minutes / shot, 1 minute / shot in Fig. 11), showing a different y-value of each trough, because the periodic troughs could be missed by the rougher scale. The occurrence of pulsing cytokinesis at higher concentrations suggests that instead of proceeding with the formation of lateral valves, some cells are still able

to divide no matter what the dosage of Oryzalin is.

Such a pulsing of cytokinesis could also be found in cells treated by Colchicine (Fig. 13), which in principle has the same effect as Oryzalin, although the periodic trough in the data graph is probably missed due to the rough scale of tracking frequency (5 minutes / shot). Colchicine is well known that it is highly effective in animal cells at the concentration level of picomolar or low micromolar (Lu et al., 2012), but less effective in plants and some other organisms if not increase the dose in hundred-times. And since it has been reported that Colchicine takes no significant effect on the calcium ion transportation in isolated mitochondrial and microsomal fraction of higher plant cells, when Colchicine is in the range between 100 μM and $10^4 \mu\text{M}$ (Hertel et al., 1980), the concentration of 200 μM Colchicine is a reasonable concentration to be administered to diatoms.

Although the mechanism of inducing the repetitive pulses is unknown, but it is reasonable to speculate that these pulses may not be related to the specific inhibition on microtubules, but is more likely induced by the side effect of the microtubule inhibition — the disturbed Ca-homeosis, because the cytokinetic contraction may depend on Ca-signalling, i.e. the Ca-modulation of plant myosins (Hepler, 2016) or the activation of animal cytoplasmic myosin II (Chang and Lu, 2000). Assuming the side effect of Oryzalin causing an enhancement of the internal calcium signaling as discussed above (Gómez et al., 2000; Kerfant et al., 2001), it is reasonable to see the occurrence of cytokinetic pulses also in this context. The occurrence of pulsing cytokinesis in fact does not contradict the occurrence of the lateral valve. Because the elevation of the cytosolic calcium may depend on the cellular regulation which is different among individuals. If a cell may react to the increase of calcium signaling with strong calcium buffering or fast efflux, the elevation of cytosolic calcium would be reduced, leading to the decrease of calcium signaling, which results in the abandoning of cytokinesis and the initiation of lateral valves.

One could also imagine that in the absence of horn bundles, the cytokinetic contraction must overcome a higher resistance because the microtubule horn bundles at telophase provide a mechanical scaffold for the incipient furrow, upon which force can be more efficiently exerted to achieve complete cleavage. In the absence of these microtubule horn bundles, the guidance that may be required is missing.

4.1.3.2 Role of the PC Precursor in the Location of the Cytokinetic Actin Ring

In the current study with normal diatom cells, it has been found that the cytokinetic actin ring assembles right above the PC precursor, both of which are located at the exact midline of the cell at preprophase (i.e., the period at late interphase but right before prophase). As a consequence, mother cells will inevitably be divided equally into two sibling cells (see Chapter 2). When the PC precursor is removed, e.g., decomposed by the complete inhibition by Oryzalin before preprophase, the cytokinetic actin ring can either remain in the midline (Fig. 10) or be dislocated away by a small but detectable distance (Figs. 6E, 9). In the case of successful division following a series of pulsing, cells may either generate two equal-sized siblings as in the normal case (not shown), or two unequal-sized ones (Figs. 11 & 12), but in either case, only one of the siblings will have a nucleus.

Even if nuclear displacement occurs, the cytokinetic actin ring may still remain close to the mid-zone of the cell. This phenomenon could be seen in the context of findings from studies on fission yeast, which have shown that a broad region at the cell middle is defined by molecules before mitosis, as the future site for ring assembly, and these molecules will narrow into a ring under the control of the mitotic spindle (Almonacid et al., 2009; Daga and Chang, 2005; Pollard, 2010; Tolic-Nørrelykke et al., 2005). And in budding yeast, the contractile ring is developed at interphase long before mitosis, and the spindle acts like a chaser and moves to the site of the ring (Pollard, 2010).

Since normal diatom cell division is always equal, it seems circumstances in *O. sinensis* are more similar to those of fission yeast, the assembly mode of the contractile ring in fission yeasts offers an option to understand the case in diatoms. And the two situations from the current data here — that the displacement of the cytokinetic actin ring can occur in the absence of the PC precursor and that this does not happen in the presence of the precursor — seem to indicate that the PC precursor is a guide. This preliminary conclusion appears to be consistent with the mode of yeasts, and thus it is reasonable to work with a model assuming a similar scenario — a broad region is marked at the midzone before mitosis and then the ring will become narrowed down at the site of PC precursor from preprophase.

In the end, whether the PC is a chaser or a guide is currently not possible to solve with the current limited data, unless further experiments are designed to see whether the displacement of the cytokinetic actin ring will occur when the PC precursor is displaced.

4.2 Taxol

The microtubule stabilizing effect of Taxol is known for more than 50 years, this effect leads to the formation of MT-bundles in vivo (Schiff and Horwitz, 1980) and interferes with spindle assembly. It also suppresses dynamic instability behavior of microtubules (Yvon et al., 1999). Due to the inhibition of mitotic spindle assembly, chromosomes fail to segregate (Long and Fairchild, 1994) and this is the reason, why Taxol (paclitaxel) is applied as anti-cancer drug. But it has potential side effects on intracellular signaling by calcium as well as phosphorylation in human cells.

4.2.1 Potential Side Effects of Taxol Treatment

4.2.1.1 Phosphorylation Status on Serine/Threonine and Tyrosine Residues of Regulatory Proteins

The application of Taxol in human cancer research lead to the discovery of side effects, such as the activation of signaling pathways leading to the induction of cytokines and the induction of tumor suppressor genes and also the secretion of tumor necrosis factor. Because the dosage of Taxol used in these studies was higher than that required for arresting mitosis, Blagosklonny and Fojo showed that even lower Taxol concentrations, such as those used in cancer therapy, can bring side effects. The reason for these effects, however, might be a consequence of mitotic arrest, which always occurred coincidentally (Blagosklonny and Fojo, 1999). All effects such as serine/threonine protein phosphorylation, as well as the phosphorylation of ribosomal S6 Kinase might be a consequence of mitotic arrest (Figuroa-Masot et al., 2001; Le et al., 2003; McCubrey et al., 2000).

Yang and Horwitz have reported that micromolar concentrations of Taxol promote tyrosine phosphorylation, whereas nano-molar concentrations promote serine phosphorylation on special human regulatory proteins involved in tumor development (Yang and Horwitz, 2000). The authors, however, pointed out that as in the previous work, these effects did not appear to result from a direct action of Taxol on protein phosphorylation but from a "dramatically prolonged time that such cells are held in the mitotic phase of the cell cycle". They also reported that the same

happens, when cells are blocked at mitosis by other microtubule-interacting drugs such as Vincristine, Vinblastine and Dolastatin, Colchicine, Colcemid and Podophyllotoxin (McCubrey et al., 2000).

In most diatoms, the silicification process requires the involvement of proteins such as silaffins, whose phosphorylation sites include serine and threonine residues (Kröger and Poulsen, 2008). Hence, if the side effects of Taxol occurs in diatoms, it is possible that the process of silicification could be a potential target. Abnormalities in silicification can indeed be found in the batch incubated at the highest concentration of 100 μ M Taxol. In that case, the control of silicification is abnormal (Figs. 19A, 20A) or the areolate pattern of the silica wall is blurred (Fig. 20c). However, further work is need to understand the role of protein phosphorylation of accessory proteins in the biosilicification process.

4.2.1.2 The Side Effects of Taxol on Ca-homeostasis

In human pancreatic cancer cells, Taxol abolishes cytosolic Ca^{2+} oscillations and as a response, rapid Ca^{2+} release from mitochondrial Ca-stores into the cytosol occurs. This response appears to be due to a change in the function of the mitochondrial membrane transport, however, whether this is downstream of the antimitotic action of Taxol and further interacts with the calcium signal cascade was not clear at that time (Kidd et al., 2002). More recently, it has been shown that it is the availability of tubulin dimers, which affects the mitochondrial membrane transport. Colchicine increases the tubulin dimers in the cytosolic pool causing a decrease in mitochondrial membrane potential, whereas Taxol decreases the availability of tubulin dimers causing an increase in the mitochondrial membrane potential. Hence, the effect of Taxol on Ca-oscillations is mediated by the degree of microtubule stability and not by a direct drug effect on the mitochondrial membrane transport mechanism (Maldonado et al., 2010; Sheldon et al., 2011).

Since all these studies were conducted on special human tissues, it is unknown, to what extend the findings are relevant for other human tissues, or tissues from other higher or even lower organisms. For the current study on a diatom species, the side effect discussion would probably be not worthy to be mentioned, if the Taxol data presented in the current work would allow a clear-cut interpretation alongside the classic inhibitory effects such the enhancement of microtubule stability. But in the light of the pleomorphic inhibitory phenotypes occurring in the

diatom samples as discussed below, it may not be entirely excluded that side effects not related to the microtubule stability have occurred.

4.2.2 Interphase: Disturbance of the Pace of Silicification and Axial Expansion

According to the Taxol inhibition result (section 3.2.1), perinuclear microtubules at interphase often extend asymmetrically towards one side of the cell and bind long actin bundles in this domain (Figs. 19 – 20). Such an asymmetrical rearrangement also indicates that they physically interact with the actin cortex nearby as well as the actin ring and this should have effects on the tension equilibrium.

One dramatic scenario seen in the samples is that the extension of microtubules is driving towards the hypothecal side and the actin ring is removed from its original site and pulled towards the same side, caused by the over-stabilization of microtubules; the PDMPO staining pattern observed in these cells has exceeded its normal distribution protruding as a wavy contour beyond the anchor point between eGB1 and eGB2 (Fig. 20). This clearly suggests that the demarcation function of the actin ring is suspended and the axial expansion is blocked but still the silica deposition at the abvalvar edge of the GB-SDV is able to continue at the time of inhibition. While this scenario would nicely support the demarcation hypothesis for the function of the actin ring, the other scenario also occurring in the samples under the influence of Taxol looks just the opposite (Fig. 19 C – F): The asymmetrically arranged microtubules are extending towards the epithecal side, but this time the actin ring is likely maintaining its correct position. However, the silica front is lagging behind, as indicated by the gap between the silica front and the actin ring. This suggests that either silicification is inhibited (due to the side effect of Taxol), or that axial expansion is promoted (due to the fact that Taxol treated microtubules were growing longer).

The common point of both scenarios is that, no matter where the asymmetrically rearranged microtubules are extending to, the nucleus is likely able to maintain its position at the middle of the cell, which then does not always coincide with the position of the latest GB-SDV. Whereas, in normal cells, when the axial expansion occurs, this process will invariably maintain the actin ring at the abvalvar edge of the SDV and put the nucleus right beneath the latest GB-SDV.

Therefore, such an abnormality of the middle maintenance clearly suggests that the nucleus location is not functionally related to the recent SDV development, but just a coincidence.

In summary, perinuclear microtubules in the SDV development have two main functions: one is that microtubule dynamic is important in tuning of silicification and axial expansion at the same pace; the other is that microtubules interacting with the actin bundles will help to keep the nucleus at the midline of the cell.

4.2.3 From Mitosis to Post-cytokinesis: Over-stabilization of the Central Spindle and Over-extension of the Microtubule Horn Bundle

At preprophase, the initialization of the PC and the cytokinetic ring can still occur in Taxol-inhibited cells (Figs. 21, 22), same as in control cells. In prophase, the morphology of mature PC and the cytokinetic ring looks normal, the only difference is that the MT root is still attaching to the nucleus due to the Taxol effect. So in general, the Taxol effect on cells at these two phases is not dramatic.

Cells at telophase are more frequently encountered in any Taxol treated batch regardless of the concentration. The central spindle seemed to be somewhat over-stabilized by Taxol, because a higher MT density is maintained than in control cells. In particular, the separation of the two halves of the central spindle at late telophase is rarely observed in Taxol treated cells. This speaks for an increase of the number of cells in the cell population arrested at a late telophase stage just before separation.

Although the central spindle is over-stabilized by Taxol, the constriction of the cytokinetic ring and the abscission of the thick central spindle eventually proceeds successfully. Also, the relocation of the daughter MC from the distal to the proximal side of the nucleus is probably not interfered with (Figs. 23C, 23D). The initiation of the horn bundles by the hb-MTOCs looks also normal whereas the density of the horn bundles is higher, which makes that the horn bundle configuration looks more prominent.

Different from the controls, the microtubule horn bundles appear to extend out of the end of the horns in post-cytokinetic cells, as if they were growing longer than the surrounding protoplasmic sleeve of the horn. However, this may not be the case, rather it may be due to the fact that the strong, tight bundles cannot shorten to accommodate the contracted protoplasmic

protrusion. This contraction is a normal process in this post-cytokinetic developmental phase (Pickett-Heaps et al., 1990; Zhang, 2012). In control cells, the horn bundles are more shrinkable so that the protoplast contraction goes hand in hand with the rearrangement of horn bundles into the radial perinuclear MT-system, whereas the Taxol-stabilized horn bundles persist longer so that their rearrangement is not synchronized with the protoplast contraction.

In summary, Taxol effects are most prominent at interphase, where they disturb the harmony between cell expansion and girdle band growth due to the creation of asymmetric tension. This effect fully supports the hypothesis that girdle band formation and axial cell expansion work hand in hand and it again emphasizes the importance of F-actin-microtubule interaction as important element in the maintenance and regulation of the tension equilibrium. Blockage of mitosis at telophase is, of course, also a severe effect, however, this is not a new discovery for a eukaryotic cell and it does not present additional information, which could have helped in understanding the role of microtubules in diatom morphogenesis.

4.3 Jasplakinolide

4.3.1 General Effect of JAS

JAS is a very effective actin inhibitor even at a concentrations as low as 0.25 μM ; it can cause a break-down of the microfilament system in the diatom *O. sinensis*. It is very effective for a break-down of the cytoplasmic actin cable system and the cytokinetic actin ring, whereas the time required for breaking down the GB-actin ring is much longer. This indicates an enhanced stability of the GB-actin ring architecture, which would be expected, given the proposed role of the GB-actin ring and also the valve actin ring (see discussion in Chapter 2), which is to serve as a demarcation of the advancing valve-SDV edge or a stable bumper for the stationary edge of the GB-SDV. Enhanced stability in this case means a low turnover between the monomer and the polymer status, a high degree of cross-linking between adjacent actin filaments, as well as a tight binding to the plasma membrane and to the SDV edge. On the other hand, the decomposition of the cytokinetic actin ring at this inhibitor concentration is dramatic in that it induces prominent actin aggregates (Figs. 28, 29), which usually accumulate into a meshwork along the curved surface of the protoplast, regardless whether the inhibition began at interphase or at the beginning of or even during cytokinesis. It suggests a big amounts of actin filaments have been converted into clusters, which is in agreement with the kinetic study by Bubb and co-workers in animal cells (Bubb et al., 2000). Besides, the curved protoplast surface at the original cleavage site suggests that the aggregate-meshwork may have a residual contractile property. Both aspects speak for a low drug resistance of the cytokinetic ring architecture but a high functional resistance of the residual aggregate components. In the same mild inhibition, silicification and axial expansion can still occur, whereas they are blocked at higher concentrations (see the paragraph below), so the actin cytoskeleton responsible for both activities must still have a residual level of organization allowing some residual function, although the immunofluorescence images do not show the corresponding structure. This may also be due to a greater lability of JAS-treated actin filaments towards fixation.

When the concentration of JAS reached up to 1 μM , a reduced GB-actin ring is present as a faint linear trace with visible aggregates in the vicinity of it (Figs. 27C – d₃); both silica deposition and axial expansion have become completely blocked, based on the fact that lysosensor-stained girdle bands are absent and no bare region of the protoplast is exposed (e.g., Figs. 27C, 27D). This suggests the silica deposition and axial expansion are F-actin based activities, and since there is no further developmental progress in the cell, it suggests that no

functional F-actin remained in the cytoplasm. At the concentration of 0.5 μM , the inhibition of both processes is less severe, based on the fact that sometimes a girdle band could be made and maintained under eGB2, but axial expansion occurring after girdle band formation had never been observed, which implies that the residual amount of F-actin was still sufficient to accomplish SDV development, but obviously not sufficient enough to promote axial expansion.

Taken together, the cytokinesis is the most sensitive actin-based cell function, because the cytokinetic actin ring is very quickly deconstructed at mild inhibition. However, the progression into the daughter cell cycle is unblocked (Section 4.3.4), i.e., the formation for daughter SDVs still occurs, in the meanwhile accompanied by the axial expansion.

The next sensitive cell function is the axial expansion, which is getting abolished from 0.5 μM upwards to 1 μM JAS. On first sight, this finding is at variance with the expectation of over-expanding as a response to the deconstruction of the actin cytoskeleton by JAS, when considering the tension-equilibrium model (see Chapter 2, Fig. 16) which states that turgor driven expansion is controlled by internal holding power of the actin-microtubule cytoskeleton system. However, it has been reported in other studies that JAS not only acts on the polymer status of the actin system but also on the turgor regulation, for instance in higher plants stomatal opening is retarded by decreasing the turgor pressure, which coincides with a breakdown of the actin cytoskeleton (Gao et al., 2009). The involvement of the actin cytoskeleton in turgor regulation appears to be a general phenomenon (Staiger, 2000), it may therefore also be relevant to the situation in the diatom *Odontella*.

The less sensitive cell function is that responsible for SDV formation, i.e., endomembrane associated actin networks, and the least sensitive one is the maintenance of the GB-actin ring.

The effects of JAS on the actin cytoskeleton of *Odontella* are consistent with those reported earlier on higher plant cells, algae (Holzinger and Blaas, 2016; Sawitzky et al., 1999), animal cells and myxamoebae in which the original actin cytoskeleton is gradually getting displaced by actin clusters (Bubb et al., 2000; Lee et al., 1998). This is explained by an imbalance in the mode of actin filament dynamics caused by an uncontrolled increase in the number of new actin polymerization seeds, which however are unsuited for the assembly of normal microfilament arrays, eventually leading to the depletion of the G-actin pool (Cramer, 1999).

Last, it is interesting to note that the classical actin inhibitors such as the Cytochalasins B and D have been much less effective in *Odontella* (data not shown), so only JAS has been

employed extensively to interfere with the actin cytoskeleton in the current study. Another potent actin inhibitor, namely, Latrunculin A, was shown to interfere with silica deposition (Zhang, 2012), however, simultaneous immunofluorescence of actin was not performed in this study, and therefore the state of the actin cytoskeleton in the presence of Lat A is still unknown.

4.3.2 The Potential Role of F-actin in the SDV Stabilization, Shaping and Initiation

When under mild inhibition (0.25 μM), the GB-actin ring is reduced but still present at the correct position (Figs. 26, 30, 31, 32, 34) and no matter whether the developing silica structures may be of aberrant shapes, the substructure of the deposited silica always shows the typical areolate pattern (e.g., Figs. 30b₂, 34). However, at the high concentration of JAS (1 μM), usually, not a trace of PDMPO signal is present, suggesting a strong impact on the whole silica deposition machinery in the cell. The lack of signal is not because that there is no new silica, but that the silica might be made in the first 2-hour pre-incubation and before the lysosensor was added, all silica deposition must have already been terminated and silica have been prematurely deployed on the protoplast surface. This conclusion is based on the principle of PDMPO staining that silica can only be labelled as long as it has undissociated Si-OH residues (Parambath et al., 2016), which is only the case, when the silica is confined in the acidic environment of the SDV, meaning not only the currently developing silica deposits but also the already laid down deposits inside the SDV will be stained; whereas PDMPO does not bind anymore to the Si-O⁻ residues exposed to sea water, and therefore, the absence of the silica staining here suggests the recently made silica was no longer wrapped by the silica lemma and also no new SDV was made. Since the silica staining of PDMPO takes no effect, when the architecture of the F-actin has been strongly perturbed by JAS inhibition, it implies that F-actin around the developing SDV, which may be in the form of a network, may play a role for instance as a scaffold of the silica lemma. This could mean that silica structures in the SDVs get prematurely deployed onto the protoplast surface, when the actin cytoskeleton gets destroyed, although there is no direct evidence to support this idea. This hypothesis can be tested, once a new dye becomes available that stains all silica regardless of whether it is in the SDV or deployed on the cell surface.

Such a role of the actin cytoskeleton in promoting exocytosis is reminiscent of its two major functions in the exocytosis of some vertebrate cell systems: In rapid exocytosis cells (e.g., neurons, neuroendocrine, endocrine, hematopoietic cells), the actin cytoskeleton acts as a physical barrier and assists vesicle docking before the fusion. Whereas, in slow ones (e.g., exocrine and other secretory cells), the actin cytoskeleton regulates the dynamics of the fusion pore, facilitates the integration of the vesicles into the plasma membrane and promotes the large cargo release after the vesicle-fusion (Nightingale et al., 2012; Porat-Shliom et al., 2013). Using the pre-synaptic actin function as a guideline, one could postulate that a fine actin network accumulates between the upper silicalemma and plasma membrane, to assist the SDV docking to the specific region to grow and acts as a barrier to avoid premature fusion. One could further assume that at the maturation of the SDV, the actin network between the silicalemma and plasma membrane (PM) gets depolymerized to allow the newly made silica being exocytosed, but at the end of exocytosis, microfilaments may accumulate into a network (MFN) under the lower silicalemma which then becomes the new part of the plasma membrane (see the **PM-MFN-SDV model** in Fig. 35-2 below). The idea of premature deployment of SDV in the presence of 1 μ M JAS can be directly examined, by using both lysosensor and a kind of new dye in a simultaneous inhibition (inhibitor plus dyes applied into the culture at the same time), if the latter of which can stain undeployed and deployed frustule components on the cell surface, by judging whether a hypothetical structure contains only the new dye stain.

The other possibility is that the supply of components required for silica deposition breaks down due to the destruction of long distance organelle actin tracks. This appears unlikely, because it has become increasingly clear in the recent years that silicon import occurs directly at the silica lemma by import proteins (Thamatrakoln and Kustka, 2009). Besides, if those components would be delivered via actin tracks, the consequence would be that the development of the SDV gets interrupted by the lack of supplies, whereas the nascent silica structure, already within it, should still be stainable by the lysosensor. But in fact there is no stains at all, which means that there is no immature silica structure in the SDV or there is even no SDV present in the cell (further discussed in Section 3.4.2.5 of Part III. General Discussion).

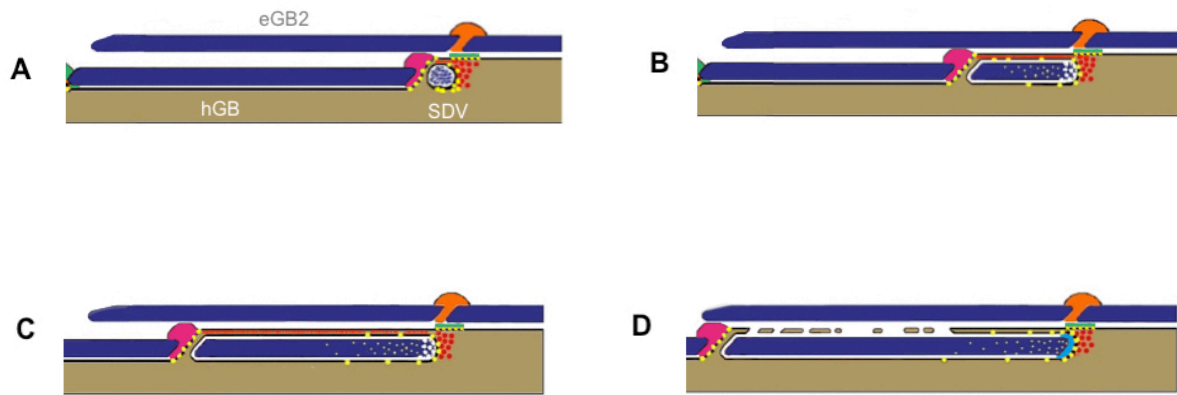


Fig. 35-2 The plasma membrane-microfilament network-SDV model (PM-MFN-SDV model).

One exception of the silica deposition in the batch of 1 μM JAS-inhibition is that lateral valves (see Section 4.3.4) in incompletely divided cells got stained by PDMPO (Fig. 31D), which appears that the silica deposition can still occur in the course of the strong inhibition. One may argue that this should not be possible, because the proposed F-actin scaffold around the SDV should be deconstructed in the first 2 hours of preincubation with this high JAS concentration, and this should abolish silica deposition all together as is the case in interphase cells, which cannot form any new SDVs (e.g., basic type #1 in Table 1). This contradiction can be resolved, because in the current example the inhibition (2-h pre-incubation without PDMPO) began after the initiation of the primary silicification sites, which occurred during cytokinesis. At this stage the F-actin scaffold around the initial SDVs should still be functionally intact. Then the cytokinetic actin ring is getting affected by JAS leading to the abortion of cytokinesis, whereas the cell cycle does not stop and hence the valve morphogenesis continues for some time producing the fused lateral valve complex, before the F-actin scaffold around the fused SDVs is also completely broken down. As long as the second phase of the inhibition schedule (48-h JAS plus PDMPO) begins, when the lateral valve complex is still confined within the SDV, the entire silica structure in its lumen will become stained. Further development is blocked because all F-actin required for SDV formation has been completely deconstructed (see Fig. 35-3 below).

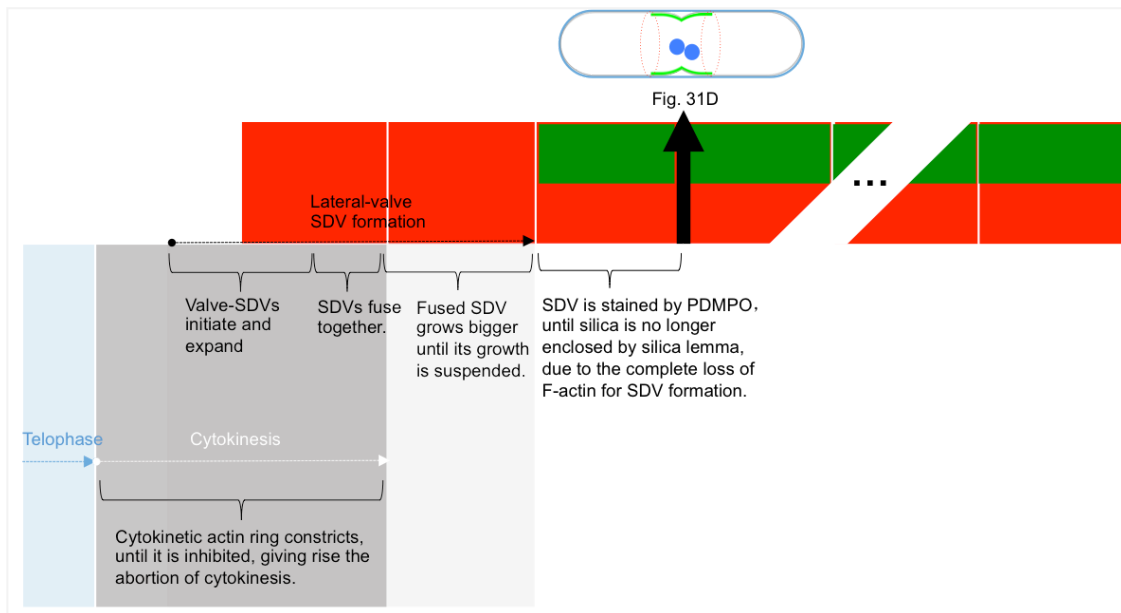


Fig. 35-3 Time course of JAS-incubation schedule aligned with the developmental stages of the cell (Fig. 31D). Red – 1 μM JAS pre-incubation takes 2 h. Green – Addition of PDMPO to the JAS-containing medium continues for the following 48 h. Black arrow – Exocytosis occurs and cell cycle is paused.

In some diatoms, vesicle spacers have been described to play a function in the three dimensional SDV molding process (Schmid, 1994). In *Odontella*, another likely candidate scaffold structure comes into play as a space holder, when the SDV begins to fold inwardly to shape the areolate chambers. These are the “fibrous balls” discovered in ultrathin sections by TEM (see Fig. 25c₂ in Chapter 1). They seem to be involved in molding the flat SDV cisterna into the three-dimensional shape of the areolate cavities, which is an advanced stage of the SDV after the virgae development. If they are composed of F-actin, their supra-molecular arrangement is unlike anything known so far, which rather speaks for a mixture between the actin polymer and actin binding proteins such as spectrins (Machnicka et al., 2014) or other long chain cross-linkers such as filamin, and by the means of the cross-linked state, the fibrous balls may be less affected by inhibitors than regular actin arrays. This could explain, why JAS-treated cells can still develop the areolate pattern. It is interesting to note that filamin is part of the actin scaffold seen in the maintenance and signaling function of the ER-contact sites ((van Vliet et al., 2017), see Section 3.4.2.5 in Part III). But the clarification of this point awaits further analysis, such as fine structure analysis of JAS-treated cells, which has not been conducted in the current work.

Further, one may argue that microtubules can also provide vesicle transportation tracks. However, when comparing the perfect areolate pattern appearing in the silica deposits of Oryzalin treated samples (e.g., Fig. 12J) with the less clear pattern appearing in the silica deposits (e.g., Fig. 31b₁ – b₃) in the JAS-treated cells, one can come to the conclusion that organic supplies to the SDV are still sufficiently delivered in the absence of microtubules, whereas they may not arrive in adequate amounts in the absence of an intact actin system.

4.3.3 Nuclear Status in JAS Treated Cells

After the 0.25 μ M JAS inhibition, the cytokinesis is often aborted and the undivided cell often contains two nuclei surrounded by a large radial array of microtubules, which occasionally look like splayed microtubule horn bundles (e.g. Fig. 28A). This obviously suggests that the cell has passed mitosis but was blocked in the course of cytokinesis so that the subsequent establishment of horn bundles was compromised.

However, sometimes cells have only one nucleus. This may be because the two MT-systems from the two daughter nuclei got tightly intermingled after mitosis, which consequently lead to the re-fusion of the two nuclei. Or alternatively, mitosis in *Odontella* may have been blocked by JAS, resulting in endomitosis or endocycling (Fox and Duronio, 2013). Or as a third possibility, one of the daughter nuclei degenerated after division, which may be deduced from the configuration of Fig. 30a₂. Which of these alternatives may be correct in the current case, remains unclear. While nothing is known about the possible function of actin in diatom mitosis, there is published evidence in different types of cells for a function of F-actin in remodeling chromatin (Olave et al., 2002) and delivering chromosomes to the spindle (Rizk and Walczak, 2005) before nuclear division, as well as interacting with microtubules of spindle during nuclear division (Forer et al., 2003; Fox and Duronio, 2013; Kunda and Baum, 2009; Lancaster et al., 2013; Ramkumar and Baum, 2016; Robinson and Snyder, 2005; Silverman-Gavrila and Forer, 2003; Woolner et al., 2008).

Hence, irrespective of how the single nucleus of lateral-valve cells was formed, it should contain a 4N DNA content, because the DNA replication is a requisite to induce the formation of lateral valves in diatoms (Oey and Schnepf, 1970). And since later on, the cell with lateral valves was able to further develop girdle bands, it suggests that completing mitosis is not necessary for the cell to enter into the next cell cycle (Fig. 32).

4.3.4 Lateral-Valve Formation Induced by JAS

Despite the massive inhibition of cytokinesis by JAS even at a low concentration the cell nevertheless attempts to proceed with developmental activities into the next cell cycle, which under normal conditions would mean that the morphogenesis of the divided daughter hypovalve gets started. Entry into the daughter cell cycle can be recognized by the fact that the cell generates lateral valves at the middle cellular domain, regardless whether there were only one or two nuclei (e.g., Fig. 30 – 33). Since the inhibition of the cell in Fig. 29 started at mid-interphase as judged by the presence of staining in the mother girdle band, the cell required the 48-hour incubation period to reach the beginning of the daughter cell cycle; whereas cells, which were inhibited from a later stage of the mother cycle such as mitosis would reach a later stage in the daughter cell cycle such as the completion of lateral valves (Figs. 30, 33) or even the completion of lateral girdle bands (Figs. 31, 32).

Lateral valves of cells that became arrested midway of protoplasmic division, may possess aberrant forms of annuli, and LP formation is sometimes aborted. This can be explained by the fact that inhibition started at a very late stage of cytokinesis, when the setting up of initial SDVs (i.e., base plate regions of LPs) has already taken place. This is clearly visible in Figs. 30a₁ and 30b₂, where the typical slit-like annular shapes can be distinguished (see arrows). Since in normal cells the two initial SDVs always fuse together to form a head plate, now in the absence of cleavage due to JAS treatment, four initial SDVs fuse together on the surface of the incompletely divided mother protoplast to form a lateral valve complex. As pointed out above, the functional status of the actin system in the presence of 0.25 μM JAS is crippled but not completely destroyed, so that, although the cytokinesis is clearly affected, other activities like SDV formation, axial expansion and maintenance of actin ring shape may continue to operate.

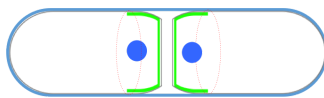
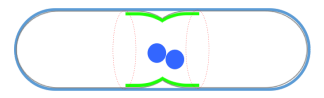
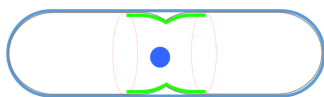
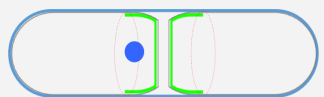
This is evident by the fact that the lateral GB structures are made at both sides of the central lateral valve complex, and they have been extruded from the cover of the mother eGB₂; both sides of actin rings show a high resistance against the deconstruction by 0.25 μM JAS in cells with lateral valves or lateral girdle bands, which leaves them with residual functional potency (see big white arrows in Figs. 30, 31a). This is an unmistakable indicator that the cell is progressing further into the daughter cell cycle stages even though cytokinesis has not been completed. Although the result of Fig. 31a comes from the undivided mother cell in the daughter cell cycle, it also supports the notion in made Chapter 2 that the capability of initiating and

developing girdle bands always resides in the actin ring. Another interesting feature of this cell is the presence of two crippled horns on the side of the deeper furrow ingression. This feature is helpful to realize that there is a relationship between the degree of furrow ingression and the horn bundle formation. In the case when the ingression is deep enough, there is a chance for the microtubule system to develop a reminiscent horn bundle architecture.

4.3.5 One Missing Inhibitory Phenotype

Interestingly, in the 0.25 μM inhibition, it has never been found that the single nucleated mother cell (e.g., basic type #5 of Table 2) can be divided into one nucleated and one enucleated daughter cell (see grey block of Table 3), instead one always sees the regular configuration with two nucleated daughter cells (basic type #3 of Table 2) or non-divided cells with two nuclei (basic type #4 of Table 2), see Table 3. In a certain percentage of Oryzalin treated cells a situation has been observed, where one nucleate and one enucleate daughter cell is produced as a result of cytokinetic cleavage. The reason for this difference may be seen in the absence of the perinuclear microtubules system in the Oryzalin-treated cells, which apparently in the JAS treated cell presents a mechanical obstruction, which cannot be bypassed by the residual contractile property of actin system.

Table 3. Basic phenotypes under the 0.25 μM JAS inhibition.

 <p>(basic type #3)</p>	 <p>(basic type #4)</p>
 <p>(basic type #5)</p>	 <p>Not found.</p>

4.4 Phalloidin

4.4.1 General Effects of Phalloidin

While JAS treatment was applied to find out, what happens, when the actin cytoskeleton was deconstructed, Phalloidin treatment was used to examine the opposite, i.e., to see what happens, if the actin system becomes stabilized and filaments are promoted to elongate, which are the major functions of this phalloxin (Cooper, 1987). The problem mentioned by Cooper that Phalloidin may not be able to penetrate the plasma membrane, when administered to live cells, does not seem to exist for cells of *Odontella*, because inhibitory effects do occur.

The results obtained with this approach present two opposite effects.

First, one would naturally expect Phalloidin will increase the amount of filamentous actin and strengthen F-actin networks (Koteliansky et al., 1983). This should give the actin cytoskeleton a stronger grip assuming that thicker actin bundles are formed for instance by the co-parallel arrangement between microfilaments. Such a grip can irritate cellular activities depending on this mechanism, and one apparent example is the absence of axial expansion, since in *Odontella* the axial microfilament bundles interact with the perinuclear microtubules (see the tension equilibrium model in Chapter 2), it is reasonable to expect that this interaction is getting stronger in Phalloidin treated cells.

Second, the promotion of actin filament elongation, which also means a decreased tendency of filament shortening, could have another effect. When the actin filaments are arranged antiparallel to each other, tension in the bundle system would depend on the shortening of actin filaments (Clark et al., 2014). The same would apply for a network, which has the function of maintaining tension by anti-parallel interaction at cross-over points between actin filaments. Such actin filament arrays would in fact lose tension, if filaments cannot get shortened and even keep getting longer by the action of Phalloidin. This may involve bipolar myosin filaments but does not necessarily to be (Sun et al., 2010).

The type of Phalloidin-induced disturbance of post-cytokinetic valve morphogenesis and also the disturbance seen in the course of cytokinetic cell constriction in *Odontella* are largely in agreement with the latter effect (second type, see Section 4.4.2, 4.4.3.1, 4.4.3.2 and 4.4.4 below), whereas the type of long-term disturbance seen with regard to the lack of cell expansion during interphase fits the former (first type, see Section 4.4.3.3).

4.4.2 Post-cytokinetic Stage: The Role of F-Actin in Valve Morphogenesis

The disturbance of the post-cytokinetic cell activities (i.e. cells at the stage of daughter hypovalve morphogenesis) by Phalloidin, may produce either slight or severe abnormalities of the valve morphology. The degree of the deformation is not related to the incubation period with the inhibitor, but rather to the stage of head plate formation, when the inhibition takes effect. Given that these abnormalities are classified into three inhibitory phenotypes according to Result 3.4.1, when the phase of head plate formation is taken as a reference time point, the first phenotype will be discussed in Section 4.4.2.1, while the other two will be discussed in Section 4.4.2.2.

4.4.2.1 Disturbance of Valve Morphogenesis Stages Starting from Head Plate Formation

In normal cells, the course of head plate morphogenesis involves the establishment of the two LP-base plates, the subsequent growth of LPs and the formation of the two compressed annuli in association with the base plates (see Fig. 19 in Chapter 2, Section 3.3.1 in Part III). This is followed by the silicification of the horns and the formation of the embossed border rim around the head plate. During this course of developmental steps, the two initial SDVs have to fuse into one by the assistance of the closed actin ring placed around them. From then on the ring begins to widen in circumference as the silica fabrication in the united SDV proceeds down the hypovalve slope (see Chapter 2).

By disturbance of the actin cytoskeleton with Phalloidin, there are three major reaction types, which will be discussed in the order of perturbation starting from slightly leading to severely abnormal (first phenotype of result 3.4.1: Figs. 36, 37 D–E).

First type: The compressed annuli presented in Fig. 36 become unusually long and exceptionally well visible, which appears like an enhancement of the annulus-stretching. As it was shown in Chapter 2, the stretched shape of an annulus is suggested to form under the guidance of the microtubule horn bundle, which runs beneath the developing SDV of the annulus, and since Phalloidin is not known to enhance microtubule stability, one can safely assume that the annulus stretching is affected by Phalloidin-stabilized F-actin enhancing the stretching process of the annular SDV but microtubules control the direction. In comparison, the

effect of JAS on the shape of the annuli is just the opposite, because the annular rims are underdeveloped and curved, formed in the shape of open hooks (Fig. 34 of Result 3.3) rather than closed circles. The open ends are curved, spreading apart from one another and they are irregularly placed in the apical domain of the hypovalve. This suggests that the partially deconstructed actin filament system by mild JAS inhibition does not sufficiently maintain the two open sides of an annulus in parallel arrangement, whereas the Phalloidin inhibition overly promotes this process, i.e. in the presence of JAS the underlying MT cytoskeleton loses its organized bundle shape and the correct placement, and the growth of annuli is disturbed, whereas in the presence of Phalloidin the bundle shape is maintained. This behavior clearly demonstrates that actin filaments work together with microtubules to create the slit shape of the annuli.

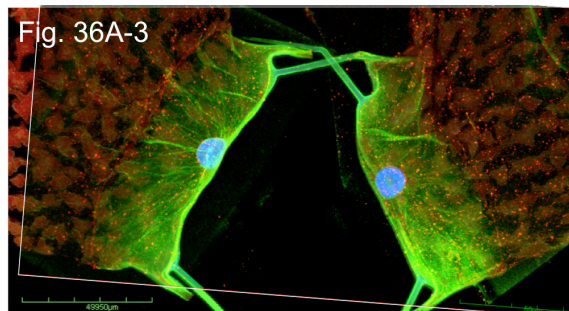
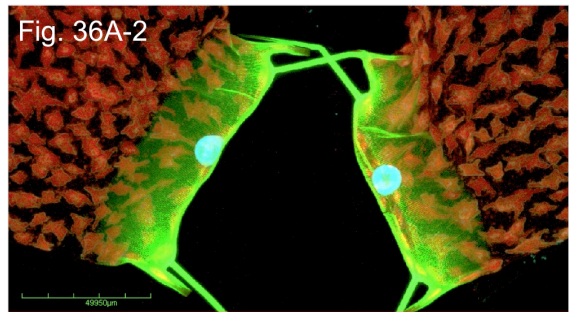
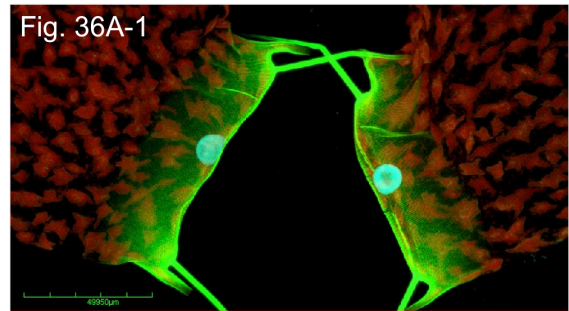
Second type: At the end of the horn bundle stage, horns remain open in the presence of Phalloidin (e.g., Figs. 36A, 36C), but the perinuclear MT system is already spreading over the apical valve domain in the typical umbrella configuration. This implies that the closure of the horn had been retarded or even blocked, because in untreated cells the establishment of the radial perinuclear MT system occurs concomitantly with the disassembly of the horn bundles and in that stage the ends of the horns get closed with the porous silica plate (the ocellus). The retardation of the horn-end-closure suggests that Phalloidin changes the configuration of the actin patch (see Section 3.4.2.4 in Part III) such that it obstructs the advancement of the SDV over the face of the ocellus, for instance by increasing the density and thickness of the actin network in the patch.

Third type: PDMPO staining of the valve in Phalloidin-treated cell significantly fades towards the basal edge of the valve. This could indicate that the actin ring travels faster down the slope of the valve than the front of growing silica within the valve SDV (Fig. 36A). Unfortunately, the true shape of the SDV cannot be seen here, only the silica is visualized by the PDMPO staining. However, the assumption that the SDV is really empty may be questioned, because artificially enhancing the signal intensity of the image (Figs. 36A-1 – 36A-3 below) reveals that, although very faint, there is still some PDMPO-signal detectable down to the basal valve edge, where a demarcating actin ring is present. This indicates that the valve actin ring and the edge of the SDV are still aligned with or even connected to each other. The significant fading of the PDMPO-signal may be due to the fact that only a thin layer of silica can be deposited because the available space is low in the flat SDV lumen.

The reason for this could lie in the disturbance by Phalloidin of the concerted action among the expansion of the valve SDV and the demarcation function of the actin ring at the edge of SDV edge, because actin filament elongation in the ring happens faster in response to Phalloidin causing it to unproportionally get wider in circumference and this in turn causes it to move more swiftly down the slope of the apical hypovalve dome than in normal cells. If the edge of the SDV and the actin ring are connected with each other, it would be logical to assume that the SDV gets stretched, which should have an impact on the overall structural integrity of the SDV, eventually even leading to the collapse of the lower onto the upper silica lemma. This would not only restrict the available space inside the SDV but actually close the SDV lumen altogether.

In addition, it is likely that a fine actin filament network is associated with either the upper or the lower silicalemma of the SDV or even with both. After all, the valve SDV in the diatom cell is a gigantic, flat membrane cisterna, which could be maintained and kept in place without additional structural support by a membrane-associated scaffold and this could be provided by the actin filament network. Phalloidin could promote the proliferation of this network, which on the one hand could enhance the two-dimensional expansion of the SDV, but on the other hand prevent the process of three-dimensional folding (see Chapter 1). The result would be that the cisterna would still be able to expand, possibly even faster than in control cells and thus work together with the actin ring moving faster. This may not so much cause a stretching of the SDV, as suggested above, but it may still weaken the structural integrity. And definitely it would allow only the formation of just one layer of silica.

Unfortunately there is currently no further supporting data available to clarify this. Future work can shed more light onto this interesting phenomenon. Clearly more fine structure analysis is necessary to clarify, whether the SDV suffers partial collapse in response to Phalloidin and



then, of course it would be very interesting to study the structure and fate of the fibrous balls in the presence of Phalloidin and in response to other treatments as well.

The pattern of faded areas in the valve domain could be different as is shown in figures 37D and 37E. Here, the daughter cell pairs have strong PDMPO-stains on the new hypovalves only in the region of the horns and the LPs and along the annuli, but the middle region from the annuli down to the valve edge also remains only lightly stained. This is consistent with the above assumption that in the lightly stained regions of the valve SDV, the process of valve morphogenesis remained stuck in the two-dimensional phase or was even completely impaired in some regions.

4.4.2.2 Disturbance of Morphogenesis before Head Plate Formation

The initiation of the valve formation in *O. sinensis* takes place midway of cytokinesis. During this course, the LPAs of this species appear and then each of them will be spatially associated with an initial SDV, based on the early TEM observation reported by Li and Volcani (Li and Volcani, 1985). The cytoskeleton data in the current work show that the two initial SDVs expand along the MT-horn bundles to form the head plate (Fig. 19D in Chapter 1), which suggests the SDV localization correlates with the horn bundles. Further, when the MT-horn bundles are deconstructed by Oryzalin, it is found that the primary silicification site is not equal to the LP initiation site, suggesting that the LPA (reported in *O. sinensis* by (Li and Volcani, 1985)) is not an essential structure for SDV initiation, and that the silica islands without associated LPs are in fact the initial annular SDVs (see Fig. 5 in Result 3.1). In conclusion, the horn bundles function as a scaffold for the placement of the initial SDV and the LPA and their association.

The dramatical inhibitory pattern of the head plate shown in Fig. 37 A – C (second phenotype in Result 3.4.1) suggests the Phalloidin inhibition took effect in the process of the initial SDV placement, because three of the silica islands are not associated with a LP and their annuli are roundish. However, the inhibition did not affect the shape of MT horn bundles and thus the horn formation is not prominently disturbed, except developing a ocellar plate (see the function of actin patch in Section 3.4.2.4 of Part III). The appearance of two extra annular SDVs and the lack of association between LPs and SDVs in the presence of normally shaped horn bundles suggest the process of the initial SDV placement are also dependent on actin filaments in the region of horn bundles. Since the association between initial SDVs and LPAs occurs in

the course of cytokinesis, as mentioned at the beginning of this section, it is reasonable to assume cortical actin filaments are involved in this association activity during cytokinesis.

Unfortunately, the cytoskeleton composition of this Phalloidin treated cell (Fig. 37 A – C) has not been visualized by fluorescent immunolabeling. Judging from the lack on any straight outline of the silica deposition edge on the downward slope of the valve, there has evidently not been any demarcating support by an actin ring.

If the inhibition takes effect in the early course of cytokinesis, probably before the initiation of primary SDVs, the hypovalve would become completely aberrant, lacking horns and LPs (third phenotype of result 3.4.1: Figs. 37F, 39 A – D). The reason for that is difficult to understand. The status of the cytoskeleton suggests that microtubules are present in high numbers forming a radial perinuclear system, but the nucleus is unusually displaced to the side. Actin filament bundles are also present in high numbers, but both cytoskeletal systems are entangled, possibly jammed into an atypical static configuration, which has lost its dynamic potentials. All this may be seen as a consequence of a disproportionate interaction between microtubules and actin bundles ending in kind of a rigor situation, which is particularly severe because of the long incubation time.

4.4.3 From Mid-Interphase to Prophase: Configuration of the Cytoskeleton after Valve Morphogenesis

Normally, the valve actin ring will find its anchorage site at the joint between eGB1 and eGB2 and with that step it begins to function as a GB-actin ring. The hGB-SDV has never been present under the cover of eGB1, which means the actin ring acts as a brake ramp preventing the GB-SDV to extend beyond the anchorage line, so that newly deposited silica will expand towards hypothecal side (see Chapter 2, Fig. 15).

In the short-term inhibition by Phalloidin, the actin system may either maintain the actin ring in normal shape demarcating the edge of the recently made GB-SDV (Fig. 40 A–B, the third phenotype of Section 4.3.2) or it may get deformed into a radiating array co-aligning with the radiating microtubule system (case 3: Figs. 40 C–D, 41 A–B, the fourth phenotype of Section 4.3.2). In Fig. 40 C&D, though, a dim actin ring is still demarcating the edge of hGB2, whereas

overall, the actin cables system in this cell (see Section 4.2.1.1 in Chapter 2) is already strongly deformed into radial arrays.

In long-term inhibition, the configuration of the cytoskeleton system appears either not (Figs. 39E, 42, 43) or only slightly affected by Phalloidin (case 2: Fig. 38, the first phenotype of Section 4.3.2). In more severe cases, the actin ring becomes deformed and the massive long microfilament system changes chaotically (case 1: Fig. 39 A–D, the second phenotype of Section 4.3.2), or the entire actin system reshapes into a radiating array focusing on the MC (case 3: 41 C–D, the fourth phenotype of Section 4.3.2).

Both types of inhibitions reveal that the frustule shape and the cytoskeleton configuration may not necessarily be affected, which may be related to the developmental stage of the cell cycle, when the inhibition starts. A closer look at the three inhibitory phenotypes may help to explain this.

4.4.3.1 Case 1: Disturbance on Actin Ring Anchorage

In the Phalloidin-treated cells of case 1 (Fig. 39 A–D), a completely aberrant valve is followed by a tilted girdle band when viewed in the lysosensor channel. The abvalvar edge of this girdle band is smooth, whereas the advalvar edge (facing the badly aberrant valve edge) is rugged, compensating the edge of the valve. This phenomenon of compensation between adjacent silica structures is similar to the situation found in Oryzalin treated cells (Fig. 15), whose advalvar edge of the GB-SDV is compensating the edge of the lateral valve complex, which means that the new SDV expands its advalvar edge into the free space left over by the previous silica structure, whereas the abvalvar edge is held in a straight shape by the GB-actin ring.

In the cytoskeleton channel of the confocal microscope (Fig. 39B), one can see the actin ring loses its compact shape and becomes spliced into several branches, which is likely a consequences of uncontrolled filament elongation. Since the valve edge is tilted, the GB also gets tilted, which suggests that the anchorage of the valve actin ring got already disturbed. It is conceivable that a cell experiencing these difficulties in the placement of girdle bands takes more time for completing morphogenesis, which could be the reason why the cell has one girdle band less than the cell of Fig. 39E, whose actin ring arrangement is normal, judging from the normal edges of the last girdle band.

4.4.3.2 Case 2: Loss of Capacity to Counteract Turgor Pressure and to Exocytose Frustule Parts

The deformation of the cytoskeleton in case 2 cells shows that, although the actin ring has reached its correct destination for anchorage under the joint between eGB1 and eGB2 (Fig. 38B), no hGB1-SDV was initiated. As it is learned from Chapter 2, the axial expansion after the valve formation occurs concomitantly with hGB1 formation, which will fill the space between the actin ring and the edge of the recently formed hypovalve. However, here in the case 2 cell, the “empty space” suggests the cell has proceeded with axial expansion, which allowed the nucleus to move out from the hypovalve, but there is no hGB1-SDV developed to fill this space. Why is this so?

Looking at the actin system, it is striking that the cables are not arranged in a normal way, instead a new focal point for the system has become established in the cortex at about the middle of the cell (asterisk in Fig. 38B). In this configuration, the actin system might not build up sufficient holding force to counteract the turgor-driven expansion, and this is what creates the “empty space”.

As shown in the short term treatments (Figs. 36A, 39A), Phalloidin took effect quickly on damaging the SDV lumen, so the reason why the entire hypovalve looks normal in the case 2 cell and is stained by PDMPO is, because the valve should have been almost completed but was still wrapped in the silica lemma, when the Phalloidin inhibition began. At that point the newly made silica must have been kept in the valve SDV for the next two hours so that it could become stainable by PDMPO, which is added in the second phase of the incubation schedule. This behavior suggests that the Phalloidin-stabilized F-actin network could even have slowed down the deployment of the silica, which in turn means that membrane associated F-actin meshworks need to be restructured in order to allow silica deployment by exocytosis. This conclusion is consistent with the previously made suggestion that deconstruction of the F-actin meshwork by JAS inhibition has the opposite effect, i.e., it promotes deployment (see Discussion 4.3.1 of Chapter 3).

This stage of the developmental block in the short term treated case 2 cell would pass over to one type of case 3 cells occurring after long-term treatment (Fig. 41 C, D), which have a

perfectly well shaped valve, no girdle band and a nucleus at about the same position as case 2 cells but an entirely reshaped cytoskeleton as described below.

4.4.3.3 Case 3: Enhancement of Radial Symmetry in the Cytoskeleton

At the stage between interphase and prophase, one of the inhibitory phenotypes is that all the long and radiating microtubules detach from the nuclear surface and connect with the MC, while the actin system changes its architecture by developing a higher preference to also anchor in the MC other than what they normally do in control cells. This phenomenon may occur either in long-term or the short-term inhibition, no matter what concentration of Phalloidin is applied (short-term, 0.5 μM : Figs. 40 C–D; short-term, 1 μM : Figs. 41 A–B; long-term, 0.5 μM : Figs. 41 C–D).

Given that Phalloidin acts as an actin filament stabilizer (Cooper, 1987) and filament elongation promoter, one would not expect it having an effect on microtubules. However, this may well occur in an indirect fashion, since actin filaments induced by Phalloidin will stabilize and dramatically increase the co-alignment with perinuclear microtubules, which is in agreement with observations in other cell systems (Mohan and John, 2015; Pacheco and Gallo, 2016; Petrášek and Schwarzerová, 2009). So that the tension, which keeps the nucleus with its associated microtubular arrays suspended between the opposite actin cable systems, focuses more strongly on the MC, causing it to get detached from the nuclear surface. It should be noted, however, that in all long-term-treated cells, which had undergone this type of cytoskeletal reorganization, the chromosomes are beginning to condense, which would be typical for the prophase stage, even though the MC is not anymore attached to the nuclear surface. This is a very interesting case of pharmacological microdissection in a living cell worthwhile to be followed up in future studies.

In the short-term inhibition, when the Phalloidin concentration is 1 μM , the arrangement of the tension equilibrium system of the cytoskeleton can be normal (Fig. 40 A&B). However, in the same inhibiting condition (drug concentration and incubation period), the entire system could completely be transformed into the radial-array configuration (Fig. 41 A&B). Besides, when the drug dose was reduced by a half, this radial configuration could occur again (Fig. 40 C&D). The latter two cases suggest the transformation of the cytoskeleton system can proceed very fast in the short term incubation either in 0.5 or 1 μM . So coming back to the first case (Fig. 40 A&B),

such a normal configuration suggests there should be some conditions of the cell different to the conditions of the cell in the latter two cases. The answer is the cell cycle stage, when the drug takes prominent effect. In the first case, the cell has just developed the last girdle band but the last axial expansion may probably have not yet occurred, so the cytoskeleton system does not rearrange to adapt for a new tension equilibrium state, and therefore Phalloidin may not have a prominent effect on the configuration of the cytoskeleton. Whereas, judging from the cell length and the PDMPO stains, it is clear that cells of the latter two cases are both in the course of the last axial expansion and halted midway, and since this is the transition stage that requires dynamic changes in the cytoskeleton — the actin ring detaches from its anchorage site and the microtubule system shifts to the new midline in untreated cells (see Chapter 2), the dynamic change of the actin system will be affected by Phalloidin, which further interferes with the interaction between actin filaments (or bundles) and microtubules, giving rise to the radial configuration of the cytoskeleton system. In conclusion, these three cases suggest the radial array of the cytoskeleton system can be induced by Phalloidin, when the cell is in the course of the last axial expansion.

In long-term inhibition (0.5 μ M Phalloidin, 2+50 hours), the configuration of the cytoskeleton system may either suffer a prominent change (Figs, 38, 41 C&D), or just a slight one (Figs. 42, 43). The difference between the two major inhibitory types is again the cell cycle stage when the inhibition takes effect. Judging from the situation of PDMPO staining, the former type must be inhibited before the hypovalve deployment, whereas the latter is inhibited after that stage.

In the former type, the deformed configuration of the cytoskeleton system is not the same in the two cells — one has its actin ring anchoring at a normal position between eGB1 and eGB2 but away from the edge of the recent made silica structure (Fig. 38), while the other has transformed its cytoskeleton system into the complete radial array although the actin system is not able to be visualized by immunolabeling (Fig. 41 C&D). Such a configuration difference again suggests that the inhibited cell cycle stages are slightly different. In Fig. 38, the cytoskeleton configuration looks normal, which suggests the inhibition took effect after the cytoskeleton system has completed the transformation of its configuration from the umbrella array in the valve apical domain to a more flattened radial array facing the girdle band. And as discussed in Section 4.4.3.2, the empty space may be due to the reason that the axial expansion was promoted by Phalloidin after the actin ring got anchored, but before the GB-SDV formation was triggered. In Fig. 41 C&D, the radial array configuration of the cytoskeleton system suggests the inhibition was taking place before the system had completed its transformation. In conclusion,

both cases suggest the radial array of the cytoskeleton system centering on the MC can be induced by Phalloidin, when the cell is in the transition stage between the valve development and the girdle band development.

In the latter type, the inhibition appears beginning from hGB1 formation and being terminated at mitosis (Figs. 42, 43). Their cytoskeleton configuration and the silica component formation look normal, except that the cytokinetic actin ring of each cell appears slightly meandering, which appears to be a typical effect caused by Phalloidin (further discussion see Section 4.4.4 below). And interestingly, both cells have successfully completed the last axial expansion, without deforming its cytoskeleton into a radial array like that occurring in the cells of Figs. 40 C&D, 41A&B. The reason for this is unknown. One possibility could be that the cytoskeleton has adapted to the intracellular changes caused by the drug, so when the last axial expansion occurs, no dramatic re-configuration of the cytoskeleton is made.

In summary, the cytoskeleton system transforming into the radial array configuration in the presence of Phalloidin, occurs in cells undergoing a sudden transition from one stage of the cell cycle to the next.

4.4.4 Cytokinesis: The Failure of Prospective Constriction

When the Phalloidin inhibition begins from the middle of interphase (defined as the stage when girdle bands are made), cells at mitotic stages have been encountered with a matured cytokinetic actin ring (Figs. 42, 43), but cells halted at the mid-way of cytokinesis, so that lateral valves did not develop. Instead, divided cells with aberrant hypoalves (Fig. 37F) have been encountered in the inhibition culture sometimes. This may be because the inhibition takes effect at the late cytokinesis, when the primary silicification of the daughter hypoalves has already occurred.

In those mitotic cells (Figs. 42, 43), the two PDMPPO-stained girdle bands look normal, which suggests that the anchorage of the actin ring, i.e., the transition from the valve to the girdle band formation stage, may probably have been completed before prominent effects are caused by Phalloidin. One cell is at metaphase and the other is at telophase. In both cases, the cytokinetic actin ring is very narrow and meandering particularly in the region, where it passes by the central spindle. This suggests the ring is too long to fit the perimeter of the cell (Figs. 42 a₁–a₅), which would be consistent with the principle effect of Phalloidin, i.e. promoting microfilament

elongation. As has been shown in other cell systems, cytokinetic contraction requires constant length adjustment of the actin filaments in the ring (Pollard, 2010), so it can be concluded that Phalloidin maintains the cytokinetic ring at its relaxed state (Barden et al., 1987; Li et al., 2016; Stachowiak et al., 2014), inducing a retardation or even the block of constriction.

In summary, inhibiting cytokinetic constriction with Phalloidin points at a construction of the cytokinetic actin ring by antiparallel arrangement of F-actin. Preliminary data were obtained with a set of inhibitors suggesting that myosin should be involved (see image plates #4.3.1 – 4.3.19 in Appendix).

5 References

- Allen, A.E., Laroche, J., Maheswari, U., Lommer, M., Schauer, N., Lopez, P.J., Finazzi, G., Fernie, A.R., and Bowler, C. (2008). Whole-cell response of the pennate diatom *Phaeodactylum tricornutum* to iron starvation. *Proc. Natl. Acad. Sci. U. S. A.* *105*, 10438–10443.
- Almonacid, M., Moseley, J.B., Janvore, J., Mayeux, A., Fraasier, V., Nurse, P., and Paoletti, A. (2009). Spatial control of cytokinesis by Cdr2 kinase and Mid1/anillin nuclear export. *Curr. Biol.* *19*, 961–966.
- Amos, L.A. (2011). What tubulin drugs tell us about microtubule structure and dynamics. *Semin. Cell Dev. Biol.* *22*, 916–926.
- Aumeier, C., Polinski, E., and Menzel, D. (2015). Actin, actin-related proteins and profilin in diatoms: a comparative genomic analysis. *Mar. Genomics* *23*, 133–142.
- Badour, S.S. (1968). Experimental separation of cell division and silica shell formation in *Cyclotella cryptica*. *Arch. Mikrobiol.* *62*, 17–33.
- Baeuerlein, E. (2004). *Biom mineralization: Progress in Biology, Molecular Biology and Application* (John Wiley & Sons).
- Bajer, A.S., and Molè-Bajer, J. (1986). Reorganization of microtubules in endosperm cells and cell fragments of the higher plant *Haemanthus* in vivo. *J. Cell Biol.* *102*, 263–281.
- Barden, J.A., Miki, M., Hambly, B.D., and Remedios, C. (1987). Localization of the phalloidin and nucleotide-binding sites on actin. *Eur. J. Biochem.* *162*, 583–588.
- Blagosklonny, M.V., and Fojo, T. (1999). Molecular effects of paclitaxel: myths and reality (a critical review). *Int. J. Cancer* *83*, 151–156.
- Bokros, C.L., Hugdahl, J.D., Hanesworth, V.R., Murthy, J.V., and Morejohn, L.C. (1993). Characterization of the reversible taxol-induced polymerization of plant tubulin into microtubules. *Biochemistry* *32*, 3437–3447.

- Bubb, M.R., Senderowicz, A.M., Sausville, E.A., Duncan, K.L., and Korn, E.D. (1994). Jasplakinolide, a cytotoxic natural product, induces actin polymerization and competitively inhibits the binding of phalloidin to F-actin. *J. Biol. Chem.* **269**, 14869–14871.
- Bubb, M.R., Spector, I., Beyer, B.B., and Fosen, K.M. (2000). Effects of jasplakinolide on the kinetics of actin polymerization. An explanation for certain in vivo observations. *J. Biol. Chem.* **275**, 5163–5170.
- Chang, D.C., and Lu, P. (2000). Multiple types of calcium signals are associated with cell division in zebrafish embryo. *Microsc. Res. Tech.* **49**, 111–122.
- Clark, A.G., Wartlick, O., Salbreux, G., and Paluch, E.K. (2014). Stresses at the cell surface during animal cell morphogenesis. *Curr. Biol.* **24**, R484–R494.
- Cooper, J.A. (1987). Effects of cytochalasin and phalloidin on actin. *J. Cell Biol.* **105**, 1473–1478.
- Cramer, L.P. (1999). Role of actin-filament disassembly in lamellipodium protrusion in motile cells revealed using the drug jasplakinolide. *Curr. Biol.* **9**, 1095–1105.
- Crews, P., Manes, L.V., and Boehler, M. (1986). Jasplakinolide, a cyclodepsipeptide from the marine sponge, Jaspis SP. *Tetrahedron Lett.* **27**, 2797–2800.
- Daga, R.R., and Chang, F. (2005). Dynamic positioning of the fission yeast cell division plane. *Proc. Natl. Acad. Sci. U. S. A.* **102**, 8228–8232.
- Darley, W.M., and Volcani, B.E. (1971). [7] Synchronized cultures: diatoms. In *Methods in Enzymology*, (Academic Press), pp. 85–96.
- D'Avino, P.P., Takeda, T., Capalbo, L., Zhang, W., Lilley, K.S., Laue, E.D., and Glover, D.M. (2008). Interaction between Anillin and RacGAP50C connects the actomyosin contractile ring with spindle microtubules at the cell division site. *J. Cell Sci.* **121**, 1151–1158.
- Davis, A.K., and Hildebrand, M. (2010). Molecular Processes of Biosilicification in Diatoms. In *Biom mineralization*, pp. 255–294.
- Dostál, V., and Libusová, L. (2014). Microtubule drugs: action, selectivity, and resistance across the kingdoms of life. *Protoplasma* **251**, 991–1005.
- Eppley, R.W. (1977). The growth and culture of diatoms. *The Biology of Diatoms* **13**, 24–64.
- Etienne-Manneville, S. (2004). Actin and microtubules in cell motility: which one is in control? *Traffic* **5**, 470–477.
- Falciatore, A., d'Alcalà, M.R., Croot, P., and Bowler, C. (2000). Perception of environmental signals by a marine diatom. *Science* **288**, 2363–2366.
- Figuroa-Masot, X.A., Hetman, M., Higgins, M.J., Kokot, N., and Xia, Z. (2001). Taxol induces apoptosis in cortical neurons by a mechanism independent of Bcl-2 phosphorylation. *J. Neurosci.* **21**, 4657–4667.
- Forer, A., Spurck, T., Pickett-Heaps, J.D., and Wilson, P.J. (2003). Structure of kinetochore fibres in crane-fly spermatocytes after irradiation with an ultraviolet microbeam: neither

- microtubules nor actin filaments remain in the irradiated region. *Cell Motil. Cytoskeleton* **56**, 173–192.
- Fox, D.T., and Duronio, R.J. (2013). Endoreplication and polyploidy: insights into development and disease. *Development* **140**, 3–12.
- Gao, X.-Q., Wang, X.-L., Ren, F., Chen, J., and Wang, X.-C. (2009). Dynamics of vacuoles and actin filaments in guard cells and their roles in stomatal movement. *Plant Cell Environ.* **32**, 1108–1116.
- Gómez, A.M., Kerfant, B.G., and Vassort, G. (2000). Microtubule Disruption Modulates Ca²⁺ Signaling in Rat Cardiac Myocytes. *Circ. Res.* **86**, 30–36.
- Hardham, A.R., Takemoto, D., and White, R.G. (2008). Rapid and dynamic subcellular reorganization following mechanical stimulation of Arabidopsis epidermal cells mimics responses to fungal and oomycete attack. *BMC Plant Biol.* **8**, 63.
- Hepler, P.K. (2016). The Cytoskeleton and Its Regulation by Calcium and Protons. *Plant Physiol.* **170**, 3–22.
- Hertel, C., Quader, H., Robinson, D.G., and Marmé, D. (1980). Anti-microtubular herbicides and fungicides affect Ca(2+) transport in plant mitochondria. *Planta* **149**, 336–340.
- Hertel, C., Quader, H., Robinson, D.G., Roos, I., Carafoli, E., and Marmé, D. (1981). Herbicides and fungicides stimulate Ca²⁺ efflux from rat liver mitochondria. *FEBS Lett.* **127**, 37–39.
- Hildebrand, M., Dahlin, K., and Volcani, B.E. (1998). Characterization of a silicon transporter gene family in *Cylindrotheca fusiformis*: sequences, expression analysis, and identification of homologs in other diatoms. *Mol. Gen. Genet.* **260**, 480–486.
- Holzinger, A., and Blaas, K. (2016). Actin-Dynamics in Plant Cells: The Function of Actin-Perturbing Substances: Jasplakinolide, Chondramides, Phalloidin, Cytochalasins, and Latrunculins. *Methods Mol. Biol.* **1365**, 243–261.
- Hugdahl, J.D., and Morejohn, L.C. (1993). Rapid and Reversible High-Affinity Binding of the Dinitroaniline Herbicide Oryzalin to Tubulin from *Zea mays* L. *Plant Physiol.* **102**, 725–740.
- Idei, M., Osada, K., Sato, S., Toyoda, K., Nagumo, T., and Mann, D.G. (2012). Gametogenesis and auxospore development in *Actinocyclus* (Bacillariophyta). *PLoS One* **7**, e41890.
- Kahl, C.R., and Means, A.R. (2003). Regulation of cell cycle progression by calcium/calmodulin-dependent pathways. *Endocr. Rev.* **24**, 719–736.
- Kerfant, B.G., Vassort, G., and Gómez, A.M. (2001). Microtubule disruption by colchicine reversibly enhances calcium signaling in intact rat cardiac myocytes. *Circ. Res.* **88**, E59–E65.
- Kidd, J.F., Pilkington, M.F., Schell, M.J., Fogarty, K.E., Skepper, J.N., Taylor, C.W., and Thorn, P. (2002). Paclitaxel affects cytosolic calcium signals by opening the mitochondrial permeability transition pore. *J. Biol. Chem.* **277**, 6504–6510.
- Koteliansky, V.E., Shartava, A.S., Belkin, A.M., Gneushev, G.N., and Smirnov, V.N. (1983). The effects of phalloidin on actin gel-sol transformation. *FEBS Lett.* **153**, 311–314.

- Kröger, N., and Poulsen, N. (2008). Diatoms—From Cell Wall Biogenesis to Nanotechnology. *Annu. Rev. Genet.* **42**, 83–107.
- Kröger, N., Bergsdorf, C., and Sumper, M. (1994). A new calcium binding glycoprotein family constitutes a major diatom cell wall component. *EMBO J.* **13**, 4676–4683.
- Kunda, P., and Baum, B. (2009). The actin cytoskeleton in spindle assembly and positioning. *Trends Cell Biol.* **19**, 174–179.
- Lancaster, O.M., Le Berre, M., Dimitracopoulos, A., Bonazzi, D., Zlotek-Zlotkiewicz, E., Picone, R., Duke, T., Piel, M., and Baum, B. (2013). Mitotic rounding alters cell geometry to ensure efficient bipolar spindle formation. *Dev. Cell* **25**, 270–283.
- Le, X.-F., Hittelman, W.N., Liu, J., McWatters, A., Li, C., Mills, G.B., and Bast, R.C., Jr (2003). Paclitaxel induces inactivation of p70 S6 kinase and phosphorylation of Thr421 and Ser424 via multiple signaling pathways in mitosis¹. *Oncogene* **22**, 484.
- Lee, E., Shelden, E.A., and Knecht, D.A. (1998). Formation of F-actin aggregates in cells treated with actin stabilizing drugs. *Cell Motil. Cytoskeleton* **39**, 122–133.
- Li, J. (2011). Zellbiologische und morphologische Untersuchungen an den Mutanten TCH3-3 und MCA1 sowie den transgenen Linien GFP-FABD2 und LIFEACT-GFP von *Arabidopsis thaliana*. Diplomarbeit Mathematisch-Naturwissenschaftlichen Fakultät. Rheinischen Friedrich-Wilhelms-Universität Bonn.
- Li, C.-W., and Volcani, B.E. (1985). Studies on the biochemistry and fine structure of silica shell formation in diatoms. X. Morphogenesis of the labiate process in centric diatoms. *Protoplasma* **124**, 147–156.
- Li, Y., Christensen, J.R., Homa, K.E., Hocky, G.M., Fok, A., Sees, J.A., Voth, G.A., and Kovar, D.R. (2016). The F-actin bundler α -actinin Ain1 is tailored for ring assembly and constriction during cytokinesis in fission yeast. *Mol. Biol. Cell* **27**, 1821–1833.
- Long, B.H., and Fairchild, C.R. (1994). Paclitaxel inhibits progression of mitotic cells to G1 phase by interference with spindle formation without affecting other microtubule functions during anaphase and telephase. *Cancer Res.* **54**, 4355–4361.
- Lu, Y., Chen, J., Xiao, M., Li, W., and Miller, D.D. (2012). An overview of tubulin inhibitors that interact with the colchicine binding site. *Pharm. Res.* **29**, 2943–2971.
- Machnicka, B., Czogalla, A., Hryniewicz-Jankowska, A., Bogusławska, D.M., Grochowalska, R., Heger, E., and Sikorski, A.F. (2014). Spectrins: a structural platform for stabilization and activation of membrane channels, receptors and transporters. *Biochim. Biophys. Acta* **1838**, 620–634.
- Maldonado, E.N., Patnaik, J., Mullins, M.R., and Lemasters, J.J. (2010). Free tubulin modulates mitochondrial membrane potential in cancer cells. *Cancer Res.* **70**, 10192–10201.
- McCubrey, J.A., May, W.S., Duronio, V., and Mufson, A. (2000). Serine/threonine phosphorylation in cytokine signal transduction. *Leukemia* **14**, 9–21.
- Mohan, R., and John, A. (2015). Microtubule-associated proteins as direct crosslinkers of actin

filaments and microtubules. *IUBMB Life* 67, 395–403.

Nightingale, T.D., Cutler, D.F., and Cramer, L.P. (2012). Actin coats and rings promote regulated exocytosis. *Trends Cell Biol.* 22, 329–337.

Oey, J.L., and Schnepf, E. (1970). Über die Auslösung der Valvenbildung bei der Diatomee *Cyclotella cryptica*. *Arch. Mikrobiol.* 71, 199–213.

Olave, I.A., Reck-Peterson, S.L., and Crabtree, G.R. (2002). Nuclear actin and actin-related proteins in chromatin remodeling. *Annu. Rev. Biochem.* 71, 755–781.

Pacheco, A., and Gallo, G. (2016). Actin filament-microtubule interactions in axon initiation and branching. *Brain Res. Bull.* 126, 300–310.

Panteris, E., Komis, G., Adamakis, I.-D.S., Samaj, J., and Bosabalidis, A.M. (2010). MAP65 in tubulin/colchicine paracrystals of *Vigna sinensis* root cells: possible role in the assembly and stabilization of atypical tubulin polymers. *Cytoskeleton* 67, 152–160.

Parambath, M., Hanley, Q.S., Martin-Martinez, F.J., Giesa, T., Buehler, M.J., and Perry, C.C. (2016). The nature of the silicaphilic fluorescence of PDMPO. *Phys. Chem. Chem. Phys.* 18, 5938–5948.

Petrásek, J., and Schwarzerová, K. (2009). Actin and microtubule cytoskeleton interactions. *Curr. Opin. Plant Biol.* 12, 728–734.

Pickett-Heaps, J.D., and Spurck, T.P. (1982). Studies on kinetochore function in mitosis. I. The effects of colchicine and cytochalasin on mitosis in the diatom *Hantzschia amphioxys*. *Eur. J. Cell Biol.* 28, 77–82.

Pickett-Heaps, J., Schmid, A.M.M., and Edgar, L.A. (1990). The cell biology of diatom valve formation. *Progress in Phycological Research* 7, 1–168. pls. 1–101.

Pollard, T.D. (2010). Mechanics of cytokinesis in eukaryotes. *Curr. Opin. Cell Biol.* 22, 50–56.

Porat-Shliom, N., Milberg, O., Masedunskas, A., and Weigert, R. (2013). Multiple roles for the actin cytoskeleton during regulated exocytosis. *Cell. Mol. Life Sci.* 70, 2099–2121.

Ramkumar, N., and Baum, B. (2016). Coupling changes in cell shape to chromosome segregation. *Nat. Rev. Mol. Cell Biol.* 17, 511–521.

Rizk, R.S., and Walczak, C.E. (2005). Chromosome Dynamics: Actin's Gone Fishing. *Curr. Biol.* 15, R841–R842.

Robinson, R.W., and Snyder, J.A. (2005). Localization of myosin II to chromosome arms and spindle fibers in PtK1 cells: a possible role for an actomyosin system in mitosis. *Protoplasma* 225, 113–122.

Rodriguez, O.C., Schaefer, A.W., Mandato, C.A., Forscher, P., Bement, W.M., and Waterman-Storer, C.M. (2003). Conserved microtubule–actin interactions in cell movement and morphogenesis. *Nat. Cell Biol.* 5, 599–609.

Sawitzky, H., Liebe, S., Willingale-Theune, J., and Menzel, D. (1999). The anti-proliferative agent jasplakinolide rearranges the actin cytoskeleton of plant cells. *Eur. J. Cell Biol.* 78,

424–433.

Schiff, P.B., and Horwitz, S.B. (1980). Taxol stabilizes microtubules in mouse fibroblast cells. *Proc. Natl. Acad. Sci. U. S. A.* 77, 1561–1565.

Schmid, A.-M. (1984). Tricornate spines in *Thalassiosira eccentrica* as a result of valve-modelling.

Schmid, A.M.M. (1980). Valve morphogenesis in diatoms : A pattern-related filamentous system in pennates and the effect of APM, colchicines and osmotic pressure. *Nova Hedwigia* 33, 811–847.

Schmid, A.-M.M. (1994). Aspects of morphogenesis and function of diatom cell walls with implications for taxonomy. In *The Protistan Cell Surface*, R. Wetherbee, J.D. Pickett-Heaps, and R.A. Andersen, eds. (Vienna: Springer Vienna), pp. 43–60.

Schmid, A.-M.M. (2003). The evolution of the silicified diatom cell wall—revisited. *Diatom Res.* 18, 191–195.

Schmid, A.-M.M., and Schulz, D. (1979). Wall morphogenesis in diatoms: Deposition of silica by cytoplasmic vesicles. *Protoplasma* 100, 267–288.

Schmid, A.-M.M., and Volcani, B.E. (1983). Wall morphogenesis in *Coscinodiscus wailesii* Gran and Angst. I. Valve morphology and development of its architecture. *J. Phycol.* 19, 387–402.

Schmid, A.-M.M., Eberwein, R.K., and Hesse, M. (1996). Pattern morphogenesis in cell walls of diatoms and pollen grains: a comparison. *Protoplasma* 193, 144–173.

Sheldon, K.L., Maldonado, E.N., Lemasters, J.J., Rostovtseva, T.K., and Bezrukov, S.M. (2011). Phosphorylation of voltage-dependent anion channel by serine/threonine kinases governs its interaction with tubulin. *PLoS One* 6, e25539.

Silverman-Gavrila, R.V., and Forer, A. (2003). Myosin localization during meiosis I of crane-fly spermatocytes gives indications about its role in division. *Cell Motil. Cytoskeleton* 55, 97–113.

Stachowiak, M.R., Laplante, C., Chin, H.F., Guirao, B., Karatekin, E., Pollard, T.D., and O’Shaughnessy, B. (2014). Mechanism of cytokinetic contractile ring constriction in fission yeast. *Dev. Cell* 29, 547–561.

Staiger, C.J. (2000). SIGNALING TO THE ACTIN CYTOSKELETON IN PLANTS. *Annu. Rev. Plant Physiol. Plant Mol. Biol.* 51, 257–288.

Sun, S.X., Walcott, S., and Wolgemuth, C.W. (2010). Cytoskeletal cross-linking and bundling in motor-independent contraction. *Curr. Biol.* 20, R649–R654.

Thamatrakoln, K., and Kustka, A.B. (2009). When to say when: can excessive drinking explain silicon uptake in diatoms? *Bioessays* 31, 322–327.

Thamatrakoln, K., Alverson, A.J., and Hildebrand, M. (2006). COMPARATIVE SEQUENCE ANALYSIS OF DIATOM SILICON TRANSPORTERS: TOWARD A MECHANISTIC MODEL OF SILICON TRANSPORT. *J. Phycol.* 42, 822–834.

Thion, L., Mazars, C., Thuleau, P., Graziana, A., Rossignol, M., Moreau, M., and Ranjeva, R.

- (1996). Activation of plasma membrane voltage-dependent calcium-permeable channels by disruption of microtubules in carrot cells. *FEBS Lett.* 393, 13–18.
- Tippit, D.H., and Pickett-Heaps, J.D. (1977). Mitosis in the pennate diatom *Surirella ovalis*. *J. Cell Biol.* 73, 705–727.
- Tolic-Nørrelykke, I.M., Sacconi, L., Stringari, C., Raabe, I., and Pavone, F.S. (2005). Nuclear and Division-Plane Positioning Revealed by Optical Micromanipulation. *Curr. Biol.* 15, 1212–1216.
- Vardi, A., Formiggini, F., Casotti, R., De Martino, A., Ribalet, F., Miralto, A., and Bowler, C. (2006). A stress surveillance system based on calcium and nitric oxide in marine diatoms. *PLoS Biol.* 4, e60.
- Vardi, A., Thamatrakoln, K., Bidle, K.D., and Falkowski, P.G. (2008). Diatom genomes come of age. *Genome Biol.* 9, 245.
- Wehland, J., Osborn, M., and Weber, K. (1977). Phalloidin-induced actin polymerization in the cytoplasm of cultured cells interferes with cell locomotion and growth. *Proc. Natl. Acad. Sci. U. S. A.* 74, 5613–5617.
- Wieland, T. (1987). 50 Jahre Phalloidin. *Naturwissenschaften* 74, 367–373.
- Woolner, S., O'Brien, L.L., Wiese, C., and Bement, W.M. (2008). Myosin-10 and actin filaments are essential for mitotic spindle function. *J. Cell Biol.* 182, 77–88.
- Wordeman, L. (1992). THE MITOTIC SPINDLE AND CELL CYCLE. *The Cytoskeleton of the Algae* 39.
- Wordeman, L., McDonald, K.L., and Cande, W.Z. (1986). The distribution of cytoplasmic microtubules throughout the cell cycle of the centric diatom *Stephanopyxis turris*: their role in nuclear migration and positioning the mitotic spindle during cytokinesis. *J. Cell Biol.* 102, 1688–1698.
- Yang, C.P., and Horwitz, S.B. (2000). Taxol mediates serine phosphorylation of the 66-kDa Shc isoform. *Cancer Res.* 60, 5171–5178.
- Yvon, A.M., Wadsworth, P., and Jordan, M.A. (1999). Taxol suppresses dynamics of individual microtubules in living human tumor cells. *Mol. Biol. Cell* 10, 947–959.
- Zhang, Y. (2012). Girdle Band Formation of *Odontella sinensis*. Master thesis. Faculty of Mathematics and Natural Sciences. Bonn University.

Part III. General Discussion

1 Fidelity of Structural Preservation and Immunolabeling

Double immunolabeling in combination with lysosensor staining has provided new insights into the developmental process of the centric marine diatom *Odontella sinensis*. Carrying cells through the inhibition together with lysosensor staining procedures at the same time, subsequently preserving structure and antigenicity for two antibodies as well as nuclear staining is not a trivial task. The additional challenge is, to end up with a sufficiently large sample size for the microscopic documentation of the cytological features, which typically emerge throughout the progression of the cell cycle. Sources of possible artifacts are manifold: Incomplete or sub-optimal fixation is among the worst. This problem depends on the right choice of the fixative mixture and on the conditions of fixation, i.e. temperature, pH, osmotic and ionic buffering components. The buffering of pH is important, because *Odontella* has a large central vacuole. Damage of the tonoplast will cause leakage, i.e., during fixation the tonoplast-barrier-function breaks down and the thin cortical cytoplasmic layer gets flooded with acid from the vacuole, possibly also with unwanted chemical components such as phenolics or polyphenolics. Also the ion-equilibrium is going to break down simultaneously (Huang and Yeung, 2015). Therefore, the buffer must have sufficient strength to counteract acidification and the other ionic components of the fixation buffer should out-compete ionic imbalances coming from the vacuole. Acidity is dangerous, because it will denature proteins, which will reduce the structural preservation and immuno-reactivity of the cellular antigens (i.e., tubulin and actin). So it has been made sure in preliminary experiments that these conditions have become optimized. One thing, that cannot reliable be standardized is the speed of diffusion. Cells covered with a wall are particularly problematic and it has been found that unicellular organism, which need to protect themselves against environmental stresses have a particularly hardy wall (Hamm and Smetacek, 2007). In case of the diatoms, the wall consists not only of the silica material, which often is porous so that molecules should be able to pass through, but also of organic matrix material and an organic layer between the silica wall and the plasma membrane (see Chapter 1 and (Brunner et al., 2009; Kotzsch et al., 2016; Tesson and Hildebrand, 2013)).

Even though protocols have been optimized in the current study, there will be always a fraction of cells within a given batch, which shows some kind of fixation-, diffusion- and

unspecific staining-artifacts. This is most prominently observed in the actin cytoskeleton, which in the case of *Odontella* can sometimes be perfectly preserved and sometimes it can be shattered to pieces. This requires selection by the observer of the best preserved examples, which inevitable carries some personal bias. Handling of the cells during transfers from one incubation step to the next could also cause damage to the cells integrity. This starts with the first step of collecting cells for fixation and continues through all changes of incubation liquids. In some lucky cases, such “rough handling” treated samples provided additional insight into cell repair mechanisms (see concentric closure of a wound, Appendix Fig. 8), but mostly the outcome was frustrating, particularly when microtubules were excellently preserved but the actin labelling was insufficient.

The evaluation of inhibitor treatments poses an additional problem, because damages stemming from the inhibitor treatment must be distinguished from artifacts. Because in the course of this study hundreds of images were obtained for each of the treatment and for every developmental stage, a sufficiently large amount of data was created for a thorough comparison and evaluation, so that misinterpretations could be minimized.

2 The Evolutionary Trends in Silica Pattern Formation

2.1 Silica Pattern of the Frustule

Silica deposition is not unique to the diatoms, it occurs in several phylogenetically unrelated branches of organisms (Raven and Waite, 2004) including radiolarians (Anderson, 1981) sponges (Müller et al., 2011) and even higher plants (Fernández Honaine et al., 2016). The mode of silica deposition may be different, as for instance shown in the sponges (Müller et al., 2011), where the enzyme silicatein catalyzes the formation of silica spicules, but in algae and protists it is a co-factor-mediated self-assembly process taking place in a special vesicular organelle, termed SDV, within which the silica deposit is processed and molded into specifically shaped covers (for the chemistry and silicic acid entry in the cell see (Knight et al., 2016)). This type of SDV is seen in the ancestral heterokont lineages leading to the diatoms (Sims et al., 2006) and in the sister branches including *Synurophyceae* (Pipes and Leedale, 1992),

Chrysophyceae, but also in unrelated protist lineages such as the choanoflagellates (Marron et al., 2013).

In the choanoflagellates, the silica covering is made of coastal stripes (Hoffmeyer and Burkhardt, 2016), whereas in the heterokont lineages leading to the diatoms, the cell covering is only made of silica scales, each of which grows by the deposition of silica in an individual SDV and then gets exocytosed to be deployed on the cell surface. However, none of these variously shaped, siliceous cell coverings are created with richly ornamental sculptures and able to enclose the protoplast into a petri-dish-like glass box as in diatoms, which consists of a bigger and a smaller ornamental cap separated by a cylinder consisting of variously shaped composite elements such as wide bands, small rings, assemblages of bracelets or scales. An example of diamond-shaped scales in diatoms is seen for instance in the polar centric *Rhizosolenia arafurensis*.

The silica frustule of the diatoms may have arisen from the dormant diplontic cyst stage of the heterokont, haploid, scaly flagellates, which are made as a closed silica casing (Mann and Marchant, 1989). It has been pointed out by Kaczmarska and co-workers (Kaczmarska et al., 2001) that diatoms fall back on the more ancestral form of silica scale formation, when they are at the stage of auxospore, which is the zygote of the diatoms, formed after gamete fusion. In some pennate species, this stage is followed by a so called perizonium stage, which has a wall composed of open, transverse bracelet-shaped bands wrapping around the cell (Sato et al., 2008). These bracelets are like an assembly of narrow girdle bands forming a long cylinder, within which the species-specific morphology consisting of valves and girdle bands is re-established with the next mitotic/vegetative divisions of the auxospore. In either way, the employment of scales or bracelets in the auxospore cell covering makes it possible for the progeny to regain the original size independent of its parent's size and morphology (Idei et al., 2012; Round et al., 2007; Schmid and Crawford, 2001). The species-specific shape develops in steps with the next vegetative divisions.

Considering the theoretical minimum number of evolutionary steps, which may have occurred, before the current-day polar-centric diatom morphology has emerged from the ancestral mode of scale production, one can think of five steps starting out from the original tendency of making scales within the SDV:

1. Enlarge the size of the first scale to the dimension of the initial valve either by expansion of a single scale or by fusion of two or more scales together.

2. Introduce a semiconservative type of cell division meaning that each daughter inherits one of the parental halves (epitheca) and forms a smaller new halve (hypotheca) thus re-establishing the parental morphology.
3. Allow for a vegetative volume increase by inserting transverse bands between epivalve and hypovalve. (for the complete treatment of valve morphogenesis see (Pickett-Heaps et al., 1990)).
4. In order to arrive at the radial, bi- or multipolar centrics, a mechanism should get installed to limit the frequency of SDV seeding to either just one at a time (radial centrics), or allowing only two or just a few iterations (polar centrics). Internally it is essential to set up and employ additional guiding structures in the cell to control the initial location of the SDV on the apical face of the recently divided daughter cell, such as linking it to the apically positioned MC mounted on the nucleus. This would create a radially centric geometry, if only one scale is initiated; alternatively, a bi-/multipolar centric geometry would be created, if two or more scale-SDVs are initiated.
5. Control the scale size. If the initial scale or the combination of two or three initial scales need to grow by expansion to reach the desired size of the future valve, a mechanism is required to control and eventually limit SDV expansion. Scales in the ancestral lineage of the diatoms as well as in the auxospore stage have a uniformly small size compared to the overall size of the cell. This raises the need for a mechanism that allows but also constrains the process of SDV expansion during the growth of the scale. Assuming that scale expansion is driven by silica deposition, no additional means are required to push expansion. And this assumption is confirmed by the current results of the Oryzalin experiments (see Chapter 3). Even more, these experiments showed that the scale size is essentially unlimited, or only limited by silica supply and the available space on the cell surface. It follows that there must have been already a mechanism in the ancestral heterokonts of diatoms to limit scale expansion. Nothing is yet known about it and even less about whether an actin ring around the scale-SDV is installed to do the job. This is only a conceivable assumption and for the time being it can only be formulated as a working hypothesis awaiting confirmation or refusal by future work. In case of an actin ring functioning as a delimiting device, it is a logical consequence that it should be able to maintain contact to the plasma membrane and at the same time also to the edge of the advancing scale-SDV with the property of increasing the diameter while keeping contact to the growing edge of the SDV.

Together, these hypothetical evolutionary steps would create a mechanism suitable for assembling a cell covering as that seen in the radial centric diatoms.

2.2 The Rise of Areola in Diatom Cell Wall

The areolate chamber is the typical structural unit composing all types of the diatom cell wall, which does not appear in the silica products from other organisms. Although it is known that the porous patterns of diatom cell wall in the two dimensional plane is dependent on different types of organic materials for the self-assembly of silicification, no one knows how the three dimensional areolate chamber is formed. Is there a common developing process of the areola formation among different diatoms?

Until now, the depositing direction of silica in the cell wall formation has been reported in several diatoms, such as *Ditylum* (Li and Volcani, 1984, 1985a), *Odontella* (Crawford and Schmid, 1986), *Aniphleira* (Stoermer et al., 1965), *Navicula* (Edgar and Pickett-Heaps, 1984), *Pinnularia* (Pickett-Heaps et al., 1979a) and *Sthatella* (Roth and De Francisco, 1977). Since this aspect varies in different diatoms, it is considered as a new criterium for taxonomy (Li and Volcani, 1984).

In most centrics, the silica is deposited towards the “biological outside” (defined by Crawford and his coworker) of the silica structure within the SDV (Crawford, 1990; Crawford and Schmid, 1986). For instance, in the radial centric diatom *Coscinodiscus wailesii*, after the development of the middle lamella (trabecular layer) under virgae, silica is added upwards to complete the upper roof (tectum) (Schmid, 1994). In contrast, the silica deposition of the bipolar centric diatom *Odontella sinensis*, goes towards “the biological inside” (Crawford, 1990; Crawford and Schmid, 1986), which agrees to the current study that the middle lamella (i.e., trabecular layer) under the roof virgae grows first, followed by the development of tectum and that of basal layer (Fig. 32).

Whereas, in the raphid pennate diatom species *Achnanthes longipes*, silica is added to the upper side of the middle lamella (trabecular layer), building the virgae and young trabeculae and then filling virgae into a tectum. In other raphids such as *Navicula sp.* (Edgar and Pickett-Heaps, 1984) and *Pinnularia sp.* (Pickett-Heaps et al., 1979a; Schmid, 1994), silica is added to both sides of the middle layer.

Obviously, the common point of the cell wall construction in diatoms is that they all first develop the middle layer — the trabeculae associated with virgae. The advantage of building this layer first is that these pillars create a physical condition for the process defined by the Reverse Ostwald Ripening Mechanism, so that embossments in the hexagonal pattern under the tectum or alternatively, big holes in micrometers (like foramina in *O. sinensis*), can be controlled in the same size (see Section 4.2.3.3 in Chapter 1).

3 Involvement of the Cytoskeleton in Valve Morphogenesis

3.1 The Geometry Pattern of the Valve Head Plate

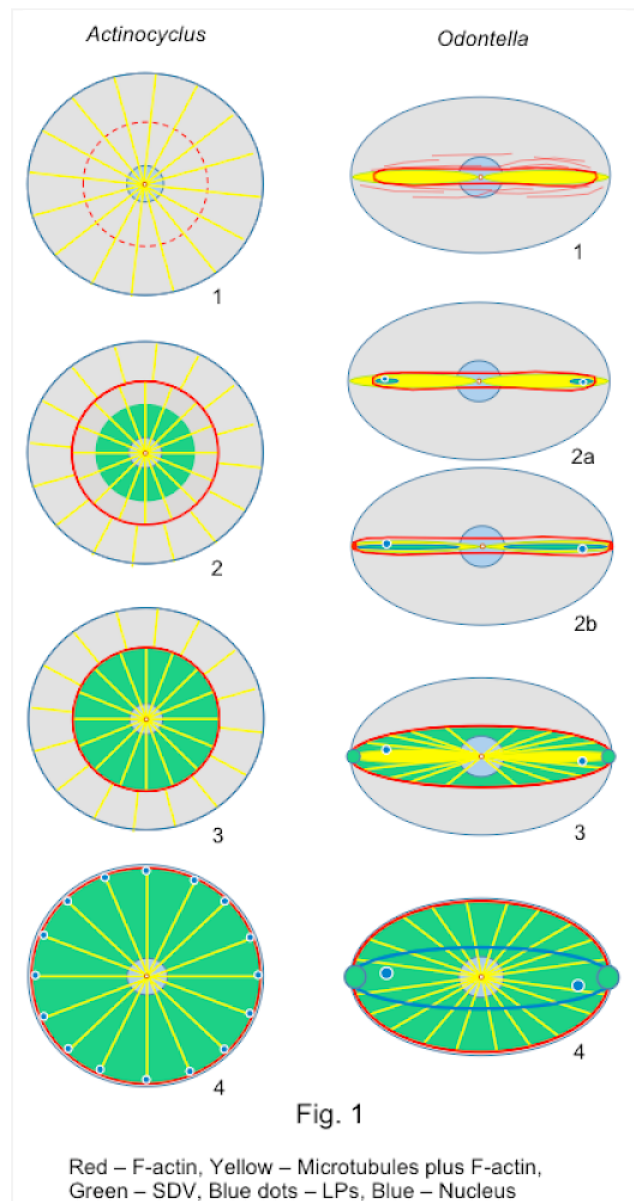
The genus *Odontella* belongs to the group of bipolar centric diatoms⁷. Its apical portion of the valve, called "head plate" here, bears the morphological features typical for this genus: an oval front face encircled by an embossed ridge, sometimes with a slight depression in the middle, two horns (ocellate elevations) at the outermost edges of the oval and two long spine-like LPs inserted somewhat inwards from the horns.

In this genus, two initial valve-SDVs sitting on the apical region of the daughter protoplast begin to form the head plate. They expand and then fuse into one unit, which quickly gets wider from the head plate downwards until it abuts against the inside of the mother frustule. Hence, the final diameter of the daughter hypovalve is dictated by the size of the mother frustule. The new valve is formed exactly alike that inherited from the mother valve (i.e., the epivalve of the daughter cell) and then the two valves are separated away by four wide girdle bands so that the cells are much longer than wide. Due to the oval cross section, most micrographs show cells lying on their cylinder face (girdle band view). Whereas, some other polar centrics, as well as

⁷ Bipolar centric diatoms means their valves present two symmetrical poles in the shape of an ellipse. Multiple polar centric diatoms means their valves present more than two symmetrical poles which result in polygon shapes of the valves. Monopolar centric diatoms present one high pole pointing out from the valve surface, whose cross section is evenly round. In radial centric diatoms, the valve face is evenly round.

some radial centrics are wider than long. Therefore, micrographs show these cells generally head-on (valve view).

As already mentioned, it is undisputed that the radial centrics are ancestral to the bipolar centrics, which in turn are ancestral to the pennates (Medlin, 2016). By comparing the configurations of the perinuclear microtubule cytoskeleton between the two groups in the centrics, it is becoming clear that the bipolar symmetry of the head plate in *Odontella* can be deduced from the overall radial symmetry of the centrics by drawing together the two opposite halves of the radial MT-system into the two massive MT-bundles extending oppositely from the MC (Fig. 1). A second determinant for creating the bipolar symmetry is the way, how the valve actin ring (red circle in Fig. 1) is modified as a consequence of the changed MT-system. How early the actin ring actually forms in the radial centrics was not determined in the current study. It is, however, clearly visible, when the daughter valve-SDV reaches about half the diameter of the mother valve before the edge of the initial SDV has reached it (see stage 2 in Fig. 1; Figs.7.6A & 7.11 in the Appendix). Very early stages of the valve actin ring have been presented in fine structural work by others, however, not in a centric but a pennate species, *Navicula cuspidata* (Edgar and Pickett-Heaps, 1984). In *Odontella*, the actin ring has not been described earlier than in the study by Zhang (Zhang, 2012); the assembly of the actin ring begins very early after cytokinesis before the occurrence of the two initial SDVs (see stage 1 and 2a in Fig. 1; Fig. 11 C – F in Chapter 2).

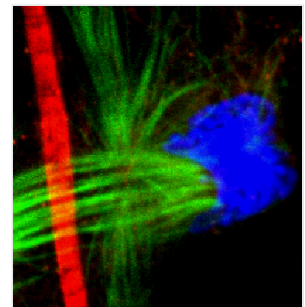


In the radial centrics and also in the pennates, the geometrical center of the initial valve SDV appears to depend on the position of the MC, which is stacked between the plasma membrane and the nucleus. As discussed in Chapter 2, the MC of the daughter is derived from the PC of the mother. I.e, it reappears, when the polar plates of the late telophase PC get decomposed (Pickett-Heaps et al., 1990). Pickett-Heaps and co-workers have suggested in the case of the monopolar, centric diatom *Ditylum*, that when the MC moves together with the nucleus away from the apical cell pole of the recently formed daughter cell, a remnant of the decomposed polar plates of the mother spindle is left behind close to the plasma membrane and they also have suggested that this is the region, where the initial daughter valve SDV forms (see (Pickett-Heaps et al., 1990) Fig. 76 on page 126). More work is required to clarify this point, but if it holds true, it offers a chance to give an explanation for the bipolar placement of the two initial SDVs in the genus *Odontella* (see Section 3.3 below). And it could as well explain the origin of multi-polarity seen in other centrics such as *Lithodesmium* or *Triceratium* (Medlin, 2016).

If it is true that there are two or more initial SDVs always alongside with the corresponding MT-bundle arms in bipolar or multipolar centric diatoms, the conclusion would be that the number of initial SDVs/MT-bundle arms can be predicted according to the number of the valve poles.

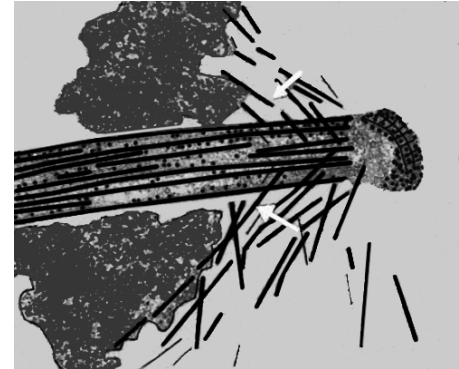
3.2 Possible Origin of the hb-MTOCs

The two ocellate elevations (horns) are typical, morphological structures of the genus *Odontella*, the development of which relies on the system of microtubule horn bundles. But different to the usual MT-initiation spot like the MC, the microtubules of the system originate from two hb-MTOCs, which are located at a point somewhat inwards from the distal ends of the central spindle. The formation of this system occurs at telophase: two arms of MT-bundles initiate from each hb-MTOC and elongate along the cytokinetic actin ring; eventually, each arm of the MT-bundle will converge on a point in the cell periphery and next will protrude out from the protoplast surface functioning as an inner scaffold of the prospective horn (see Chapter 2).



The appearance of the hb-MTOCs raises questions: It is a unique cytoskeletal configuration, which has not been seen in other centric diatoms studied so far (see Fig. 2 above, taken from

Fig. 22d₂ of Chapter 3). Further, the mere phenomenon that new microtubules are initiated from within the central spindle appears to be novel for any type of mitotic spindle. It can only be speculated that the polar plates of the spindle in *Odontella* get separated as it occurs in the pennate diatom *Surirella ovalis* at anaphase (see Fig. 3, from Fig. 38b (Tippit and Pickett-Heaps, 1977)); then each polar plate may be split into two parts, one remaining associated with the newly forming daughter nucleus and eventually becoming the MC (see Fig. 4 below), and one lagging somewhat behind on the central spindle becoming the hb-MTOC.



It must be acknowledged that the suggestion regarding the fragmentation of the spindle poles at the end of mitosis is not new. There was an observation made by Pickett-Heaps a long time ago that the spindle poles of the centric diatom *Ditylum* at anaphase separate into several structural components, one of which is associated with the future LPA of the initial SDV (see Fig. 76 on page 109 of (Pickett-Heaps et al., 1990)). This leaves the option for the situation here in *Odontella* that other components, i.e. those that give rise to the hb-MTOC, may also separate, but move a small distance back from the spindle pole towards the center where they express or acquire the hb-MTOC function.

There is also an alternative explanation possible, i.e., this hb-MTOC might be the remnant of the polar initiation region of the kinetochore fibres, which were formed earlier in the spindle development and then disappeared, when chromosomes have reached the poles. It is just a coincidental observation, but this region appears to be less well defined in the diatom spindle than in spindles of other cell types. At least this much is seen in electron micrographs such as those in the early work of Tippit and Pickett-Heaps (see Fig. 3 here, re-drawn as overlay from Fig. 15 in (Tippit and Pickett-Heaps, 1977) to allow a direct comparison with the confocal image Fig. 2). The EM image is taken from an anaphase spindle in the pennate diatom *Surirella ovalis* and it shows that the kinetochore microtubules (kMTs) originate from a broad collar region somewhat inwards from the actual spindle pole at anaphase (pointed by the two small arrows in Fig. 3) (Tippit and Pickett-Heaps, 1977). It would be this collar region that roughly matches the position of the hb-MTOC in the *Odontella* spindle (Fig. 2). Therefore, it is a possibility, which however currently has no additional support from other work, that a convergent center of kMTs may occur at this region and turn into the hb-MTOC in *Odontella* at late telophase, by initiating a second population of microtubules, which however, in the absence of any available anchoring

points (no kinetochores present anymore) begin to radiate further out and reorganize into bundles.

The function of the horn bundles in *O. sinensis* may be two folds: First they provide the scaffold and mold the cytoplasmic protrusions for the development of the horns; second they help to position the initial silicification sites, which are associated with the initiation of the LPs (proved by the Oryzalin results, see Discussion 4.1.3.2.1 and 4.1.3.2.2 in Chapter 3). The molding of the horns by the MT-bundles appears to be a straight-forward-interpretation, whereas the positioning of the LPs requires further considerations. In agreement with the early work cited above, it is proposed here that the determinants for the positioning of the initial silicification sites in *Odontella* are related with components coming off from the original polar region of the spindle.

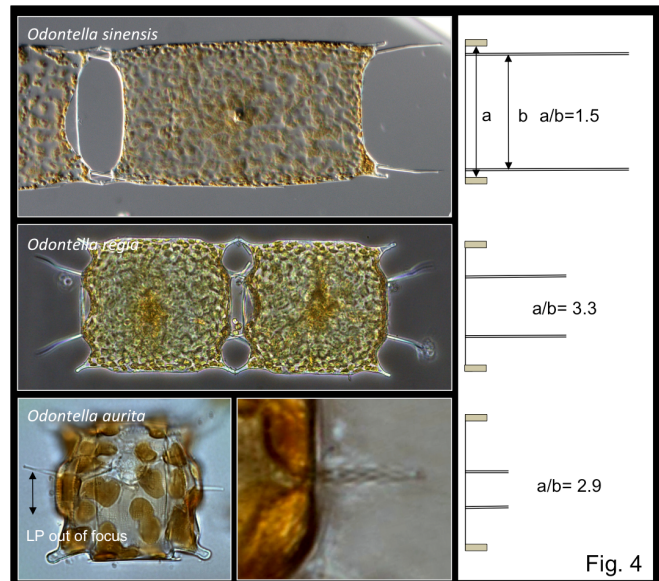
3.3 Placement of Initial SDVs

3.3.1 A Comparison among Bipolar, Monopolar and Radial Centrics

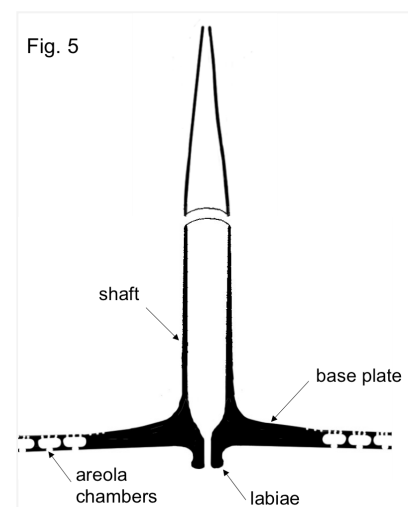
It is obvious that these split-off remnants of the PCs must have affinity to microtubules, because the mitotic spindle pole itself definitely has this property, and it is conceivable that this PC material can get transported along microtubules. Looking at the situation in *Odontella*, such a mechanism could give rise to the pair of initial SDVs placed along the pair of horn-bundle-arms, which give rise to the annuli. The only question remains, as to how their positioning to a certain point along the horn bundles is determined. One assumption appears to be safe that the symmetry in the placement of the initial SDVs is dictated by the symmetry of the horn bundles. But what determines the distance?

Since it has been suggested, based on the EM observation of fine structures in *Odontella sinensis* and *Odontella aurita* (Li and Volcani, 1985b), that the annuli, from which the base plates of the LPs are formed, are the primary silicification sites, the reverse conclusion should also be valid in this genus, i.e., that the LPs can reveal, where the initial SDVs were positioned. In the three *Odontella* species (Fig. 4, samples were collected from Helgoland), it turns out that the positioning of LPs is species-specifically different (Note that in the case of *O. aurita*, the orientation of the two LPs on one valve of the cell is opposite to the other, so that the orientation of LPs on a valve may not be in the same plane as the other, like that shown in Fig. 4). That means, the placement process of SDVs is under genetic control. It should, however, be

mentioned that there is a slight plasticity in the geometrical features of LP insertion. This is a frequent observation made in the current study on *Odontella sinensis*. The plasticity could be due to the culturing conditions, because twin LPs coming off the same base were observed once in a while on one side of the head plate but not on the other and sometimes horns were crippled on one side but not on the other. This kind of plasticity did not occur in samples collected from the sea.



Obviously the initiation site/location of the LP is associated with the primary silicification site where usually the annulus is formed, but the LP location is not identical with the site (see discussion in (Pickett-Heaps et al., 1990)). In the monopolar centric diatom *Ditylum brightwelli*, the silicification starts out as a siliceous ring (circular annulus) at the center of the valve face. And a labiate process apparatus (LPA) situated under the center of siliceous ring is developed as a differentiation of the lower silica lemma at the same time, followed by the expansion of base plate from which next the LP shaft extrudes out; the LPA will disappear after the maturation of the LP ((Li and Volcani, 1985b), for the structure of LP see Fig.5). Next the SDV spreads centrifugally from the base plate-annulus complex to form the valve head plate with a geometrical pattern ranging from triangular via star-shaped to round depending on the genotype of this species (see Fig. 7 in the Appendix) and continues over the rest part of the valve. There is as yet no confirmation from other work for the presence of an actin ring at the developing edge of the valve SDV in *Ditylum*, though the assumption that it must exist would be in line with all other observations discussed here. So in the monopolar centrics (e.g., *Ditylum*) and the bipolar centrics (e.g., *Odontella*), the LP location and the primary silicification site are combined together within a unit in the same spot.



This situation is apparently different in the radial centrics, where the LP location and the primary silicification site are not at the same spot (see Fig. 1). The existence of the circumvalvar actin ring has been observed by means of fluorochrome labelled Phalloidin in *Cyclotella* and *Coscinodiscus* (Tesson and Hildebrand, 2010a, 2010b) and this is now confirmed on the basis of the immunofluorescence data on the radial centric diatom *Coscinodiscus sp.* and *Actinocyclus sp.* (presented in Figs. 7.1C, 7.3E, 7.6A, 7.7B₁, 7.10B, 7.11 in Appendix). So in this group of radial centrics the LPs (also termed “rimoportulae” in the radial centrics) are, unlike the situation in *Ditylum* and *Odontella*, located far away from the primary silicification site, which is at the center of the valve. They are inserted at the outermost edge of the valve face (blue dots in Fig. 1, left row, stage 3).

Based on these aspects, one can conclude that the primary silicification site of the SDV is not equal to the initiation site of the LP, which is dependent on the site of the LPA (Li and Volcani, 1985b). And this view can also be proven by the Oryzalin results on *Odontella* (Chapter 3), where silica in the form of roundish annular islands is deposited in the SDV in the protoplast surface without any LPs extruding out from it. Therefore, the annulus on its own does not initiate the LP. It requires additional information/cues (e.g., LPAs), which gets destroyed by the absence of either microtubules or actin filaments nearby.

In agreement with data from Tesson and Hildebrand on *Cyclotella* and *Coscinodiscus* (Tesson and Hildebrand, 2010a, 2010b), it is shown here for *Actinocyclus* that microtubules and actin filaments run in a radial fashion from the nucleus associated MC in the middle of the forming valve towards the border of the valve surface, where many of them point directly at the positions of the LPs at the margin of the valve (see Figs. 7.1, 7.3, 7.4 in Appendix). The lysosensor data indicate that LPs will be made at the moment when the valve SDV, encircled by the actin ring, has reached the valve margin, which is the maximum diameter of the daughter valve face, where the radiating cytoskeleton bends sharply down by 90° to form the side wall of the valve, and in the meanwhile the entire plane of the actin ring goes down vertically from the apical surface of the valve along the side wall. And since it is known that LPA localization occurs before the silicification (Li and Volcani, 1985b), one can assume that its development proceeds as follows: LPAs as a whole or split into their component parts get transported along radiating microtubules and they get anchored at the edge of the valve surface, although it remains unknown how the anchorage is done. In addition, the other interesting question is, how the LPAs or their component parts are evenly distributed along the circumference of the valve. Both aspects await explanation in future research.

As to the situation in *Odontella sinensis*, the LPA localization also occurs before both the silicification and the actin ring initiation. It has been shown by EM that the initial SDV is associated with the LPA and then the silica is deposited within it, both of which occur already at a time point before the completion of cytokinesis (Li and Volcani, 1985b), even though the lysosensor data presented in Chapter 2 cannot show any discrete fluorescence signal on the newly divided cell surface at this stage (Fig. 11C of Chapter 2), probably because of the low density of silica. Besides, the valve-SDV-actin ring initiates only after the completion of cytokinesis, so it means the LPA localization is not mediated by the actin ring.

The question, how the two initial SDVs are associated with the LPAs in *O. sinensis*, can be answered by understanding how those supernumerary initial SDVs can be formed in the Oryzalin inhibited valve (see Section 3.4 above or Section 4.1.2.2.1 in Chapter 3) and how extra annular SDVs are formed in Phalloidin inhibited valve (see Discussion 4.4.2.2 in Chapter 3) — MT horn bundles act as scaffold and cortical actin filaments guide initial SDVs to the sites of LPAs. Currently the origins of neither the LPAs nor the SDV precursor vesicles are known, but a proposal is made here, how the initial SDVs together with the LPAs get anchored at certain site in *Odontella* (see Fig. 6).

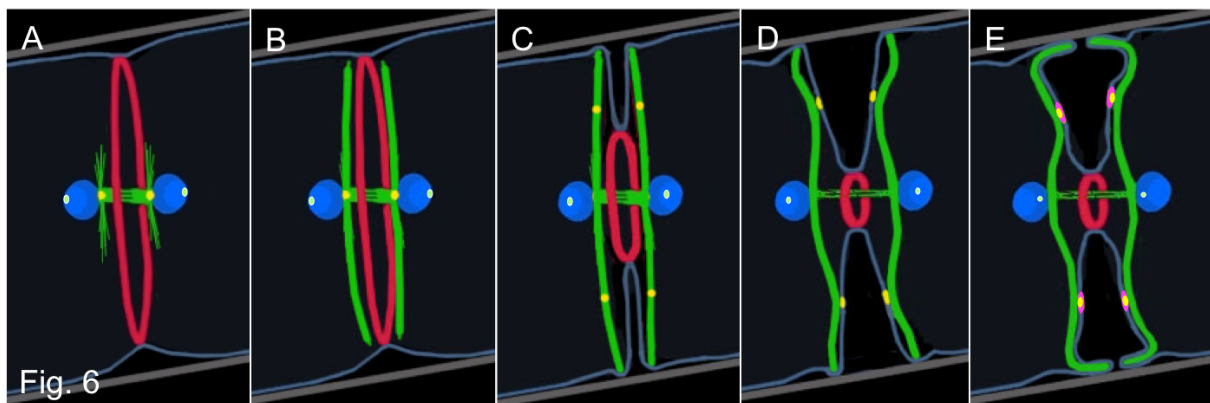


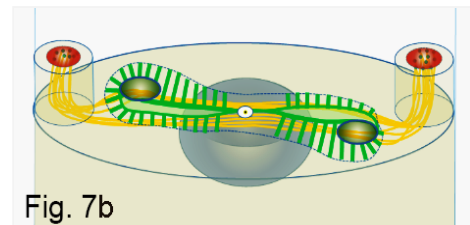
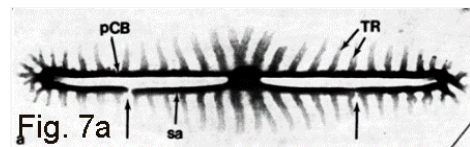
Fig. 6 The hb-MTOCs (A and B, yellow marks, see also Chapter 2, Fig. 10A and Chapter 3, Fig. 22), representing the proximal remnants of the former PC give rise to two new rays of microtubules (A), which extend along the nearby upper bow of the cytokinetic actin band (B). The MCs (white dots) derived from the distal fragment of the former PCs are placed on the distal side of the nuclei becoming the new MCs. As the cytokinesis sets in (C), the LPAs (yellow) are mobilized and get transported outwards along each branch of the horn bundles. In the course of constriction, the tips of the horn bundles intercept with (or come close to) the plasma membrane at the side walls and begin to buckle most likely aided by the retraction of the two daughter protoplasts from one another (D). The remnants of the hb-MTOC or fragments of polar plates separate from the MT bundles as they get associated with the plasma membrane in the cleavage furrow (in analogy with the situation in *Ditylum* see above); each group of remnants (LPA) being attached with an initial SDV (magenta pads), under the guidance by actin filaments;

then each initial SDV will develop an annulus with an LP attached to it. Since the tips of the horn bundles continue to elongate they bend forward (E). This process may further be facilitated by the gradual retraction of the daughter cell poles from one another (E), as has been suggested by Pickett-Heaps; he also proposed that an adhesion of the protruding horn to the inner wall of the mother girdle band could be involved (Pickett-Heaps et al., 1990).

Coming back to the question, how the difference between the three *Odontella* species could be explained, the answer may be that this should lie in subtle difference in the timing of the process, the density of microtubule bundles, the types and the regulation of microtubule-based motors and the like. All of this remains to be explored further in future work.

3.3.2 Comparison of Valve Initiation between Pennates and Bipolar Centrics

The valve geometry is indeed strikingly similar, when comparing the raphe of the raphid pennate diatom *Navicula pelliculosa* (Fig. 7a, reproduced from (Chiappino and Volcani, 1977)) with the head plate of the bipolar centric diatom *Odontella sinensis* (see Fig. 11 of Chapter 1 and Fig. 7b), i.e., two slit like annular rims, positioned to the left and right of a central region (in the pennates this region will develop a central nodule).



This is in line with the notion that pennates have evolved from the centrics (Medlin, 2016; Sims et al., 2006). Further, there are striking examples in the recent araphid pennate diatoms showing ocellate elevations or pseudo-raphe serving as secretory structures for the formation of adhesive stalks or connecting pads (Hasle, 1974; Pickett-Heaps et al., 1990; Round et al., 2007; Wang et al., 2000), and this trait seems to have evolved as a means to allow cell chain formation at the transition from the bipolar centrics to the pennates in the Cretaceous age (Witkowski et al., 2011), when the pennates first appeared.

However, their developing processes of the valve geometry are completely different. It has been concluded that the valve of *O. sinensis* initiates from two opposite SDVs, both of which extend in the central symmetrical way towards the center of the valve (see Fig. 8a), but their

fusion at the middle does not give rise to a nodule. Whereas, the valve of pennate initiates from a SDV, which is located at the center of the valve and give rise a nodule; ribs at the two opposite sides of the nodule extend outwards in a mirror symmetrical way (see Fig. 8b). This cytological detail may be taken as another hint that the intracellular mechanism used for setting up the head plate symmetry has become streamlined in the pennates, i.e., they are more advanced than in the polar centrics.

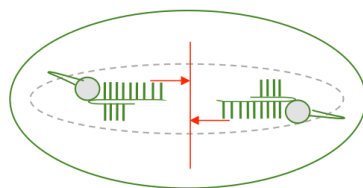


Fig. 8a

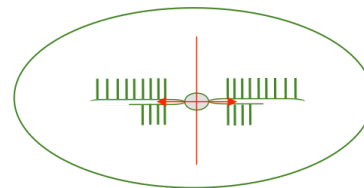


Fig. 8b

It is known that the head plate geometry of *O. sinensis* is governed by the cytoskeleton, shown as the graphic (Fig. 7b)⁸ compiled from the data on the early head plate stage obtained in the current study. And the cytoskeleton organization appears to work in a similar fashion in the pennates, i.e., microtubule bundles that stem from the MC also run along the major axis of the SDV to accompany both sides of the forming raphe slits, which is concluded by reconstructing the three dimensional arrangement of cytoskeletal elements around the SDV according to the EM images of *Navicula* (Chiappino and Volcani, 1977; Edgar and Pickett-Heaps, 1984).

But the difference of developing process of the valve-SDV between the two types of diatoms, suggests the cytoskeleton guidance for the SDV formation would be different: In the genus *Odontella*, the external force for the stretching of the initial SDVs towards the valve center along the MT horn bundles, can be offered by dyneins. Or alternatively, this may be achieved by the actin cytoskeleton in an as yet unknown fashion since actin filaments are distributing along the MT-horn-bundles and the Phalloidin data presented in Chapter 3.4, suggest an involvement of actin (see section 3.4.2.2, Fig. 36 of Chapter 3). Whereas, in the pennate diatom, since the SDV extending direction is opposite, the external force may be achieved by kinesin.

⁸ In this graphic the microtubules are yellow, MC is white positioned on top of the dark-grey nucleus. Silica ribs are green, LP base plates are dark green, the annuli are depicted as two slits to both sides of the nucleus, and the actin patches at the top ends of the horn protrusions are red. The actin ring will assemble along the dotted line around the SDV.

3.4 Cytoskeletal Interactions during Stages of Valve Morphogenesis

3.4.1 Functions of the Microtubules

In the case of the bi- or multipolar centrics two or more SDVs need to be initiated, which subsequently expand to fuse with each other and the advancing edge of the resulting co-joint SDV combines with the actin ring and continues to expand until the valve dome is completed (Chapter 2). Different from the situation of the monopolar centric geometry as seen in *Ditylum* an additional guidance mechanism should be required to exactly place these supernumerary SDVs. In Fig. 1, it was explained how this might work out in the bipolar centrics.

In addition to the structural aspects discussed above, the functional significance of the microtubule system is evident from the Oryzalin experiments, which show that supernumerary annular island-like SDVs spontaneously appear on the valve dome of the drug treated cells at the stage of valve initiation. Without any guidance by microtubules, they start their activity in quite a normal fashion, each with a circular pattern center, the annulus, from the rim of which radially oriented silica ribs are built by self-assembly. This way, cells seem to fall back on the ancestral mode of scale formation discussed above in section 2. Next the SDVs expand until they encounter each other and fuse creating a large convoluted silica domain (for instance see Fig. 5A of Chapter 3). It follows, that the removal of microtubules has no adverse effect on the initiation of SDVs and it also does not prevent SDV expansion and fusion. However, in the absence of microtubules the orderly bipolar geometry is lost, because the SDVs are not initiated at the correct positions and their number is not limited to two per valve.

How are those supernumerary initial SDVs formed? Given the fact that horn bundles were absent and the formation of LPs was aborted, it is reasonable to speculate that a number of LPAs was getting scattered around near the protoplast surface, and it could be these substances, which are at the onset of the daughter cell cycle, are target sites for SDV precursor vesicles to attach, giving rise to individual annular pattern centers. The fact that the sizes of the centrally located annuli were quite variable among these silica islands supports this speculation.

The islands themselves, scattered around on the valve domains in Oryzalin-treated cells, are of variable size. Does this mean that the absence of microtubules affect the regular advancement of the SDV edge? Probably not, because given enough freedom for expansion a

single island can grow perfectly round and quite large, whereas islands remain smaller and become irregular, when the available space is limited. It is very likely that the positioning and efficiency of the valve actin ring is also affected in the sense that its assembly is more or less irregular without guidance by the microtubules and therefore its expansion is irregular. This is quite impressively seen in Fig. 5C of Chapter 3, where an actin ring has assembled but without guidance, so it did not adopt a proper circular shape. The conclusion from this behavior is that there is a spatial interdependence between the actin and the microtubule cytoskeleton, even though it is likely that the assembly process of the actin ring can occur independently of microtubules, its overall shape might be guided by microtubules. Interestingly some of the SDVs extended impressively far-out creating very large silica islands in the absence of microtubules (Chapter 3, Fig. 7A, 14b₁), suggesting that microtubules could function as a brake (drag shoe hypothesis stated in Section 4.1.2.2.1 of Chapter 3) to limit the speed of valve-SDV expansion.

3.4.2 Functions of the Actin System

3.4.2.1 Head Plate Morphogenesis with a Deconstructed Cytokinetic Actin Ring

What happens with regard to valve morphogenesis, when microtubules are left undisturbed but the actin cytoskeleton is deconstructed by pharmacological treatment. As shown in Chapter 3 (Section 3.3), the JAS application causes a severe modification of the actin cytoskeleton and this in turn has consequences on two levels of the valve morphogenesis. One concerns the direct function of actin, which is implicated by the observation that silica deposition is sensitive to JAS at 1 μM concentration (also see Section 3.4.2.5 below), the other is a more indirect effect concerning the interaction between the actin cytoskeleton and microtubules. This gives further support to the conclusion made before (see above) that both systems depend on each other.

This is particularly important in the process of cytokinesis and the early post-cytokinetic stage of valve morphogenesis. Because cytokinesis is dramatically affected by JAS, subsequent steps of valve morphogenesis, which require microtubules are likewise dramatically disturbed. One common feature of all inhibitory phenotypes is that horn bundles in the regular shape do not form in the absence of JAS, although there are plenty of microtubules present (Figs. 28, 29 of Chapter 3). This shows that the cytokinetic actin ring has a guiding function (compare with Fig. 10b₁ and Fig. 8A in Chapter 2); without it, the microtubules cannot adopt a bipolar configuration but instead they form a radial configuration around each of the nuclei. Since the

post-mitotic nuclei are not properly separated from one another, due to the absence of the cleavage furrow, they get drawn back towards each other and their perinuclear domains tend to fuse, forming a giant radiating microtubular array around the two nuclei. In less severe inhibitory phenotypes, nuclei succeed to remain separated from one another, but still the MT horn bundles do not form. Instead, each of the two perinuclear domains begins to set up its own aberrant silica island starting out from misshaped and misplaced annuli (probably two per domain, although that was difficult to see) and eventually both domains fuse and the combined domain continues to grow becoming just one big lateral valve system, which may or may not bear some crippled LPs. This shows the initial SDVs responsible for the formation of the annuli are still formed but without the cleavage furrow, the MT-cytoskeleton around the daughter nuclei does not configure correctly, so that these SDVs do not get positioned correctly and also do not adopt the typical slit-like shape** (Fig. 34 of Chapter 3).

3.4.2.2 Valve Morphogenesis in Cells with an Over-stabilized Actin System

Over-stabilizing the actin system by Phalloidin should produce effects opposite to those obtained by JAS treatment, however, as it turned out, this expectation is far too naive. The reason for this is the configuration of the actin cytoskeleton, i.e., actin networks react differently from actin bundles towards the phalloxin (see Discussion 4.4 in Chapter 3), which shall not be repeated here.

The aspect addressed here shall be the shape of the annuli and the interaction between valve SDV and the valve actin ring. In those few cells, which managed to divide, because Phalloidin was applied without preincubation and late in the mother cell cycle, when division was almost or at least halfway accomplished, valve morphogenesis was still severely affected. The most critical stage of the early valve morphogenesis requiring cytoskeletal guidance again appears to be the generation and placement of the compressed, slit-like shapes of the annuli including the shaping and growth of the LPs. This confirms all the previous conclusions that the horn bundles need the microfilament system to get properly positioned. And if that part fails, the initial SDVs cannot be placed correctly (Fig. 37 of Chapter 3), which gives further support to the above conclusion made in Section 3.4.2.1 (see the double asterisks) that microtubules shaping into bundles requires the microfilament system; in weak inhibitory phenotypes, when they were correctly placed, they had the correct slit-like shape but were oversized (Fig. 36 of Chapter 3)

suggesting a subtle function of F-actin in the very early stages of the initial SDV shaping process. What this function could be, has not been ultimately elucidated in the current study.

The recurring theme encountered in this study is that microtubules and actin appear cooperate with each other. It has been established in the past decade that this type of interaction is very common in eukaryotic cells (Basu and Chang, 2007; Dugina et al., 2016; Goode et al., 2000; Mohan and John, 2015; Pacheco and Gallo, 2016). In the case of annular slit shaping, actin filaments appear to run parallel along the MT horn bundles just in the area, where the annuli are placed. This already suggests a role of the cytoskeleton in the placement of the annuli, which is next supported by the pharmacological effects: (1) The deconstruction of the actin system by JAS leads to an asymmetric opening of the annuli and a loss of symmetry in the placement in the apical valve domain (see Section 3.4.2.1). (2) The Phalloidin effects appear to be in line with this idea, because now the slit shape and the orientation along the horn bundles are maintained, but the slits extend further than in control towards the nuclei, as if the annuli have been further stretched in length along the underlying microtubule bundle co-aligned with actin filaments. This is in agreement with the well-established fact that actin filaments and microtubules can interact in various ways and that the parallel alignment leads to mutual enhancement of both systems (see for instance the summary graphic, Fig. 1D, in (Pacheco and Gallo, 2016)).

3.4.2.3 SDV Expansion and the Cytoskeletal Composition of the Valve Actin Ring

Davis and Hildebrand have speculated that the expansion of the valve-SDV is mediated by microtubules via motor proteins (Davis and Hildebrand, 2010). The umbrella-like distribution of the microtubules would be consistent with such an idea, however, mediation should be exclusively in the aspect of spatial control, rather than in that of the driving force, because the results of Oryzalin inhibition presented in Chapter 3 have shown that the self-assembly of silica in the SDV lumen can autonomously enlarge the size of the SDV with areola rows arranged in a perfect radial fashion.

Nevertheless, one should still think about the possibility that there is an external force mediating the SDV to grow outward and that this is not due to microtubules but to the actin ring. The way how this could happen would not be by the classical model of myosin exerting force along linear actin tracks, but rather by an indirect fashion involving three physically interacting elements: (1) an expandable valve actin ring; (2) a physical link of some kind between the actin

ring and the edge of the advancing valve SDV; (3) a radial microtubule system, where individual microtubules are oriented perpendicular to the actin ring. The attempt to challenge this system experimentally by removing the actin ring was unfortunately not entirely successful in the current study, because the actin ring turned out to be the most JAS-resistant structure in the actin cytoskeletal system (Discussion 4.3.1 in Chapter 3). But the phenomenon of the occurrence of silica depleted regions in the SDV (e.g., Figs. 36A, 37D, 37E and 39A in Chapter 3) seen in the Phalloidin result may point at a solution as to how the actin ring could be involved in the expansion of the SDV. The explanation has been addressed in Discussion 4.4.2.1 of Chapter 3 as the third major type of Phalloidin-induced disturbance and it was interpreted as the consequence of a stretching action of the actin ring on the entire SDV structure, because it is postulated that the ring expands and moves faster down the slope of the valve domain than the speed of expansion of the SDV would allow (e.g., Figs. 36A-1 – 36A-3 from Discussion 4.4.2.1 in Chapter 3). A slight disparity between the two expanding processes may probably be sufficient to have a big effect on the SDV integrity considering the huge size of the valve SDV. We do not know enough yet about the properties of the cortical actin network and whether its function could be to serve as a submembrane scaffold for the SDV, but it is not far-fetched to envision a major change of its property caused by Phalloidin. If the two aspects – a drag on the SDV edge by a speeding actin ring and a change in the scaffold function of the submembrane actin network – come together, the lower silica lemma could be forced to collapse onto the upper silica lemma thus decreasing or even abolishing the internal luminal space.

The characteristic of the valve actin ring that it can modulate its circumference suggests its cytoskeletal composition contains myosins, like that in the cytokinetic actin ring. This suggestion can be supported by the evidence from the NEM inhibition that a prominent constriction at the edge of valve-SDV after the NEM inhibition (Fig. 4.3.16 in the Appendix), where myosins are forced to be in a rigor state (Karlsson and Lindberg, 1985). However, this suggestion is not to say that both rings are in the same composition (see Discussion in Chapter 2), but the valve actin ring should be able to adjust the filament length on the one hand and the internal circumferential tension on the other.

3.4.2.4 Role of the Distal Actin Patch in the Formation of the Ocellar Plate

SEM images in Chapter 1 (Fig. 18a₃) have shown that horns at the early stage of valve morphogenesis are open at the tips, while the shaft of the horn is fully silicified. In the result of

control cells (Section 3.3 of Chapter 2), a patch is immuno-labeled by anti-actin (C11) which appears at each tip of the MT horn bundle (Fig 11e of Chapter 2), and then disappears, when the horn formation is completed and the bipolar MT system transforms into a radial system for the development of the shoulder of the valve dome.

The fact that open horns have not been spotted in PDMPO stained samples of normal cells can only mean that this developmental step is very short, which reduces the chance to see that. Cells treated with Phalloidin however, regularly show this phenomenon (see Figs. 36C, 37A in Chapter 3 and Fig. 9 in this section), which can only mean that the process is greatly slowed down. Similar effects can be achieved by using myosin inhibitors NEM (N-ethylmaleimide, Fig. 4.3.16 in Appendix), BDM (2,3-butanedione monoxime, Figs. 4.3.1 – 4.3.2), or Blebbistatin (Fig. 4.3.7). The interpretation here is that the SDV membrane in normal cells slowed down because it is forced to expand more slowly through the maze of a knotted meshwork of actin filaments eventually creating a porous silica plate. In Phalloidin treated cells as well as in cells treated with myosin inhibitors, the actin network may tend to become a dense uniform pad rather than a knotted network with free spaces between the knots, so that the silica lemma is stalled. The formation of dynamic actin networks is well studied in animal cells and with computer simulations, it has been possible to visualize how bipolar myosin-II filaments drive the reorganization of an actin/fascin network leading to the emergence of aggregated clusters, i.e. knots leaving spaces between them (Köhler et al., 2011), which demonstrates that relatively few molecular components are sufficient to generate such patterns in an actin network.

Hence it is a model, worthwhile to be followed in future studies to test, whether the actin patch at the tips of the horn may have a function in molding the detailed structures (pores and knobs) of the ocellar front plate of the horn and whether by Phalloidin induced over-stabilization, the actin filament network is becoming too rigid for the dynamic interaction between silicalemma and actin filaments in the course of the molding process (see also Phalloidin Discussion 4.4.2.1 in Chapter 3).

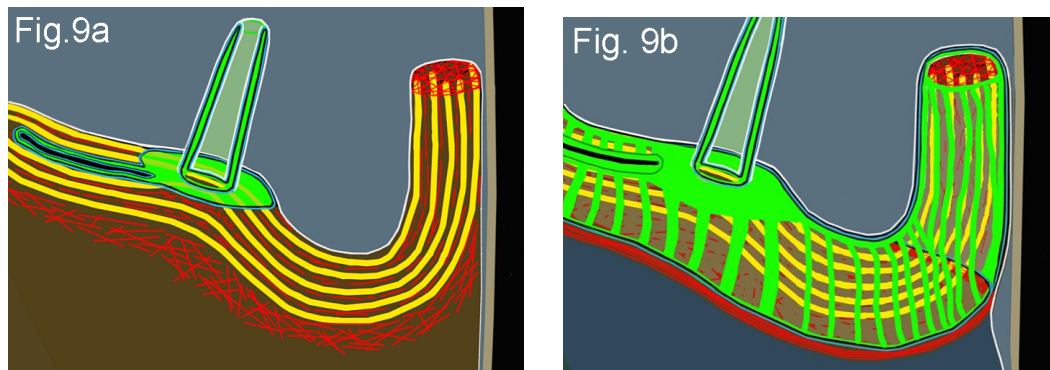


Fig. 9 The initial SDV forms the LP base plate and the compressed annulus that grows towards the left and the as yet short LP growing out from the base (a). Imagining that the cell nucleus is placed to the left of this initial SDV, the second initial SDV would be further to the left in centro-symmetrical configuration. The two initial SDVs extend along the horn bundles until they meet in the middle above the nucleus, where they fuse (not shown here) and they extend further towards the sides flowing around the shafts of the protruding protoplasmic sleeve of the horns until they reach the top ends with the actin patch (b). As the SDV extends, silica ribs form first within the SDV, shown here as green stripes, which then get filled in by further silica deposition as described in Chapter 2. The way how microtubules terminate in the actin patch opens a number of options, how cofactors, such as crosslinkers and motors could be transported and targeted for the dynamics in the patch (see Phalloidin Discussion 4.4.2.1 in Chapter 3).

3.4.2.5 The Credibility of the PM-MFN-SDV Model

In Discussion 4.3.2 of Chapter 3, the premature deployment of SDV in the presence of $1 \mu\text{M}$ JAS raises the attention on the role of actin filaments in stabilizing the membrane structure of the SDV during silica deposition. A **PM-MFN-SDV model** has been proposed to suggest that a microfilament network (MFN) is developed between the plasma membrane (PM) and the upper silicalemma of the SDV, which restrains the frustule component within the SDV from premature exocytosis.

However this model suffers from the disadvantage that the upper silica lemma and the plasma membrane are so closely stacked upon each other that there is apparently no free space between them to harbor an actin filament network (see images in Chapter 1). These features make the PM-MFN-SDV model derived from the architecture of the nerve terminal (Nelson et al., 2013) rather impossible. Looking for a better suited model, one would rather think of the cell-cell adhesion sites in animal tissues, facilitated by transmembrane protein connectors for instance those of the e-cadherin type (Niessen and Gottardi, 2008), or an even

better model would be the plasma membrane-ER (PM-ER) contact sites known from all eukaryotic cells (Saheki and De Camilli, 2017), for the convenience named **PM-ER contact site model**, which are mediated by a number of different types of protein connectors including ion-channels. Another fitting feature is that the type of organelle involved in plasma membrane adhesion is directly comparable with the situation in the diatoms, only that SDV needs to be replaced by ER⁹, for the convenience named **PM-SDV contact site model**. One recent finding, which makes this model even more attractive, is that an actin filament network is located underneath the ER, which functions as a scaffold platform for the cross-talk of cytoplasmic signal factors with an ER-luminal signal mediator (van Vliet et al., 2017). And therefore, applying this model to the situation in diatoms the location of the actin filament network should rather be underneath the SDV.

Although there is no visible evidence here for the actin network underneath the SDV of *O. sinensis*, which might either have to do with a fixation problem, or such an actin filament network is usually too fine to be seen in the ultrathin sections, unless the filaments are very regularly organized like that observed in the silica lemma of the centric diatom *Chaetoceros* during setae morphogenesis. Setae are very long cell processes, which get stabilized with a ribbed silica wall, while they are still extending outwards. Between the ribs, Pickett-Heaps and coworker have identified periodic arrays of very fine filaments in the size range of actin filaments at the inner lining of the SDV-membrane (Pickett-Heaps et al., 1994). Similar situation could be present in other diatom species but obscured by the lower degree of order.

The idea that actin filaments assemble on the cytoplasmic side of the SDV is already about 30 years old (Robinson and Sullivan, 1987) and it has been proposed that the organization pattern of actin may influence the silica macro-pattern developing inside the SDV (Hildebrand and Lerch, 2015; Robinson and Sullivan, 1987). And this idea is still attractive today and on the whole, it appears to be promising to follow the guideline provided by the PM-SDV contact site model, when designing future experimental approaches for the elucidation of interactions among plasma membrane, SDV and microfilament model (**PM-SDV-MFN model**) in the diatoms.

⁹ The origin of the SDV from any specific endomembrane compartment is still unresolved, candidates are Golgi, ER or endosomes.

4 Dynamics of the Cytoskeleton during Girdle Band Formation and Axial Expansion

4.1 Tensional Force Centers on the Nucleus not on the MC

On the basis of the data obtained in the present study, the tension equilibrium model has been developed to explain how girdle band formation is integrated with the generation and release of axial tension (see Fig. 16 of Chapter 2 for details). The instrument for tension generation is the interaction between the perinuclear microtubules and the actin cable system (also see the drag shoe hypothesis stated in Discussion 4.1.2.1 of Chapter 3). Radial perinuclear MT arrays are common in animals and yeast, where the centrosome or the spindle pole body, respectively, serves as an organizing center (Bornens, 2012), whereas, different from plants, cortical MTs not connected to the centrosome are basically absent. The same principle organization is found in the brown algae, where, however, the centrosome duplicates early in the cell cycle so that two prominent MT-asters emerge from the nuclear surface long before mitosis (Katsaros et al., 2006). Green algae may also feature radial perinuclear arrays during certain stages of the life cycle. One classic example is the cyst stage in the dasyclad green alga *Acetabularia* (Menzel et al., 1996). Even higher plants maintain MT-organization centers on the nuclear surface in specialized cell types (Otegui and Staehelin, 2000; Smirnova and Bajer, 1994), but also in regular plant tissue (Baluška et al., 1996; Hepler and Hush, 1996). It has even been shown that isolated plant nuclei are capable of nucleating microtubules in-vitro at their surface (Stoppin et al., 1994). In contrast to the situation in all the non-green organisms listed above, however, lower and higher plants are famous for their cortical MT-systems, which play a role for cell wall formation (Deinum and Mulder, 2013; Paradez et al., 2006). Such cortical arrays are completely absent in the diatoms as studied so far.

The question that should be considered here is, what kind of role the MC plays in the interaction between microtubules and the actin system. This point is raised here because of the importance, which some researchers have placed on the MC in guiding the post-cytokinetic migration/repositioning of the nucleus, suggesting that traction force might be involved (Pickett-Heaps et al., 1990; Tippit and Pickett-Heaps, 1977).

With the exception of mitosis and the horn bundle stage, the MT-cytoskeleton in *Odontella* is organized as a radial array around the nucleus during the major part of interphase (see Chapter 2). The primary organization center appears to be the MC attached to the nuclear surface, which appears to take control from mid-horn bundle stage through interphase. However, during interphase the majority of MTs does not converge on the MC but is attached all over the nuclear surface, onto which MTs appear to converge in many smaller nodes, suggesting that secondarily, the nuclear surface has adopted MT-organizing properties. This creates a cage-like MT structure around the nucleus plus a massively bundled MT-root, which emerges from the cage. This solid mode of MT anchoring constitutes a highly useful architecture, because the nuclear surface as a whole will be able of bearing tensional forces much better than the MC alone.

The existence of tensional force has become clear in the Phalloidin treated cells, when the microtubule cage around the nucleus became rearranged in some cells and all perinuclear MTs became reattached to the MC. The consequence was, that the MC was lifted off from the nuclear surface (Figs. 40C, 41 of Chapter 3). This is a massive effect, which however cannot be explained by tensional force alone, but must involve a dramatic rearrangement of MTs from the nuclear surface back to the MC. The reason for this could be seen in the dual role of the MC, organizing both the microtubules and the actin filaments (discussed detailedly in Section 4.4.3.3 of Chapter 3). However, if both cytoskeletal polymers are left undisturbed, the affinity of the microtubule system to the nuclear surface outweighs or even exceeds the affinity to the MC. Phalloidin on the other hand strengthened the actin cable system, which gets exceedingly focused on the MC, and this in turn stabilized microtubules coming off the MC and tension eventually causes the MC to be plucked off from the nuclear surface. Indeed, the MC shares this feature of attracting microtubules as well as actin filaments/bundles with the animal centrosome (Farina et al., 2016), which supports the scenario outlined above.

4.2 The Girdle Band Actin Ring

In addition to the axial actin bundle system and the cytokinetic actin ring in the cleavage furrow, another circumferential actin ring is present in association with the advancing edge of the valve SDV and in association with the advalvar (facing the hypovalve) edge of the forming girdle band. This is clearly shown here for *Odontella* and together with some reports on other diatom species, which is suggested that this type of actin ring could be a unique feature in the diatoms

and it probably is, when conceived together as a functional unit with the expanding SDV during the stages of frustule morphogenesis (see Fig. 16 in Chapter 2).

In valve morphogenesis the actin ring begins to assemble at about the time, when the valve head plate is nearing completion (see Chapter 2). Its major function may be seen it confining the advancing edge of the valve SDV and controlling its further expansion down the slope of the apical dome. At completion, the bottom edge of the valve has arrived at the junction between eGB2 and eGB1 and this is the position, where the actin ring is locked into place throughout girdle band formation.

4.2.1 The Role of Chimeric Chitin Synthases in Anchoring the Actin Ring

From the lysosensor data obtained on the frustule morphogenesis of *Odontella* combined with immunofluorescence and the WGA labelling data, the hypothesis was developed (see discussion in Chapter 2, Fig. 17) that anchoring the GB-actin ring underneath the junction between eGB1 and eGB2 could be due to the activity of an unusual, chimeric form of chitin synthase, which has been discovered in a genomic study on the centric diatom *Thalassiosira* (Durkin et al., 2009). Provided that the *Odontella* genome contains similar genes, which is likely given the close evolutionary relationship between bipolar and radial centrics, the proteins encoded by these genes may take a center role in the mechanism of axial cell expansion. The unique domain structure of some of these chimeric proteins allows them to potentially interact with the underlying actin ring by an N-terminal myosin motor domain on the cytoplasmic side of the plasma membrane, while the C-terminal chitin synthase domain on the luminal side of the SDV or on the extracellular face of the plasma membrane is engaged in spinning out chitin fibers. Given the highly conserved nature of frustule construction in the diatoms (i.e., two valves separated by a number of girdle bands), it is legitimate to assume that the way, how girdle bands are made in the SDV, deployed on the cell surface and adhered together by chitin containing adhesive material is highly conserved in the diatoms (see discussion in Chapter 2).

It is also an interesting finding that the presence of chimeric chitin synthases is not unique to the diatoms. Chimeric myosin-chitin synthases have been discovered in *Aspergillus* (Fujiwara et al., 1997) and were subsequently found in many plant-pathogenic fungi such as those of the genera *Fusarium*, *Ustilago* and the like. They even occur in bivalve mollusks (Weiss et al., 2006). In the filamentous fungi, chimeric chitin synthases always occur together with regular types of chitin synthases and beta glucan synthases in the membranes of secretory vesicles, at

the hyphal tip and at the sites of septum formation. The chimeric enzymes contribute to chitin cell wall formation but are not essential for it. However, they are most important for proper septum placement and also the efficiency of the pathogen attack very much depends of the presence of the chimeric myosin-chitin synthases. The myosin domain in these proteins does not have to do with long distance actin-based transport but instead, it is needed for the anchoring of the secretory vesicles at the intracellular target site, which in turn promotes secretion at these sites (Treitschke et al., 2010).

Cytokinesis and septum formation has not been studied in detail in the hyphae fungi possessing the chimeric chitin synthases but studies on the fission yeast could fill in some information relevant to this topic. In the fission yeast it has been shown that a special isoform of beta-glucan-synthase, Bgs1p, is delivered from the Golgi to the future division site, where it is thought to help anchor the contractile actin ring operating during cytokinesis (Arasada and Pollard, 2014). It must be pointed out that, although Bgs1p does not have a myosin motor domain itself, its function does depend on myosin II (Myp2p), to which it is bounded via a protein complex consisting of actin-binding and membrane-binding proteins (Arasada and Pollard, 2014; Ge and Balasubramanian, 2008). As soon as Bgs1 with the accompanying protein complex including myosin is installed at the cleavage site, the ring begins to contract and linear beta glucan chains are delivered into the extracellular space becoming the primary septum. This process is smoothly choreographed so that constriction of the ring and the closure of the septum proceed at the same speed and at exact cross-sectional geometry (Davì and Minc, 2015). If one of the molecular partners is experimentally interfered with, for example Bgs1 or one of the proteins in the associated protein complex, the actin ring gets displaced and the septum may either not form at all, become deformed or aborted (Arasada and Pollard, 2014).

These observations can be used to complete the picture and explain, how potentially the anchoring of the GB-actin ring might work in *Odonella*. The shared principle here is that glucan/chitin synthesis is intrinsically linked with anchoring to the underlying actin ring at the site of septum formation. This is a fascinating mechanism serving as a role model for the future work on actin ring positioning in *Odontella*.

4.2.2 Secretion of Chitin Fibres when the Axial Expansion is Inhibited

A very unusual observation should be briefly mentioned here, which appears to be relevant to chitin secretion. When the axial expansion is blocked by myosin inhibiting drugs, such as BDM, NEM and Blebbistatin (Bond et al., 2013), barely visible thin fibres become secreted into the outside medium (see video series #5–7 in Appendix). These fibers have never been seen in the medium, when other cytoskeleton structures are inhibited or by any other treatment. The fiber secreting organelles, the composition of these fibers, the reason why they are secreted and the secretion mechanism, all of this is not yet known.

Regarding the cellular location of secretion, it appears likely that fibres come out from the entire cell surface rather than a specific site. They are likely excreted through pores on the cell wall (see mentioned videos). It is shown in Chapter 1 that the frustule has smaller pores and a kind of bigger pores are also seen in the SEM (see Fig. 5a₂, 9E, 11c₂, 12D in Chapter 1). The bigger ones should be the candidates for chitin secretion, whereas the smaller ones, which are inserted at a higher density in the frustule wall, might be better suited for the exchange of small molecules and gasses between intra- and extracellular environment. The big question is, why chitin fibres are driven out through pores, when myosin is inhibited, whereas they are secreted into the extracellular space between the protoplast surface and the inner surface of the frustule in uninhibited cells, particularly strongly at all junctions between frustule parts (the overlap between epi-and hypotheca and the overlaps between adjacent girdle bands). The reason for this phenomenon may have to do with the fact that myosin inhibition leads to an inhibition of axial cell expansion, and because of that there is no increase of the cell surface, which would provide sufficient space in the gap between frustule and protoplast surface to accommodate the secreted chitin fibres. Future work will have to clarify this point.

5 The Diversity of Circumferential Actin Rings

5.1 For Adhesion

Circumferential actin rings as such are not as rare in the eukaryotic realm as one would think. Most of these appear to be modifications of the same general principle encountered in the

contractile cytokinetic actin ring, but not all. There are several examples of actin rings known from different cell types.

For instance, the adherens junction (zonula adherens) is very common in animal epithelial cells. It is a closed, circumferential ring of actin filaments together with associated proteins in each cell separating the apical domain from the rest of the cell body (Yonemura, 2011). Since this type of actin ring links-up through the plasma membrane with extracellular proteins via the transmembrane proteins (E-cadherin) and because it generates circumferential tension by means of non-muscle myosin II, it may serve as a role model for the construction of the valve- and GB-actin rings in *Odontella*. One only needs to replace E-cadherin by **chitin synthase**.

E-cadherin is attached to the actin ring in the zonula adherens either by the actin binding proteins, vinculin, or by myosin VI (Breshears and Titus, 2007). The latter is the type of scenario similar to the one postulated here in the diatoms, where the N-terminal myosin motor domain of the chimeric chitin synthases could serve this function (see also Section 4.2.1 above).

5.2 For Constriction

Another type of circumferential actin ring forms during the process of cellularization in *Drosophila* embryogenesis. At this early developmental stage the synthetic outer layer of the fly egg transforms into an epithelium. First the "sidewalls" of the future cells are formed creating a layer of open cylinders, each with a nucleus inside. And then the open, inner sides of the cell cylinders are sealed by concentric closure of the plasma membrane, which is accomplished in each cell by the constriction of a circumferential actomyosin ring in the plane of the closing membrane (Xue and Sokac, 2016). The molecular mechanism has two phases, one requiring myosin II and the other requiring actin filament shortening. However, both phases are not dependent on each other, in the contrary, ring closure can be accomplished by one or the other alone. So the two phases appear to be redundant mechanisms serving the same purpose. The authors of this report point out that in the animal cleavage furrow, the phase 1 mechanism involving myosin II has been conceived as the major mechanism, but this view is now changing in the sense that the two mechanisms seem to occur simultaneously (Xue and Sokac, 2016). There are, however, cases where the cytokinetic actin ring can get closed by means of actin depolymerization as the sole driving mechanism (Mendes Pinto et al., 2012).

In the light of these considerations, the Phalloidin effect on the cytokinetic actin ring in *Odontella* is easier to understand. As has been reported in the results section of Chapter 3, successful divisions have been rarely encountered in Phalloidin-treated cells, even though cells with a fully developed cytokinetic actin ring do frequently occur in the samples. These actin rings had a conspicuous, meandering shape suggesting that their circumference exceeded that of the cell, which intuitively suggests that instead of undergoing contraction, these rings even appeared to expand. In agreement with the situation in the *Drosophila* embryo, this indicates that contraction of the cytokinetic ring in *Odontella* also requires actin filament shortening.

The circumferential actin ring at the edge of the SDV of the valve and the girdle band might be constructed differently when compared with the cytokinetic actin ring. It may provide limited tension at one time but then also may relax and become wider at another time. The hypothesis has been put forward here, that it links to the SDV by a special type of chitin-synthase-myosin chimeras (see Section 4.2.1).

Yet another type of circumferential actin structure is worth to be mentioned here. In an early stage of embryogenesis (tubulogenesis) of the ascidian sea squirt *Ciona intestinalis* a belt-shaped actin system forms in the equatorial region of notochord cells, which causes circumferential compression and this in turn is thought to drive cell elongation (Dong et al., 2011). Apparently this actin belt contracts until the cells have been compressed to about 65% of the original width and concomitantly their individual length has doubled. Since the actin belt contains myosin II in addition to actin it has features resembling a halfway condensed cytokinetic contractile ring, though it apparently does not require spindle or astral microtubules for its orientation. The other difference is that constriction stops half way through and subsequently relaxes again until the reduction of cell width reaches about $\frac{3}{4}$ of the original size. This could be seen as a single pulse of contraction followed by partial relaxation (see discussion on pulsed contraction below, Section 6.2).

5.3 Two Different Types of Actin Rings Sitting Side by Side

Other circumferential actin rings are found in some specialized animal cell types, such as very thin rings placed in a periodic fashion along the length of the nerve axon. Their construction involves spectrin and filament end-tracking proteins serving a static function (Xu et al., 2013). This would be an example, where molecular construction and function are clearly different to

that of the contractile cytokinetic actin ring. It is conceivable then, that two types of rings, if they are sufficiently different from one another, can exist side by side in the same cell and that one of them might just be forming, while the other is becoming deconstructed as has been suggested for the SDV-actin ring of the girdle band and the cytokinetic actin ring in *Odontella* (see discussion of Chapter 2). Looked at it from a wider perspective, it is indeed a common feature of eukaryotic cell architecture that different actin cytoskeleton assemblies can be maintained side by side in the same cytoplasm (Michelot and Drubin, 2011).

6 The Cytokinetic Actin Ring of *Odontella*

6.1 Does the PC Precursor/ PCs of the Diatom Spindle Controls the Cleavage Plane Determination?

As mentioned above, the position of the cytokinetic actin ring in *Odontella* coincides precisely with the gap between the two polar complexes (PCs), where the central spindle is about to develop. All the way during spindle assembly and subsequent constriction, the ring maintains this position. The obvious consequence is that daughter nuclei come to lie on both sides of the ring and become segregated into the two separated daughter cell protoplasts, when cleavage is completed. Destroying the cytokinetic actin ring by JAS leads to a rapprochement of the nuclei followed by a merger of the two perinuclear microtubule systems into one. The Oryzalin experiments have shown that in the absence of microtubules mitosis fails and the single nucleus tends to wander away from the central position, whereas formation of the ring may still occur close to the original equatorial plane, but it may also sometimes occur elsewhere along the cell axis. Hence it is clear that constriction of the ring does not require spatial proximity to the PCs (i.e. to the nucleus, because in Oryzalin-treated cells the fate of the PCs is not clear). This shows that even though the PC appears to have a guiding function for the positioning of the contractile ring in control cells, neither the initiation of the contractile ring, nor the contraction process as such require an intervention of the PCs. In other words, and in agreement with the previous conclusions by Wordemann and co-workers (Wordeman et al., 1986; Wordemann, 1992), cytokinesis in the diatoms can work independently of mitosis.

But how does determination of the division plane in diatoms compare to the situation in other organisms?

Cell division in plant cells is entirely different, because the spindle is acentric and division does not involve a contractile ring but a phragmoplast. There is, however, a guiding mechanism involving the so called preprophase band made of microtubules and in turn, the positioning of the preprophase band is guided by the nucleus (Rasmussen et al., 2013). In yeast, the spindle poles are formed by the spindle pole bodies (SPBs). They originate from the duplication of the single interphase SPB and the formation of the cytokinetic actin ring coincides with the location of the recently divided SPBs, before they move to opposite poles of the pre-mitotic nucleus. Therefore, Arai and coworkers conclude that fission yeast SPBs have a function in the positioning of the cytokinetic actin ring (Arai and Mabuchi, 2002). This suggests some kind of molecular crosstalk between the SPB and the cell cortex (Eng et al., 1998; Hedman et al., 2015).

Animal spindles have radiating microtubule asters originating from the centriole poles and there is increasing evidence that the positioning of the contractile ring has to do with the astral microtubules or with the centrioles. For example, recent work of von Dassow and coworkers (von Dassow et al., 2009) on cell division in sea urchin embryos shows (1) cytokinesis can occur in anucleated cells, as long as two far-separated domains of asters remain in the cytoplasm; (2) in nucleated cells, cleavage furrow appears at microtubule poor region; thus they concluded that the spatial balance between the two domains of asters affects the placement of the cleavage plane but not the capability to construct a cytokinetic ring.

So in essence, the situations in yeast and animals have important features in common, although the structure of the spindle poles, the size of the astral arrays are different. For the diatoms, one can only make a note here of the conspicuous spatial correlation between the PC (precursor) and the forming cytokinetic actin ring. Any speculations on potential molecular mechanisms remain premature.

6.2 How Common is the Pulsed Contraction?

An hitherto unknown phenomenon observed in Colchicine-treated or Oryzalin-treated *Odontella* cells is that the cytokinetic cleavage furrow undergoes pulsed contraction, no matter whether the

nucleus lies directly in the path of the ingrowing furrow. Is such a behavior known from other systems (leaving autonomously contracting heart muscle cells aside) and how can it be explained?

Pulsed contraction is indeed known from other systems. In the process of epithelial folding during *Drosophila* gastrulation (a developmental stage following that of cellularization, discussed above), pulsed contraction generated by the cortical actomyosin system drives apical cell constriction so that the cell assumes a pyramidal shape. The unique nature of this motile process is that the amount of constriction achieved during every single pulse is stored between pulses so that the surface area of the apical cell pole gets smaller in a stepwise fashion until the flat epithelial cell layer is forced into a fold shape in the local area, where these contractions occur (Martin et al., 2009). This has prompted the authors to envision a molecular ratchet-like mechanism. The molecular basis for the intermittent stop phases could lie in the activation of actin cross-linkers, which need to be released with the next contraction phase or it could simply be a step up in myosin persistence. The latter has indeed been found in amnioserosa cells of *Drosophila*, which undergo pulses of contraction and relaxation before the onset of dorsal closure (see Fig. 7 in (Martin and Goldstein, 2014)). In the case, when the result of apical cell contraction becomes stabilized, it is quite clear that this intermittent stop allows for an adaptation of the cytoskeleton to adjust for the reduced cell circumference by a rearrangement in the cortical actomyosin network thus optimizing the conditions for the next contraction pulse to come.

It is currently premature to decide, what the causes for the contraction pulses are in the Oryzalin-treated *Odontella* cells. But the mechanism, just described for *Drosophila* epithelium folding serves as an attractive model. Following this model, it is tempting to speculate, that in the situation, when the cleavage furrow encounters the obstructing nucleus, the persistence in the myosin motor activity during cytokinetic contraction is gradually building up until it overcomes the additional resistance caused by the obstruction in the path the incipient furrow. This suggests that the nucleus acts as a mechanical resistance against the force of the incoming furrow. However, the nucleus is often but not always in the path of the pulsing cleavage furrow and in addition, the idea of the nucleus serving as an obstruction is at variance with the observations made by others that in other diatoms the cleavage furrow can exert immense physical strength capable of pushing large organelles out of the way (see for instance (Pickett-Heaps, 1991; Pickett-Heaps et al., 1979b), also see the movie by (Pickett-Heaps and Pickett-Heaps, 2003)). To reconcile these differences, it may be conceivable

that the contractile mechanism is less focused in *Odontella* as a result of the Colchicine or Oryzalin treatment (see videos # 2 & 3 in the Appendix), i.e., spread further around the cell circumference than in control cells. This suggestion comes from the observation that the cell surface shows local contractile activities further away from the position of the cleavage furrow.

7 References

- Anderson, O.R. (1981). Radiolarian Fine Structure and Silica Deposition. In *Silicon and Siliceous Structures in Biological Systems*, T.L. Simpson, and B.E. Volcani, eds. (New York, NY: Springer New York), pp. 347–379.
- Arai, R., and Mabuchi, I. (2002). F-actin ring formation and the role of F-actin cables in the fission yeast *Schizosaccharomyces pombe*. *J. Cell Sci.* *115*, 887–898.
- Arasada, R., and Pollard, T.D. (2014). Contractile ring stability in *S. pombe* depends on F-BAR protein Cdc15p and Bgs1p transport from the Golgi complex. *Cell Rep.* *8*, 1533–1544.
- Baluška, F., Barlow, P.W., Parker, J.S., and Volkmann, D. (1996). Symmetric reorganizations of radiating microtubules around pre- and post-mitotic nuclei of dividing cells organized within intact root meristems. *J. Plant Physiol.* *149*, 119–128.
- Basu, R., and Chang, F. (2007). Shaping the actin cytoskeleton using microtubule tips. *Curr. Opin. Cell Biol.* *19*, 88–94.
- Bond, L.M., Tumbarello, D.A., Kendrick-Jones, J., and Buss, F. (2013). Small-molecule inhibitors of myosin proteins. *Future Med. Chem.* *5*, 41–52.
- Bornens, M. (2012). The centrosome in cells and organisms. *Science* *335*, 422–426.
- Breshears, L.M., and Titus, M.A. (2007). Motor Proteins: tightening your belt with myosin VI. *Curr. Biol.* *17*, R915–R917.
- Brunner, E., Richthammer, P., Ehrlich, H., Paasch, S., Simon, P., Ueberlein, S., and van Pée, K.-H. (2009). Chitin-based organic networks: an integral part of cell wall biosilica in the diatom *Thalassiosira pseudonana*. *Angew. Chem. Int. Ed.* *48*, 9724–9727.
- Chiappino, M.L., and Volcani, B.E. (1977). Studies on the biochemistry and fine structure of silica shell formation in diatoms VII. Sequential cell wall development in the pennate *Navicula pelliculosa*. *Protoplasma* *93*, 205–221.
- Crawford, R.M. (1990). Transmission Electron Microscopy and Diatom Research. J.P. Kociolek, ed. (California Academy of Sciences), pp. 5–19.
- Crawford, R.M., and Schmid, A.M. (1986). Ultrastructure of silica deposition in diatoms. *Biomineralization in Lower Plants and Animals* 291–314.

- von Dassow, G., Verbrugghe, K.J.C., Miller, A.L., Sider, J.R., and Bement, W.M. (2009). Action at a distance during cytokinesis. *J. Cell Biol.* *187*, 831–845.
- Davì, V., and Minc, N. (2015). Mechanics and morphogenesis of fission yeast cells. *Curr. Opin. Microbiol.* *28*, 36–45.
- Davis, A.K., and Hildebrand, M. (2010). Molecular Processes of Biosilicification in Diatoms. In *Biom mineralization*, pp. 255–294.
- Deinum, E.E., and Mulder, B.M. (2013). Modelling the role of microtubules in plant cell morphology. *Curr. Opin. Plant Biol.* *16*, 688–692.
- Dong, B., Deng, W., and Jiang, D. (2011). Distinct cytoskeleton populations and extensive crosstalk control *Ciona* notochord tubulogenesis. *Development* *138*, 1631–1641.
- Dugina, V., Alieva, I., Khromova, N., Kireev, I., Gunning, P.W., and Kopnin, P. (2016). Interaction of microtubules with the actin cytoskeleton via cross-talk of EB1-containing +TIPs and γ -actin in epithelial cells. *Oncotarget* *7*, 72699–72715.
- Durkin, C.A., Mock, T., and Armbrust, E.V. (2009). Chitin in diatoms and its association with the cell wall. *Eukaryot. Cell* *8*, 1038–1050.
- Edgar, L.A., and Pickett-Heaps, J.D. (1984). VALVE MORPHOGENESIS IN THE PENNATE DIATOM NAVICULA CUSPIDATA1. *J. Phycol.* *20*, 47–61.
- Eng, K., Naqvi, N.I., Wong, K.C., and Balasubramanian, M.K. (1998). Rng2p, a protein required for cytokinesis in fission yeast, is a component of the actomyosin ring and the spindle pole body. *Curr. Biol.* *8*, 611–621.
- Farina, F., Gaillard, J., Guérin, C., Couté, Y., Sillibourne, J., Blanchoin, L., and Théry, M. (2016). The centrosome is an actin-organizing centre. *Nat. Cell Biol.* *18*, 65–75.
- Fernández Honaine, M., Paolicchi, M., Osterrieth, M., and Benvenuto, M.L. (2016). Root silicification of grasses and crops from Pampean region and its relevance on silica and silicophytolith content of soils. In *International Meeting on Phytolith Research*,.
- Fujiwara, M., Horiuchi, H., Ohta, A., and Takagi, M. (1997). A novel fungal gene encoding chitin synthase with a myosin motor-like domain. *Biochem. Biophys. Res. Commun.* *236*, 75–78.
- Ge, W., and Balasubramanian, M.K. (2008). Pxl1p, a paxillin-related protein, stabilizes the actomyosin ring during cytokinesis in fission yeast. *Mol. Biol. Cell* *19*, 1680–1692.
- Goode, B.L., Drubin, D.G., and Barnes, G. (2000). Functional cooperation between the microtubule and actin cytoskeletons. *Curr. Opin. Cell Biol.* *12*, 63–71.
- Hamm, C., and Smetacek, V. (2007). Armor: why, when, and how. In *Evolution of Primary Producers in the Sea*, (Elsevier), pp. 311–332.
- Hasle, G.R. (1974). The “mucilage pore” of pennate diatoms. *Nova Hedwigia Beiheft*, 167–194.
- Hedman, A.C., Smith, J.M., and Sacks, D.B. (2015). The biology of IQGAP proteins: beyond the cytoskeleton. *EMBO Rep.* *16*, 427–446.
- Hepler, P.K., and Hush, J.M. (1996). Behavior of Microtubules in Living Plant Cells. *Plant*

Physiol. 112, 455–461.

Hildebrand, M., and Lerch, S.J.L. (2015). Diatom silica biomineralization: Parallel development of approaches and understanding. *Semin. Cell Dev. Biol.* 46, 27–35.

Hoffmeyer, T.T., and Burkhardt, P. (2016). Choanoflagellate models - *Monosiga brevicollis* and *Salpingoeca rosetta*. *Curr. Opin. Genet. Dev.* 39, 42–47.

Huang, B.Q., and Yeung, E.C. (2015). Chemical and Physical Fixation of Cells and Tissues: An Overview. In *Plant Microtechniques and Protocols*, E.C.T. Yeung, C. Stasolla, M.J. Sumner, and B.Q. Huang, eds. (Cham: Springer International Publishing), pp. 23–43.

Idei, M., Osada, K., Sato, S., Toyoda, K., Nagumo, T., and Mann, D.G. (2012). Gametogenesis and auxospore development in *Actinocyclus* (Bacillariophyta). *PLoS One* 7, e41890.

Kaczmarek, I., Ehrman, J.M., and Bates, S.S. (2001). A review of auxospore structure, ontogeny and diatom phylogeny. In *Proceedings of the 16th International Diatom Symposium*, (Athens, Greece, University of Athens), pp. 153–168.

Karlsson, R., and Lindberg, U. (1985). Changes in the organization of actin and myosin in non-muscle cells induced by N-ethylmaleimide. *Exp. Cell Res.* 157, 95–115.

Katsaros, C., Karyophyllis, D., and Galatis, B. (2006). Cytoskeleton and morphogenesis in brown algae. *Ann. Bot.* 97, 679–693.

Knight, M.J., Senior, L., Nancolas, B., Ratcliffe, S., and Curnow, P. (2016). Direct evidence of the molecular basis for biological silicon transport. *Nat. Commun.* 7, 11926.

Köhler, S., Schaller, V., and Bausch, A.R. (2011). Structure formation in active networks. *Nat. Mater.* 10, 462–468.

Kotzsch, A., Pawolski, D., Milentyev, A., Shevchenko, A., Scheffel, A., Poulsen, N., Shevchenko, A., and Kröger, N. (2016). Biochemical Composition and Assembly of Biosilica-associated Insoluble Organic Matrices from the Diatom *Thalassiosira pseudonana*. *J. Biol. Chem.* 291, 4982–4997.

Li, C.-W., and Volcani, B.E. (1984). Aspects of Silicification in Wall Morphogenesis of Diatoms. *Philos. Trans. R. Soc. Lond. B Biol. Sci.* 304, 519–528.

Li, C.-W., and Volcani, B.E. (1985a). Studies on the biochemistry and fine structure of silica shell formation in diatoms. *Protoplasma* 124, 147–156.

Li, C.-W., and Volcani, B.E. (1985b). Studies on the biochemistry and fine structure of silica shell formation in diatoms. *Protoplasma* 124, 10–29.

Mann, and Marchant (1989). The origin of the diatom and its life cycle.

Marron, A.O., Alston, M.J., Heavens, D., Akam, M., Caccamo, M., Holland, P.W.H., and Walker, G. (2013). A family of diatom-like silicon transporters in the siliceous loricate choanoflagellates. *Proc. Biol. Sci.* 280, 20122543.

Martin, A.C., and Goldstein, B. (2014). Apical constriction: themes and variations on a cellular mechanism driving morphogenesis. *Development* 141, 1987–1998.

- Martin, S., Bonnin, A., Furio, V., Coronado, P.J., Vidart, J.A., and Arencibia, J.M. (2009). 8017 Tspan13 expression in epithelial ovarian cancer. *Eur. J. Cancer Suppl.* 7, 454–455.
- Medlin, L.K. (2016). Evolution of the diatoms: major steps in their evolution and a review of the supporting molecular and morphological evidence. *Phycologia* 55, 79–103.
- Mendes Pinto, I., Rubinstein, B., Kucharavy, A., Unruh, J.R., and Li, R. (2012). Actin depolymerization drives actomyosin ring contraction during budding yeast cytokinesis. *Dev. Cell* 22, 1247–1260.
- Menzel, D., Jonitz, H., and Elsner-Menzel, C. (1996). The perinuclear microtubule system in the green alga *Acetabularia*: anchor or motility device? *Protoplasma* 193, 63–76.
- Michelot, A., and Drubin, D.G. (2011). Building distinct actin filament networks in a common cytoplasm. *Curr. Biol.* 21, R560–R569.
- Mohan, R., and John, A. (2015). Microtubule-associated proteins as direct crosslinkers of actin filaments and microtubules. *IUBMB Life* 67, 395–403.
- Müller, W.E.G., Wang, X., Chen, A., Hu, S., Gan, L., Schröder, H.C., Schloßmacher, U., and Wiens, M. (2011). The unique invention of the siliceous sponges: their enzymatically made bio-silica skeleton. *Prog. Mol. Subcell. Biol.* 52, 251–281.
- Nelson, J.C., Stavoe, A.K.H., and Colón-Ramos, D.A. (2013). The actin cytoskeleton in presynaptic assembly. *Cell Adh. Migr.* 7, 379–387.
- Niessen, C.M., and Gottardi, C.J. (2008). Molecular components of the adherens junction. *Biochim. Biophys. Acta* 1778, 562–571.
- Otegui, M., and Staehelin, L.A. (2000). Syncytial-type cell plates: a novel kind of cell plate involved in endosperm cellularization of *Arabidopsis*. *Plant Cell* 12, 933–947.
- Pacheco, A., and Gallo, G. (2016). Actin filament-microtubule interactions in axon initiation and branching. *Brain Res. Bull.* 126, 300–310.
- Paradez, A., Wright, A., and Ehrhardt, D.W. (2006). Microtubule cortical array organization and plant cell morphogenesis. *Curr. Opin. Plant Biol.* 9, 571–578.
- Pickett-Heaps, J. (1991). Cell Division in Diatoms. In *International Review of Cytology*, K.W. Jeon, and M. Friedlander, eds. (Academic Press), pp. 63–108.
- Pickett-Heaps, J.D., and Pickett-Heaps, J. (2003). Diatoms [videorecording]: life in glass houses (Cytographics).
- Pickett-Heaps, J., Schmid, A.-M.M., and Edgar, L.A. (1990). The cell biology of diatom valve formation. *Progress in Phycological Research* 7, 1–168. pls. 1–101.
- Pickett-Heaps, J.D., Tippit, D.H., and Andreozzi, J.A. (1979a). Cell division in the pennate diatom *Pinnularia*. IV. Valve morphogenesis. *Biologie Cellulaire*.
- Pickett-Heaps, J.D., Tippit, D.H., and Andreozzi, J.A. (1979b). Cell division in the pennate diatom *Pinnularia*. III. The valve and associated cytoplasmic organelles. *Biologie Cellulaire*.
- Pickett-Heaps, J.D., Carpena, J., and Koutoulis, A. (1994). Valve and seta (spine)

- morphogenesis in the centric diatom *Chaetoceros peruvianus* Brightwell. In *The Protistan Cell Surface*, R. Wetherbee, J.D. Pickett-Heaps, and R.A. Andersen, eds. (Vienna: Springer Vienna), pp. 269–282.
- Pipes, L.D., and Leedale, G.F. (1992). Scale formation in *Tessellaria volvocina* (Synurophyceae). *British Phycological Journal* 27, 11–19.
- Rasmussen, C.G., Wright, A.J., and Müller, S. (2013). The role of the cytoskeleton and associated proteins in determination of the plant cell division plane. *Plant J.* 75, 258–269.
- Raven, J.A., and Waite, A.M. (2004). The evolution of silicification in diatoms: inescapable sinking and sinking as escape? *New Phytol.* 162, 45–61.
- Robinson, D.H., and Sullivan, C.W. (1987). How do diatoms make silicon biominerals? *Trends Biochem. Sci.* 12, 151–154.
- Roth, L.E., and De Francisco, A. (1977). marine diatom, *Striatella unipunctata*. II. Siliceous structures and the formation of intercalary bands. *Cytobiologie*.
- Round, F.E., Crawford, R.M., and Mann, D.G. (2007). *Diatoms: Biology and Morphology of the Genera* (Cambridge University Press).
- Saheki, Y., and De Camilli, P. (2017). Endoplasmic Reticulum–Plasma Membrane Contact Sites. *Annu. Rev. Biochem.* 86, 659–684.
- Sato, S., Mann, D.G., Nagumo, T., Tanaka, J., Tadano, T., and Medlin, L.K. (2008). Auxospore Fine Structure and Variation in Modes of Cell Size Changes in *Grammatophora Marina* (Bacillariophyta). *Phycologia* 47, 12–27.
- Schmid, A.-M.M. (1994). Aspects of morphogenesis and function of diatom cell walls with implications for taxonomy. *Protoplasma* 181, 43–60.
- Schmid, A.-M.M., and Crawford, R.M. (2001). *Ellerbeckia arenaria* (Bacillariophyceae): formation of auxospores and initial cells. *Eur. J. Phycol.* 36, 307–320.
- Sims, P.A., Mann, D.G., and Medlin, L.K. (2006). Evolution of the diatoms: insights from fossil, biological and molecular data. *Phycologia* 45, 361–402.
- Smirnova, E.A., and Bajer, A.S. (1994). Microtubule converging centers and reorganization of the interphase cytoskeleton and the mitotic spindle in higher plant *Haemanthus*. *Cell Motil. Cytoskeleton* 27, 219–233.
- Stoermer, E.F., Pankratz, H.S., and Bowen, C.C. (1965). FINE STRUCTURE OF THE DIATOM *AMPHIPLEURA PELLUCIDA*. II. CYTOPLASMIC FINE STRUCTURE AND FRUSTULE FORMATION. *Am. J. Bot.* 52, 1067–1078.
- Stoppin, V., Vantard, M., Schmit, A.C., and Lambert, A.M. (1994). Isolated Plant Nuclei Nucleate Microtubule Assembly: The Nuclear Surface in Higher Plants Has Centrosome-like Activity. *Plant Cell* 6, 1099–1106.
- Tesson, B., and Hildebrand, M. (2010a). Dynamics of silica cell wall morphogenesis in the diatom *Cyclotella cryptica*: substructure formation and the role of microfilaments. *J. Struct. Biol.* 169, 62–74.

- Tesson, B., and Hildebrand, M. (2010b). Extensive and intimate association of the cytoskeleton with forming silica in diatoms: control over patterning on the meso- and micro-scale. *PLoS One* 5, e14300.
- Tesson, B., and Hildebrand, M. (2013). Characterization and localization of insoluble organic matrices associated with diatom cell walls: insight into their roles during cell wall formation. *PLoS One* 8, e61675.
- Tippit, D.H., and Pickett-Heaps, J.D. (1977). Mitosis in the pennate diatom *Suirella ovalis*. *J. Cell Biol.* 73, 705–727.
- Treitschke, S., Doehlemann, G., Schuster, M., and Steinberg, G. (2010). The myosin motor domain of fungal chitin synthase V is dispensable for vesicle motility but required for virulence of the maize pathogen *Ustilago maydis*. *Plant Cell* 22, 2476–2494.
- van Vliet, A.R., Giordano, F., Gerlo, S., Segura, I., Van Eygen, S., Molenberghs, G., Rocha, S., Houcine, A., Derua, R., Verfaillie, T., et al. (2017). The ER Stress Sensor PERK Coordinates ER-Plasma Membrane Contact Site Formation through Interaction with Filamin-A and F-Actin Remodeling. *Mol. Cell* 65, 885–899.e6.
- Wang, Y., Chen, Y., Lavin, C., and Gretz, M.R. (2000). Extracellular matrix assembly in diatoms (Bacillariophyceae). iv. ultrastructure of *Achnanthes longipes* and *Cymbella cistula* as revealed by high-pressure freezing/freeze substitution and cryo-field emission scanning electron microscopy. *J. Phycol.* 36, 367–378.
- Weiss, I.M., Schönitzer, V., Eichner, N., and Sumper, M. (2006). The chitin synthase involved in marine bivalve mollusk shell formation contains a myosin domain. *FEBS Lett.* 580, 1846–1852.
- Witkowski, J., Sims, P.A., and Harwood, D.M. (2011). Rutilariaceae redefined: a review of fossil bipolar diatom genera with centrally positioned linking structures, with implications for the origin of pennate diatoms. *Eur. J. Phycol.* 46, 378–398.
- Wordeman, L., McDonald, K.L., and Cande, W.Z. (1986). The distribution of cytoplasmic microtubules throughout the cell cycle of the centric diatom *Stephanopyxis turris*: their role in nuclear migration and positioning the mitotic spindle during cytokinesis. *J. Cell Biol.* 102, 1688–1698.
- Wordemann, L. (1992). The cytoskeleton in the diatoms. The mitotic spindle and cell cycle dependent organization. *The Cytoskeleton of Algae*. CRC Press, Boca Raton 39–57.
- Xu, K., Zhong, G., and Zhuang, X. (2013). Actin, spectrin, and associated proteins form a periodic cytoskeletal structure in axons. *Science* 339, 452–456.
- Xue, Z., and Sokac, A.M. (2016). -Back-to-back mechanisms drive actomyosin ring closure during *Drosophila* embryo cleavage. *J. Cell Biol.* 215, 335–344.
- Yonemura, S. (2011). Cadherin–actin interactions at adherens junctions. *Curr. Opin. Cell Biol.* 23, 515–522.
- Zhang, Y. (2012). Girdle Band Formation of *Odontella sinensis*. Master. Bonn University.

Summary

Despite significant advances in diatom research over the past decade very little is known on the more detailed mechanisms of frustule morphogenesis, such as how the geometry of the valve at the microscale is established, how the frustule surface is sculptured, how girdle bands are produced and how a newly deployed silica structure is inserted into the frustule. Such important questions concerning frustule morphogenesis and to what extent the cytoskeleton is involved have been addressed in the current thesis using the marine centric diatom species *Odontella sinensis* grown in laboratory culture as a model system.

To this end, a variety of experimental approaches have been taken. The fine structure of the frustule has been studied by scanning electron microscopy (SEM) using specimens either fixed directly from the culture medium or after pretreatments ranging from gently opening cells to completely disintegrating them so that only cleaned silica was left behind. Further, ultra-thin sections as well as acid cleaned frustule parts were analyzed by transmission electron microscopy (TEM). The previously established fluorescent lysosensor dye staining method (Zhang 2012) was exploited to visualize all stages of frustule morphogenesis in great detail by high resolution multi-color confocal microscopy as a complementation of the fine structural methods. Successive steps of silica deposition were studied by sequential application of two types of lysosensors, whose spectral properties are different. As a further refinement, lysosensor staining was combined with immunocytochemical fluorochrome labelling of cytoskeletal proteins to study the relationship between frustule morphogenesis and the cytoskeletons. And finally the cytochemical localization of chitin, which has been attempted before (Zhang 2012, "Girdle Band Formation of *Odontella sinensis*", Master thesis, Bonn University.), was further refined by using specific binding of fluorochrome-conjugated lectin.

In order to learn more about the role of the cytoskeleton, the microtubule system has been challenged by the inhibitors Oryzalin and Taxol; whereas the actin system was put under stress by Jasplakinolide (JAS) and Phalloidin. Preliminary data were also obtained on myosin function by using inhibitors such as N-ethylmaleimide (NEM), 2,3-butanedione monoxime (BDM) and Blebbistatin. The data of myosin inhibitions are shown in the Appendix of this thesis.

- ❖ The fine structure work revealed that the frustule wall of *O. sinensis* consists of three layers — the tectum (upper layer), the trabeculae (columns between the upper and lower layer) and the foramen layer (base layer). The principle of cell morphogenesis in

diatoms is well known, i.e. that all frustule parts are fabricated in the lumen of the silica deposition vesicle (SDV), but the process of molding within the SDV is shown here in further detail; especially, the molding in the vertical direction appears to be related to a kind of hitherto unknown structure — the fibrous balls. It is further demonstrated that the development of the frustule wall starts with the virgae of the tectum, continues with the trabecular columns and closes with the foramen layer.

❖ Valve morphogenesis can be separated in several steps and the cytoskeleton involvements during the corresponding process has been discussed:

1. Initiation and LP formation: Two SDVs are initiated and positioned on the apical dome of each daughter protoplasmic surface. It is demonstrated that the cytoskeletal basis for the SDV positioning is the horn bundle system of microtubules, which can be traced back to an unusual MTOC from within the late telophase spindle. The horn bundle system of microtubules require the guidance of the contractile cytokinetic actin ring, when the actin system is deconstructed by JAS, the microtubule system by itself, is not able to set up the horn bundles, which suggests a close cooperation between both cytoskeletal systems. Horn bundles are not only instrumental for the positioning of the initial SDVs, which sets the bipolar symmetry of the valve, they also are responsible for the molding of the cytoplasmic protrusion coming from the sides of the polar region as two horns. At the primary silicification site of each SDV on the horn bundle, a long and hollow labiate process (LP) begins to grow out.
2. Shaping of annuli: Actin filaments begin to gather surrounding the two expanding initial SDVs until a compressed ring structure is established. Next, the SDVs expand towards the middle of the apical domain along the microtubule horn bundles to form two slit-like annuli and then further expand to fuse into one single valve SDV, which then further expands until its advancing edge encounters the actin ring. Then the valve SDV and its associated actin ring expand to cover the entire head plate region.
3. Shaping of horns and completion of head plate: The valve SDV associated with the actin ring further expands to the side along the horn bundles, thereby wrapping around the cytoplasmic protrusions, giving rise of the horns. The

closing of the horn appears to be mediated by the dynamic of actin cytoskeleton.

4. Completion of the hypovalve: At this point, the apical head plate of the valve has been completed and the formation of the valve dome continues, which is characterized by an umbrella configuration of perinuclear microtubules – transformed from the horn bundles – centering on the microtubule center (MC) at the nucleus. The SDV edge advances further driven by silica deposition within the lumen of the SDV. Through the entire process, the actin ring remains associated with the advancing SDV edge until the valve is completed and becomes deployed on the cell surface.

The specific configuration of the valve SDV, microtubules and the valve actin ring, give rise to the formulation of a novel functional model, according to which the actin ring limits the SDV expansion, in cooperation with the radial microtubule system until the SDV edge reaches a specific position with respect the mother frustule identified as the joint between the two epithelial girdle bands (eGB1 and eGB2). This model, along with a large number of results from inhibitor experiments, is discussed very thoroughly with literature data, leading to the conclusion that the actin ring is destined to reach this location by the interaction with chitin, which is exactly present at this joint.

- ❖ After the deployment of the valve, the girdle band morphogenesis sets in by the formation of a new SDV along the cell circumference exactly at the last position of the former valve SDV edge with the persisting actin ring right behind it. Different to the motile state during the valve development, it is concluded that the actin ring statically remains at the joint between eGB1 and eGB2, when it is involved in the girdle band formation, acting as a bumper to prevent the GB-SDV from growing beyond its epithelial side, so that the SDV grows towards the hypothecal side and pushes against the hypotheca.

Meanwhile, the nucleus together with its radial perinuclear microtubule system moves away from the valve pole and faces to the forming girdle band. The reason for this repositioning lies within the establishment of the axially oriented actin cable system, which consists of two groups of actin cables anchored at the epithelial LP-labiae. The actin cables spread in the middle of the cell into finer branches and associate with the perinuclear MTs. A similar actin system is developing on the hypothecal side. When MTs associate with the new actin bundles anchored at the hypothecal LP-labiae, the tension between the two opposite unites of the actin cytoskeleton will eventually reach a

balance, so that the nucleus will be held in the exact middle of the cell. During such a cytoskeleton regulation, girdle bands develop and get deployed on the protoplasmic surface one after the other. These observations leads to formulate the model of tension equilibrium system, which, combining many data from inhibitor experiments challenging one or the other cytoskeletal system, tries to explain how the cell grows axially and keeps the nucleus at the demanding position.

- ❖ Late interphase cells are observed to proceed into prophase by the conspicuous condensation of chromosomes. All the while, the MC has remained located on the nucleus, although it appears dormant, i.e. it is not functioning as a microtubule organizer, in the sense that all microtubules converge on it. But it definitely has this capacity, as is demonstrated in a striking way under the conditions of Phalloidin treatment, which is discussed in conjunction with data from the literature showing that the animal centrosome acts as an unique organizer for both microtubules and actin filaments, which is seen here for the first time also in a diatom. Under normal conditions, this MC, however, is suggested to be dormant and get degraded, as the spindle precursor (also termed polar complexes, PCs) emerges in the vicinity at the onset of prophase. While this emersion is known from work on other species, it has not been known, that the cytokinetic actin ring forms exactly from the position of the PCs and remains there as PCs expand to develop a spindle, so that the ring can be seen straddling the central spindle throughout mitosis and cytokinesis. Therefore, the reforming daughter nuclei come to lie on both sides of it and will eventually get separated from each other at the completion of division.

Since the former GB-actin ring persists to the moment, when the cytokinetic actin ring is becoming assembled, the question is discussed, how it could be possible to have two oppositely directed dynamics (one assembling, one disassembling) of the actin cytoskeleton occurring so close to each other in the same cell. This also prompted a literature search on the presence of actin rings in various types of cells, which is described in the general discussion (Part III).

- ❖ A large body of data is obtained describing what happens in cells with deconstructed actin system and cells with deconstructed microtubule system, and they are compared with normal cells. The comparison results are consistent with the ideas developed on the mode of valve morphogenesis and on the role of cytoskeleton in the tension-equilibrium

model which aims to explain the mechanism of axial cell growth and the cell wall formation. One particular phenomenon should be separately mentioned here, and this is the propensity of diatoms to form, what is called lateral valves, when either the microtubule system or the actin system is crippled or even absent in the cell. This phenomenon, which has been discovered already in the 1960s, is so striking, because it demonstrates that the transit from the mother cell cycle to the daughter cell cycle does not require successful cell division and further it shows to what a large degree silica deposition can occur autonomously and continue with frustule wall formation without the guidance of any microtubules, but it still requires some F-actin.

The large degree of autonomy of silica deposition and the very close interaction of both the microtubules and the actin system in the guidance of these processes resulting in a specific cell morphology, makes the diatoms a fascinating model for morphogenesis studies. Given the tremendous diversity of cell shapes in the diatoms, one may wonder, how the principles of valve morphogenesis and axial growth may become adapted in various ways or become transformed into something new in the different diatom lineages. This point is addressed in the general discussion (Part III) and also a very small preview of cytoskeletal features in centric diatoms is presented in the Appendix as kind of a teaser for future scientists interested in diatom cell morphogenesis.